

Acquisitions and Bibliographic Services Branch

395 Wellington Street Ottawa, Ontario K1A 0N4 Bibliothèque nationale du Canada

Direction des acquisitions et des services bibliographiques

395, rue Wellington Ottawa (Ontario) K1A 0N4

Your life. Votre rélérence

Our file Notre rélérence

NOTICE

The quality of this microform is heavily dependent upon the quality of the original thesis submitted for microfilming. Every effort has been made to ensure the highest quality of reproduction possible.

La qualité de cette microforme dépend grandement de la qualité de la thèse soumise au microfilmage. Nous avons tout fait pour assurer une qualité supérieure de reproduction.

AVIS

If pages are missing, contact the university which granted the degree.

S'il manque des pages, veuillez communiquer avec l'université qui a conféré le grade.

Some pages may have indistinct print especially if the original pages were typed with a poor typewriter ribbon or if the university sent us an inferior photocopy. La qualité d'impression de certaines pages peut laisser à désirer, surtout si les pages originales ont été dactylographiées à l'aide d'un ruban usé ou si l'université nous a fait parvenir une photocopie de qualité inférieure.

Reproduction in full or in part of this microform is governed by the Canadian Copyright Act, R.S.C. 1970, c. C-30, and subsequent amendments. La reproduction, même partielle, de cette microforme est soumise à la Loi canadienne sur le droit d'auteur, SRC 1970, c. C-30, et ses amendements subséquents.

Canadä¹

Laminar Heat Transfer to Viscous Non-Newtonian Fluids in Non-Circular Ducts

Seyed Gholamreza Etemad

Department of Chemical Engineering



McGill University Montreal, Quebec, Canada

A thesis submitted to the Faculty of Graduate Studies and Research in partial fulfillment of the requirements for the degree of

Doctor of Philosophy

© S. Gh. Etemad Feb. 1995



National Library of Canada

Acquisitions and Bibliographic Services Branch

395 Wellington Street Ottawa, Ontario K1A 0N4 Bibliothèque nationale du Canada

Direction des acquisitions et des services bibliographiques

395, rue Wellington Ottawa (Ontario) K1A 0N4

Your file Votre rélèrence

Our file Notre référence

THE AUTHOR HAS GRANTED AN IRREVOCABLE NON-EXCLUSIVE LICENCE ALLOWING THE NATIONAL LIBRARY OF CANADA TO REPRODUCE, LOAN, DISTRIBUTE OR SELL COPIES OF HIS/HER THESIS BY ANY MEANS AND IN ANY FORM OR FORMAT, MAKING THIS THESIS AVAILABLE TO INTERESTED PERSONS.

L'AUTEUR A ACCORDE UNE LICENCE IRREVOCABLE ET NON EXCLUSIVE PERMETTANT A LA BIBLIOTHEQUE NATIONALE DU CANADA DE REPRODUIRE, PRETER, DISTRIBUER OU VENDRE DES COPIES DE SA THESE DE QUELQUE MANIERE ET SOUS QUELQUE FORME QUE CE SOIT POUR METTRE DES EXEMPLAIRES DE CETTE THESE A LA DISPOSITION DES PERSONNE INTERESSEES.

THE AUTHOR RETAINS OWNERSHIP OF THE COPYRIGHT IN HIS/HER THESIS. NEITHER THE THESIS NOR SUBSTANTIAL EXTRACTS FROM IT MAY BE PRINTED OR OTHERWISE REPRODUCED WITHOUT HIS/HER PERMISSION.

L'AUTEUR CONSERVE LA PROPRIETE DU DROIT D'AUTEUR QUI PROTEGE SA THESE. NI LA THESE NI DES EXTRAITS SUBSTANTIELS DE CELLE-CI NE DOIVENT ETRE IMPRIMES OU AUTREMENT REPRODUITS SANS SON AUTORISATION.

ISBN 0-612-05700-3



Heat Transfer to Viscous Non-Newtonian Fluids in Non-Circular Ducts

Abstract

A computational and experimental study was made of the steady developing laminar convective heat transfer to viscous non-Newtonian fluids described by the power law model flowing in straight channels of circular and several non-circular cross-sections. In the numerical study the governing conservation equations in three dimensions subject to suitable boundary conditions were solved after appropriate discretization, using the Galerkin finite element method. Fourteen different cross-sectional geometries were studied numerically. Effects of temperature-dependent apparent viscosity, viscous dissipation as well as Prandtl number were included in the model. The thermal boundary conditions tested were: uniform wall temperature and uniform wall heat flux on the entire duct surface. Predicted velocity fields, pressure drop, and heat transfer distributions were compared with available data and simulation results as appropriate. Results are presented on the comparative thermal performance of various cross-sectional ducts.

In the experimental study the critical Reynolds numbers were measured for distilled water flowing through a semi-circular and an equilateral triangular duct. Local Nusselt number distributions are presented for ducts with the horizontal bottom plane sides subjected to uniform heat flux while the rest of the channel is well insulated. The measured pressure drop and Nusselt number distribution for Carbopol solutions compared very well with the numerical predictions.

Résumé

Dans cette thèse, on présente une étude numérique et expérimentale sur la convection thermique d'un fluide non-Newtonien dans un écoulement laminaire en voie de développement en régime établi qui circule dans une gaine droite d'une section circulaire ainsi que plusieurs autres sections non-circulaires. Dans l'étude numérique les équations de base décrivant le principe de conservation de masse, d'énergie et de quantité de mouvement en trois dimensions, sont résolues numériquement en utilisant la méthode des éléments finis de Galarkin et des conditions limites appropriées. Des gaines avec 14 profils géométriques différents sont examinées. L'influence de la température locale sur la viscosité, le nombre de Prandtl ainsi que la dissipation visqueuse ont été pris en compte. Les deux conditions limites thermiques d'une paroi à une température constante et à un flux thermique constant sont considérées. Les prédictions numériques pour le profil de vitesse, la chute de pression et le coefficient local de transfert de chaleur sont comparées avec les résultats numériques et expérimentaux des autres auteurs. La performance comparée des gaines à différentes géométries a été discuté en détail.

Dans létude expérimentale, le nombre de Reynolds critique est mesuré pour de l'eau distillée circulant dans une gaine à section demi-circulaire et triangulaire. La distribution du nombre local de Nusselt est donnée dans une gaine dont l'un des côtés est chauffé avec un flux thermique constant tandis que les autres côtés sont isolés. Les valeurs mesurées de la chute de pression et la distribution du nombre de Nusselt pour des solutions de Carbopol se comparent très favorablement avec les prédictions numériques.

Acknowledgments

First of all I would like to express my great appreciation to Professor Arun S. Mujumdar, my thesis advisor, for his constant support, guidance and encouragement throughout the course of this study. Also, I would like to thank Professor A. D. Rey for his comments on my thesis research.

I gratefully acknowledge the financial support of Isfahan University of Technology (Isfahan, Iran) and Iranian Ministry of Culture and Higher Education to pursue the present study. The research support of Natural Sciences and Engineering Council of Canada as well as Exergex Corporation is gratefully acknowledged.

I wish to thank Mr. A. Gagnon of the Chemical Engineering machine shop for his excellent construction of the apparatus. Also the assistance of Mr. A. Côte of the Mechanical Engineering Department of E.T.S., University of Quebec, with the experimental set-up is acknowledged. I am indebted to the Computing Center of McGill University for their generous allocation of mainframe computing time on IBM 9000 machines and to Dr. H. Yang and Mr. M. Head for their consulting help.

The author gratefully recognizes Professor R. Nassef for his financial help towards the experimental apparatus and for providing suitable laboratory space for it. I am indebted to Professor H.S. Ramaswami of the Food Science Department for allowing us the use of a rheometer and to Ms. S. Basak for making the rheological measurements.

I wish to thank my friends specially Mr. S. H. Seyedein for the scientific discussions during this study.

I would like to dedicate this effort to the memories of my parents for the love and excellent support they gave me all my life, and to my family for their patience, understanding, sacrifices, constant support and encouragement and their belief in me and my ability even when I have had my doubts. I will always be grateful for this.

Table of Contents

Ab	stract .		i
Rés	sumé		ii
Acl	cnowled	lgments	iii
Lis	t of figu	res	ix
Lis	t of tabl	les	xv
Noi	nenclat	ure	xix
Cha	apter 1	Introduction and Background	1-16
1.1	Introduc	etion	1
		es and scope	
1.3	Backgro	ound	4
	1.3.1	Circular tubes	4
	1.3.2	Rectangular cross-sectional ducts	7
		1.3.2.1 Parallel plates	7
		1.3.2.2 Other rectangular ducts	9
	1.3.3	Circular-sector ducts	10
	1.3.4	Triangular ducts	10
	1.3.5	Summary of various studies	11
Cha	apter 2	Mathematical Model	17-29
2.1	Governi	ng equations	17
2.2	Constitu	tive equation for purely viscous non-Newtonian fluids	18
2 2	Dimensi	onless governing equations	10

2.4	Boundar	conditions		21
2.5	Solution	nethodology		. 22
2.6	Definitio	s of dimensionless parameter	s	. 27
Cha	apter 3	Flow and Heat Transi	er in Different Geometry Ducts 30	-72
3.1	Compari	on with prior studies		. 31
	3.1.1	Circular tube		. 31
	3.1.2	Parallel plates	•••••••••••••••••••••••••••••••••••••••	34
	3.1.3	Rectangular ducts		. 39
		3.1.3.1 Square duct	••••••	39
		3.1.3.2 Rectangular duct w	ith different aspect ratios	41
	3.1.4	Circular-sector ducts		43
	3.1.5	Triangular ducts		45
3.2	Effect of	power law index		47
	3.2.1	Fluid flow		47
	3.2.2	Heat transfer		60
3.3	Conclus	ons		72
Ch	apter 4	•	erature-Dependent Viscosity, Viscosity, 73-	
4.1	Effect o	temperature-dependent appa	rent viscosity	73
4.2	Effect o	viscous dissipation		84
4.3	Simulta	eous effects of temperature-o	lependent viscosity and viscous dissipation	92
4.4	Effect o	Prandtl number		95
4 5	Conclus	 .		100

Ch	apter 5	Miscellaneous Geometrical Effects	101-120
5.1	Effect of	rounding corners of a square duct	101
5.2	Effect of	aspect ratio of rectangular ducts	105
5.3	Effect of	Papex angle of circular-sector ducts	109
5.4	Compari	son between circular-sector and triangular ducts	113
5.5	Effect of	geometric parameter of cross-shaped duct	116
5.6	Conclusi	ons	120
Cha	apter 6	Comparison of Thermal Performance of Variou	
6.1	Fully dev	veloped conditions	
6.2	Effect of	cross-sectional factor on fully developed friction factor and Nusse	elt number
	***********	***************************************	126
6.3		son of $f_{app}Re$ for different geometries	
6.4	Compari	son of entrance region Nusselt numbers for different geometries .	131
6.5	Goodnes	s factor comparison	134
	6.5.1 A	rea goodness factor comparison	134
	6.5.2 ·\	olume goodness factor comparison	138
6.6	Conclusi	ons	142
Cha	apter 7	Experimental Studies	144-171
7.1	Experim	ental apparatus	144
		Flow system	
	7.1.2	Test section	147
7.2	Test Flui	ds	149
		Physical properties of Carbopol solutions	
		Rheological measurements	150

7.3	Results a	and discussion	152
	7.3.1	Critical Reynolds number	153
	7.3.2	Pressure drop measurements	156
	7.3.3	Heat transfer results	162
		7.3.3.1 Newtonian fluids	162
		7.3.3.1.1 Effect of Rayleigh number	164
		7.3.3.2 Viscous non-Newtonian fluids	167
7.4	Conclus	ions	171
	4		
Cna	ipter {	8 Conclusions, Contributions to Knowledge Recommendations	
8.1	Conclus	ions	172
8.2	Contribu	ution to knowledge	174
8.3	Recomn	nendations for future research	175
Ref	erences	s	77-186
Apj	pendix .	A	- A-14
A.1	U_{max} an	$\mathrm{id}f_{app}Re$ for different geometries	A-1
A.2	Nusselt	numbers for different geometries	A-8
Ap	pendix i	B-1	- B-15
B.1	Effect of	of temperature-dependent viscosity on Nusselt number for $n=1.0$	B-1
B.2	Effect of	of viscous dissipation on Nusselt number for $n=1.0$	В-4
B.3	Simulta	meous effects of temperature-dependent viscosity and viscous dissip	ation on
	Nusselt	number for n=1.0	B-6
R A	Effect (of Prandtl number on Nucselt number for $n=1.0$	R_8

Table of Contents

B.5	Effects	of temper	ature-dependent viscosity and viscous	lissipation on flow and heat
	transfer (characteri	stics	В-10
B.6	Nusselt	number fo	or <i>Pr=1.0</i>	B-15
App	pendix (••••••	C-1 - C-7
C.1	Mean N	usselt nur	nber	C-1
			•	•
App	endix I			D-1 - D-15
D.1	Resistan	ce variati	on with temperature	D-1
D.2	Local bo	ttom plat	e Nusselt number	D-2
D.3	Physical	and rheo	logical properties of Carbopol solution	D-4
D.4	Error an	alysis		D-5
D.5	Experim	ental resu	lts	D-7
	D.5.1	Pressure	drop	D-7
	D.5.2	Nusselt	number	D-9
		D.5.2.1	Distilled water	D-9
		D.5.2.2	Viscous non-Newtonian fluid	D-12

List of Figures

Chapter 3

Figure 3.1 Comp	parison of the fully developed center-plane axial velocity profile: circul-	ar
tube	3	2
Figure 3.2 (a - b)	Comparison of $f_{app}Re$ and $K(x)$: circular tube	3
Figure 3.3 (a - b)	Comparison of Nusselt numbers in combined entrance region: circula	Г
	tube	33
Figure 3.4 (a - b)	Comparison of U_f and $f_{app}Re$: parallel plates	35
Figure 3.5 (a - b)	Comparison of Nusselt number in the combined entrance region:	
	parallel plates	36
Figure 3.6 (a - b)	Comparison of dimensionless center-plane axial velocity profile and	
	U _{max} : square duct	39
Figure 3.7 Comp	parison of Nusselt number: square duct	11
Figure 3.8 Comp	parison of fully developed velocity profile at different circumferential	
locat	tions: semi-circular duct	43
Figure 3.9 Comp	parison of $f_{app}Re$: equilateral triangular duct	45
Figure 3.10 (a - h) Dimensionless axial velocity profiles at $x^+=0.002$ and fully develope	d
	condition for different power law indices and various geometries	
		48
Figure 3.11 (a - d) Dimensionless maximum velocity for different power law indices ar	ıd
	various geometries, Re=500	51
Figure 3.12 (a - 1)	Product of apparent friction factor and Reynolds number $(f_{app}Re)$ ar	ıd
	incremental pressure drop $(K(x))$ vs. dimensionless axial distance for	Γ
	different power law indices and various geometries, Re=500	52
Figure 3.13 (a - c) Secondary flow for different power law indices at $x^{\dagger}=0.002$: circula	μΓ
~	tube (a)- $n=0.5$, (b)- $n=1.0$, (c)- $n=1.25$	58

Figure 3.14 (a - c)	Secondary flow for different power law indices at $x^{+}=0.002$: square
	duct (a)- $n=0.5$, (b)- $n=1.0$, (c)- $n=1.25$
Figure 3.15 (a - c)	Secondary flow for different power law indices at $x^{+}=0.002$: semi-
	circular duct (a)- $n=0.5$, (b)- $n=1.0$, (c)- $n=1.25$
Figure 3.16 (a - c)	Secondary flow for different power law indices at $x^{\dagger}=0.002$:
	equilateral triangular duct (a)- $n=0.5$, (b)- $n=1.0$, (c)- $n=1.25$
Figure 3.17 (a - x)	Nusselt number and dimensionless bulk temperature vs. dimensionless
	axial distance for different power law indices and various geometries,
	<i>Re=500, Pr=10</i>
Figure 3.18 (a - f)	Circumferential wall heat flux (T b.c.) and circumferential wall
•	temperature (H2 b.c.) for different power law indices and various
	geometries, Re=500, Pr=10
Chapter 4	
Figure 4.1 (a - h)	Effect of temperature-dependent viscosity on the velocity profile for
Figure 4.1 (a - h)	Effect of temperature-dependent viscosity on the velocity profile for different power law indices and various geometries. $Re=500$. $Pr=10$.
Figure 4.1 (a - h)	different power law indices and various geometries, $Re=500$, $Pr=10$.
	different power law indices and various geometries, Re=500, Pr=10.
	different power law indices and various geometries, Re=500, Pr=10. 76 Effect of temperature-dependent viscosity on the dimensionless
Figure 4.2 (a - h)	different power law indices and various geometries, $Re=500$, $Pr=10$. 76 Effect of temperature-dependent viscosity on the dimensionless maximum velocity for different geometries, $Re=500$, $Pr=10$ 78
Figure 4.2 (a - h)	different power law indices and various geometries, $Re=500$, $Pr=10$. 76 Effect of temperature-dependent viscosity on the dimensionless maximum velocity for different geometries, $Re=500$, $Pr=10$ 78 Effect of temperature-dependent viscosity on the apparent friction
Figure 4.2 (a - h) Figure 4.3 (a - h)	different power law indices and various geometries, $Re=500$, $Pr=10$. 76 Effect of temperature-dependent viscosity on the dimensionless maximum velocity for different geometries, $Re=500$, $Pr=10$ 78 Effect of temperature-dependent viscosity on the apparent friction factor for different geometries, $Re=500$, $Pr=10$ 80
Figure 4.2 (a - h) Figure 4.3 (a - h)	different power law indices and various geometries, $Re=500$, $Pr=10$. 76 Effect of temperature-dependent viscosity on the dimensionless maximum velocity for different geometries, $Re=500$, $Pr=10$
Figure 4.2 (a - h) Figure 4.3 (a - h) Figure 4.4 (a - h)	different power law indices and various geometries, $Re=500$, $Pr=10$. 76 Effect of temperature-dependent viscosity on the dimensionless maximum velocity for different geometries, $Re=500$, $Pr=10$ 78 Effect of temperature-dependent viscosity on the apparent friction factor for different geometries, $Re=500$, $Pr=10$ 80
Figure 4.2 (a - h) Figure 4.3 (a - h) Figure 4.4 (a - h)	different power law indices and various geometries, $Re=500$, $Pr=10$. 76 Effect of temperature-dependent viscosity on the dimensionless maximum velocity for different geometries, $Re=500$, $Pr=10$
Figure 4.2 (a - h) Figure 4.3 (a - h) Figure 4.4 (a - h) Figure 4.5 (a - h)	different power law indices and various geometries, $Re=500$, $Pr=10$. 76 Effect of temperature-dependent viscosity on the dimensionless maximum velocity for different geometries, $Re=500$, $Pr=10$
Figure 4.2 (a - h) Figure 4.3 (a - h) Figure 4.4 (a - h) Figure 4.5 (a - h)	different power law indices and various geometries, $Re=500$, $Pr=10$. 76 Effect of temperature-dependent viscosity on the dimensionless maximum velocity for different geometries, $Re=500$, $Pr=10$

Figure 4.7 (a - h)	Effect of viscous dissipation on thermal characteristics for T boundary
	condition for different geometries, Re=500, Pr=10, Br=-2.0 90
Figure 4.8 (a - h)	Simultaneous effects of temperature-dependent viscosity and viscous
	dissipation on Nusselt number and dimensionless bulk temperature for
	different geometries, $n=0.5$, $Re=500$, $Pr=10$
Figure 4.9 (a - b)	Heat transfer characteristics vs. X for T boundary condition for
	different Prandtl number, Re=500
Figure 4.10 (a - b)	Heat transfer characteristics vs. x^* for T boundary condition for
	different Prandtl number, Re=500
Figure 4.11 (a - b)	Heat transfer characteristics vs. X for H boundary condition for
	different Prandtl number, Re=500
Figure 4.12 (a - b)	Heat transfer characteristics vs. x for H boundary condition for
	different Prandtl number, Re=500
Figure 4.13 (a - h)	Effect of Prandtl number on Nusselt number and dimensionless bulk
	temperature for different geometries, Re=500
Chapter 5	
-	Effect of rounding corners of a square duct on the dimensionless
-	
Figure 5.1 (a - d)	Effect of rounding corners of a square duct on the dimensionless
Figure 5.1 (a - d)	Effect of rounding corners of a square duct on the dimensionless maximum velocity and apparent friction factor, Re=500
Figure 5.1 (a - d) Figure 5.2 (a - d)	Effect of rounding corners of a square duct on the dimensionless maximum velocity and apparent friction factor, $Re=500$
Figure 5.1 (a - d) Figure 5.2 (a - d)	Effect of rounding corners of a square duct on the dimensionless maximum velocity and apparent friction factor, $Re=500$
Figure 5.1 (a - d) Figure 5.2 (a - d) Figure 5.3 (a - d)	Effect of rounding corners of a square duct on the dimensionless maximum velocity and apparent friction factor, $Re=500$
Figure 5.1 (a - d) Figure 5.2 (a - d) Figure 5.3 (a - d)	Effect of rounding corners of a square duct on the dimensionless maximum velocity and apparent friction factor, $Re=500$
Figure 5.1 (a - d) Figure 5.2 (a - d) Figure 5.3 (a - d) Figure 5.4 (a - d)	Effect of rounding corners of a square duct on the dimensionless maximum velocity and apparent friction factor, $Re=500$
Figure 5.1 (a - d) Figure 5.2 (a - d) Figure 5.3 (a - d) Figure 5.4 (a - d)	Effect of rounding corners of a square duct on the dimensionless maximum velocity and apparent friction factor, $Re=500$
Figure 5.1 (a - d) Figure 5.2 (a - d) Figure 5.3 (a - d) Figure 5.4 (a - d) Figure 5.5 (a - d)	Effect of rounding corners of a square duct on the dimensionless maximum velocity and apparent friction factor, $Re=500$

Figure 5.7 (a - d)	Comparison of flow characteristics between the circular-sector and
	triangular ducts with the same apex angles, Re=500114
Figure 5.8 (a - d)	Comparison of Nusselt number between the circular-sector and
	triangular ducts with the same apex angles, Re=500
Figure 5.9 (a - d)	Effect of geometric parameter of cross-shaped duct on dimensionless
	maximum velocity and apparent friction factor, Re=500
Figure 5.10 (a - d)	Effect of geometric parameter of cross-snaped duct on the local
	Nusselt number distribution, Re=500
Chanter 6	
Chapter 6	
	developed values of f.Re and Nusselt number vs. cross-sectional factor

Figure 6.2 (a - c)	$f_{app}Re \text{ vs. } x^+ \text{ for different geometries at } Re=500 \text{ (a)- } n=0.5,$
•	(b)-n=1.0, (c)-n=1.25
Figure 6.3 (a - c)	Nu_T vs. x^* for different geometries at $Re=500$, $Pr=10$ (a)- $n=0.5$,
	(b)- n=1.0, (c)- n=1.25
Figure 6.4 (a - c)	Nu_{H2} vs. x° for different geometries at $Re=500$, $Pr=10$ (a)- $n=0.5$,
	(b)- n=1.0, (c)- n=1.25
Chapter 7	
Figure 7.1 Experi	imental apparatus 146
Figure 7.2 (a - b)	Shear stress vs. shear rate for partially neutralized Carbopol 934
	solutions neutralized to different levels151
Figure 7.3 (a - b)	Critical Reynolds number at different locations over duct cross-section
	(a)- semi-circular duct, (b)- equilateral triangular duct
Figure 7.4 (a - b)	Comparison of numerical and experimental results for $\Delta P'$
	(a)- semi-circular duct, (b)- equilateral triangular duct

Figure 7.5 (a - b)	Dimensionless pressure drop vs. dimensionless axial distance X for
	n=0.623 (a)- semi-circular duct, (b)- equilateral triangular duct
Figure 7.6 (a - b)	Dimensionless pressure drop vs. dimensionless axial distance X for
	n=0.727 (a)- semi-circular duct, (b)- equilateral triangular duct
Figure 7.7 (a - b)	Dimensionless pressure drop vs. dimensionless axial distance x^{+} for
	n=0.623 (a)- semi-circular duct, (b)- equilateral triangular duct
Figure 7.8 (a - b)	Dimensionless pressure drop vs. dimensionless axial distance x^+ for
	n=0.727 (a)- semi-circular duct, (b)- equilateral triangular duct
	bottom plate wall temperature vs. dimensionless axial distance X for
	circular and equilateral triangular ducts
_	tom plate Nusselt number vs. dimensionless axial distance X for semi-
	ular and equilateral triangular ducts
Figure 7.11 (a - d	Nusselt number vs. dimensionless axial distance x for different
	Reynolds and Rayleigh numbers for semi-circular and equilateral
Ph 710 (- 1)	triangular ducts
Figure 7.12 (a - b)	Comparison of the local Nusselt number distribution from numerical
	and experimental results $(n=0.623)$ (a)- semi-circular duct,
T' 510/	(b)- equilateral triangular duct
Figure 7.13 (a - c	l) Local Nusselt number vs. dimensionless axial distance x^* for
	different Rayleigh numbers 169
Appendix B	
Figure B1 (a - h)	Effect of temperature-dependent viscosity on Nusselt number and
	dimensionless bulk temperature, $n=1.0$. $Re=500$, $Pr=10$ B-1

4

 $\dot{\phi}$

Ç,

List of Figures

Figure B2 (a - h)	Effect of viscous dissipation on Nusselt number and dimensionless bulk
	temperature, n=1.0, Re=500, Pr=10
Figure B3 (a - h)	Simultaneous effects of temperature-dependent viscosity and viscous
	dissipation on Nusselt number and dimensionless bulk temperature,
	n=1.0, Re=500, Pr=10
Figure B4 (a - h)	Effect of Prandtl number on Nusselt number and dimensionless bulk
	temperature, n=1.0, Re=500, Pr=10 B-8

List of Tables

Chapter 1

Ü

5

Table 1.1	Summary of laminar fluid flow and / or heat transfer studies: circular tube 12
Table 1.2	Summary of laminar fluid flow and / or heat transfer studies: Rectangular
	ducts
Table 1.3	Summary of laminar fluid flow and / or heat transfer studies: circular-sector
	ducts
Table 1.4	Summary of laminar fluid flow and / or heat transfer studies: triangular ducts
Chapter	2
Table 2.1	Generated mesh for different geometries
Chapter	
Table 3.1	Comparison of the fully developed flow and heat transfer characteristics for
	circular tube: present study and other available results
Table 3.2	Comparison of the fully developed flow and heat transfer characteristics for
	•
	parallel plates: present study and other available results
Table 3.3	•
Table 3.3	parallel plates: present study and other available results
	parallel plates: present study and other available results
Table 3.4	parallel plates: present study and other available results

Table 3.6	Comparison of the fully developed flow and heat transfer characteristics for rectangular duct with A.R.=0.5: present study and other available results
Table 3.7	
	rectangular duct with A.R.=0.2: present study and other available results
	42
Table 3.8	Comparison of the fully developed flow and heat transfer characteristics for
	semi-circular duct: present study and other available results
Table 3.9	Comparison of the fully developed flow and heat transfer characteristics for
	circular-sector duct ($\alpha = 90^{\circ}$): present study and other available results 44
Table 3.10	Comparison of the fully developed flow and heat transfer characteristics for
	circular-sector duct ($\alpha = 60^{\circ}$): present study and other available results 44
Table 3.11	Comparison of the fully developed flow and heat transfer characteristics for
	equilateral triangular duct: present study and other available results 46
Table 3.12	Comparison of the fully developed flow and heat transfer characteristics for
	right isosceles triangular duct: present study and other available results 46
Table 3.13	Predicted fully developed flow and heat transfer characteristics for different
	power law indices and various duct geometries
Table 3.14	The locations of maximum velocity for different geometries
Table 3.15	$\frac{Nu_{H2}}{Nu_T}$ in the developing and fully developed regions for different geometries
	63
Chapter	5
Table 5.1	Comparison of flow and heat transfer characteristics for rounded corner square
	ducts for different power law indices
Table 5.2	Comparison of flow and heat transfer characteristics for rectangular ducts with
	different aspect ratio106

Table 5.3	Comparison of flow and heat transfer characteristics for circular-sector ducts
	with different apex angles
Table 5.4	Comparison of flow and heat transfer characteristics between circular-sector
	and triangular ducts with the same apex angles
Table 5.5	Comparison of flow and heat transfer characteristics for cross-shaped ducts
	with different geometric parameters
Chapter	• 6
Table 6.1	Fluid flow characteristics for different power law indices and various geometric
	configurations for fully developed conditions
Table 6.2	Nusselt number for different power law indices and various geometric
	configurations for fully developed conditions
Table 6.3	Cross-sectional factor for various duct geometries
Table 6.4	$\frac{Nu}{f.Re}$ for various power law indices and duct geometries for fully developed
	condition, constant property fluids
Appendi	ix A
Table A.1	through A.12 $f_{app}Re$ and U_{max} for different power law indices and different
	axial locations: various duct geometries A-1 - A-7
Table A.1	3 through A.24 $Nu_{T,x}$ and $Nu_{H2,x}$ for different power law indices and different
	axial distances, $Re=500$, $Pr=10$: various duct geometries
	A-8 - A-14
Append	ix B
Table B1	through B4 $f_{app}Re$ and U_{max} for T and H2 boundary conditions for different
	values of B: various duct geometries

Table B5 t	hrough B8	$Nu_{T,x}$ and $Nu_{H2,x}$ for specific values of B and Br: various	s duct
		geometries	B-12 - B-13
Table B9 t	through B12	$Nu_{T,x}$ and $Nu_{H2,x}$ for $Pr=1.0$: various duct geometries	
			B-14 - B-15
	مار مار		****
Appendi	x C	·	
Table C1 through C12 $Nu_{T,m}$ and $Nu_{H2,m}$ for different power law indices and different		different	
		axial locations: various duct geometries	C-1 - C-7
Appendi	x D		
11ppcnu-			
Table D1	Consistency	index of Carbopol 934 solutions ($n=0.623$ for solution	n # 1 and
	n=0.727 for	r solution # 2)	D-4
Table D2	Uncertainty	for different parameters	D- 6
Table D3	Experimenta	al results	D-7 - D-15

Nomenclature

ls

$$A_c$$
 Cross-sectional area

$$A_T$$
 Cross-sectional area of the foil at temperature T

Brinkman number
$$(=\frac{k_o u_e^{n+1}}{D_h^{n-1}(T_e - T_w)K})$$
 for T and

$$= \frac{k_o u_e^{n+1}}{D_h^n q} \text{ for H2 boundary conditions)}$$

$$D_h$$
 Hydraulic diameter (= $\frac{4A_c}{p'}$)

ಡ್ಲು_{ಡಿಸಿದರ}

f	Friction factor $(=\frac{\tau_w}{\frac{1}{2}\rho u_e^2})$
f_{app}	Apparent friction factor
f(T)	Temperature dependence function of the consistency index
	defined by equation 2.10
$F(\theta)$	Dimensionless temperature dependence function of the
	consistency index defined by equation 2.20
F	Defined by equation 2.19
g	Gravity acceleration
\boldsymbol{G}	Defined by equation 2.19
Gr	Grashof number $Gr = \frac{\rho^2 D_h^{2n+2} \beta q'' g u_e^{2-2n}}{k_o^2 K}$ for H2 boundary
	condition
h_x	Local heat transfer coefficient, defined by equation 2.29
H	Defined by equation 2.19
H b.c.	Constant heat flux boundary condition for circular tube and
	parallel plates
H2 b.c.	Constant wall heat flux both axially and peripherally
HI b.c.	Constant wall heat flux axially and constant wall temperature
	peripherally
H2(1) b.c.	Constant heat flux (H2) at one wall while other walls are insulated
H1(1) b.c.	Constant heat flux (H1) at one wall while other walls are insulated
I	Electrical current
K	Thermal conductivity
k	Consistency index at temperature T
k_o	Consistency index at reference temperature
K(x)	Incremental pressure drop, defined by equation 2.26

:==:

O

$K(\infty)$	Dimensionless incremental pressure drop, defined by
	equation 2.27
1	Hydrodynamic entrance length
ľ	Peripheral distance
L	Dimensionless hydrodynamic entrance length (= $\frac{l}{D_h}$)
$\overline{\mathcal{L}}$	Length of the channel
L'	Dimensionless peripheral distance $(\frac{l'}{D_h})$
$L^{\!\scriptscriptstyle +}$	Dimensionless hydrodynamic entrance length (= $\frac{l}{D_h Re}$)
$\overline{L}_{\!\scriptscriptstyle T}$	Length of the foil at temperature T
$\overline{L}_{\!\scriptscriptstyle R}$	Length of the foil at temperature T_R
m ⁱ	Mass flow rate
n	Power law index
N	Dimensionless normal distance
$Nu_{b,x}$	Local Nusslet number based on bottom plate for H2
	boundary condition
Nu_{H2}	Fully developed Nusselt number for H2 boundary condition
Nu_l	Nusselt number based on the temperature difference
	between the wall and the inlet fluid
Nu _m	Mean Nusselt number $(=\frac{1}{X}\int_0^X Nu_x dX)$
Nu_T	Fully developed Nusselt number for T boundary condition

$$Nu_x$$
 Local Nusselt number ($Nu_x = \frac{\left(\frac{\partial \theta}{\partial N}\right)_{w,m}}{\theta_{w,m} - \theta_{b,x}}$ for H2 and

$$Nu_x = \frac{\left(\frac{\partial \theta}{\partial N}\right)_{w,m}}{\theta_{b,x}}$$
 for T boundary conditions)

P Dimensionless pressure (=
$$\frac{p - \rho gz}{\rho u_{\bullet}^2}$$
)

$$\overline{P}$$
 Pumping power, defined by equation 6.7

$$\Delta p$$
 Axial pressure drop

$$\Delta P'$$
 Axial dimensionless pressure drop $(=\frac{\Delta p}{\frac{1}{2}\rho u_e^2})$

Pe Peclet number (=
$$\frac{\rho C_p u_e D_h}{K}$$
)

Pr Prandtl number
$$(=\frac{k_o C_p \left(\frac{u_o}{D_h}\right)^{n-1}}{K})$$

Q Dimensionless wall heat flux
$$(=\frac{qD_h}{K(T_w - T_e)})$$
 for T and $=\frac{q}{q_w}$ for H2 boundary conditions)

$$\overline{Q}$$
 Total energy generated electrically within the foil

$$\overline{Q}_x$$
 The heat supplied electrically from the beginning of the

R	Radius of the channel
\overline{R}	Electrical resistance
$\overline{R}_{\!\scriptscriptstyle R}$	Electrical resistance at temperature T_R
\overline{R}_{T}	Electrical resistance at temperature T
r'	Dimensionless radial coordinate (= $\frac{r}{D_h}$)
Ra	Rayleigh number (=Gr.Pr)
R.C.	Rounded corner radius of square duct
Re	Reynolds number $(=\frac{\rho u_e^{2-n}D_h^n}{k_o})$
Recrit	Critical Reynolds number
T :-	Temperature
t_f	time
T b.c.	Isothermal wall condition
T(1) b.c.	Constant temperature at one wall while other walls are insulated
Tw_{x}	Mean bottom plate temperature at specific axial location, x
u	Axial velocity
u_i	Relative uncertainty for measured quantity i
U	Dimensionless axial velocity (= $\frac{u}{u_e}$)
U_f	Dimensionless axial velocity at fully developed condition
$U_{ extit{max}}$	Dimensionless maximum velocity
ν	Velocity in y direction
V	Dimensionless velocity in y direction (= $\frac{v}{u_e}$)
V'	Volume of the channel
w	Velocity in z direction
W	Dimensionless velocity in z direction (= $\frac{w}{t}$)

ij

9

43

x Axial distance

X Dimensionless axial distance (= $\frac{x}{D_{h}}$)

 ΔX Dimensionless distance between two axial locations

 x^{+} Dimensionless axial coordinate (= $\frac{x}{D_{L}Re}$)

 x^* Dimensionless axial coordinate (= $\frac{x}{D_1 Pe}$)

y Transverse distance

Y Dimensionless transverse distance (= $\frac{y}{D_h}$)

z Transverse distance

Z Dimensionless transverse distance (= $\frac{z}{D_h}$)

Greek symbols

α Apex angle

 α_L Temperature coefficient of the expansion of the length

 α_R' Temperature coefficient of electrical resistance

 α'_{p} Temperature coefficient of electrical resistivity

β Circumferential angle from the bottom plate and from the

origin of the channel

 β Volume expansion of the fluid

β' Surface compactness, defined by equation 6.6

ý Shear rate

Δ Rate of deformation tensor in Cartesian coordinates defined

by equation 2.7

θ	Dimensionless temperature (= $\frac{T - T_w}{T_e - T_w}$ for T and = $\frac{T - T_e}{\frac{qD_h}{K}}$
	for H2 boundary conditions)
$\theta_{b,x}$	Dimensionless bulk temperature evaluated at x axial
	position
λ	Geometric parameter of cross-shape channel
μ	Viscosity of the Newtonian fluid
п	Defined by equation 2.19
ρ	Density
ρ_T	Electrical resistivity at temperature T
τ	Shear stress tensor
$ au_{w}$	Wall shear stress

Subscripts

b	Evaluated at bulk condition
b,x	Evaluated at bulk temperature and at local x position
e	Evaluated at inlet condition
fd	Fully developed condition
H2,x	Evaluated at local x position for H2 boundary condition
H2,m	Mean value for H2 boundary condition
m	Mean value
P.P	Refers to parallel plate channel
R.T	Refers to right isosceles triangular channel
T,x	Evaluated at local x position for T boundary condition
<i>T</i> , <i>m</i>	Mean value for T boundary condition
x	Evaluated at local x position
y	Evaluated at local y position

Nomenclature

z	Evaluated at local z position
w	Evaluated at wall condition
w,m	Mean value evaluated at wall condition
w,x	Evaluated at wall condition and local x position

Chapter 1

Introduction and Background

1.1 Introduction

Thermal processing of highly viscous non-Newtonian fluids is encountered in several industrial sectors, e.g. chemical, petrochemical, polymer, foods etc. For reliable design and optimization of such process equipment it is essential to have information on the heat transfer rates for such liquids flowing through channels. Since liquids of interest are often very viscous, if the hydraulic diameter of the flow passage is small the flow is laminar. Also, a large class of such liquids display negligible elasticity at least over the flow ranges of interest. Thus it is of practical interest to study the laminar heat transfer characteristics of purely viscous non-Newtonian fluids flowing in straight ducts.

Much of earlier studies in this area have focused on flows through circular tubes, rectangular channels and between infinitely large parallel plates. This thesis research was designed to examine at a fundamental level the simultaneously developing laminar flow and heat transfer of purely viscous non-Newtonian fluids (described by the well known power law model) flowing in straight channels of various uniform non-circular cross-sections. The prime objective was to make a comparative evaluation of many different geometries and include cocurrently the effects of such additional parameters as: temperature-dependent apparent viscosity, viscous dissipation, Prandtl number as well as two commonly employed thermal boundary conditions viz. uniform wall temperature and uniform wall heat flux.

Details of the flow and thermal fields were studied numerically using the finite element technique to solve the governing conservation equations of mass, momentum and energy along with the power law model constitutive equation and appropriate boundary conditions. Fourteen different cross-sectional geometries were examined numerically and two were selected for experimental validation.

Since little information exists on the critical Reynolds numbers for non-circular ducts, flow visualization experiments were conducted to measure the Reynolds number at which the laminar flow suffered transition. This information gives the upper limit on the applicability of the laminar flow model. Also, an experimental facility was developed to measure the pressure drop and local Nusselt number distribution for the entrance flow of viscous non-Newtonian fluids through two non-circular straight ducts. A semi-circular and an equilateral triangular channels were used as test cases for the experimental part of this thesis work. Experimental results are compared with the numerical simulation results.

This thesis is divided into eight chapters. This chapter is followed by objectives and scope of the thesis as well as a brief literature review. Chapter 2 covers the mathematical model used for numerical solution and also the basic definitions. Governing equations in dimensionless form and boundary conditions are presented. Description on the mesh generation for different geometries and the numerical solution are also presented. In the third chapter the effects of power law index on fluid flow and heat transfer characteristics are examined. The results cover both isothermal wall and constant wall heat flux boundary conditions.

Chapter 4 covers the effects of temperature dependent viscosity, viscous dissipation, the simultaneous effects of temperature dependent viscosity and viscous dissipation, and Prandtl number on flow and heat transfer performance. Miscellaneous effects such as: effects of rounding of the corners of a square duct, aspect ratio of rectangular ducts, apex angle of circular sector channels and a specially defined geometric parameter of a cross-shape channels on fluid flow and heat transfer characteristics are presented in Chapter 5. Chapter 6 presents the effects of geometry on friction factor and

Nusselt number distribution. Several criteria are defined and calculated for different duct geometries to compare their thermal performance.

Chapter 7 is devoted to the experimental study. A description of the experimental apparatus is given along with the experimental methodology. Data on the critical Reynolds number for semi-circular and equilateral triangular ducts are presented. Nusselt number measurements for distilled water experiments include the effect of the Rayleigh number. Also, for viscous non-Newtonian fluids, pressure drop and heat transfer results are presented and compared with numerical results.

Chapter 8 includes a summary of the major conclusions of this study and also some recommendations for future research.

1.2 Objectives and scope

S

The prime objectives of this study were:

- (a)- To develop finite element simulation results for simultaneously developing laminar flow and heat transfer to purely viscous non-Newtonian fluids described by power law model. The governing conservation equations subjected to selected boundary conditions were solved using the FIDAP solver upon appropriate mesh generation and discretization procedures. Effects of temperature-dependent viscosity, viscous dissipation as well as Prandtl number are included in the model.
- (b)- To apply the finite element solver to fourteen different duct geometries of current and potential practical interest and evaluate the results by comparison with existing literature where possible.
- (c)- To investigate on the effects of rounding the corners of a square duct, aspect ratio for rectangular channels, apex angles of circular sector ducts and the geometric parameter of cross-shape channels on fluid flow and heat transfer characteristics.
- (d)- To develop an experimental test apparatus to measure the critical Reynolds numbers and to measure the pressure drop and local Nusslet number distribution in the entrance region of a semi-circular and an equilateral triangular ducts.

1.3 Background

The present review focuses only on fluid flow and heat transfer through straight, uniform and singly connected ducts of different cross-sections. Only steady, incompressible, and laminar flows are considered.

For Newtonian fluids, Shah and London (1978) and Shah and Bhatti (1987) have published excellent reviews on laminar flow and heat transfer through the ducts of circular and non-circular cross sections. In these reviews different conditions of flow and thermal development are considered. Literature on laminar forced convection of Newtonian fluids in the combined entry region of ducts has been reviewed by Kakac and Yener (1983). The fully developed flow and heat transfer characteristics of various channels were discussed by Shah (1983a).

Fluid flow and heat transfer problems involving non-Newtonian fluids have been reviewed by Metzner (1965), Skelland (1967), Cho and Hartnett (1985) and Irvine Jr. and Karni (1987). An extensive literature review has been published by Lawal and Mujumdar (1989b) which deals with non-Newtonian fluids flowing in non-circular ducts; they included studies on temperature-dependent viscosity and viscous dissipation effects.

Studies dealing with simultaneously developing flow and heat transfer are cited in the following sections. Relevant published works under different flow and thermal development conditions are tabulated in Tables 1.1 through 1.4. Some of these works are referred to and interpreted in the results and discussion chapters of this thesis. Studies discussed in Shah and London (1978) are noticited here except when they are directly compared with the results of this study.

1.3.1 Circular tubes

Simultaneously developing flow and heat transfer for Newtonian fluids flowing in circular tubes was considered numerically by Kays (1955) for constant wall temperature (T) and constant heat flux (H) conditions and Pr=0.7. He employed a finite difference technique ignoring the radial velocity component as well as axial conduction in the energy

equation. A finite difference method also was used by Hornbeck (1965) with linearization of the momentum equation. This investigation was for T and H boundary conditions and for Pr=0.7, 2, and 5.

Jensen (1989) employed a control volume finite difference method to obtain accurate results for the isothermal wall boundary condition and for various Prandtl numbers. In this study very fine grids were used close to the entrance of the channel. Local and mean Nusselt numbers were presented over a wide range of Pr (0.01 - 50). Simultaneous development of flow and heat transfer was investigated by Pagliarine (1989) using the finite element method. He computed the local Nusselt number distribution in a circular tube for Prandtl numbers ranging from 0.1 to 100 and Peclet numbers from 5 to 500.

Huhn (1992) has correlated the data of various investigators and developed an empirical correlation for the entrance Nusselt number in circular, rectangular, triangular, and concentric annular ducts as well as parallel plates. He published an equation which relates the entrance region Nusselt number to the fully developed Nusselt number through coefficients, which depend on the boundary conditions as well as the duct geometry. Al-Ali and Selim (1992) presented an integral boundary layer solution for the case of constant heat flux for different Prandtl number fluids. Their results were in close agreement with the predictions of Hornbeck (1965). They tabulated thermal entrance length and Nusselt number results for different Prandtl numbers. Also, Shome and Jensen (1993) employed the control volume finite difference technique for the general convective boundary condition which in special cases become T and H boundary conditions. They used fine grids close to the entrance and employed different Prandtl numbers for both T and H boundary conditions. Their results cover Prandt numbers from 0 to ∞; here the∞ case is the same as the hydrodynamically developed and thermally developing condition. They developed a correlation for the product of the apparent friction factor and Reynolds number and also the local Nusselt number and thermal entrance length. Nguyen (1993) considered the combined entry length problem for a circular duct using finite difference methods for T and H boundary conditions but presented local Nusselt number results only

for Pr=0.7. He tabulated local Nusselt number for both boundary conditions and also presented correlations for the hydrodynamic and thermal entrance lengths over I < Re < 1000.

The problem of simultaneously developing flow and heat transfer to viscous non-Newtonian fluids was solved by McKillop (1964) using a boundary layer solution near the entrance and a perturbation solution farther downstream. The results of McKillop (1964) for Newtonian fluids are in very good agreement with those obtained by Kays (1955). He tabulated the local Nusselt number for different power law indices and various Prandtl numbers for both T and H boundary conditions. In a subsequent work McKillop et al. (1970) included temperature-dependent viscosity in their analysis of the same problem.

Victor and Shah (1976), Lin (1977), and Lin and Shah (1978) employed a control volume finite difference method with a forward marching procedure to obtain numerical solution for yield power law fluids flowing in tubes. The solution of the energy equation was obtained for two boundary conditions (T and H). The results of Lin (1977) cover the fully developed and entrance Nusselt numbers for different power law indices and various yield numbers.

Heat transfer to a Bingham plastic fluid flowing through a circular tube was investigated by Samant and Marner (1971) and more recently by Vradis et al. (1993). Vradis et al. (1993) employed a finite difference method and presented friction factor and local Nusselt number results for the T boundary condition and different yield, Prandtl, and Brinkman numbers.

The effects of viscous dissipation were investigated numerically by Lawal (1985), Lawal and Mujumdar (1989a and 1992). They employed the control volume finite difference technique, marching method and an orthogonal coordinate transformation technique to transform the physical space into a new computational space wherein the physical boundaries coincide with the transformed boundaries. Their results covered different values of the power law indices for the T boundary condition but only for Pr=0.1. The scope of their work was limited by available computing power and facilities.

100

...

Later Lawal (1989) considered mixed convection heat transfer for power law fluids in circular ducts.

Recently Isazadeh (1993) developed a control volume based finite difference code to compute the laminar heat and mass transfer in flows with reactions, for tubes of arbitrary cross section. However, his results do not cover the range of interest in this study and hence could not be compared with directly.

1.3.2 Rectangular cross-sectional ducts

In a comprehensive and elegant review Hartnett and Kostic (1989) have summarized the numerous investigations of fluid flow and heat transfer to Newtonian and non-Newtonian fluids flowing through rectangular ducts and between parallel plates. Only selected studies will be cited in this section.

1.3.2.1 Parallel plates

5

Hwang and Fan (1964) used a finite difference method to obtain velocity distributions for a Newtonian flow and numerically integrated the energy equation for both T and H boundary conditions. These results were given by Shah and London (1978) and were later claimed by Shah and Bhatti (1987) to be more accurate than other results available in the literature. Mercer et al. (1967) also used a finite difference solution for T and T(1) (isothermal condition at one wall while another wall is insulated) boundary conditions with Pr=0.7. They also investigated experimentally using interferometer measurements for the same conditions as used in their numerical work and reported good agreement between the two. They also proposed a correlation for the mean Nusselt number.

The problem of combined entrance region heat transfer was investigated analytically by Rostami and Mortazavi (1990) assuming a linear profile for the axial component of the velocity and solving the energy equation by the similarity method. They obtained a closed form expression for the Nusselt number as a function of x^* and the

Prandtl number. This method is less applicable for low Prandt number, because the assumption of a linear velocity profile in the thermal boundary layer introduces significant error. This problem for the T and H boundary conditions was solved numerically by Nguyen (1991) and Nguyen and Maclaine-Cross (1991). The results of Nguyen (1991) are valid for Pr=0.7 and Reynolds number between 1 and 20 while the results of Nguyen and Maclaine-Cross (1991) cover for Pr=0.2 to 100 and Re=40 to 2000. Nguyen (1991) proposed correlations for the incremental pressure drop and heat transfer and also the hydrodynamic and thermal entrance lengths. The results of Nguyen and Maclaine-Cross (1991) are in good agreement with those of Hwang and Fan (1964).

Campos Silva et al. (1992) employed a linearization procedure to solve the flow problem in the developing flow region. They solved the decoupled energy equation using a generalized integral transform technique. Results were given for the isothermal wall condition, and for Pr=0.72 and 10.

For purely viscous non-Newtonian fluids Yau and Tien (1963) employed the momentum and energy integral method of von Kármán and Pohlhausen to solve the laminar entrance heat transfer problem for the T boundary condition. As noted by Hartnett and Kostic (1989) their Nusselt number predictions appear to be in error when recalculated on the basis of local Nusselt number versus x^* with Prandtl number as a parameter. The numerical finite difference and marching method was used by Lin (1977) and Lin and Shah (1978) for T and H boundary conditions which cover a wide range of power law index and yield number values.

Klemp et al. (1992) applied a finite difference method to account for the temperature-dependent viscosity variation of purely viscous non-Newtonian fluids subjected to the H boundary condition. They presented results for both Reynolds and Peclet numbers equal to 1. Recently Etemad et al (1994) solved the simultaneously developing thermal entry problem using the Galerkin finite element technique for viscous non-Newtonian fluids flowing through parallel plates subjected to four different thermal boundary conditions; T, T(1), H and H(1). They presented results which include the effects of power law index, temperature-dependent viscosity, viscous dissipation,

Ñ

مرتني

simultaneous effects of temperature-dependent viscosity and viscous dissipation, and Prandtl number on the entrance Nusselt number distribution.

1.3.2.2 Other rectangular ducts

1

Wibulswas (1966), and Montgomery and Wibulswas (1967) investigated the combined entry problem for rectangular ducts of different aspect ratios. They employed a numerical finite difference method for T and H1 boundary conditions for Newtonian fluids. They specified the transverse velocity components to be zero and neglected both axial momentum and thermal diffusion terms. Wibulswas (1966) also presented experimental work for air flowing through a rectangular duct of $I'' \times 2''$ cross section for the H1 boundary condition. Based on the results of Montgomery and Wibulswas (1967), Shah and London (1978) calculated the thermal entrance length for the H1 boundary condition and found that this parameter decreases with decreasing aspect ratio.

Simultaneously developing steady laminar flow and heat transfer to Newtonian fluids flowing through square cross section ducts was considered by Neti and Eichhorn (1983) and Asako and Faghri (1988) using a control volume finite difference method and a marching technique for solution. Neti and Eichhorn (1983) presented results for the T boundary condition for Pr=6. The study of Asako and Faghri (1988) is related to rhombic ducts which square duct was as a special case.

Abou-Ellail and Morcos (1983), Incropera and Schutt (1985), and Mahaney et al. (1988) employed the control volume finite difference method to solve the mixed convection heat transfer in the entrance region of a rectangular duct. Incropera et al. (1987) considered experimentally mixed convection in a rectangular duct with aspect ratios of 0.1 and 0.2 when the bottom plate was heated by direct current. They used dye injection to visualize the fluid flow and measure Grashof and Reynolds numbers for transition from laminar to turbulence due to the buoyancy-driven secondary flow.

For viscous non-Newtonian fluids Chandrupatla (1977) employed a finite difference technique and marching method to solve the governing equations for the T, H1,

and H2 boundary conditions at various power law indices (only pseudoplastic fluid) and Prandtl numbers. Lawal (1985), Lawal and Mujumdar (1984, 1985, 1989a and 1992) considered the combined entry region of Newtonian and viscous non-Newtonian fluids flowing through a square duct using a control volume finite difference method. The work of Lawal (1985) and Lawal and Mujumdar (1989a and 1992) also were included the effect of viscous dissipation for Pr=0.1. Lawal (1989) has presented some numerical results on mixed convection heat transfer in a square duct.

Hartnett and Kostic (1981) studied experimentally the entrance non-Newtonian flow and heat transfer distribution in a rectangular duct with aspect ratio of 0.5. They heated the bottom and top stainless steel plates of the channel electrically while other walls were insulated. They reported local Nusselt number distribution for different Reynolds and Rayleigh numbers. Recently Shin and Cho (1994) considered numerically the heat transfer through a rectangular channel with aspect ratio of 0.5 when top plate was heated while other sides were insulated. They considered viscous non-Newtonian fluids and temperature-dependent apparent viscosity and proposed a correlation for the apparent friction factor and local Nusselt number.

1.3.3 Circular-sector ducts

There is no published work on simultaneously developing of flow and heat transfer to Newtonian and viscous non-Newtonian fluids flowing through circular-sector ducts.

1.3.4 Triangular ducts

Simultaneously developing steady laminar flow and heat transfer of Newtonian and viscous non-Newtonian fluid for the T boundary condition was considered by Lawal (1985) and Lawal and Mujumdar (1984, 1985, 1989a and 1992). The results of Lawal (1985) include the effects of variable viscosity and viscous dissipation for Pr=0.1 and Re=1000.

1.3.5 Summary of various studies

Tables 1 through 4 contain a listing of various published investigations on steady laminar channel flow and heat transfer. The following symbols and abbreviations are used in these tables in the interest of conciseness:

*1	Hydrodynamically and thermally fully developed
*2	Hydrodynamically developing flow
*3	Hydrodynamically fully developed and thermally developing
*4	Simultaneously developing flow and heat transfer
*A	Temperature-dependent viscosity
*B	Viscous dissipation
*N	Natural convection
T	Isothermal wall condition
T(1)	Constant temperature at one wall while other walls are insulated
H2	Constant wall heat flux both axially and peripherally
H1	Constant wall heat flux axially and constant wall temperature peripherally
H2(1)	Constant heat flux (H2) at one wall while other walls are insulated
H1(1)	Constant heat flux (H1) at one wall while other walls are insulated
Hv	Wall heat flux varies circumfrentially
F.D.M.	Finite difference method
C.V.F.D.M.	Control volume finite difference method
F.E.M.	Finite element method
Int.	Integral method
Exp.	Experimental study
N	Newtonian fluid
V.N.	Viscous non-Newtonian fluid
B.P.	Bingham plastic fluid
VE	Viscoelastic fluid

Table 1.1 Summary of laminar fluid flow and / or heat transfer studies: circular tube.

References	Studied fluid	Description
Kays (1955)	N N	T, H, *4, F.D.M.
Powlek & Tien (1964)	V.N.	T, *4, Int.
McKillop (1964)	V.N.	T, H, *4, Int.
Hornbeck (1965)	N	T, H, *4, F.D.M.
McKillop et al. (1970)	V.N.	T, *4, *A, Int.
Samant & Marner (1971)	<i>B.P.</i>	T, *4, Int.
Lin (1977)	V.N.	T, H, *4, C.V.F.D.M.
Lin & Shah (1978)	V.N.	T, H, *4, C.V.F.D.M.
Joshi & Bergles (1980)	V.N.	Н, *3, Ехр.
Filkova et al. (1987)	V.N.	Н, *4, Ехр.
Conley et al. (1985)	N	T, *3, C.V.F.D.
Lawal (1985)	V.N.	T, *4,*A, *B, C.V.F.D.M.
Prikh & Mahalingam (1988)	<i>V.N</i> .	H, Hv, *1, Superposition
Pagliarini (1989)	N	T, H, *4, F.E.M.
Mansour (1989)	V.N.	T, *3, Laplace transformation
Poirier & Mujumdar (1989)	N	T, *3, F.D.M.
Jensen (1989)	N	T, *4, C.V.F.D.M.
Lawal & Mujumdar (1989a)	<i>V.N</i> .	T, *4, *B, C.V.F.D.M.
Salazar & Campo (1990)	N	T, H, *3, Separation of variables
Flores et al. (1991)	V.N.	T, *3, *B, Laplace transformation

Table 1.1 (Continued)

Lawal & Mujumdar (1992)	V.N.	T, *4, *B, C.V.F.D.M.
Nguyen (1992)	N	T, H, *3, F.D.M.
Al-Ali & Selim (1992)	N	H, *4, Int.
Nguyen (1993)	N	T, H, *4, F.D.M.
Shome & Jensen (1993)	N	T, H, *4, C.V.F.D.M.
Vradis et al. (1993)	B.P.	T, *4, *B, F.D.M.
Isazadeh (1993)	V.N.	T, *4, C.V.F.D.M.
Prusa & Manglik (1994)	V.N.	T, *3, *1, F.D.M.
Weber (1995)	<i>N</i>	H,*1

Table 1.2 Summary of laminar fluid flow and / or heat transfer studies: Rectangular ducts.

References	Studied Fluid	Aspect Ratio	Description
Siegel & Sparrow (1959)	N	0	H, *4, Int.
Bodoia & Osterle (1961)	N	0	*2, F.D.M.
Yau & Tien (1963)	V.N.	o	T, *4, Int.
Hwang & Fan (1964)	N	o	T, H, *4, F.D.M.
Mercer et al. (1967)	N	о .	T, T(1), *4, F.D.M., Exp.
Montgomery & Wibulswas (1967)	N	0.167 - 1.0	T, H1, *4, F.D.M.
Shah (1975)	N	0 - 1.0	T, H1, H2, Least square method
Natio (1975)	N	0	H, H(1), *4, Int.

Table 1.2 (Continued)

Bhatti and Savery (1977)	N	0	H, *4, Int.
Lin (1977)	V.N.	0	T, H, C.V.F.D.M.
Chandrupatla (1977)	V.N.	1:0	T, H1, H2, *4, F.D.M.
Chandrupatla & Sastri (1977)	V.N.	1.0	T, H1, H2, *3, F.D.M.
Lin & Shah (1978)	V.N.	0	T, H, C.V.F.D.M.
Abou-Ellail & Morcos (1983)	N	0.25, 1.0	H2, *4, *N, C.V.F.D.M.
Neti & Eichhorn (1983)	N	1.0	T, *4, C.V.F.D.M.
Lawal & Mujumdar (1984)	<i>V.N</i> .	1.0	T, *4, *A, C.V.F.D.M.
Incropera & Schutt (1985)	N	0.5	H2(1), *4, *N, C.V.F.D.M.
Lawal (1985)	V.N.	1.0	T, *4, *A, *B, C.V.F.D.M.
Lawal & Mujumdar (1985)	V.N.	1.0	T, *4, C.V.F.D.M.
Hartnett & Kostic (1985)	VE	0.5	H1, *4, Exp.
Natio (1985)	N	0	H, H2(1), *4, F.D.M.
Mahaney et al. (1987)	N	0.5	H2(1), *4, C.V.F.D.M.
Incropera et al. (1987)	N	0.1, 0.2	H(1), *4, Exp.
Mahaney et al. (1988)	N	0.5	H2(1), *4, C.V.F.D.M.
Asako & Faghri (1988)	N	1.0	T, H1, *4, C.V.F.D.M.
Nonino et al. (1988)	N	1.0	T, H2, *4, F.E.M.
Lawal & Mujumdar (1989a)	<i>V.N</i> .	1.0	T, *4, *B, C.V.F.D.M.
Rostami & Mortazavi (1990)	N.	0	T, *4, Similarity solution

Table 1.2 (Continued)

Aparecido and Cotto (1990)	N	0.1 - 1.0	T, *3, Int.
Nguyen (1991)	N	o	T, H, *4, F.D.M.
Nguyen & Maclaine-Cross (1991)	N	0	T, H, *4, F.D.M.
Yang & Camarero (1991)	N	1.0	*2, F.D.M.
Campos Silva et. al. (1992)	N	0	T, *4, Int.
Lawal & Mujumdar (1992)	V.N.	1.0	T, *4, *B, C.V.F.D.M.
Klemp et al. (1992)	V.N.	О	H, *A, *4, F.D.M.
Xie & Hatnett (1992)	N	0.5	H1, *4, *A, Exp.
Gao & Hartnett (1992)	V.N.	0.2 - 1.0	T, H1, H2, *1, F.D.M.
Isazadeh (1993)	V.N.	0.5,0.66,1.0	T, *4, C.V.F.D.M.
Shin & Cho (1994)	V.N.	0.65	H1, *4,*3, *A, C.V.F.D.M.
Etemad et al. (1994)	V.N.	o	, T(1), H, H2(1), *4, *A, *B, F.E.M

Table 1.3 Summary of laminar fluid flow and / or heat transfer studies: Circular-sector ducts.

References	Studied Fluid	Apex Angle	Description
Hong & Bergles (1976)	. N	180°	H1, H1(1), *3, F.D.M.
Soliman et al. (1982)	N	5.6° - 45°	*2, F.D.M.
Trupp & Lau (1984)	N	8°-180°	T, H1, *1, F.D.M.
Manglik & Bergles (1988)	N	180°	T, T(1), *3, F.D.M.

Table 1.3 (Continued)

Lei & Trupp (1989a)	N	0°-360°	*1, Fourier transformation
Lei & Trupp (1989b)	N	0°-360°	H1, *1, Fourier transformation
Trup & Lei (1989)	N	0°-360°	H2, *1, Fourier transformation
Ben-Ali et al. (1989)	N	5°-350°	T, H1, H2, *1, F.D.M.
Lei & Trupp (1990)	N	20°-360°	H1, H2, *3, C.V.F.D.M.
Lei (1990)	N	0°-360°	T, H1, H2, *1, *3, Fourier transformation, C.V.F.D.M., Exp.
Lei & Trupp (1991)	N	180°	H1, *3, Exp.
Manglik and Bergles (1987)	N	180°	T, *3

Table 1.4 Summary of laminar fluid flow and / or heat transfer studies: Triangular ducts.

References	Studied Fluid	Apex Angle	Description
Wibulswas (1966)	·N	60°, 90°	T, H1, *4, F.D.M.
Shah (1975)	N	0°-180°	T, H1, H2, Least square method
Schneider & LeDain (1981)	N	10°-120°	T, H1, H2, *I, F.E.M.
Lawal (1985)	<i>V.N</i> .	60°	T, *4, *A, *B, C.V.F.D.M.
Lawal & Mujumdar (1989a)	V.N.	60°	T, *4, *B, C.V.F.D.M.
Isazadeh (1993)	V.N.	60°	T, *4, C.V.F.D.M.
Lakshminarayana & Haji-Sheikh (1992)	N	2.5°-170°	T, *3, Integral method
Lawai & Mujumdar (1992)	V.N.	60°	T, *4, *B, C.V.F.D.M.

Chapter 2

Mathematical Model

This chapter is concerned with the formulation of the mathematical model for simultaneously developing steady laminar flow and heat transfer in a straight duct of arbitrary but uniform cross-section. The governing equations of continuity, momentum, energy as well as the pertinent boundary conditions are given. Finally the computational procedure to solve these equations is described briefly.

2.1 Governing equations

The flow and heat transfer characteristics of fluids in various geometric domains are obtained theoretically by solving either analytically or numerically the conservation equations of mass, momentum and energy subjected to appropriate boundary conditions.

The equations for continuity, momentum, and energy for steady state and constant density conditions in rectangular coordinates are:

Continuity:
$$\frac{\partial u}{\partial x} + \frac{\partial v}{\partial y} + \frac{\partial w}{\partial z} = 0$$
 (2.1)

x-Momentum:
$$\rho \left(u \frac{\partial u}{\partial x} + v \frac{\partial u}{\partial y} + w \frac{\partial u}{\partial z} \right) = -\frac{\partial p}{\partial x} + \left(\frac{\partial \tau_{xx}}{\partial x} + \frac{\partial \tau_{yx}}{\partial y} + \frac{\partial \tau_{zx}}{\partial z} \right) + \rho g_x \qquad (2.2)$$

y-Momentum:
$$\rho \left(u \frac{\partial v}{\partial x} + v \frac{\partial v}{\partial y} + w \frac{\partial v}{\partial z} \right) = -\frac{\partial p}{\partial y} + \left(\frac{\partial \tau_{xy}}{\partial x} + \frac{\partial \tau_{yy}}{\partial y} + \frac{\partial \tau_{zy}}{\partial z} \right) + \rho g_y \qquad (2.3)$$

z-Momentum:
$$\rho \left(u \frac{\partial w}{\partial x} + v \frac{\partial w}{\partial y} + w \frac{\partial w}{\partial z} \right) = -\frac{\partial p}{\partial z} + \left(\frac{\partial \tau_{yz}}{\partial x} + \frac{\partial \tau_{yz}}{\partial y} + \frac{\partial \tau_{zz}}{\partial z} \right) + \rho g_z \qquad (2.4)$$

Energy:

٦Ŀ,

$$\rho C_{p} \left(u \frac{\partial T}{\partial x} + v \frac{\partial T}{\partial y} + w \frac{\partial T}{\partial z} \right) = -\left[\frac{\partial q_{x}}{\partial x} + \frac{\partial q_{y}}{\partial y} + \frac{\partial q_{z}}{\partial z} \right] + \left\{ \tau_{xx} \frac{\partial u}{\partial x} + \tau_{yy} \frac{\partial v}{\partial y} + \tau_{zz} \frac{\partial w}{\partial z} \right\} + \left\{ \tau_{xy} \left(\frac{\partial u}{\partial y} + \frac{\partial v}{\partial x} \right) + \tau_{zz} \left(\frac{\partial u}{\partial z} + \frac{\partial w}{\partial x} \right) + \tau_{yz} \left(\frac{\partial v}{\partial z} + \frac{\partial w}{\partial y} \right) \right\} \tag{2.5}$$

2.2 Constitutive equation for purely viscous non-Newtonian fluids

The simplest mathematical model for a purely viscous non-Newtonian fluid is the power law model of Ostwald-de Waele expressed by equation 2.6.

$$\tau = k_o f(T) \left| \frac{1}{2} (\Delta : \Delta) \right|^{\frac{n-1}{2}} \Delta \tag{2.6}$$

in which Δ is the symmetrical "rate of deformation tensor" with Cartesian components:

$$\Delta_{ij} = \left(\frac{\partial v_i}{\partial x_j}\right) + \left(\frac{\partial v_j}{\partial x_i}\right) \tag{2.7}$$

$$(\Delta:\Delta) = \Delta_{ij}\Delta_{ji} \tag{2.8}$$

where:

্

$$\frac{1}{2}(\Delta : \Delta) = \left\{ 2 \left[\left(\frac{\partial u}{\partial x} \right)^2 + \left(\frac{\partial v}{\partial y} \right)^2 + \left(\frac{\partial w}{\partial z} \right)^2 \right] + \left(\frac{\partial u}{\partial y} + \frac{\partial v}{\partial x} \right)^2 + \left(\frac{\partial w}{\partial y} + \frac{\partial v}{\partial z} \right)^2 + \left(\frac{\partial u}{\partial z} + \frac{\partial w}{\partial x} \right)^2 \right\}$$
(2.9)

Here n is power law index and k_o is the consistency index at reference temperature (T_o) while f(T) specifies the temperature dependence of the consistency index as follows:

$$f(T) = e^{B'(T-T_o)} (2.10)$$

where B' is temperature-viscosity coefficient. From equation 2.6, the expression reduces to the Newtonian law of viscosity for n=1.0; therefore n can be viewed as an indicator of non-Newtonian behavior. For n < 1 the fluid is a shear thinning fluid and for n > 1 it is a shear thickening fluid. At very high and low shear rates, pseudoplastic fluids exhibit linearity in their flow curves (Newtonian behavior). It is evident that a constitutive equation which completely describes the shear stress over the entire shear rate range must contain several constants. Fortunately, for many engineering problems only a portion or portions of the entire flow curve need to be considered, and therefore only a few constants are required.

2.3 Dimensionless governing equations

The governing equations are non-dimensionalized with respect to appropriate characteristics values. The dimensionless parameters are defined as follows:

$$U = \frac{u}{u_{e}}, V = \frac{v}{u_{e}}, W = \frac{w}{u_{e}}, X = \frac{x}{D_{h}}, Y = \frac{y}{D_{h}}, Z = \frac{z}{D_{h}}$$

$$P = \frac{p - \rho gz}{\rho u_{e}^{2}}$$
(2.11)

where the subscript e indicates entrance condition. Hydraulic diameter, D_h , equals 4 times the duct cross-section area, A_c , divided by the wetted perimeter p'.

For the constant wall temperature boundary condition (T):
$$\theta = \frac{T - T_w}{T_e - T_w}$$
 (2.12)

For the constant wall heat flux boundary condition (H2):
$$\theta = \frac{T - T_{\bullet}}{\frac{qD_{h}}{K}}$$
 (2.13)

The heat flux is nondimensionalized in terms of the heat flux on one wall $(Q = \frac{q}{q_w})$.

The dimensionless governing equations in Cartesian coordinates then become:

1.

Continuity:
$$\frac{\partial U}{\partial X} + \frac{\partial V}{\partial Y} + \frac{\partial W}{\partial Z} = 0$$
 (2.14)

x-Momentum:
$$U\frac{\partial U}{\partial X} + V\frac{\partial U}{\partial Y} + W\frac{\partial U}{\partial Z} = -\frac{\partial P}{\partial X} + \frac{I}{Re}\left(\frac{\partial C}{\partial X} + \frac{\partial D}{\partial Y} + \frac{\partial E}{\partial Z}\right)$$
 (2.15)

y-Momentum:
$$U\frac{\partial V}{\partial X} + V\frac{\partial V}{\partial Y} + W\frac{\partial V}{\partial Z} = -\frac{\partial P}{\partial Y} + \frac{I}{Re}(\frac{\partial F}{\partial Y} + \frac{\partial D}{\partial X} + \frac{\partial G}{\partial Z})$$
 (2.16)

z-Momentum:
$$U\frac{\partial W}{\partial X} + V\frac{\partial W}{\partial Y} + W\frac{\partial W}{\partial Z} = -\frac{\partial P}{\partial Z} + \frac{I}{Re}\left(\frac{\partial H}{\partial Z} + \frac{\partial G}{\partial Y} + \frac{\partial E}{\partial X}\right)$$
 (2.17)

Energy:

$$U\frac{\partial \theta}{\partial X} + V\frac{\partial \theta}{\partial Y} + W\frac{\partial \theta}{\partial Z} = \frac{I}{Pe} \left(\frac{\partial^{2} \theta}{\partial X^{2}} + \frac{\partial^{2} \theta}{\partial Y^{2}} + \frac{\partial^{2} \theta}{\partial Z^{2}} \right) + \frac{\partial^{2} \theta}{\partial Z} + F\frac{\partial^{2} \theta}{\partial Y} + H\frac{\partial^{2} \theta}{\partial Z} + D\left(\frac{\partial^{2} \theta}{\partial Y} + \frac{\partial^{2} \theta}{\partial X} \right) + E\left(\frac{\partial^{2} \theta}{\partial Z} + \frac{\partial^{2} \theta}{\partial X} \right) + G\left(\frac{\partial^{2} \theta}{\partial Z} + \frac{\partial^{2} \theta}{\partial Y} \right)$$
(2.18)

where:

$$\frac{\Pi}{2} = \left\{ 2 \left[\left(\frac{\partial U}{\partial X} \right)^{2} + \left(\frac{\partial V}{\partial Y} \right)^{2} + \left(\frac{\partial W}{\partial Z} \right)^{2} \right] + \left(\frac{\partial U}{\partial Y} + \frac{\partial V}{\partial X} \right)^{2} + \left(\frac{\partial W}{\partial Y} + \frac{\partial V}{\partial Z} \right)^{2} + \left(\frac{\partial U}{\partial Z} + \frac{\partial W}{\partial X} \right)^{2} \right\}$$

$$C = 2 \left(\frac{\Pi}{2} \right)^{\frac{n-1}{2}} \frac{\partial U}{\partial X} F(\theta) \quad ; \quad D = \left(\frac{\Pi}{2} \right)^{\frac{n-1}{2}} \left(\frac{\partial U}{\partial Y} + \frac{\partial V}{\partial X} \right) F(\theta)$$

$$E = \left(\frac{\Pi}{2} \right)^{\frac{n-1}{2}} \left(\frac{\partial U}{\partial Z} + \frac{\partial W}{\partial X} \right) F(\theta) \quad ; \quad F = 2 \left(\frac{\Pi}{2} \right)^{\frac{n-1}{2}} \frac{\partial V}{\partial Y} F(\theta)$$

$$G = \left(\frac{\Pi}{2} \right)^{\frac{n-1}{2}} \left(\frac{\partial V}{\partial Z} + \frac{\partial W}{\partial Y} \right) F(\theta) \quad ; \quad H = 2 \left(\frac{\Pi}{2} \right)^{\frac{n-1}{2}} \frac{\partial W}{\partial Z} F(\theta)$$

where:
$$Re = \frac{\rho u_e^{2-n} D_h^n}{k_o}$$
, $Pr = \frac{k_o C_p \left(\frac{u_e}{D_h}\right)^{n-1}}{K}$ (2.20)

For T boundary condition
$$Br = \frac{k_0 u_e^{n+1}}{D_h^{n-1} (T_e - T_w) K} , \quad F(\theta) = e^{B'\theta(T_e - T_w)} = e^{B\theta}$$

For H2 boundary condition
$$Br = \frac{k_0 u_e^{n+1} \left(\frac{I}{D_h}\right)^n}{q}$$
, $F(\theta) = e^{B'\theta q \frac{D_h}{K}} = e^{B\theta}$

2.4 Boundary conditions

The fluid enters the duct with uniform velocity and temperature profiles. Thus:

$$X = 0 \begin{cases} U = 1, V = 0, W = 0 \\ \theta = 1 \text{ for T boundary condition} \\ \theta = 0 \text{ for H2 boundary condition} \end{cases}$$
 (2.21)

The no-slip condition is applied at the channel walls. For thermal boundary conditions at the walls a large variety of thermal boundary conditions can be specified. Shah and London (1974 and 1978) attempted to systematize a possible set of thermal boundary conditions that can be applied at the walls.

Three commonly encountered thermal boundary conditions at the wall are:

- a. uniform wall temperature (T) everywhere
- b. uniform heat flux axially as well as peripherally (H2)
- c. uniform heat flux axially and uniform temperature peripherally (H1)

For circular tubes and parallel plates H1 and H2 boundary conditions are the same; therefore for these geometries the constant heat flux boundary condition is indicated simply as H.

In the numerical study attention is given only to the T and H2 boundary conditions while in the experimental work only the H2 boundary condition could be applied.

The dimensionless temperature at the walls for the T boundary condition is zero while for the H2 boundary condition the dimensionless heat flux at the heated walls is unity. The gradient of all dependent variables across the symmetry plane are zero except for the velocity perpendicular to the symmetry plane for which the velocity itself at the symmetry plane is zero. A fully developed condition could be prescribed at the outlet boundary due to the long axial length of the plates (120 times the hydraulic diameter).

2.5 Solution methodology

11

Equations (2.14)-(2.18), which is a system of highly nonlinear partial differential equations with associated boundary conditions, were solved using FIDAP (a fluid dynamic and heat transfer analysis package, based on the Galerkin finite element method). The Galerkin finite element method is well documented in the literature e. g. Zienkiewicz (1977), Pittman (1989), and Engleman (1991) and hence will not be discussed in this thesis.

The flow domain was discretized and the governing equations were converted into algebraic equations using appropriate number of grids (based on the geometry). Table 2.1 presents the number of nodes employed and the type of mesh used for different duct geometries. The number of meshes was based on the requirement of mesh-independence of the numerical solution. The number was chosen such that doubling the node numbers showed less than 1 % difference in the apparent friction factor as well as the local Nusselt numbers.

The penalty approach was chosen for pressure with the penalty parameter set at 10^{-8} to satisfy continuity without solving an additional partial differential equation. The penalty function approximation is well known and described by several investigators e.g. Hughes et. al. (1979) and Heinrich and Yu (1988).

Due to the higher velocity and temperature gradients in the entrance region and in the vicinity of the walls, finer mesh distributions were used in these regions (Table 2.1). For some geometries (using symmetry of the cross section) the solution was obtained for only half of the channels, while for a few the whole geometry was considered. The reason for the latter was to allow investigation of the secondary flow pattern in the entrance region. For the triangular duct identical mesh in the corner region could be obtained only when the whole geometry is considered (due to the mesh generation capability of FIDAP).

The solution of the set of algebraic equations generated by the discretization of the governing equations is the most time-consuming stage of the solution. Due to the high radius of convergence of the fixed iteration method and also the high rate of convergence

of the quasi-Newton-Raphson method, a combination strategy used to solve the algebraic equations which starts with the fixed iteration method and then switches to the quasi-Newton-Raphson approach. The combination strategy results in a significant saving in computational time.

The streamline upwinding formulation was used to improve the probable numerical oscillation. In this method the artificial diffusion is added to the physical diffusion, and a Galerkin finite element discritization is employed. In the streamline upwinding method the artificial diffusion acts in such a way that it only affects and modifies the true viscosity for the streamline component of the viscosity. This is due to elimination of the crosswind diffusion effect. The streamline upwind formulation is explained in details by Brooks and Hughes (1982) and Engleman (1991).

The iteration was ended when the relative error was less than 10^{-4} . The relative error was calculated as follows:

$$\frac{\|\Delta \varphi_i\|}{\|\varphi_i\|} \le 10^{-4} \quad \text{where } \Delta \varphi_i = \varphi_i - \varphi_{i-1} \text{ and } \varphi_i \text{ is solution vector at iteration } i.$$

The operator $\| \cdot \|$ is the Euclidean norm. Although this convergence criterion is quite effective for Newton-Raphson method, a more suitable convergence criterion is based on the residual vector itself which must tend to zero when φ_i approaches the correct solution. The normalized residual vector is defined as:

$$\frac{\|R(\varphi_i)\|}{\|R_o\|} \le 10^{-4} \qquad \text{where } R(\varphi_i) \text{ is the residual vector and } R_o \text{ is the reference}$$

vector, typically $R(\varphi_o)$. In this study the convergence criterion was set at 10^{-4} for relative difference between successive solution and also the relative residual.

Table 2.1 Generated mesh for different studied geometries.

5

	Geometry		Node Numbers & Type of Element
·	Circular Z	R=0.5	X×Y×Z 61×11×19 8-node bricks
· · · · · · · · · · · · · · · · · · ·	Square Z X Y o	a=1.0 a o	61×9×17 27-node bricks
	Rounded corner square (R.C.= a/20) Z X T	a=0.981	61×11×21 8-node bricks
0	Rounded corner square $(R.C.=a/6)$ X $Y \longleftarrow 0$	a=0.951	61×11×21 8-node bricks

Table 2.1 (continued)

o	Rectangular (A.R.=0.5) Z X Y O	a=1.5, b=0.75 b 0	X×Y×Z 61×17×17 27-node bricks
0	Rectangular (A.R.=0.2) Z	a=3.0, b=0.6 b	61×13×21 27-node bricks
0	Parallel Plates Y X	$H' = 0.5$ $H' \int_{0}^{\infty}$	121 × 33 9-node elements
	Semi-circular Z Y	R=0.818	61×13×17 8-node bricks
·	Circular $Sector(\alpha = 90^{\circ})$ X $Y \leftarrow$	R=1.137	61×19×19 8-node bricks

. New C

 ${\cal E}$

Table 2.1 (continued)

	Circular Sector $(\alpha = 60^{\circ})$	R=1.455	X×Y×Z 61×19×19 8-node bricks
	Equilateral Triangular Z X • Q	a=1.732 $a = 1.732$ $a = 1.732$ $a = 1.732$	61×17×17 27-node bricks
•	Right Isosceles Triangular Z X Y	a=2.414, h=1.207	61×17×17 27-node bricks
·	Cross-Shape $(\lambda = 0.25)$ X $Y \leftarrow 0$	$a=1.067$ $\begin{bmatrix} a \\ b \end{bmatrix}^{\frac{\lambda a}{2}}$	61×11×21 27-node bricks
·	Cross-Shape $(\lambda = 0.5)$ Z X	$a=1.333$ $a=\frac{\lambda a}{2}$ 0	61×13×25 27-node bricks

2.6 Definitions of dimensionless parameters

In the solution and analysis of the governing equations the following dimensionless groups are of most interest:

Dimensionless axial distance

For the hydrodynamically developing flow the dimensionless axial distance (x^{\dagger}) is defined as:

$$x^{+} = \frac{x}{D_{h} Re} \tag{2.22}$$

For the thermally developing region non-dimensional axial distance (x^*) is expressed as:

$$x^{\bullet} = \frac{x}{D_h Re Pr} = \frac{x^{+}}{Pr}$$
 (2.23)

Hydrodynamic entrance length

The hydrodynamic entrance length (1) is defined here as the axial length of the straight duct which is required to achieve maximum axial velocity within 99% of its corresponding fully developed value. This parameter is nondimensionalized as follows:

$$L = \frac{l}{D_h} \quad , \quad L^+ = \frac{L}{Re} \tag{2.24}$$

Friction factor

The Fanning friction factor, f, is defined as the ratio of the local wall shear stress to the fluid kinetic energy per unit volume. For a fully developed flow

.

$$f = \frac{\tau_w}{\frac{1}{2}\rho u_e^2} = \frac{\Delta p}{\frac{1}{2}\rho u_e^2} \frac{1}{4\Delta X}$$
 (2.25)

where p is the cross-section. Average pressure. In the entrance region f is called the apparent friction factor, f_{app} , and is based on the pressure drop over the axial length from X = 0 to X = X.

Incremental pressure drop

In a hydrodynamic entrance region, the pressure drop can be considered to consist of two components: (1) pressure drop based on fully developed flow and (2) an additional pressure drop due to change of the velocity profile. The second part of the pressure drop is called as the incremental pressure drop, K(x), and it is defined as follows:

$$\Delta P' = \frac{\Delta p}{\rho u_e^2 / 2} = f(4X) + K(x)$$

$$\Delta P' = (f.Re)(4x^+) + K(x) = (f_{app} Re)(4x^+)$$
(2.26)

In the fully developed region, K(x) is designated as $K(\infty)$. For a long duct the following equation relates $K(\infty)$ and f.Re to $\Delta P'$.

$$\Delta P' = (f.Re)(4x^{+}) + K(\infty) \tag{2.27}$$

Dimensionless bulk temperature

The local dimensionless bulk temperature at any axial location is defined by:

$$\theta_{b,x} = \frac{\int_{A_c} U\theta \, dA_c}{\int_{A_c} U \, dA_c} \tag{2.28}$$

Local Nusselt number

The local Nusselt number is defined as:

$$Nu_x = \frac{h_x D_h}{K} \tag{2.29}$$

For the constant wall temperature (T) case:

$$Nu_{x} = \frac{\left(\frac{\partial \theta}{\partial N}\right)_{w,m}}{\theta_{hx}} \tag{2.30}$$

For constant wall heat flux (both axially and peripherally) (H2):

$$Nu_{x} = \frac{\left(\frac{\partial \Theta}{\partial N}\right)_{w,m}}{\Theta_{w,m} - \Theta_{b,x}} \tag{2.31}$$

where N is normal vector to the surface of the duct. The peripheral mean wall temperature $\theta_{w,m}$ at an arbitrary cross section is defined as:

$$\theta_{w,m} = \frac{1}{L'} \int_{\Gamma} \theta_{w} dL' \tag{2.32}$$

The mean Nusselt number over length X measured from the inlet is then given by:

$$Nu_{m} = \frac{1}{X} \int_{0}^{X} Nu_{x} dX \tag{2.33}$$

7/2

Chapter 3

Flow and Heat Transfer in Different Geometry Ducts

This chapter deals with the numerical results for fully developed as well as simultaneously developing laminar flow and heat transfer for Newtonian and power law non-Newtonian fluids through various cross-sectional ducts. The results are presented for two different thermal boundary conditions; constant wall temperature (T) and constant wall heat flux (H2). The results presented in this chapter are restricted to forced convection heat transfer without temperature-dependent viscosity and viscous dissipation effects.

The numerical results are compared with available analytical, experimental, and computational results where appropriate. The influences of power law index and entrance region on flow and thermal characteristics and also the effects of the wall thermal boundary conditions on heat transfer are covered.

For all duct geometries, results were obtained for Re=500 and Re=1000. The computed $f_{app}Re$ as well as Nu_T and Nu_{H2} distribution were found to be independent of Reynolds number when were plotted vs. x^+ and x^- as dimensionless axial distances, respectively. For the sake of brevity results showing the effect of the Reynolds number on Nusselt number are not included in this thesis. The effect of the initial guess on the flow and heat transfer results (specially on the secondary flow) was examined by making two different initial guesses for all dependent variables. No noticeable difference in the dependent variables was obtained as a result of the differences in the initial guess.

This thesis provides tabulated data for various hydrodynamic and heat transfer parameters to three significant digits. Clearly, from the engineering viewpoint the third digit is not significant. However, this format is retained for the benefit of future studies which may wish to compare their results (particularly numerical) with those of this investigation.

3.1 Comparison with prior studies

In the following section the flow and heat transfer characteristics, e.g. product of friction factor and Reynolds number (f.Re), dimensionless maximum velocity (U_{max}) and Nusselt numbers $(Nu_{T,x})$ and $Nu_{H2,x}$ for hydrodynamically and thermally fully developed conditions are presented for different power law indices and various duct geometries. For each geometry, the results are compared with those in the literature most of which are for fully developed conditions.

3.1.1 Circular tube

For power law fluids, the fully developed center-plane velocity distribution (U_f) and f.Re are given by Skelland (1967) as follows:

$$U_f = \frac{3n+1}{n+1} \left[1 - \left| (2r'-1)^{\frac{n+1}{n}} \right| \right]$$
 (3.1)

$$f.Re = 2^{n+1} \left(\frac{3n+1}{n}\right)^n \tag{3.2}$$

where $r' = \frac{r}{D_h}$

The fully developed velocity profiles for different power law indices (Fig. 3.1) obtained in this investigation are in excellent agreement with equation (3.1).

The computed results for friction factor and incremental pressure drop are shown in Fig. 3.2 (a - b) and compared with the data of Hornbeck (1965) who used a finite

difference technique and boundary layer approximation to solve the Newtonian flow problem in the entrance region of a circular tube. The work of Hornbeck (1965) is believed to be the most accurate of published results (Shah and Bhatti (1987)). Also the results of Lawal (1985) obtained by employing the control volume finite difference method are shown in Fig. 3.2 (a) for comparison. The comparison is seen to be quite favorable.

Table 3.1 presents the fully developed values of flow characteristics and also the Nusselt number which for comparison includes the analytical results of Bird et al. (1977) who used the separation of variables technique.

For simultaneously developing flow and heat transfer of a Newtonian fluid, Fig. 3.3 (a) compares the results of this investigation with the results obtained by Nguyen (1993) and McKillop (1964) for the H boundary condition and the results of Hornbeck (1965) and Jensen (1989) for the T boundary condition. For non-Newtonian fluids Fig. 3.3 (b) presents a comparison between the results of this study and the results of McKillop (1964) for n=0.5. From Fig. 3.3 (a - b) good agreement exists between the results of this investigation and available studies.

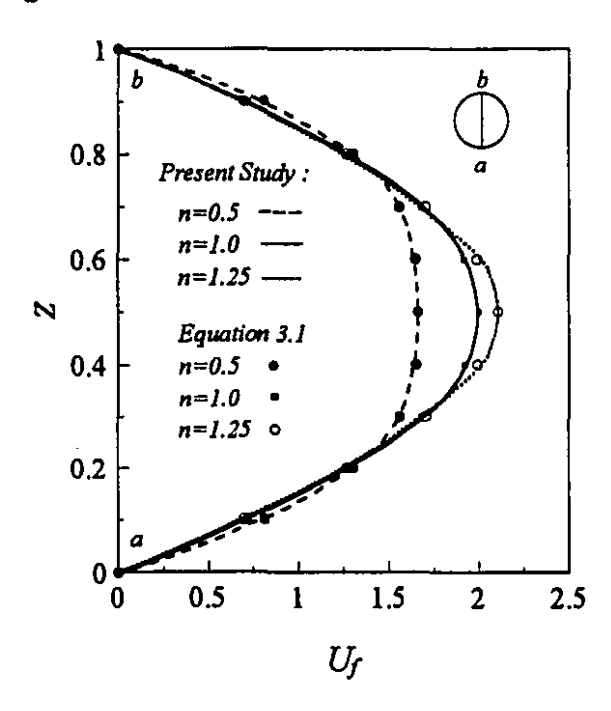


Figure 3.1 Comparison of the fully developed center-plane axial velocity profile: circular tube.

-1

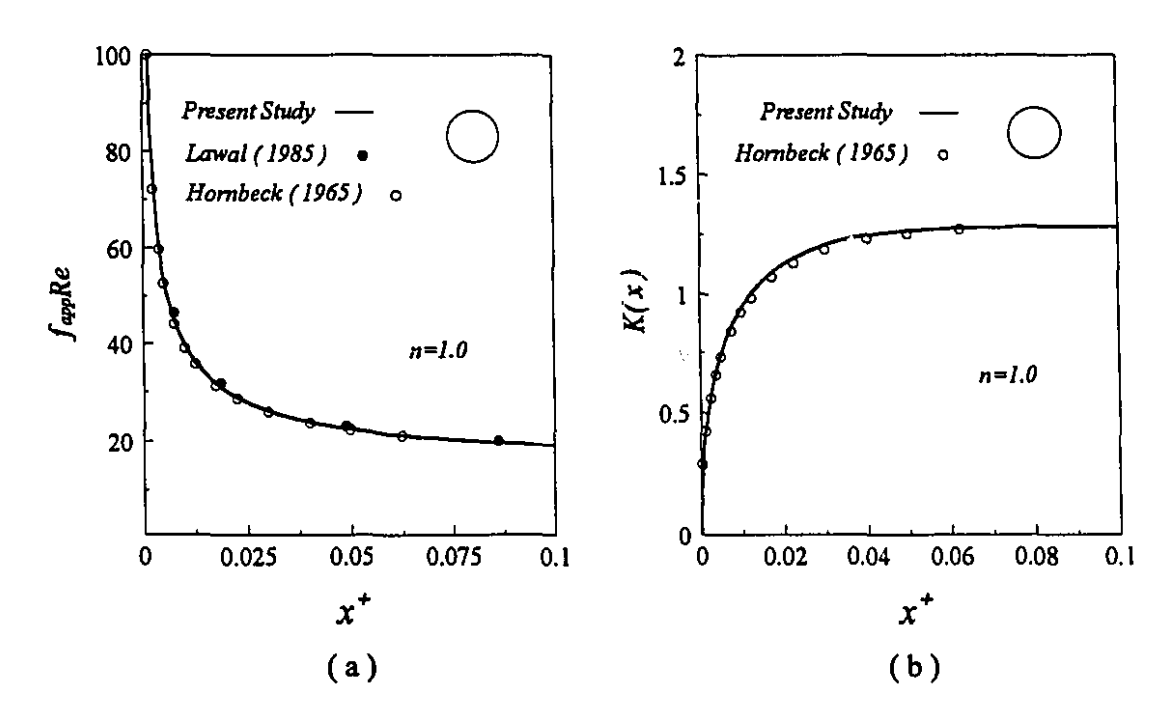


Figure 3.2 (a - b) Comparison of $f_{app}Re$ and K(x): circular tube

. -----

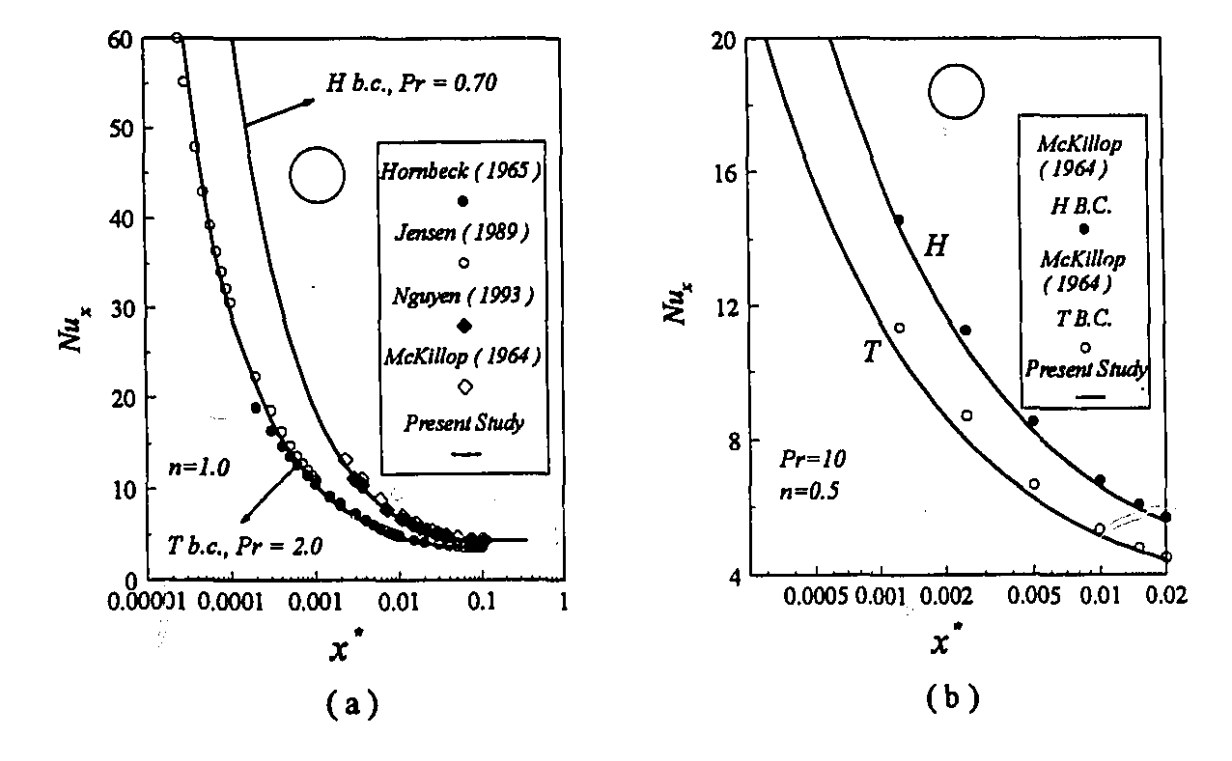


Figure 3.3 (a - b) Comparison of Nusselt numbers in combined entrance region: circular tube

ır:

ĭ

		f.Re	U_{max}	Nu_T	Nu_{H2}
	Skelland (1967)	6.325	1.667		
n=0.5	Bird et al. (1977)			3.949	4.746
ľ	Present Study	6.321	1.665	3.950	4.744
	Skelland (1967)	16.000	2.000		
n=1.0	Bird et al. (1977)			3.657	4.364
	Present Study	15.995	1.996	3.659	4.363
	Skelland (1967)	25.238	2.111		
n=1.25	Bird et al. (1977)				4.275
ľ	Present Study	25.231	2.108	3.590	4.272

Table 3.1 Comparison of the fully developed flow and heat transfer characteristics for circular tube: present study and other available results.

3.1.2 Parallel plates

For power law non-Newtonian fluids flowing in laminar flow between parallel plates the fully developed dimensionless velocity profile (U_f) and f.Re as a function of power law index are given by the following analytical expressions (Skelland (1967)):

$$U_f = \frac{2n+1}{n+1} \left[1 - \left| \frac{Y - 0.25}{0.25} \right|^{\frac{n+1}{n}} \right]$$
 (3.3)

$$f.Re = 2^{2n+1} \left(\frac{2n+1}{n}\right)^n$$
 (3.4)

Fig. 3.4 (a) displays the fully developed dimensionless velocity profile, while Table 3.2 indicates f.Re and U_{max} in comparison with the results obtained by Skelland (1967). Again, good agreement is found between the computational and analytical results.

For parallel plates the boundary layer type solution of Bodoia and Osterle (1961) is claimed by Shah and Bhatti (1987) as the most accurate. Fig. 3.4 (b) compares the

2

product of the apparent friction factor and Reynolds number $(f_{app} Re)$ for a Newtonian fluid as obtained in this investigation with the results of Bodoia and Osterle (1961). Furthermore, Table 3.2 contains Nusselt numbers for hydrodynamically and thermally developed conditions. For all boundary conditions, the Newtonian Nusselt numbers obtained in this study are in excellent agreement with the exact solution of Shah and London (1978).

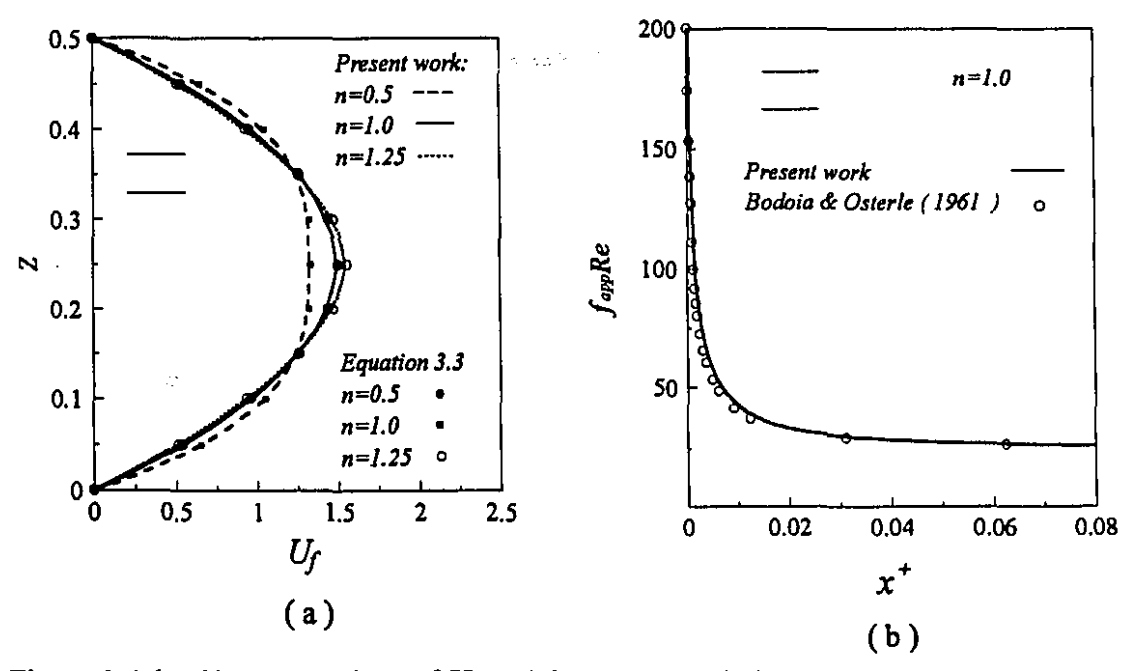


Figure 3.4 (a - b) Comparison of U_f and f_{app} Re: parallel plates

ريد. مريا

Table 3.2 Comparison of the fully developed flow heat transfer characteristics for parallel plates: present study and other available results.

		f.Re	Umax	$Nu_{T(I)}$	Nu_T	Nu _{H(I)}	Nu_H
	Skelland (1967)	8.000	1.333				
n=0.5	Lin (1977)	-	<u> </u>		7.940		8.762
	Present Study	7.994	1.327	4.898	7.950	5.398	<i>8.758</i>
	Skelland (1967)	24.000	1.500				
n=1.0	Shah & London (1978)			4.861	7.541	5.385	<i>∝8.235</i>
	Present Study	23.879	1.491	4.862	7.541	5.386	8.235
n=1.25	Skelland (1967)	40.978	1.555				
	Present Study	40.694	1.546	4.857	7.442	5. <u>380</u>	8.109

The constant wall temperature boundary conditions (T and T(1)) were investigated by Mercer et al. (1967) experimentally using an interferometer. Fig. 3.5 (a - b) shows a comparison of the present results with their experimental data obtained for air. Again, the agreement is found to be good in the light of the experimental uncertainties. Note that the local Nusselt number defined by Mercer et al. (1967) is based on the temperature difference between the wall and the inlet fluid. For Fig. 3.5 (a - b), our results were calculated according to the Mercer et al. definition although in rest of this work the local Nusselt number in based on the temperature difference between the wall and the local fluid mixing cup temperature.

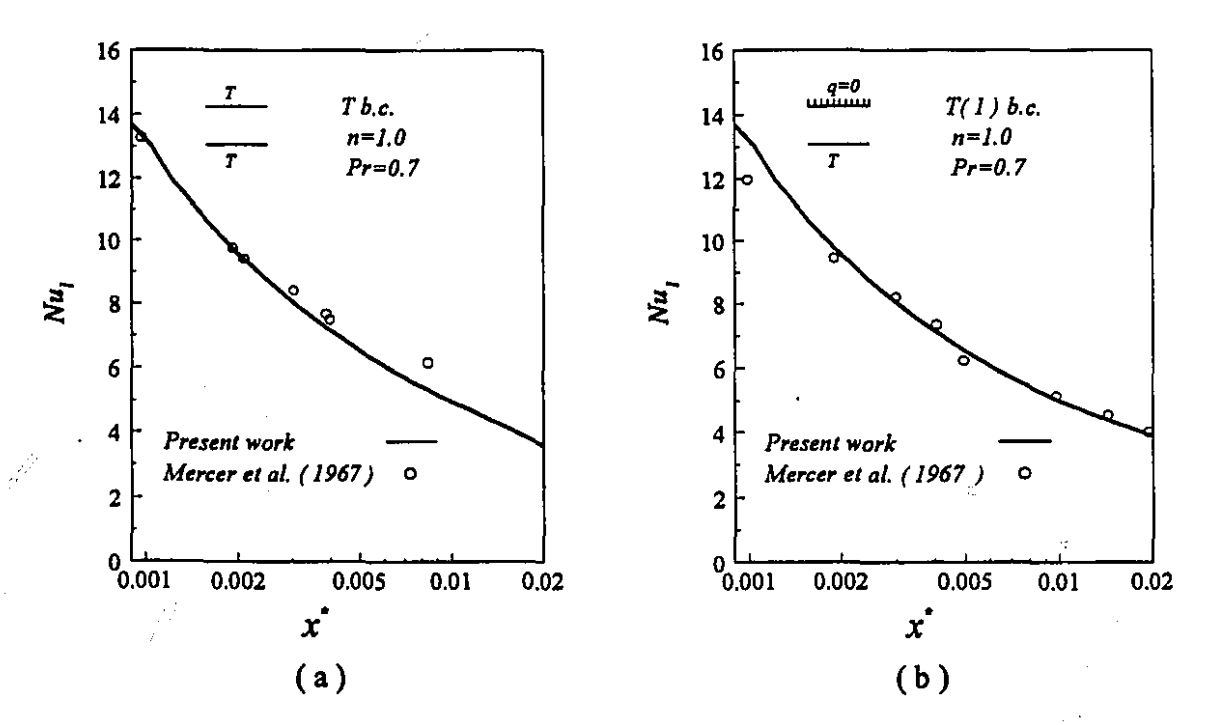


Figure 3.5 (a - b) Comparison of Nusselt number in the combined entrance region: parallel plates

Table 3.3 compares the results of this study with those reported by Shah and London (1978), and Hwang and Fan (1964) using a finite difference method for Newtonian fluids. They obtained velocity distributions and then numerically integrated the energy equation for both T and H boundary conditions; their Prandtl number values

0

1

ranged from 0.01 to 50. These results are claimed by Shah and Bhatti (1987) to be more accurate than other literature values (as of 1978). Table 3.3 also includes the results of Nguyen and Maclaine-Cross (1991) who used a finite difference method to solve the momentum and energy equations using the stream function as an independent variable.

This problem was also investigated analytically by Rostami and Mortazavi (1990) using a linear profile for the axial component of the velocity and solving the energy equation by the similarity method. Their results (Table 3.3) show good agreement with those of this investigation except in the downstream region where large discrepancies occur due to the linear velocity profile assumption. The values of $Nu_{T,x}$ obtained by Campos Silva et al. (1992) are also tabulated in Table 3.3. Far downstream their results are comparable to present results but close to the entrance they are greater probably because of their linearization method.

Table 3.4 compares the Nusselt numbers obtained in the present investigation and those reported by Lin (1977) for a non-Newtonian fluid (n=0.5) at different Prandtl numbers (Pr=10 and Pr=1). This comparison shows very good agreement in the entire channel.

Table 3.3 Comparison of Nusselt numbers reported by various researchers for Pr=10, n=1 and Re=500: parallel plates

		Nı	$t_{T,m}$		Nu	ſ _i x	Nı	Nu _{H,x}	
x.	Nguyen & Maclaine -Cross (1991)	&	Rostami & Mortazavi (1990)	Present work	Campos Silva et al. (1992)	Present work	Hwang & Fan (1964)	Present work	
0.00012		46.68	47.46	47.18	27.75	24.72	34.07	34.24	
0.00043		27.88	27.84	27.42	16.80	15.82	20.66	20.92	
0.00075		21.94	22.28	21.86	13.70	13.34	17.03	17.18	
0.0020	13.96	15.44	15.63	15.31	10.10	10.27	12.60	12.58	
0.00625	10.49	11.01	11.33	10.95	8.20	8.15	9.50	9.51	
0.010	9.54	9.86	10.4	9.80	7.79	7.72	8.80	8.76	
0.0125	9.15	9.40	10.14	9.38	7.70	7.63		8.55	

Table 3.4 Comparison of $Nu_{T,x}$ for n=0.5 and Re=500: parallel plates

	Pr=10	-		Pr=1			
x.	Lin (1977)	Present Work	<i>x</i> ·	Lin (1977)	Present Work		
0.000781	15.21	14.83	0.00061	20.71	20.97		
0.000999	13.86	13.59	0.00110	16.57	15.98		
0.001205	13.29	12.76	0.00217	12.29	12.12		
0.001803	11.43	11.28	0.00405	<i>9.87</i>	9.86		
0.002335	10.6	10.52	0.00571	9.05	9.03		
0.004017	9.29	9.29	0.01047	<i>8.27</i>	8.20		
0.006026	8.65	8.64	0.02055	8.00	7.97		
0.010110	8.21	8.14	0.02653	7.96	7.95		
0.020525	7.94	7.95					

3.1.3 Rectangular ducts

3.1.3.1 Square duct

Fig. 3.6 (a - b) displays the center-plane velocity profile and dimensionless maximum velocity for n=1 obtained in this investigation and the experimental results of Goldstein and Kreid (1967). They made laser Doppler anemometer measurements in a square duct with water as the working fluid. The results of this study are in very close agreement with those of Goldstein and Kreid (1967). Fig. 3.6 (b) also includes the numerical results of Lawal (1985) for different power law indices.

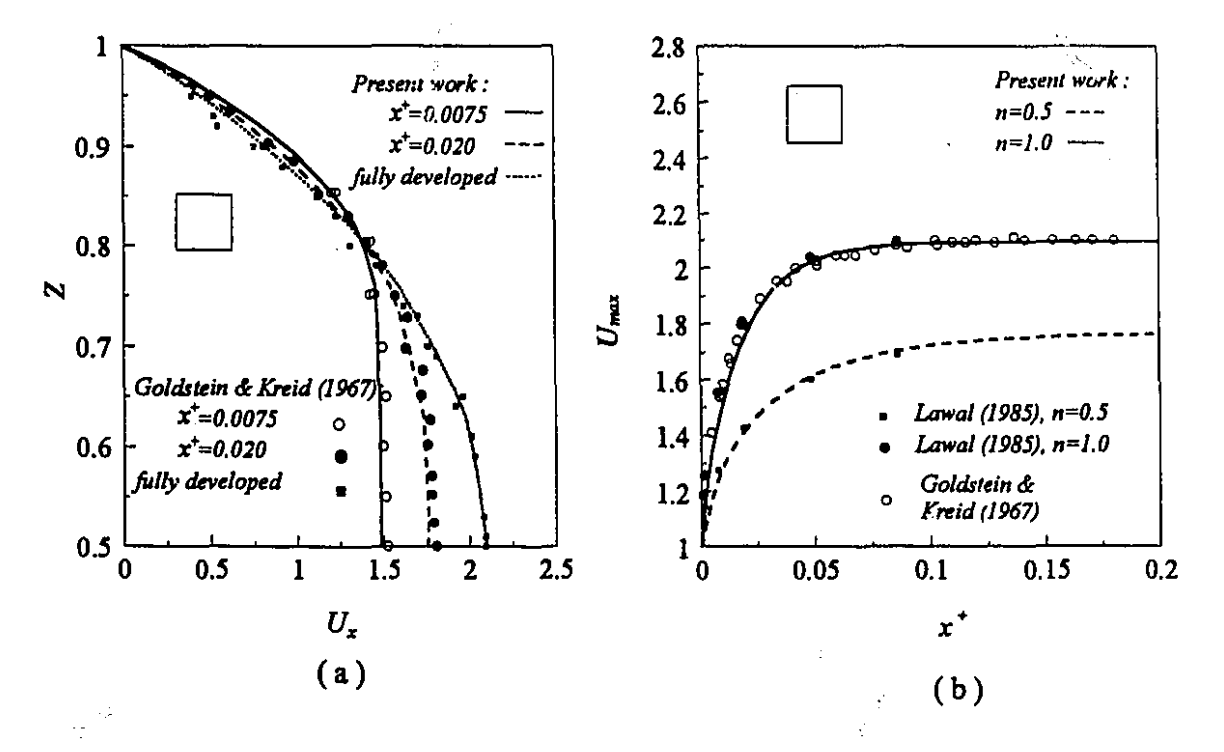


Figure 3.6 Comparison of dimensionless center-plane axial velocity profile and U_{max} : square duct

Table 3.5 presents the fully developed values of the key flow characteristics and Nusselt number. This table contains the results of Kozicki et al. (1966) who introduced a new Reynolds number for which the relationship $f = \frac{10}{R_{e'}}$ is applicable for fully developed laminar flow of a power law fluid through non-circular channels of uniform cross section.

~---!!

1

This table also includes the computational results of Gao and Hartnett (1992) for the hydrodynamically and thermally fully developed condition and for various power law indices. Table 3.5 includes the results of Chandrupatla (1977) for different boundary conditions. This table demonstrates very good agreement between the results of this work and other available data in the literature.

Table 3.5 Comparison of the fully developed flow and heat transfer characteristics for square duct: present study and other available results

		f.Re	U_{max}	Nu _T	Nu _{H2}
	Kozicki et al. (1966)	5.935		*****	
	Chandrupatla (1977)	5.733	1.763	3.184	3.274
n=0.5	Gao & Hartnett (1992)	5.723		_	3.309
	Present Study	5.772	1.760	3.190	3.310
	Kozicki et al. (1966)	14.219		40.49-44	
	Chandrupatla (1977)	14.228	2.096	2.975	3.095
n=1.0	Gao & Hartnett (1992)	14.229			
	Present Study	14.234	2.092	2.979	3.090
n=1.25	Kozicki et al. (1966)	21.858			
	Present Study	22.248	2.209	2.925	3.032

For simultaneous development of flow and heat transfer Fig. 3.7 compares the results of this study with the results obtained by Chandrupatla (1977). $Nu_{T,x}$ has not been reported by Chandrupatla (1977), hence for the T boundary condition comparison is made with $Nu_{T,m}$ reported by Chandrupatla (1977). The agreement between the two results is good.

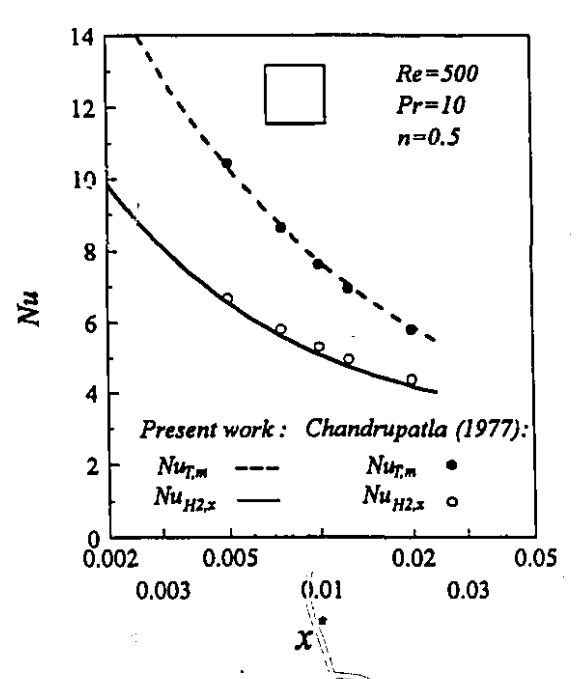


Figure 3.7 Comparison of Nusselt number: square duct

3.1.3.2 Rectangular duct with different aspect ratios

Hydrodynamically developing flow in rectangular ducts was studied by Sparrow et al. (1967) who used a pitot tube to measure the velocity profiles at different locations for air flowing through rectangular ducts with aspect ratios of 0.2 and 0.5. Table 3.6 and Table 3.7 indicate the results of the present investigation which are compared with available results in the literature showing good agreement.

Table 3.6 Comparison of flow and heat transfer characteristics for rectangular duct with A.R.=0.5: present study and other available results

		f.Re	$U_{ m max}$	Nu _T	Nu_{H2}
	Kozicki et al. (1966)	6.237			<u> </u>
n=0.5	Gao & Hartnett (1992)	6.002			3.180
	Present Study	6.060	1.734	3.600	3.150
	Kozicki et al. (1966)	15.546			
	Shah & London (1978)			3.391	3.020
n=1.0	Gao & Hartnett (1992)	15.551			
	Sparrow et al. (1967)	15.550	1.991		
	Present Study	15.570	1.992	3.388	3.021
n=1.25	Kozicki et al. (1966)	24.342			
	Present Study	24.805	2.053	3.350	2.998

Table 3.7 Comparison of flow and heat transfer characteristics for rectangular duct with A.R.=0.2: present study and other available results

		f.Re	U_{max}	Nu _T	Nu _{H2}
	Kozicki et al. (1966)	7.019			
n=0.5	Gao & Hartnett (1992)	6.805			2.743
	Present Study	6.860	1.600	4.922	2.717
	Kozicki et al. (1966)	19.071			
Ī	Shah & London (1978)			4.803	2.930
n=1.0	Gao & Hartnett (1992)	19.075			
	Sparrow et al. (1967)	19.075	1.715		
	Present Study	19.077	1.714	4.831	2.924
n=1.25	Kozicki et al. (1966)	31.087		4.922 4.803 4.831	
	Present Study	31.456	1.749	4.817	2.996

3.1.4 Circular-sector ducts

Fig. 3.8 shows the fully developed velocity profiles for Newtonian fluids flowing through semi-circular duct at different circumferential locations and indicates the excellent agreement between the results of this investigation and the results of Manglik and Bergles (1988) who used the finite difference method.

Table 3.8 presents the fully developed flow and heat transfer results for a semi-circular duct. This table compares the results of this study with those of Shah and London (1978); it also includes the results obtained by Lei (1990) who used the Fourier transform technique to obtain results for a fully developed steady laminar Newtonian flow for the H2 thermal boundary.

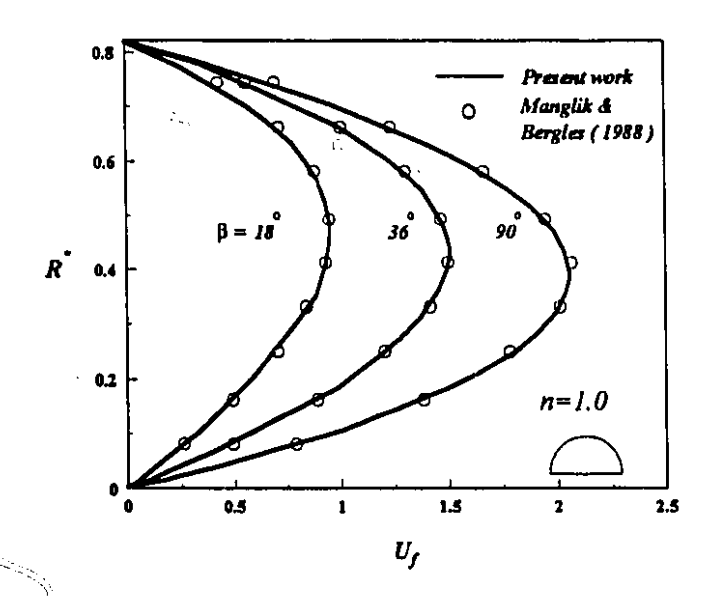


Figure 3.8 Comparison of fully developed velocity profile at different circumferential locations: semi-circular duct

condition in circular sector ducts.

Table 3.8 furthermore contains

the results of Trupp and Lau (1984) obtained by the finite difference technique for laminar heat transfer in circular sector ducts with isothermal walls, and those of Ben-Ali et al. (1989) who applied the same numerical method to predict the heat and fluid flow behavior for different boundary conditions in annular sector and circular sector channels with different apex angles.

Table 3.8 shows that the present results and other available data are in very close agreement, which supports the accuracy of the computational model.

 $\cdot \succeq_{\zeta}$

for semi-circular duct: present study and other available results

f.Re U____ Nu_T Nu_H2

Table 3.8 Comparison of the fully developed flow and heat transfer characteristics

		f.Re	U_{max}	Nu_T	Nu_{H2}
n=1.0	Shah & London (1978)	15.767			2.923
	Lei (1990)	15.767	2.061	-	2.920
	Ben-Ali et al.(1989)	15.790		3.316	2.930
	Trupp & Lau (1984)			3.316	
	Present Study	15.860	2.058	3.318	2.920

For other circular sector channels ($\alpha = 90^{\circ}$ and $\alpha = 60^{\circ}$) Table 3.9 and Table 3.10 present the fully developed values of flow and heat transfer characteristics; which are compared with the limited results available in the literature.

Table 3.9 Comparison of the fully developed flow and heat transfer characteristics for circular-sector duct ($\alpha = 90^{\circ}$): present study and other available results

		f.Re	U _{max}	Nu_T	Nu _{H2}
	Lei (1990)	14.769	2.102		2.987
n=1.0	Ben-Ali et al.(1989)	14.790		3.060	2.984
	Present Study	14.820	2.079	3.060	2.980

Table 3.10 Comparison of the fully developed flow and heat transfer characteristics for circular-sector duct ($\alpha = 60^{\circ}$): present study and other available results

		f.Re	Umax	Nu _T	Nu _{H2}
n=1.0	Shah & London (1978)	14.171			
	Lei (1990)	14.171	2.149		2.448
	Ben-Ali et al.(1989)	14.200	_	2.822	2.421
	Trupp & Lau (1984)			2.819	
	Present Study	14.248	2.134	2.820	2.430



 \mathcal{J}^{p}

3.1.5 Triangular ducts

Fig. 3.9 presents the computed apparent friction factor results Newtonian and non-Newtonian fluids compared with the computational results of Lawal (1985). Fully developed friction and dimensionless maximum factor velocity and the fully developed Nusselt number values (Nu_T) are compared in Table 3.11 with the results of Shah (1975) who employed a least squares matching technique to analyze the fully developed laminar flow and heat transfer in ducts of arbitrary cross-section. Also included in Table 3.11 are results of Schneider and

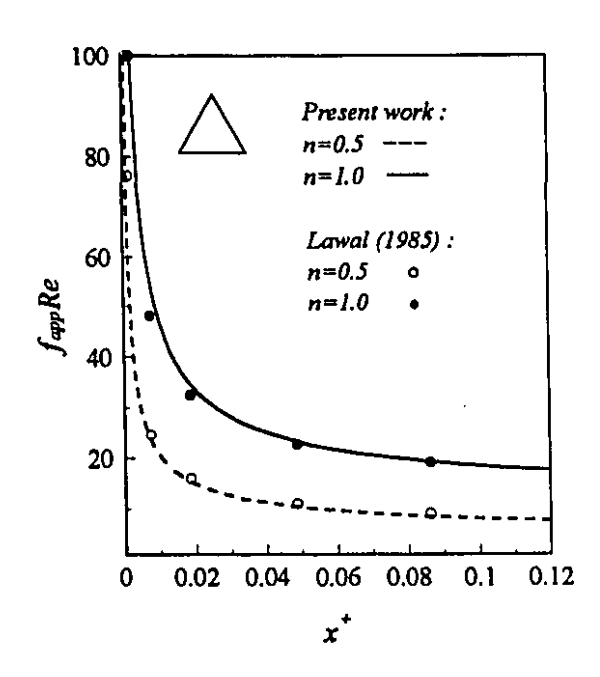


Figure 3.9 Comparison of f_{app} Re: equilateral triangular duct

LeDain (1981) who used the finite element method. The agreement between the results of present study and other mentioned results was found to be excellent. Lawal (1985) did not provide the fully developed Nusselt number values as a result of computational limitations.

The Nusselt number (T boundary condition) distribution in the entrance region for n=0.5 was compared with the results of Lawal (1985). This comparison is not shown here. The results of Lawal (1985) were between 10 and 25 percent (depending on the axial location) higher than results of the present work. Due to high velocity and temperature gradients close to the walls, a finer non-uniform mesh must be employed in this region of the channel. The difference between the results of Lawal (1985) and this work can be attributed to the uniform mesh used in the former work.

Table 3.11 Comparison of the fully developed flow and heat transfer characteristics for equilateral triangular duct: present study and other available results

		f.Re	U_{max}	Nu_T	Nu _{H2}
	Shah (1975)	13.333	2.222		1.892
n=1.0	Schneider & LeDain (1981)	13.340		2.497	1.890
	Present Study	13.340	2.230	2.503	1.896

Table 3.12 compares the flow and heat transfer characteristics for a right isosceles triangular duct obtained in this study and those available in the literature.

Table 3.12 Comparison of the fully developed flow and heat transfer characteristics for right isosceles triangular duct: present study and other available results

		f.Re	U_{max}	Nu_T	Nu _{H2}
	Shah (1975)	13.154			1.340
n=1.0	Schneider & LeDain (1981)	13.161		2.358	1.351
	Present Study	13.167	2.268	2.350	1.351

3.2 Effect of power law index

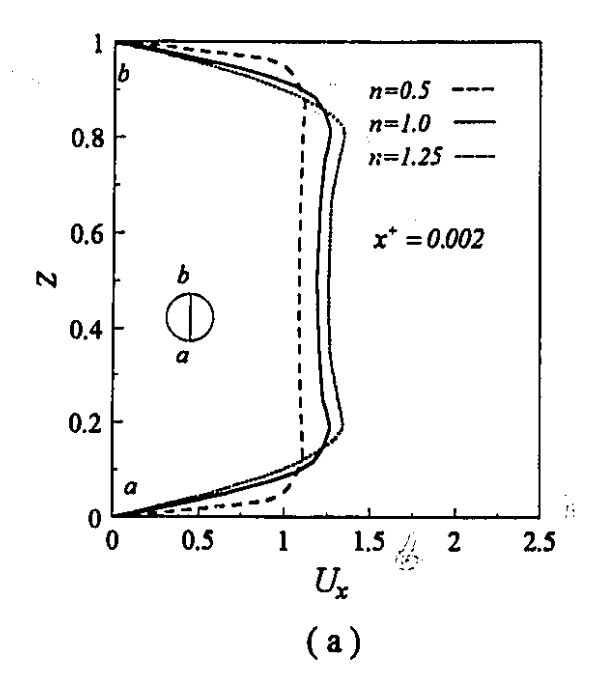
3.2.1 Fluid flow

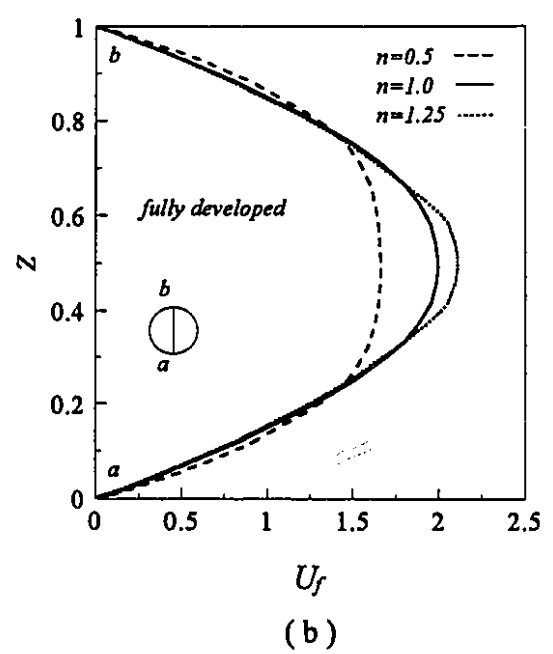
₹.

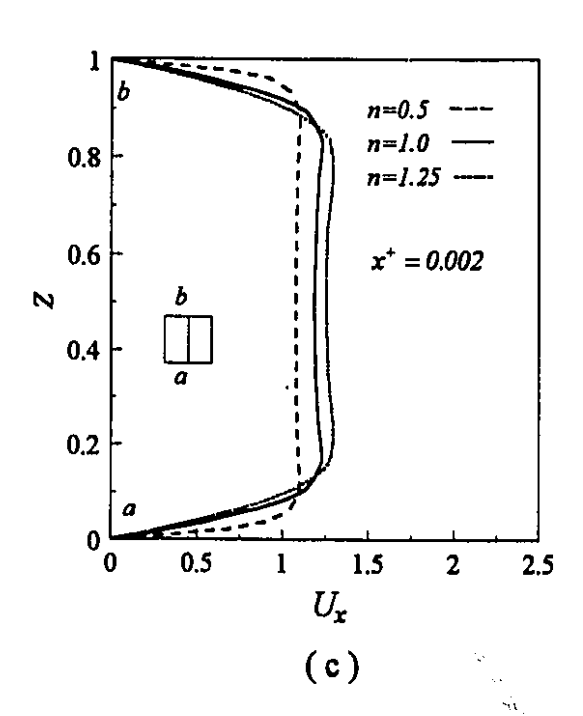
Figs. 3.10 (a - h) presents the computed dimensionless axial velocity profiles at $x^{+}=0.002$ and fully developed condition for different power law indices and various geometries. The velocity profiles close to the entrance display a local maximum near the wall. Due to the no-slip condition at the walls to satisfy the continuity equation the velocity of the fluid must increase in other sections. This increase in velocity can not reach the center instantaneously; therefore for small x, bulges appear near the walls. Further downstream, the rise in axial velocity reaches the center of the duct and the maximum velocity is transferred to the center. It is evident from Fig. 3.10 (a - h) that for pseudoplastic fluids the increase in velocity due to the no-slip condition at the walls can not sustain a bulge in the velocity profile. That is a result of the flatness of the velocity profiles for these fluids. Therefore these bulges are bigger for larger values of the power law index. Bunke and Berman (1969) conducted a series of experiments using a laser-Doppler velocimeter to measure the velocity profile in the entrance region of a circular tube. They observed overshoots in the velocity profile at Re=304, 206 and 108 in the entrance section as predicted. Both experimental and analytical results support the existence of overshoots in the velocity profile in the entrance region of the duct (Shah and London (1978)).

Close to the wall for the same value of shear rate and consistency index the apparent viscosity of a pseudoplastic fluid is lower than that of a shear-thickening fluid. In the entrance region of a duct, due to the viscous effects close to the walls and the high shear rate in the wall region, the velocity of the pseudoplastic fluid is higher than that of a dilatant fluid. Requirement of mass conservation forces the fluids to correspondingly slow down in the core of the duct. Further downstream, viscous effects propagate to the centerplane of the channel and the influence of the power law index decreases.

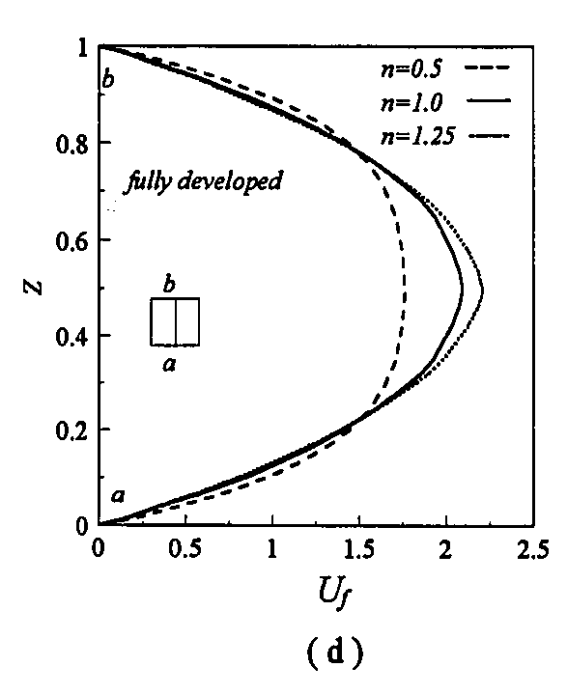








Ö



40

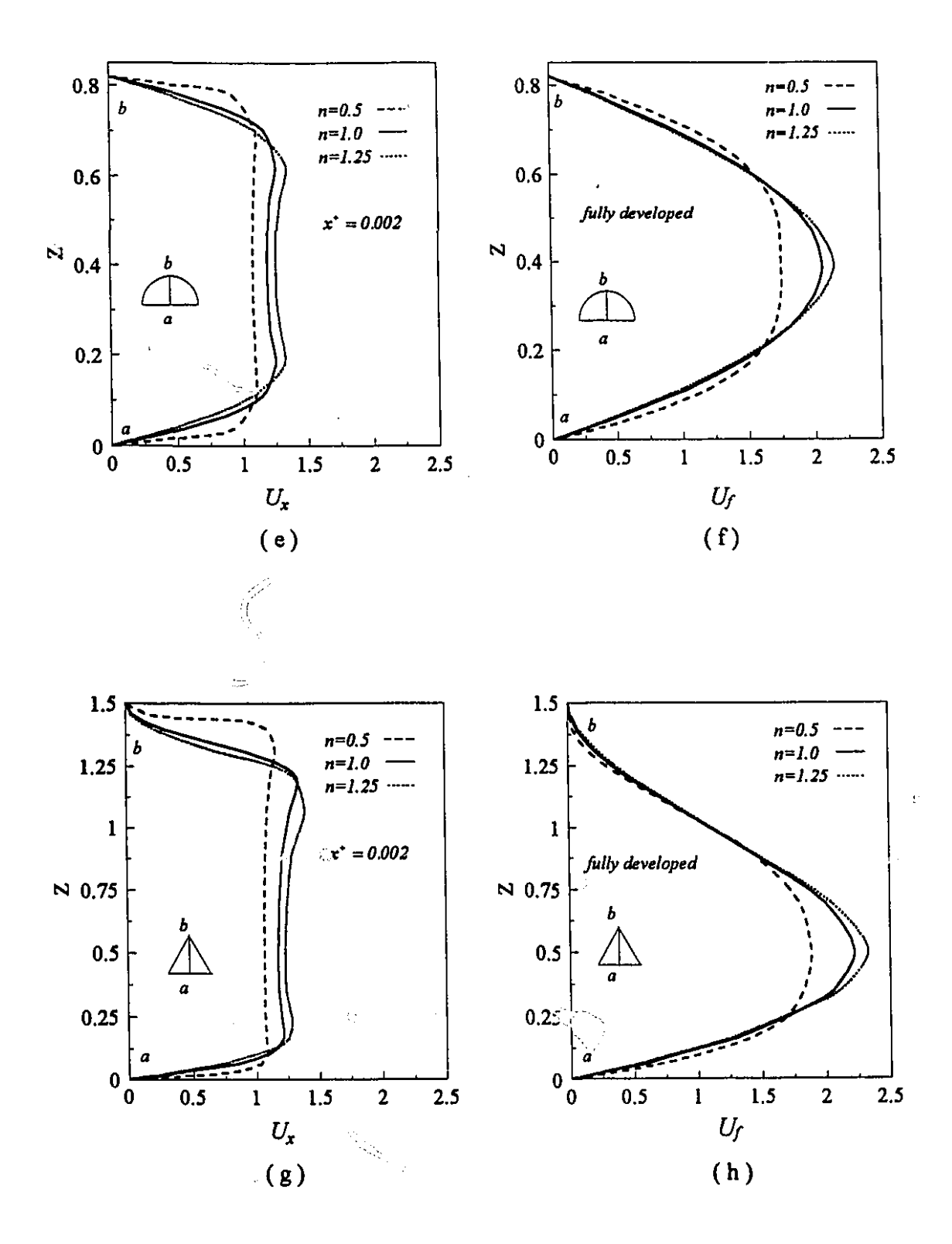


Figure 3.10 (a - h) Dimensionless axial velocity profiles at $x^{+}=0.002$ and fully developed condition for different power law indices and various geometries.

 U_{max} as well as $f_{app}Re$ and K(x) for different power law indices and various geometries are presented in Fig. 3.11 (a - d) and Fig. 3.12 (a - l) respectively. Also the results for U_{max} and $f_{app}Re$ are tabulated in Tables A1 through A12 in Appendix A. The fully developed flow and heat transfer characteristics for different power law indices and various geometries are given in Table 3.13.

Due to the flatter velocity profile for lower power law index, U_{max} decreases with decreasing n values. From Fig. 3.12 (a - l) and Table 3.13 it is observed that lower n results in lower K(x) and $K(\infty)$, but higher L^+ . Also the power law index has a significant effect on the pressure drop. The lower apparent viscosity close to the walls for shearthinning fluids causes smaller dimensionless pressure drop in comparison with that due to a shear thickening fluid for the same Re. Thus, from Fig. 3.12 (a - l) and Tables A1 through A12 (Appendix A) two important observations can be made concerning the apparent friction factor, entrance region and power law index. The hydrodynamically developing section has a higher $f_{app}Re$ than the fully developed condition. For the duct geometries studied for n=0.5, $f_{app}Re$ at $x^+=0.002$ are appreciably higher than f.Re, ranging from 228 % higher for parallel plates to 884 % higher for the right isosceles triangular duct. The effect of power law index on $f_{app}Re$ is also appreciable. For example, at $x^+=0.002$, $f_{app}Re$ of n=0.5 is smaller than f_{app} Re of n=1.0 which ranges from 57 % for right isosceles triangular duct to 72 % for cross-shaped duct ($\lambda=0.5$).

医温度

R

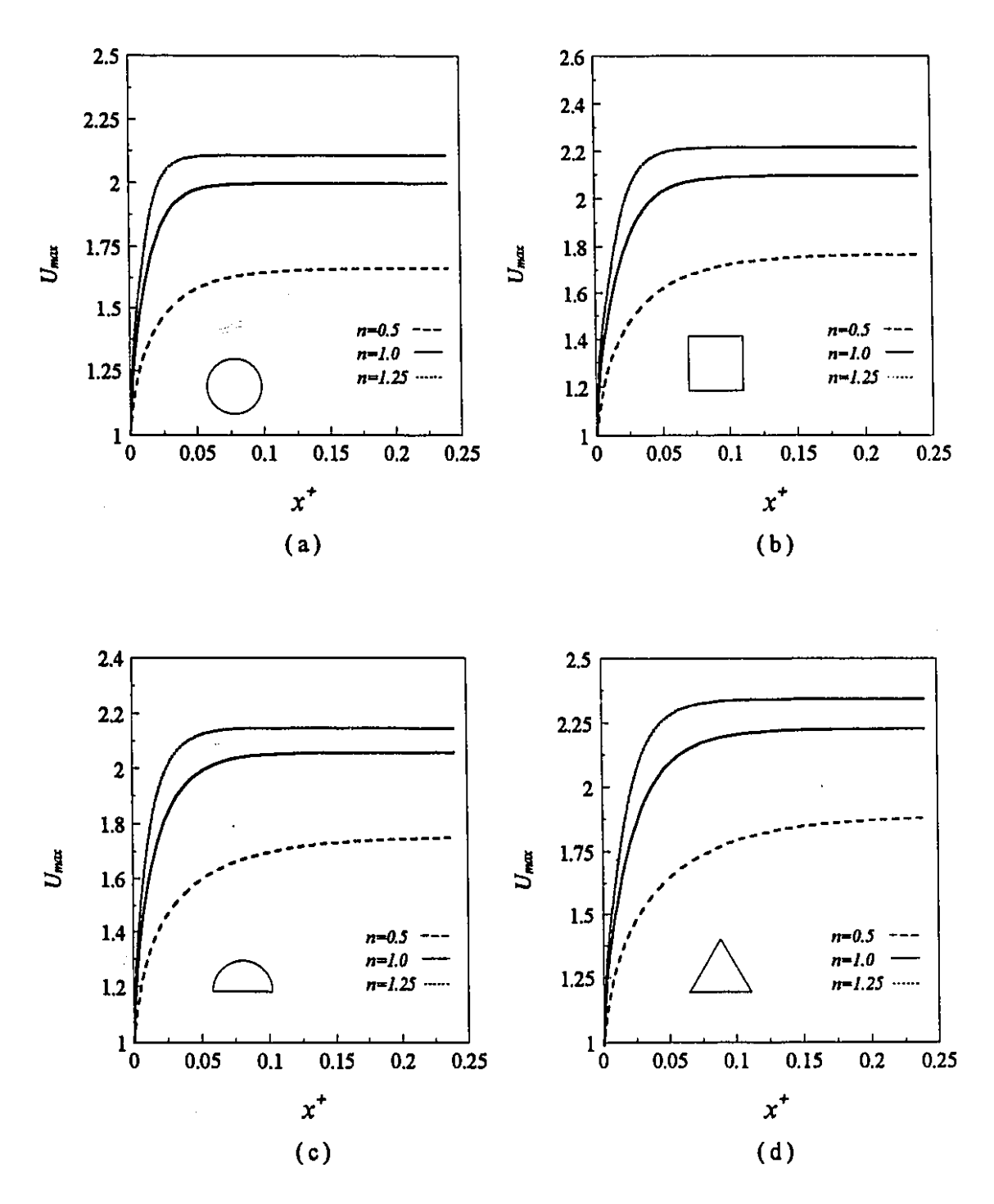
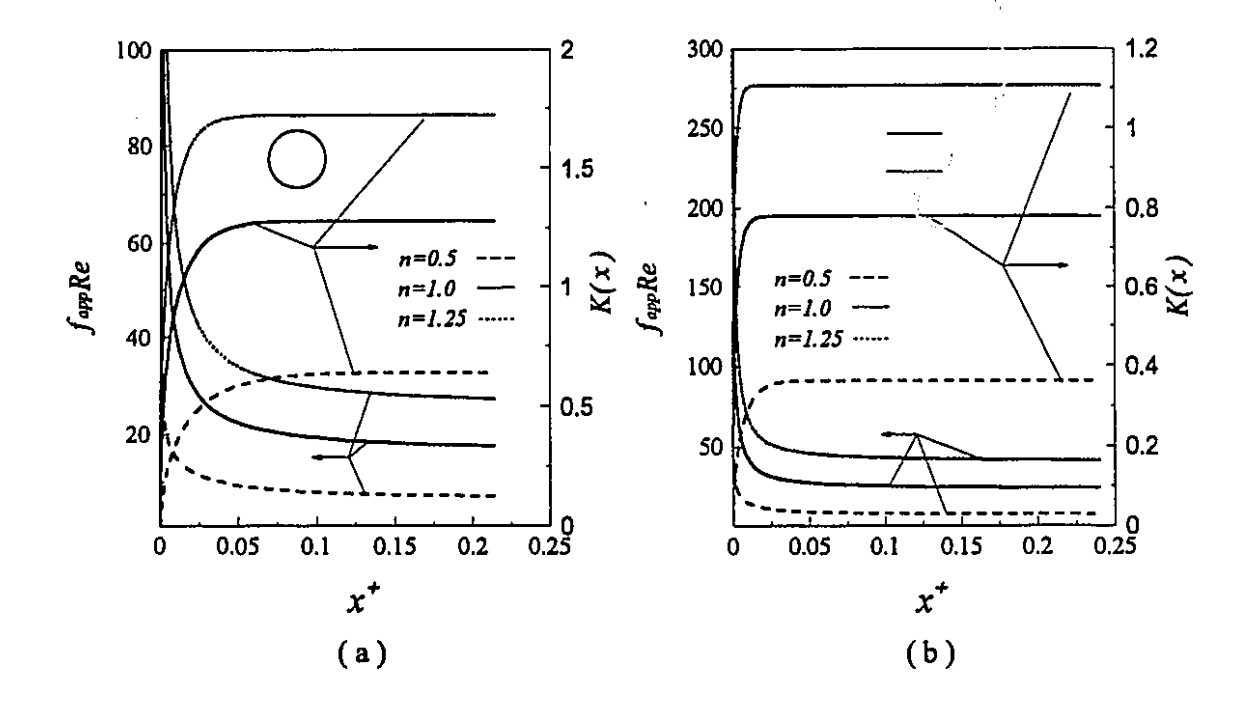
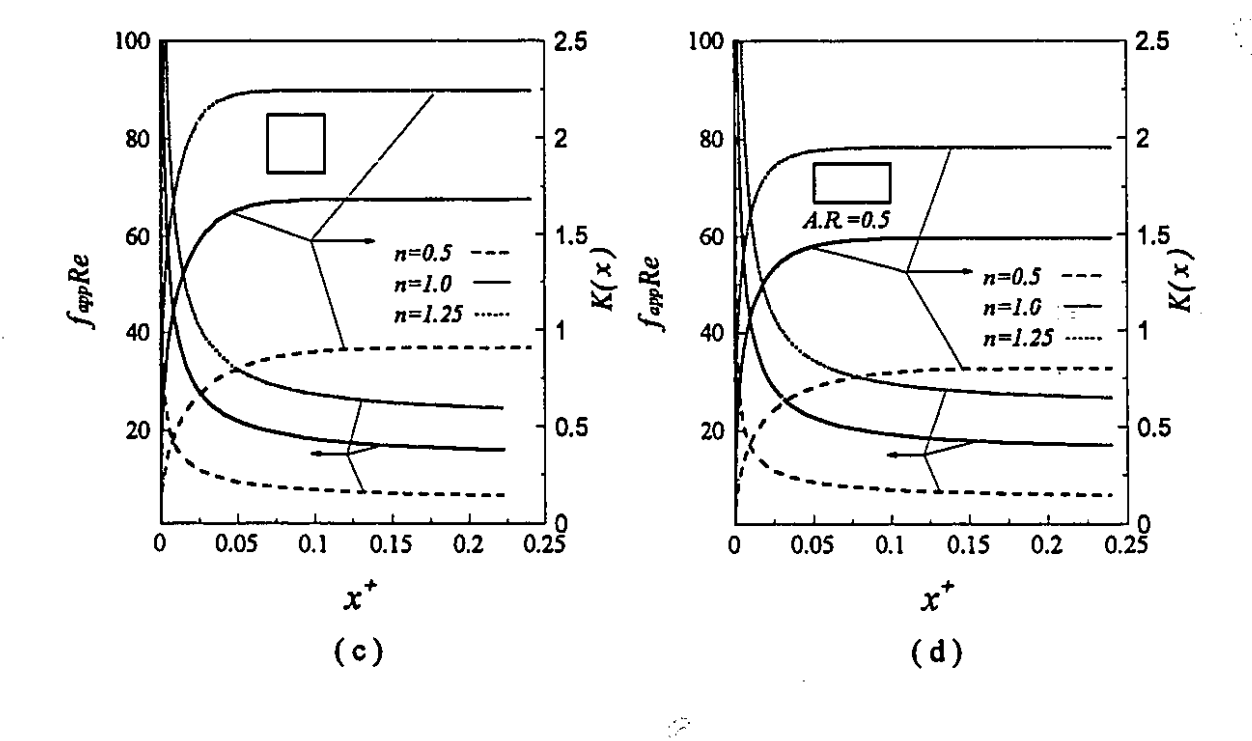
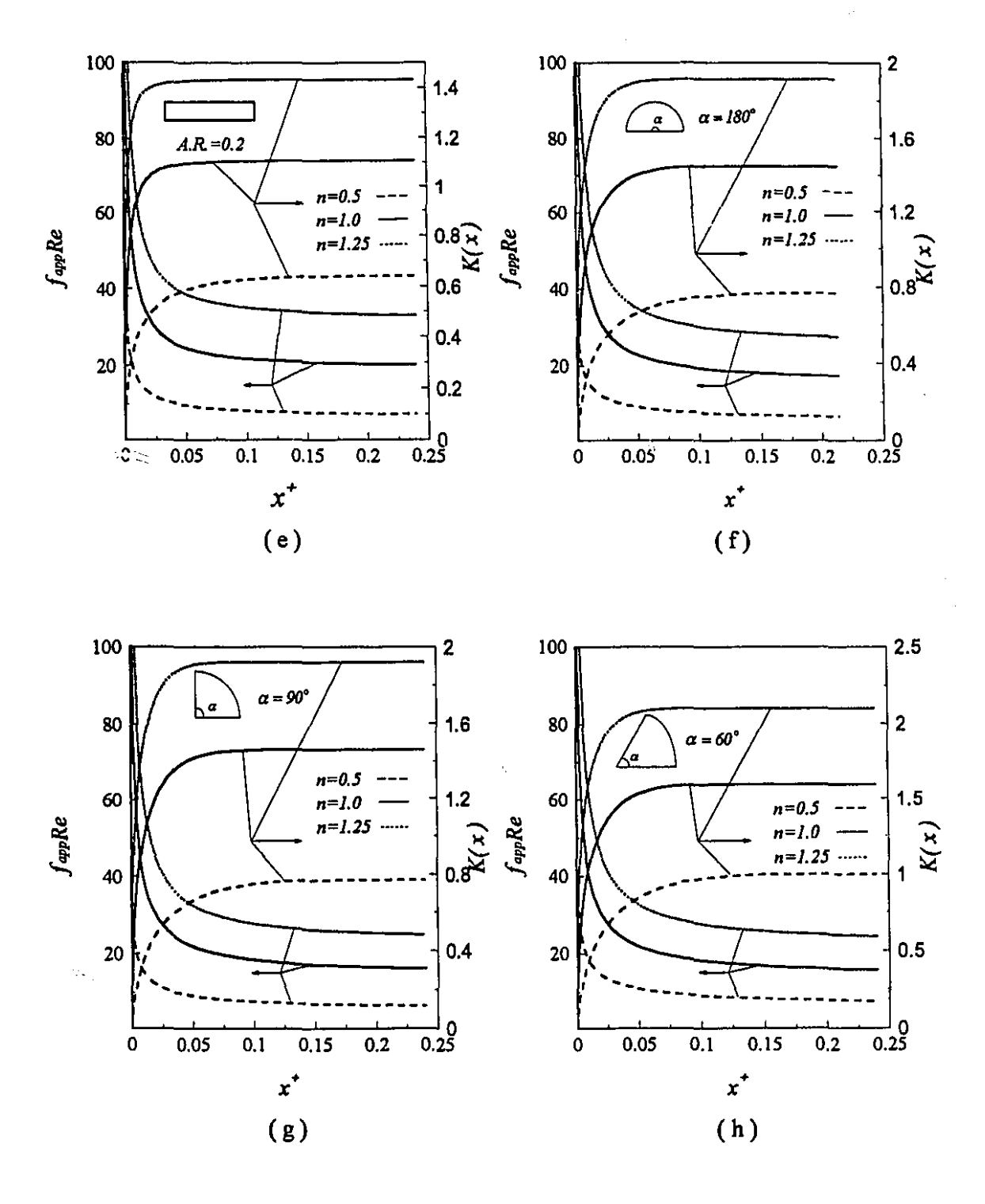


Figure 3.11 (a - d) Dimensionless maximum velocity for different power law indices and various geometries, Re=500.

....







쉿.:

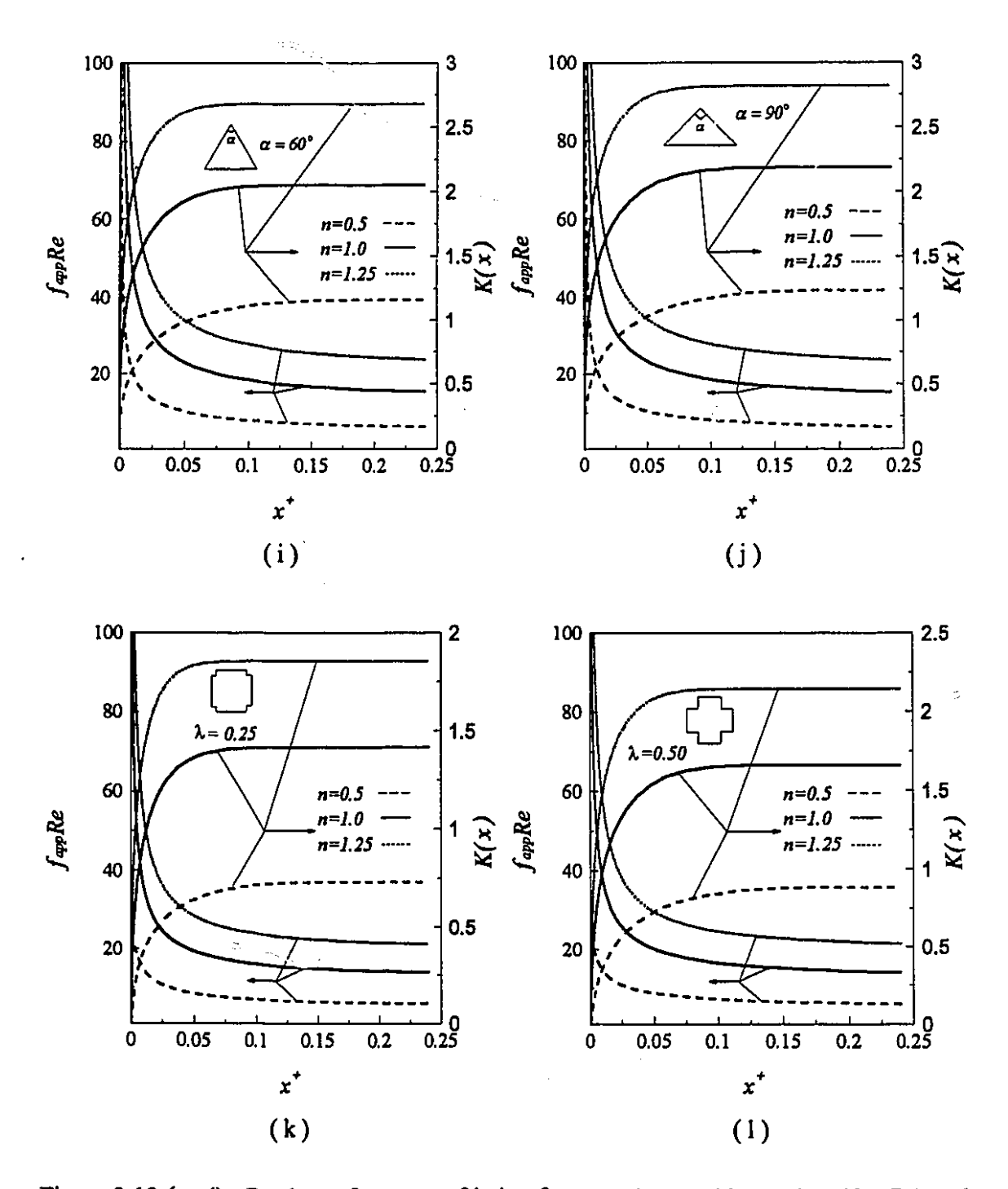


Figure 3.12 (a - 1) Product of apparent friction factor and Reynolds number $(f_{app} Re)$ and incremental pressure drop (K(x)) vs. dimensionless axial distances for different power law indices and various geometries, Re=500.

Table 3.13 Predicted fully developed flow and heat transfer characteristics for different power law indices and various duct geometries.

		f.Re	Umax	K (∞)	L^{\star}	Nu _T	Nu _{H2}
	n=0.5	6.321	1.665	0.632	0.098	3.950	4.744
Circular	n=1.0	16.005	1.996	1.268	0.054	3.659	4.363
	n=1.25	25.231	2.108	1.701	0.037	3.590	4.272
	n=0.5	7.994	1.327	0.351	0.025	7.950	8.758
Parallel plates	n=1.0	23.879	1.491	0.763	0.011	7.541	8.235
	n=1.25	40.694	1.546	1.089	0.050	7.442	8.109
	n=0.5	5.772	1.760	0.901	0.131	3.190	3.310
Square	n=1.0	14.234	2.092	1.670	0.071	2.979	3.090
	n=1.25	22.248	2.209	2.222	0.050	2.925	3.032
	n=0.5	6.060	1.734	0.801	0.147	3.600	3.150
Rectangular (A.R.=0.5)	n=1.0	15.570	1.992	1.475	0.084	3.388	3.021
	n=1.25	24.805	2.053	1.935	0.052	3.350	2.998
	n=0.5	6.860	1.600	0.639	0.165	4.922	2.717
Rectangular (A.R.=0.2)	n=1.0	19.077	1.714	1.103	0.074	4.831	2.924
	n=1.25	31.456	1.749	1.417	0.034	4.817	2.996
	n=0.5	6.223	1.747	0.764	0.143	3.480	3.038
Semi-circular	n=1.0	15.860	2.058	1.437	0.076	3.318	2.920
1	n=1.25	25.365	2.146	1.894	0.051	3.265	2.880

Table 3.13 continued

			_				
	n=0.5	5.951	1.744	0.765	0.133	3.206	3.121
Circular-sector ($\alpha = 90^{\circ}$)	n=1.0	14.820	2.079	1.451	0.072	3.060	2.980
:	n=1.25	23.216	2.181	1.901	0.048	3.013	2.937
	n=0.5	5.761	1.792	0.837	0.143	2.936	2.510
Circular-sector ($\alpha = 60^{\circ}$)	n=1.0	14.248	2.134	1.582	0.077	2.820	2.430
	n=1.25	22.332	2.242	2.078	0.052	2.789	2.408
	n=0.5	5.455	1.877	1.159	0.165	2.594	1.951
Equilateral triangular	n=1.0	13.340	2.230	2.043	0.100	2.503	1.896
·	n=1.25	20.978	2.343	2.662	0.069	2.478	1.880
	n=0.5	5.383	1.916	1.236	0.175	2.409	1.370
Right isosceles triangular	n=1.0	13.167	2.268	2.176	0.112	2.350	1.351
:	n=1.25	20.748	2.377	2.799	0.077	2.335	1.344
	n=0.5	5.317	1.711	0.727	0.130	2.883	3.170
Cross-shape ($\lambda = 0.25$)	n=1.0	12.625	2.034	1.404	0.074	2.667	2.956
	n=1.25	19.356	2.148	1.835	0.053	2.628	2.903
	n=0.5	5.209	1.821	0.881	0.159	2.508	2.598
Cross-shape ($\lambda = 0.50$)	n=1.0	12.479	2.171	1.648	0.097	2.338	2.443
<u></u>	n=1.25	19.349	2.287	2.121	0.068	2.300	2.413
	n=1.25	19.349	2.287	2.121	0.068	2.300	2.413

The location of the maximum axial velocity is different for various geometries. Table 3.14 summarizes the predicted location for various ducts. It should be noted the origins of the coordinates are based on Table 2.1 in Chapter 2.

Table 3.14 The locations of maximum velocity for different geometries

Geome	tries	Y	Z
Circular		0.000	0.500
Parallel Plates	A.R.=0.0	0.250	
	A.R.=0.2	0.000	0.300
Rectangular	A.R.=0.5	0.000	0.375
	A.R.=1.0	0.000	0.500
	$\alpha = 60^{\circ}$	0.829	0.479
Circular Sector	$\alpha = 90^{\circ}$	0.478	0.478
	$\alpha = 180^{\circ}$	0.000	0.393
Triangular	$\alpha = 60^{\circ}$	0.866	0.500
	α = 90°	1.207	0.472
Cross Shape	$\lambda = 0.25$	0.000	0.533
	$\lambda = 0.50$	0.000	0.667

Secondary flow (cross-stream velocity vector) in the hydrodynamically developing region due to the growing boundary layer for different power law indices and various geometries are presented in Figs. 3.13 (a - c) through 3.16 (a - c). The maximum secondary flow at specified axial distance for higher power law index is stronger which can be attributed to higher deviation of axial velocity profile from fully developed condition for higher power law index.

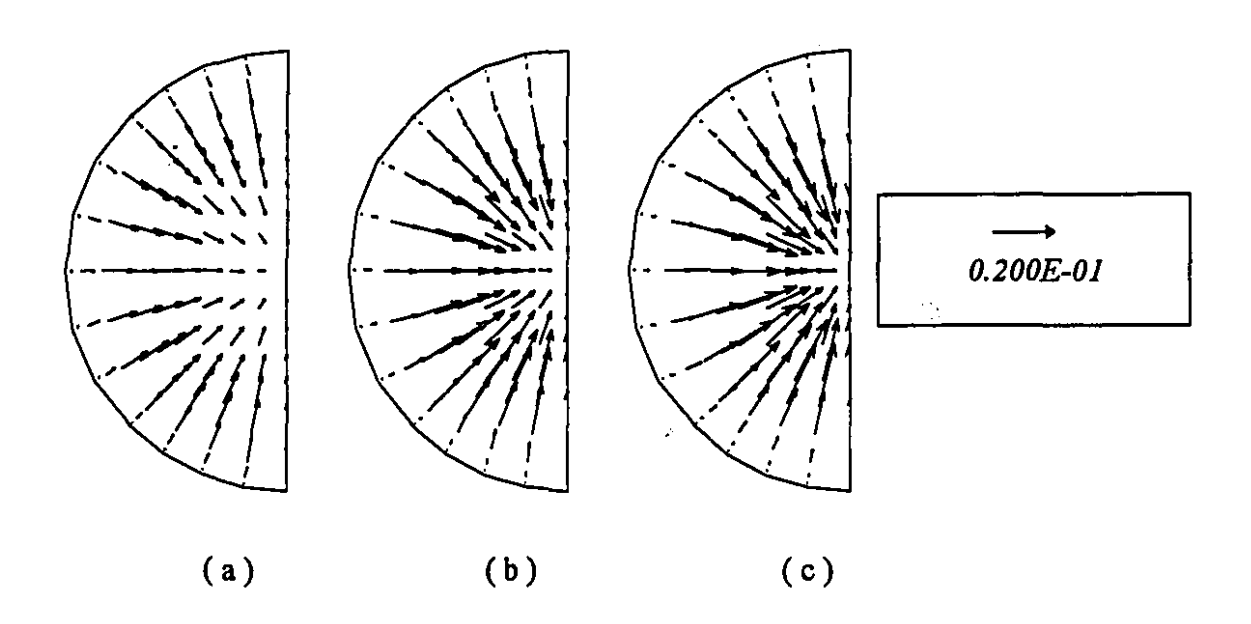


Figure 3.13 (a - c) Secondary flow for different power law indices at $x^{+}=0.002$: circular tube (a)-n=0.5, (b)-n=1.0, (c)-n=1.25.

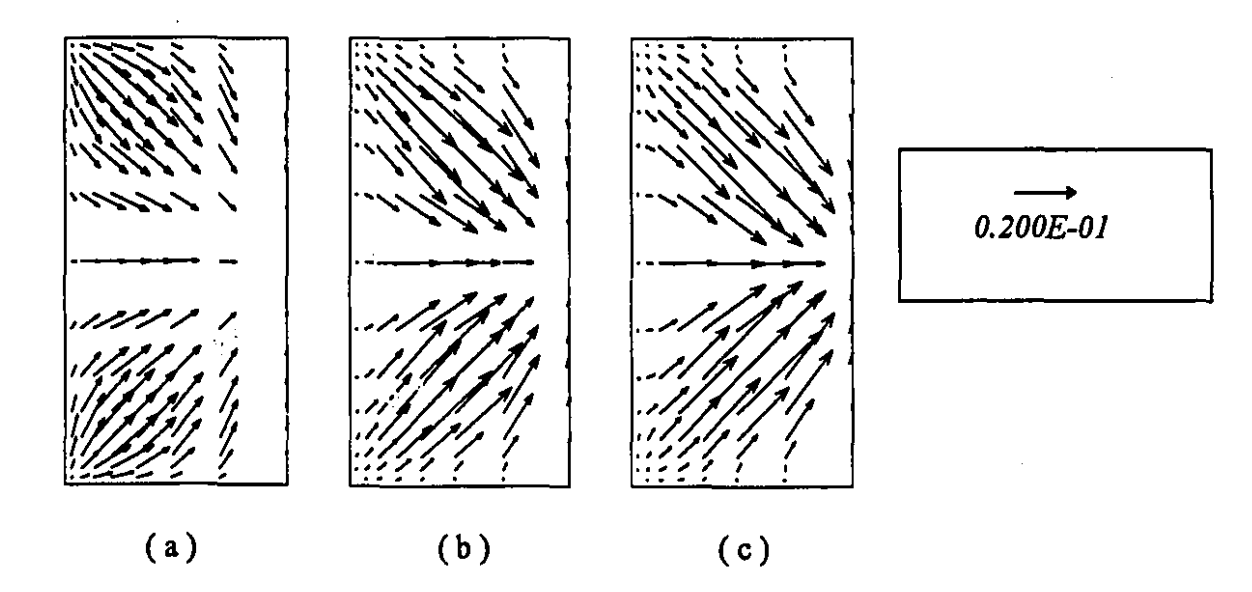


Figure 3.14 (a - c) Secondary flow for different power law indices at $x^{+}=0.002$: square duct (a)-n=0.5, (b)-n=1.0, (c)-n=1.25.

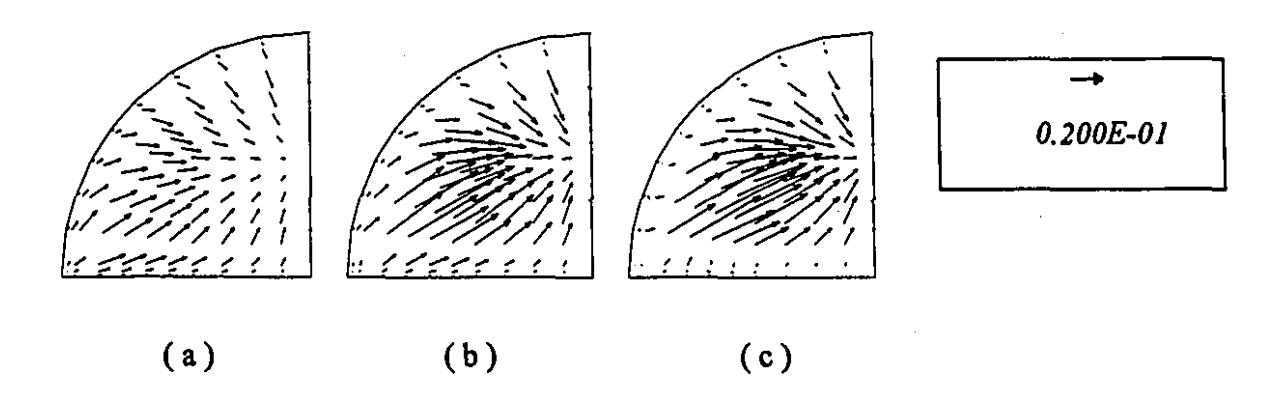


Figure 3.15 (a - c) Secondary flow for different power law indices at $x^+=0.002$: semi-circular duct (a)-n=0.5, (b)-n=1.0, (c)-n=1.25.

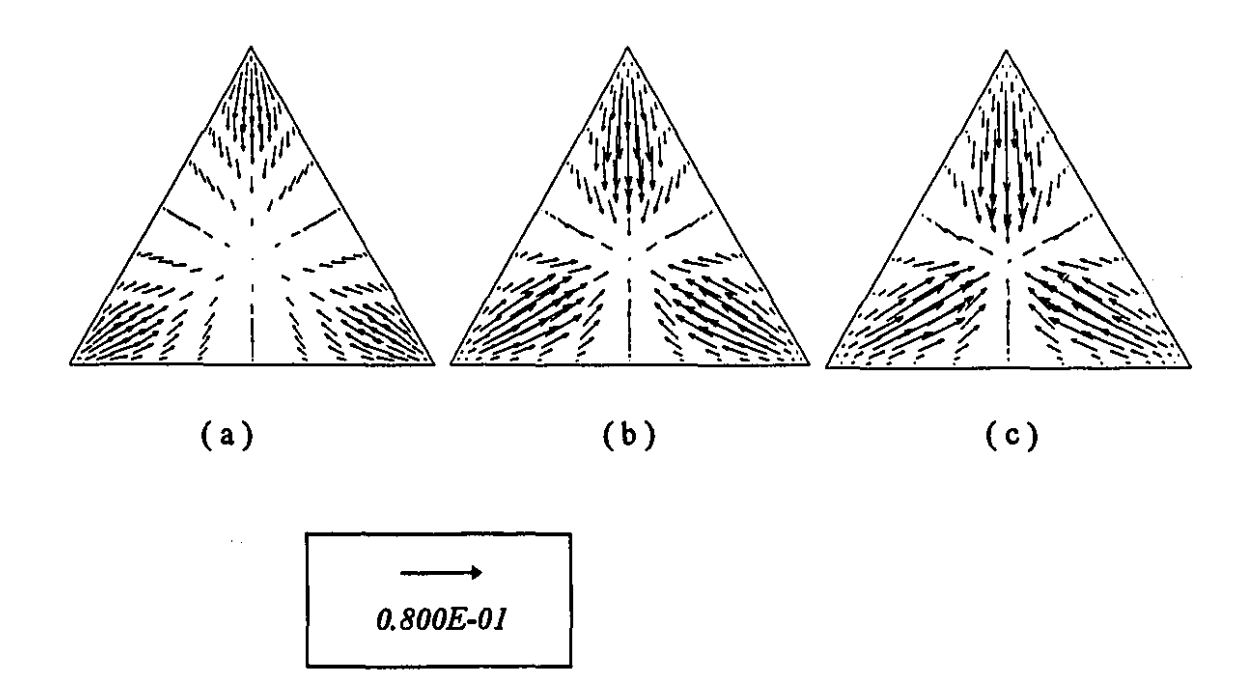


Figure 3.16 (a - c) Secondary flow for different power law indices at $x^{+}=0.002$: equilateral triangular duct (a)-n=0.5, (b)-n=1.0, (c)-n=1.25.

3.2.2 Heat transfer

Fig. 3.17 (a - x) and Tables A13 through A24 in Appendix A show the local Nusselt number and dimensionless bulk temperature for different power law indices, T and H2 boundary conditions, and various geometries. Fully developed Nusselt number values for various geometries are tabulated in Table 3.13. Generally the Nusselt number for both T and H2 boundary conditions increases with decreasing n because of the steeper velocity gradient in the wall region for lower n values. Due to flow development, this difference decreases further downstream. For the H2 boundary condition, $\theta_{b,x}$ is not affected by n. This can be explained by the fact that the heat flux is the same for different power law indices, therefore the difference in velocity profiles for different n's is not reflected in the bulk temperature.

The influence of n on Nusselt number for both T and H2 boundary conditions and for all geometries is significant. For example from Tables A13 through A24 at $x^*=0.0002$ the enhancement of $Nu_{T,x}$ for n=0.5 relative to n=1.0 ranges from about 23 % for the semi-circular duct to 45 % for the equilateral triangular duct. The corresponding values for $Nu_{H2,x}$ are from 26% for parallel plates to 36 % for right isosceles triangular duct. Also, the entrance region is very important factor which influences heat transfer. From Tables A13 through A24, $Nu_{T,x}$ and $Nu_{H2,x}$ for all power law indices studied are noticeably higher in the developing region than their fully developed values.

At the fully developed condition for all geometries decreasing n values results in increasing Nu_T and Nu_{H2} except for the rectangular duct with an aspect ratio of 0.2 for which Nu_{H2} decreases. This behavior may be is due to the reversed effect of the wall velocity gradient on the short side of the channel.

Fig. 3.18 (a - f) presents the dimensionless circumferential heat flux for the T boundary condition and the dimensionless circumferential wall temperature distribution for the H2 boundary condition for different power law indices and various geometries. For ducts with sharp corners subjected to the H2 boundary condition, due to the lower velocity in the corner region, the fluid temperature in this region is higher than that close

to the central part of the walls. Thus the maximum wall temperature occurs at the corners and the minimum wall temperature midway between the corners. At the fully developed condition because of the constant heat flux around the periphery and the higher wall temperature at the corners the peripheral average wall temperature increases causing a reduction of Nu_{H2} relative to its counterpart in geometries without sharp corners (e.g. parallel plates and circular duct).

For the T boundary condition, for ducts with sharp corners the lower velocity in the corner region yields a higher fluid temperature close to the corners (lower dimensionless temperature), lowering the heat flux close to the corners (Fig. 3.18). Therefore the minimum wall heat flux occurs at the corners and the maximum wall heat flux midway between the corners. For the fully developed condition lower heat flux from the corners causes a lower Nusselt number relative to ducts without sharp corners. As mentioned earlier the higher velocity gradient close to the walls for lower power law index result in higher heat fluxes for pseudoplastic fluids (Fig. 3.18).

Generally for the T boundary condition and for circular cross-sectional ducts as well as parallel plates the temperature of the fluid close to the walls approaches the wall temperature; so the temperature gradient of the fluid at the wall is smaller for the T boundary condition than that for the constant heat flux case. This results in a lower Nusselt number for the former case. This difference in Nusselt numbers for a duct with sharp corners is different compared to round ducts or parallel plate channels. As was explained before, for ducts with sharp corners fully developed Nusselt numbers for both T and H2 boundary conditions are lower than those for circular tubes and parallel plates, but the decrease in Nusselt numbers due to the presence of sharp corners is more pronounced for H2 than for the T boundary condition. Thus the difference in Nusselt numbers between T and H2 boundary conditions decreases and sometimes (depending on the geometry) the Nusselt number for H2 is less than that for T boundary condition.

In the fully developed region the presence of sharp corners reverses the effect of n on the velocity gradient close to the corner (Fig 3.10 (h)). Therefore the difference

between Nu_{H2} of different power law indices diminishes with decrease in the angle of the corner or increase in the number of corners.

Table 3.15 presents the ratio $\frac{Nu_{H2}}{Nu_T}$ at the fully developed condition for different power

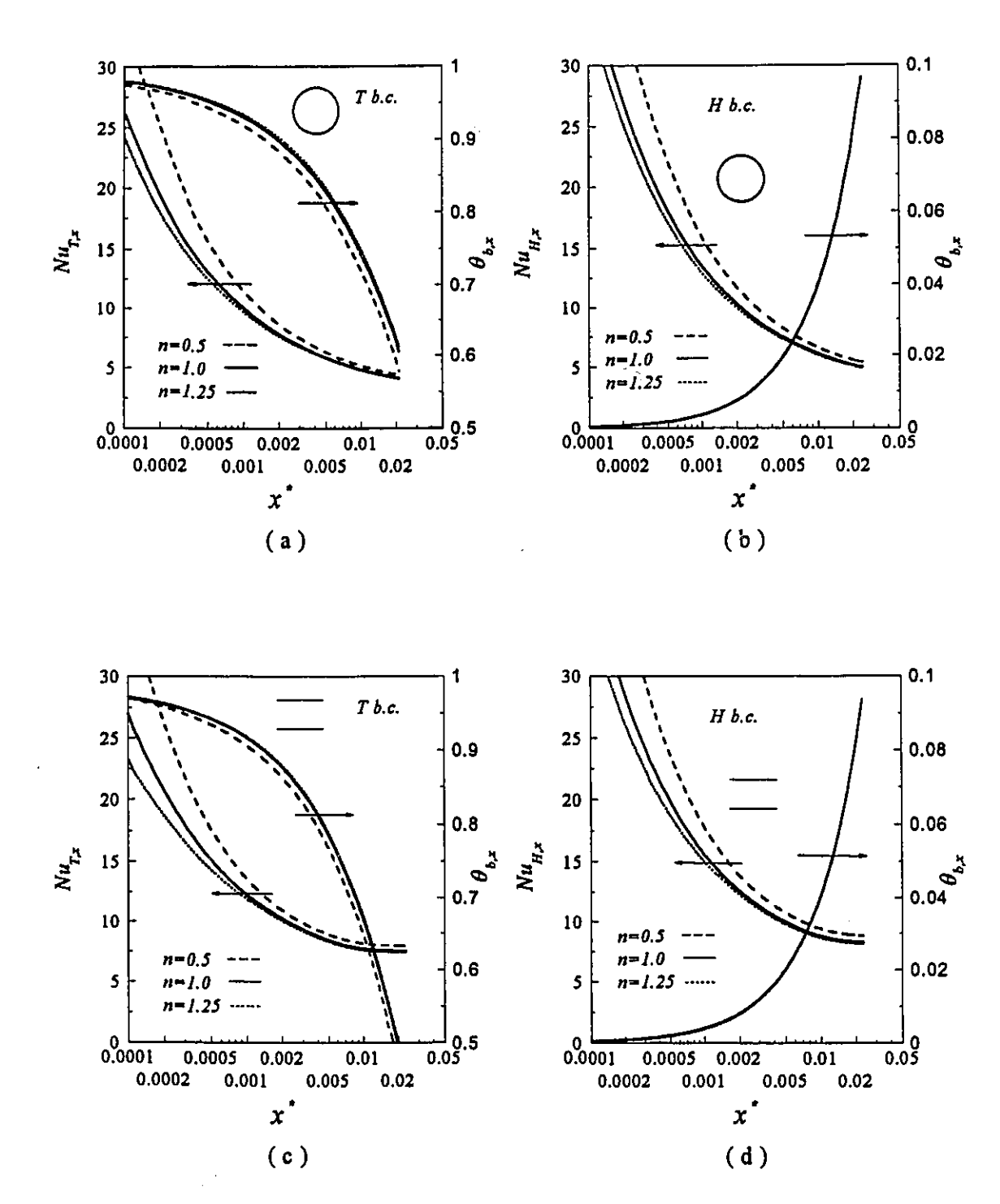
law indices for the various geometries studied. From this table, for n=0.5, $\frac{Nu_{H2}}{Nu_T}$ for all geometries ranges from 0.55 for the rectangular duct with aspect ratios of 0.2 to 1.2 for the circular tube which reflects the strong effect of the presence of sharp corner on Nu_{H2} .

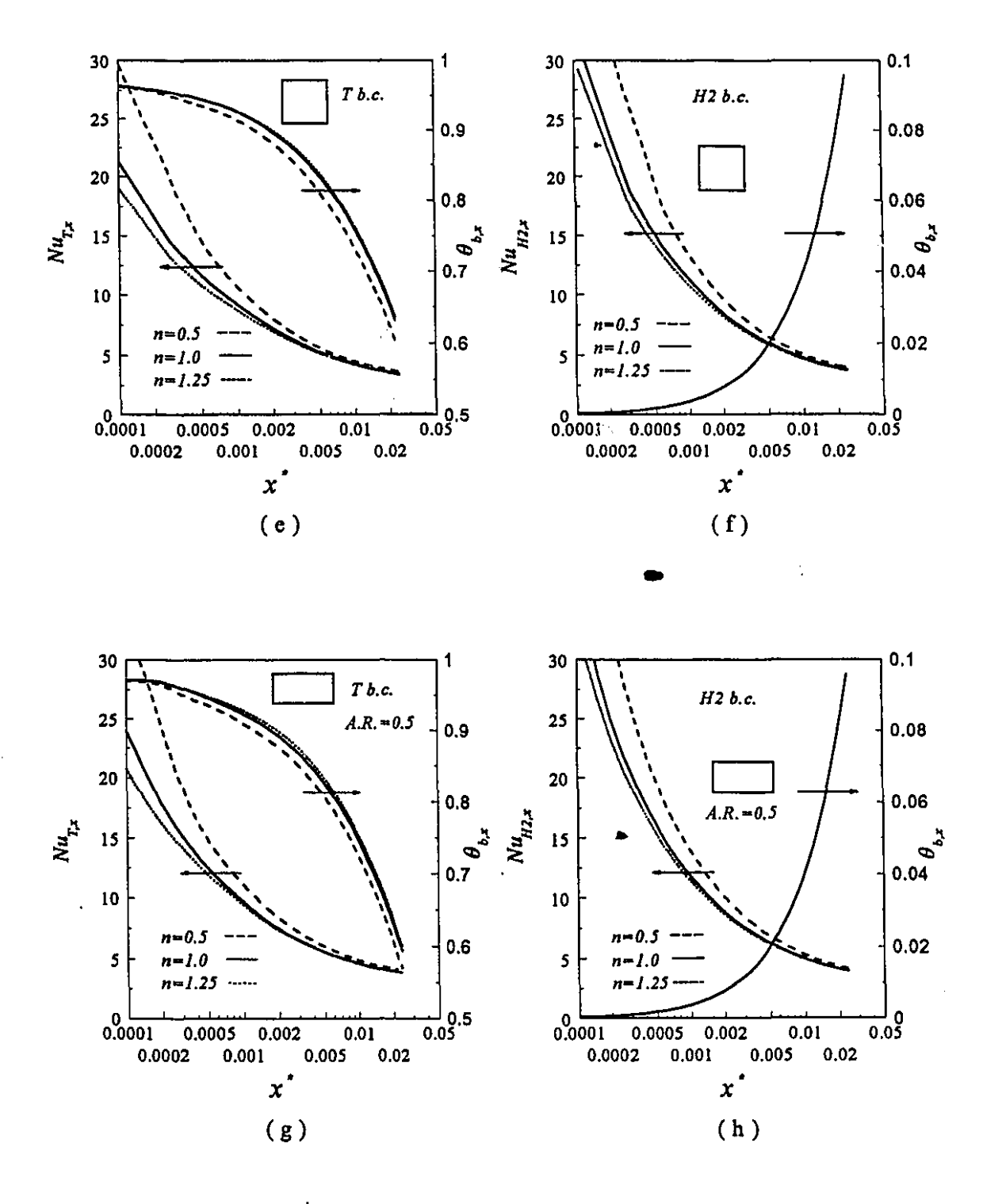
To investigate the effect of rounding the corners on Nusselt number two 'rounded' square channels were tested numerically with rounding corner radii of a/20 and a/6, where a is the length of the side of the channel. Table 3.15 includes the ratio of Nusselt numbers for rounded corner square ducts. From this table rounding corner (R.C.=a/6) yields an increase of 5.8 % and 4.8 % in $\frac{Nu_{H2}}{Nu_T}$ for n=0.5 and n=1.0,

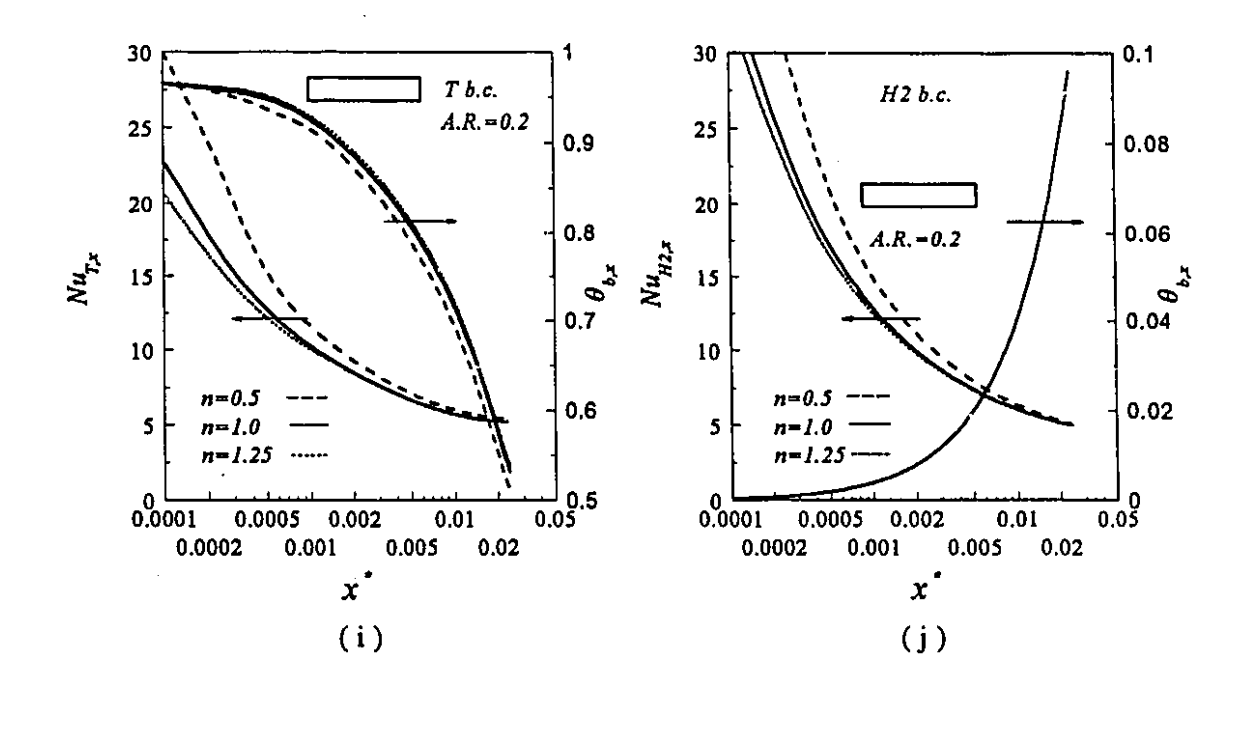
respectively. The effect of the rounding of corners of square duct on the flow and heat transfer characteristics is explained in detail in Chapter 4.

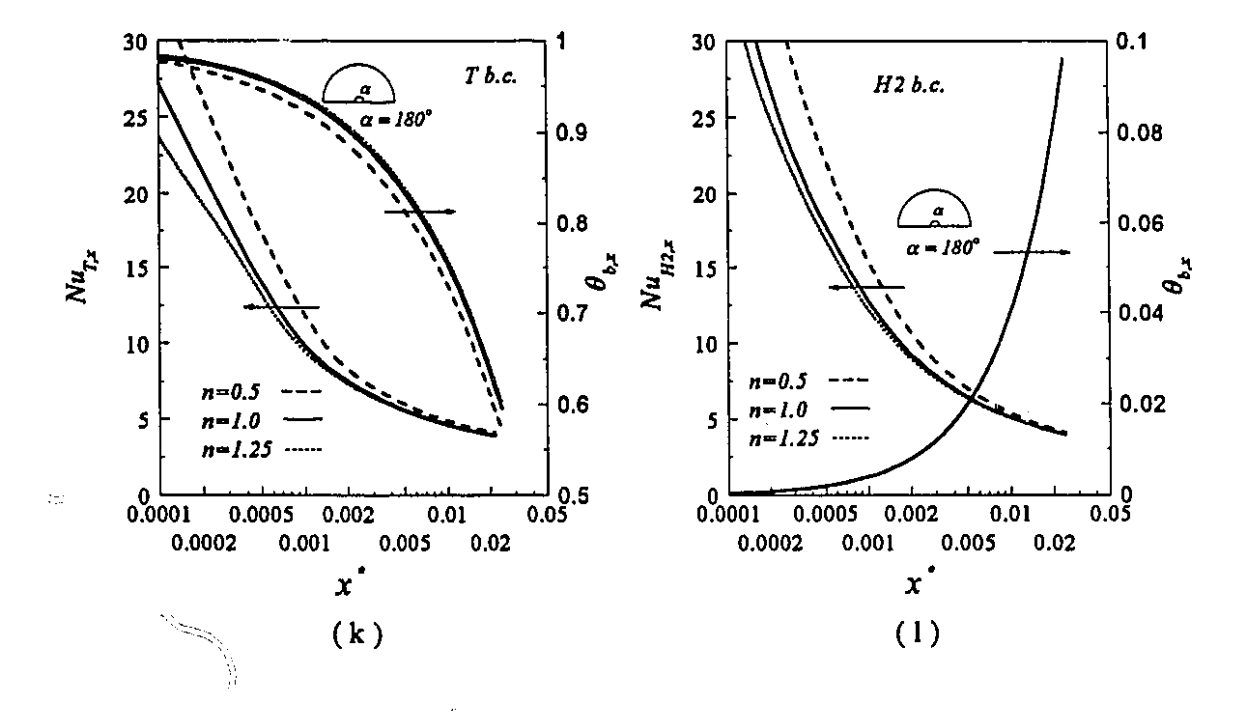
Table 3.15 $\frac{Nu_{H2}}{Nu_T}$ in the fully developed regions for different geometries.

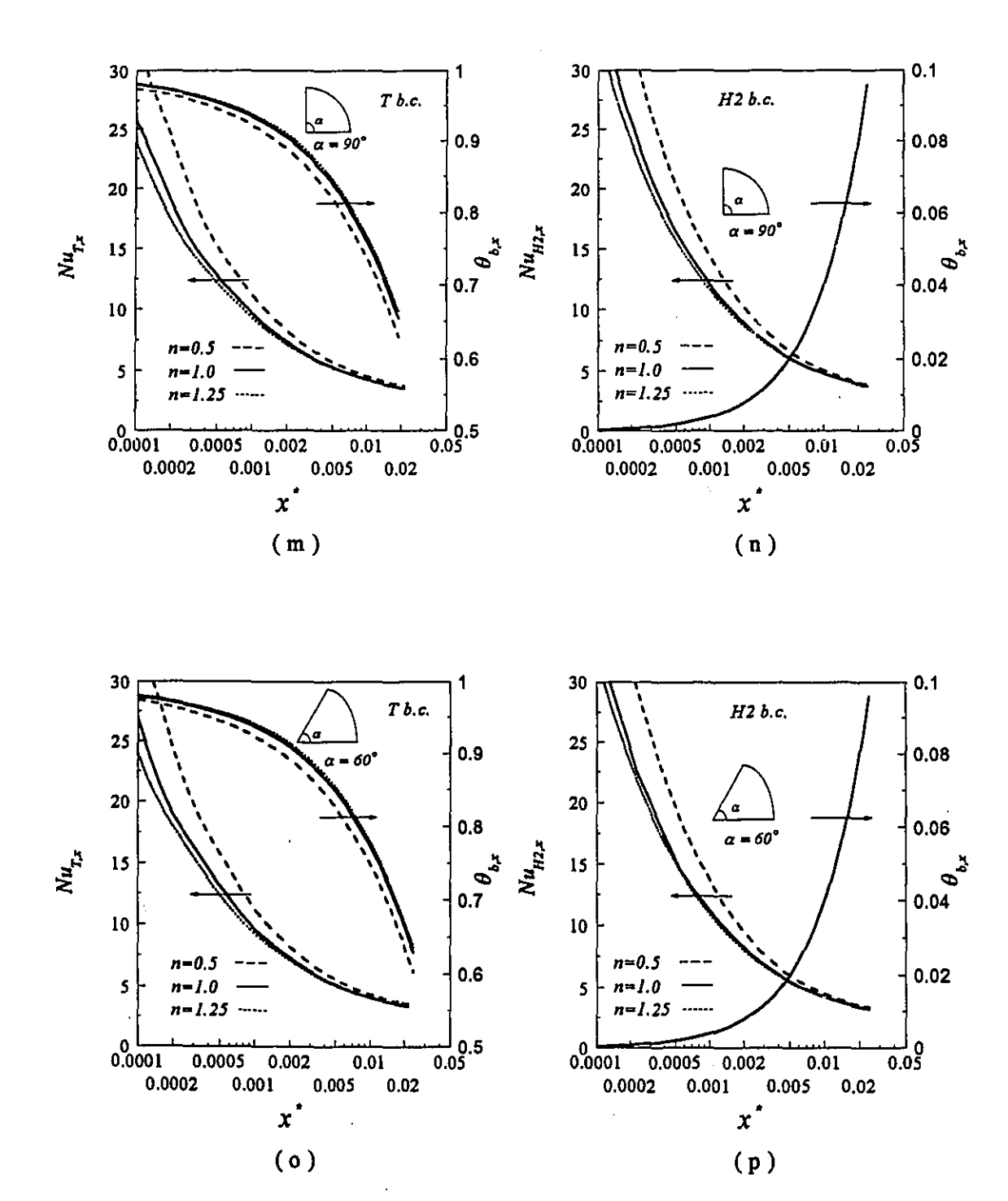
Geom	$\frac{\mathit{Nu_{H2}}}{\mathit{Nu_{T}}}$		
		n=0.5	n=1.0
Circular		1.20	1.19
Parallel Plates	A.R. =0.0	1.10	1.09
	A.R.=0.2	0.55	0.61
Rectangular	A.R.=0.5	0.88	0.89
	A.R.=1.0	1.04	1.04
Rounded Corners	R.C.=a/20	1.06	1.06
Square	R.C.=a/6	1.10	1.09
	$\alpha = 60^{\circ}$	0.86	0.86
Circular-Sector	α = 90°	0.97	0.97
	$\alpha = 180^{\circ}$	0.87	0.88
	$\alpha = 60^{\circ}$	0.75	0.76
Triangular	$\alpha = 90^{\circ}$	0.57	0.57
	$\lambda = 0.25$	1.10	1.10
Cross-Shape	$\lambda = 0.5$	1.04	1.04



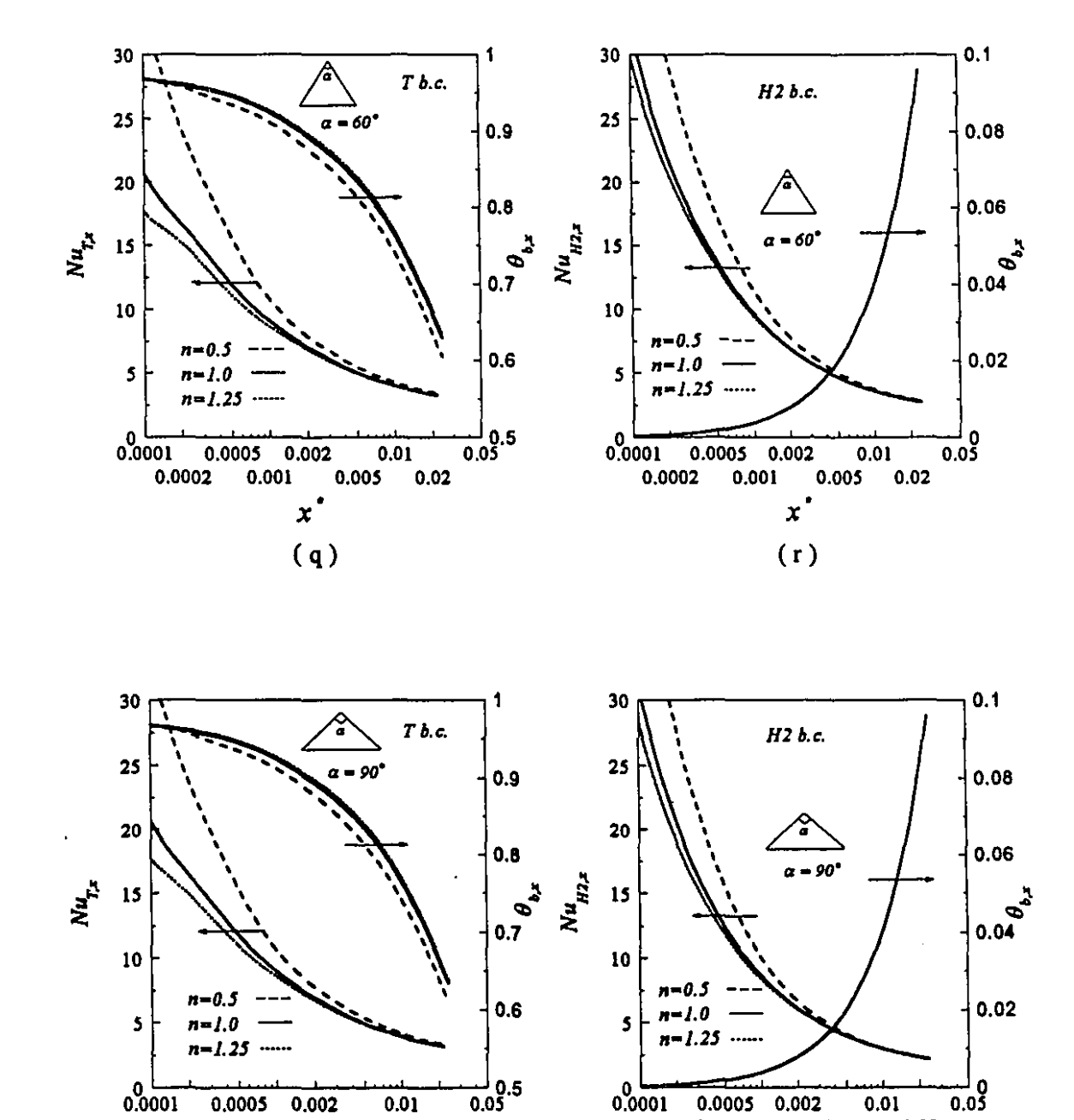








......



0.0002

0.001

x.

(t)

0.005

0.02

0.0002

0.001

(s)

0.005 0.02

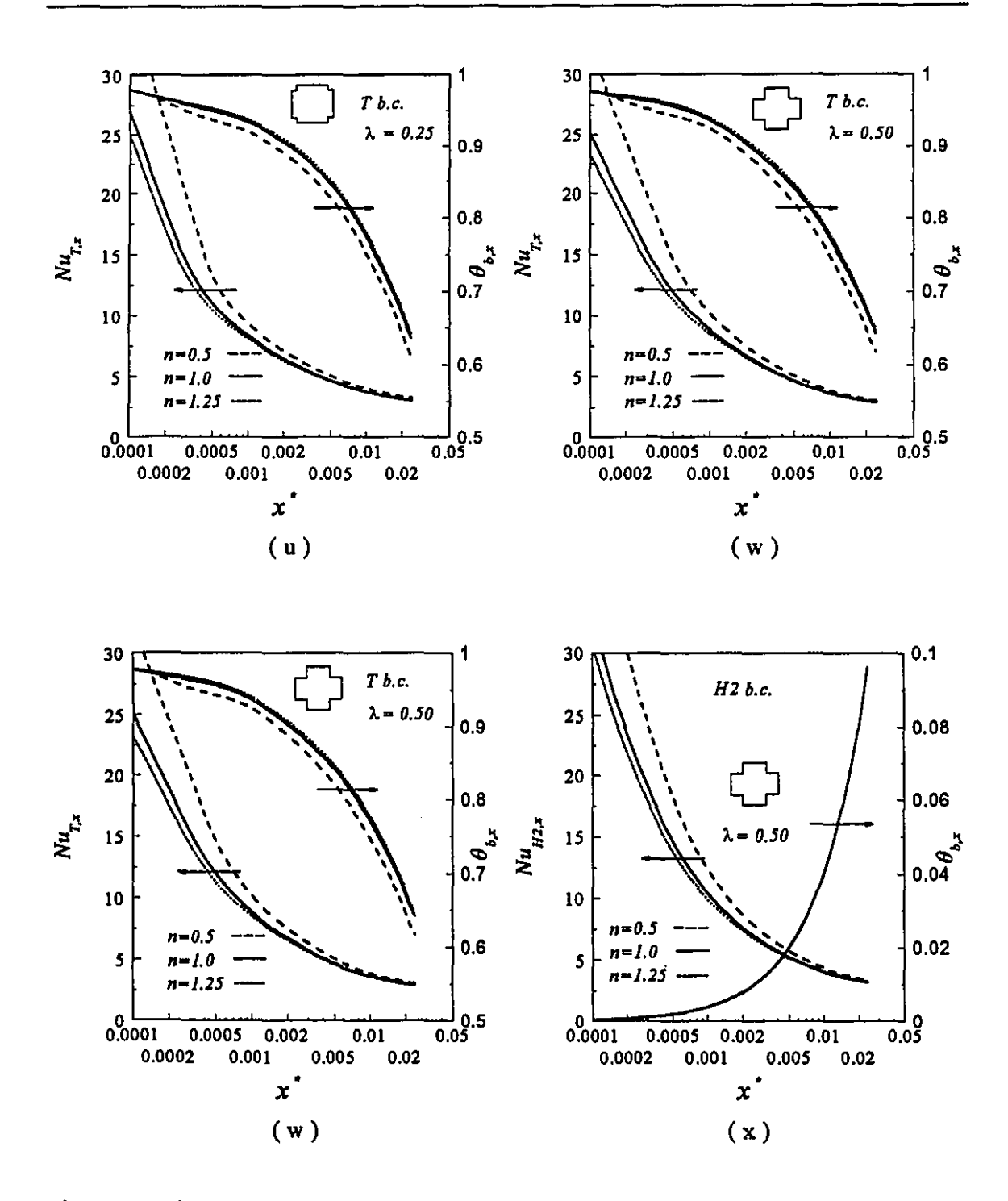
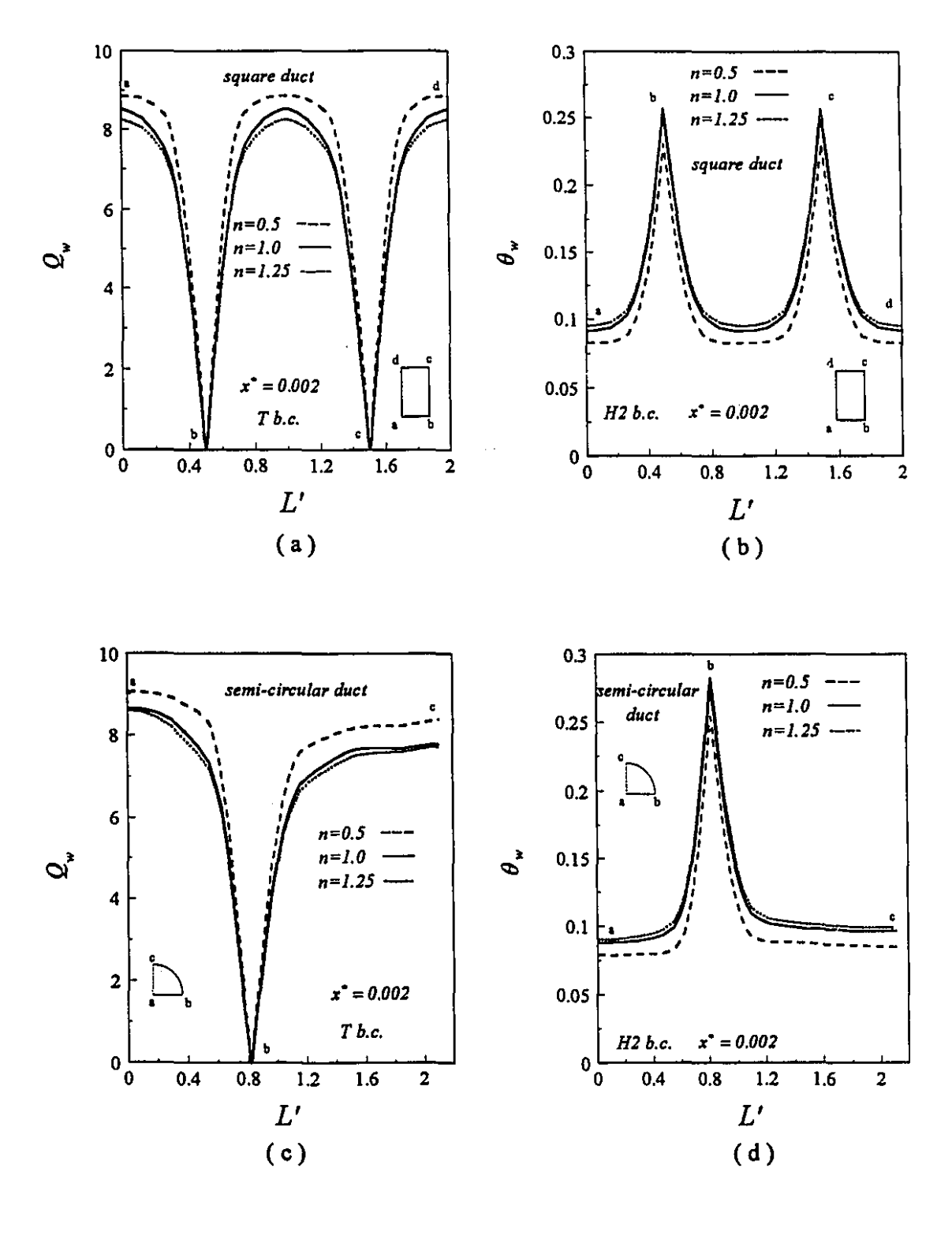


Figure 3.17 (a - x) Nusselt number and dimensionless bulk temperature vs. dimensionless axial distance for different power law indices and various geometries, Re=500, Pr=10.



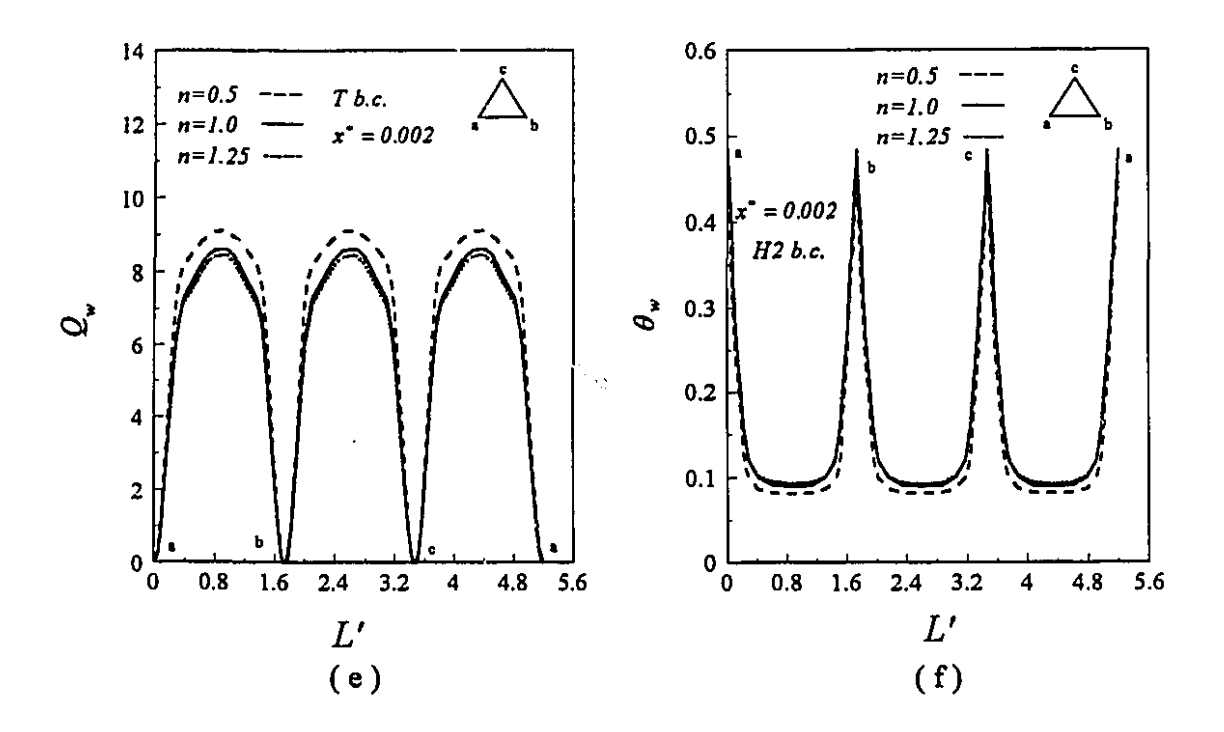


Figure 3.18 (a - f) Circumferential wall heat flux (T b.c.) and circumferential wall temperature (H2 b.c.) for different power law indices and various geometries, Re=500, Pr=10.

Ç

3.3 Conclusions

Numerical results for the steady laminar heat transfer under hydrodynamically and thermally developed as well as simultaneously developing conditions of Newtonian and power law non-Newtonian fluids flowing through various geometries were presented. The analysis considered the effects of the power law index under both T and H2 boundary conditions. The favorable comparison of the present results with available experimental data as well as analytical and numerical results supports the accuracy of this study.

This work has shown that the influence of the entrance region of the channels and also the effect of the power law index on the flow and heat transfer characteristics can be significant. $f_{app}Re$ for pseudoplastic fluids is appreciably lower than that for dilatant fluids. For both boundary conditions the local Nusselt number for lower power law index is noticeably higher.

1

Chapter 4

Effects of Temperature-Dependent Viscosity, Viscous Dissipation, and Prandtl Number

This chapter includes the results of numerical simulation for the effects of several key parameters on simultaneously developing laminar flow and heat transfer through circular, square, semicircular, and equilateral triangular ducts. The parameters examined are: temperature-dependent viscosity, viscous dissipation, simultaneous effects of temperature-dependent viscosity and viscous dissipation, and Prandtl number.

Results are given for both T and H2 thermal boundary conditions as well as different power law indices. It should be noted that it is not possible to generalize the results including simultaneous effects of all parameters. Each case must be solved numerically. However, the results presented in this chapter can be used to anticipate the influence of the key parameters involved on both the flow and heat transfer characteristics.

4.1 Effect of temperature-dependent apparent viscosity

The apparent viscosity of most liquids decreases with increase in temperature. Thus for the case of heating the temperature-viscosity coefficient (B) is positive for T and negative for H2 boundary conditions.

The effect of temperature-dependent viscosity on the dimensionless central-plane axial velocity profile for both T and H2 boundary conditions can be observed from Fig. 4.1 (a - h). Dimensionless maximum velocity for various values of B are presented in Fig. 4.2 (a - h).

In the case of heating, for both boundary conditions, due to the effects of temperature-dependent viscosity velocity and velocity gradients near the wall increase (Fig. 4.1(a - h)). Consequently temperature-dependence of viscosity results in lower maximum velocities (Fig. 4.2 (a - h)).

Fig. 4.3 (a - h) and Tables B1 through B4 (Appendix B) show the effect of variable viscosity on the apparent friction factor for both T and H2 boundary conditions. For the T boundary condition, the reference temperature for viscosity is the wall temperature. When variable viscosity (heating case) is considered, the viscosity and velocity gradient in the momentum boundary layer are higher than that for the case of constant viscosity which cause a higher dimensionless pressure drop and consequently higher friction factor.

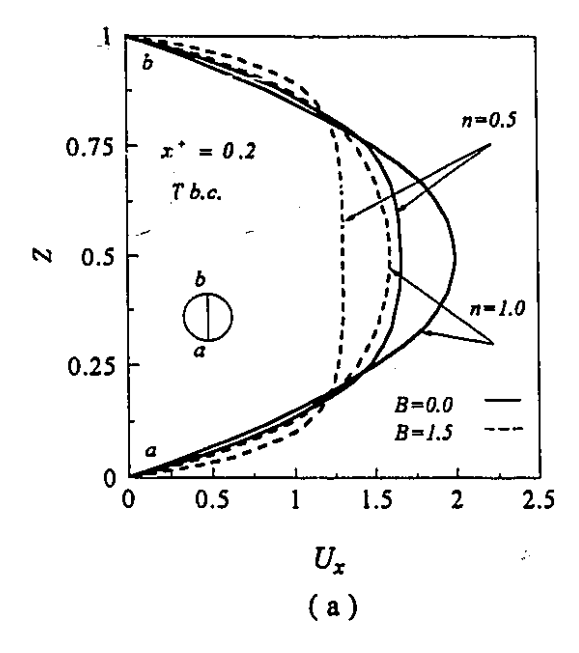
For the H2 boundary condition the inlet fluid temperature is chosen as the reference temperature, therefore considering variable viscosity results in a lower dimensionless pressure drop. For example at x^+ =0.002, f_{app} Re for n=0.5, B=1.5 and T boundary condition increases by about 26 %, 74 %, 24 % and 24 % relative to constant viscosity condition for circular tube, square, semicircular and equilateral triangular ducts, respectively. For the H2 boundary condition $f_{app}Re$ decreases noticeably only far downstream in the channel.

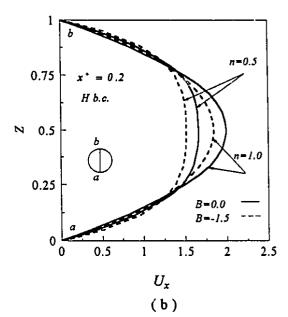
Fig. 4.4 (a - h) presents $Nu_{T,x}$ and $Nu_{H2,x}$ for n=0.5 for various duct geometries. Nusselt numbers for n=1.0 are given in Fig. B1 (a - h) (Appendix B). Also $Nu_{T,x}$ and $Nu_{H2,x}$ for n=0.5 and n=1.0 are tabulated in Tables B5 through B8. For both T and H2 boundary conditions considering temperature-dependent viscosity enhances Nusselt number which is due to the higher velocity close to the walls.

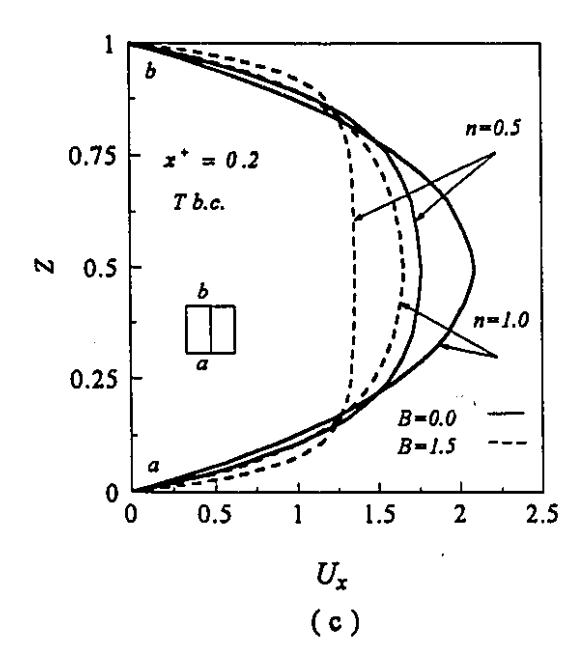
For the T boundary condition, a large difference between the wall and the bulk fluid temperature exists close to the entrance, therefore considering temperaturedependent viscosity induces significant changes in the velocity gradient close to the wall.

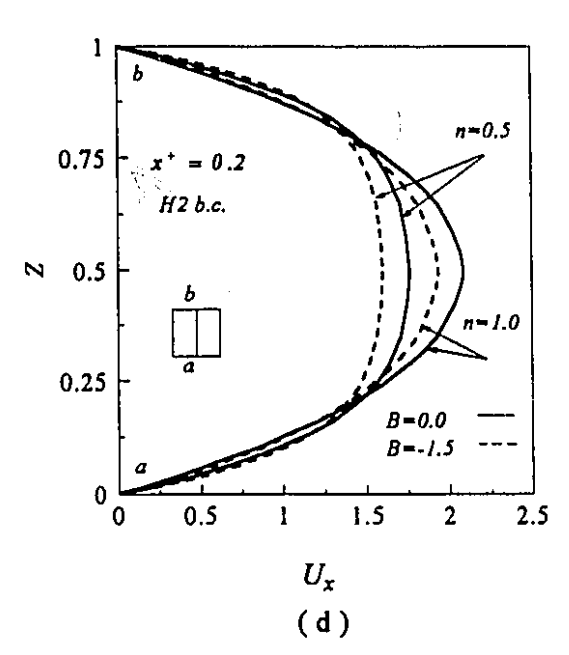
On the other hand, the axial velocity profile in the entrance region is quite flat and the velocity and velocity gradient close the wall are rather high; therefore the temperature-dependence of viscosity does not produce large effects on the velocity profile. Competition between these two factors affects both the pressure drop and the Nusselt number. For example at $x^*=0.0002$ the enhancement of $Nu_{T,x}$ for n=0.5 and B=1.5 is about 18.8 %, 11.7 %, 17.8 %, and 11.5 % relative to the constant viscosity condition for circular, square, semi-circular and triangular ducts, respectively.

For the H2 boundary condition by reason of small temperature difference between the channel walls and the bulk temperature and also because of the relatively flat velocity profiles at locations close to the entrance, the effect of variable viscosity is negligible in this section. Further downstream the increase in $(\theta_{w,x} - \theta_{b,x})$ and development of the velocity make these effects more notable. At $x^*=0.0002$ for n=0.5 and B=-1.5, $Nu_{H2,x}$ increases by only 1.4 % relative to constant viscosity condition for the triangular duct among all studied geometries, while at $x^*=0.01188$ increases of 4.9 %, 7.6 %, 8.9 %, and 10.6 % are observed for circular, square, semi-circular and triangular ducts, respectively. Comparison of the $Nu_{T,x}$ and $Nu_{H2,x}$ results shows smaller effect of temperature-dependent viscosity for the H2 boundary condition.









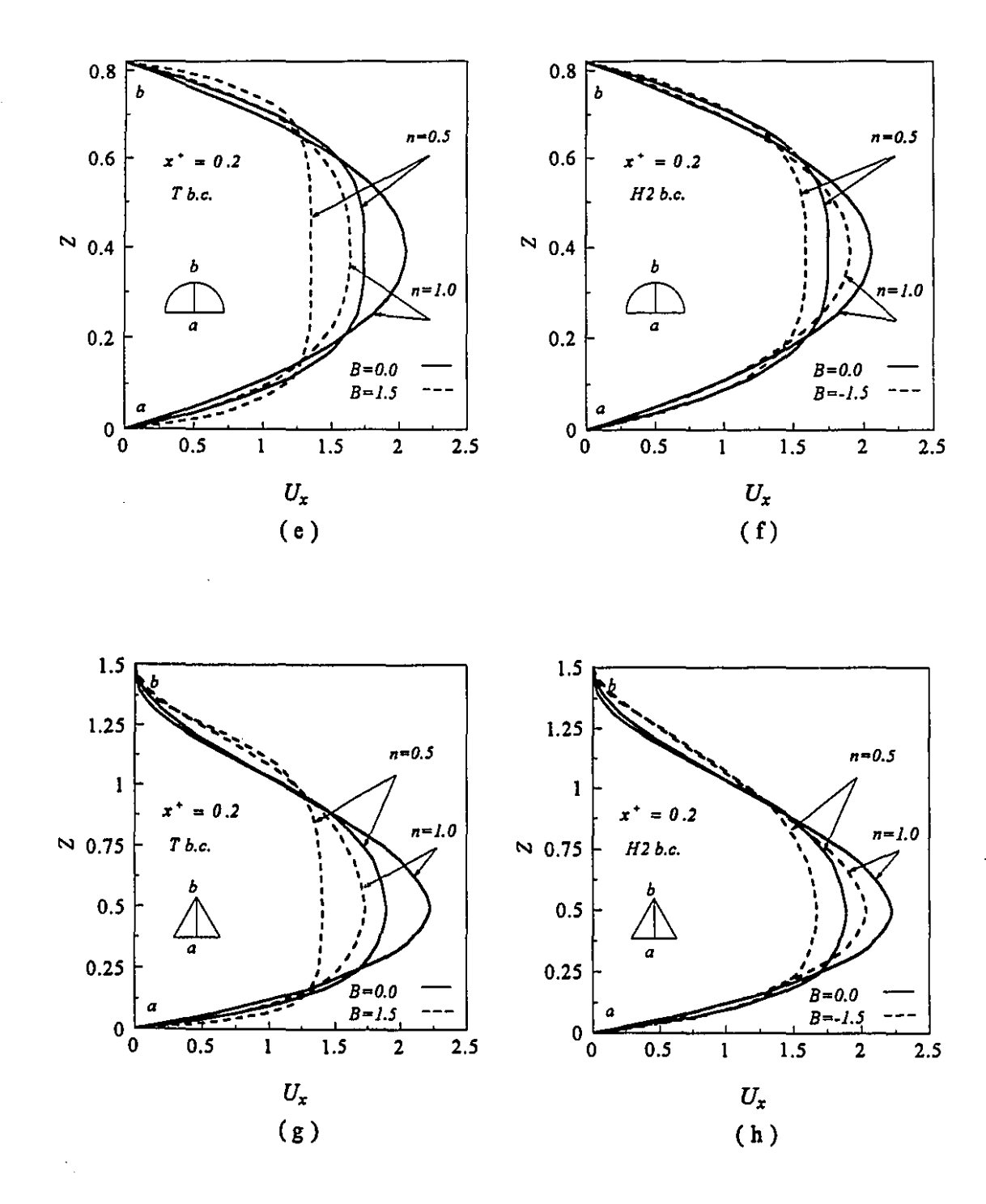
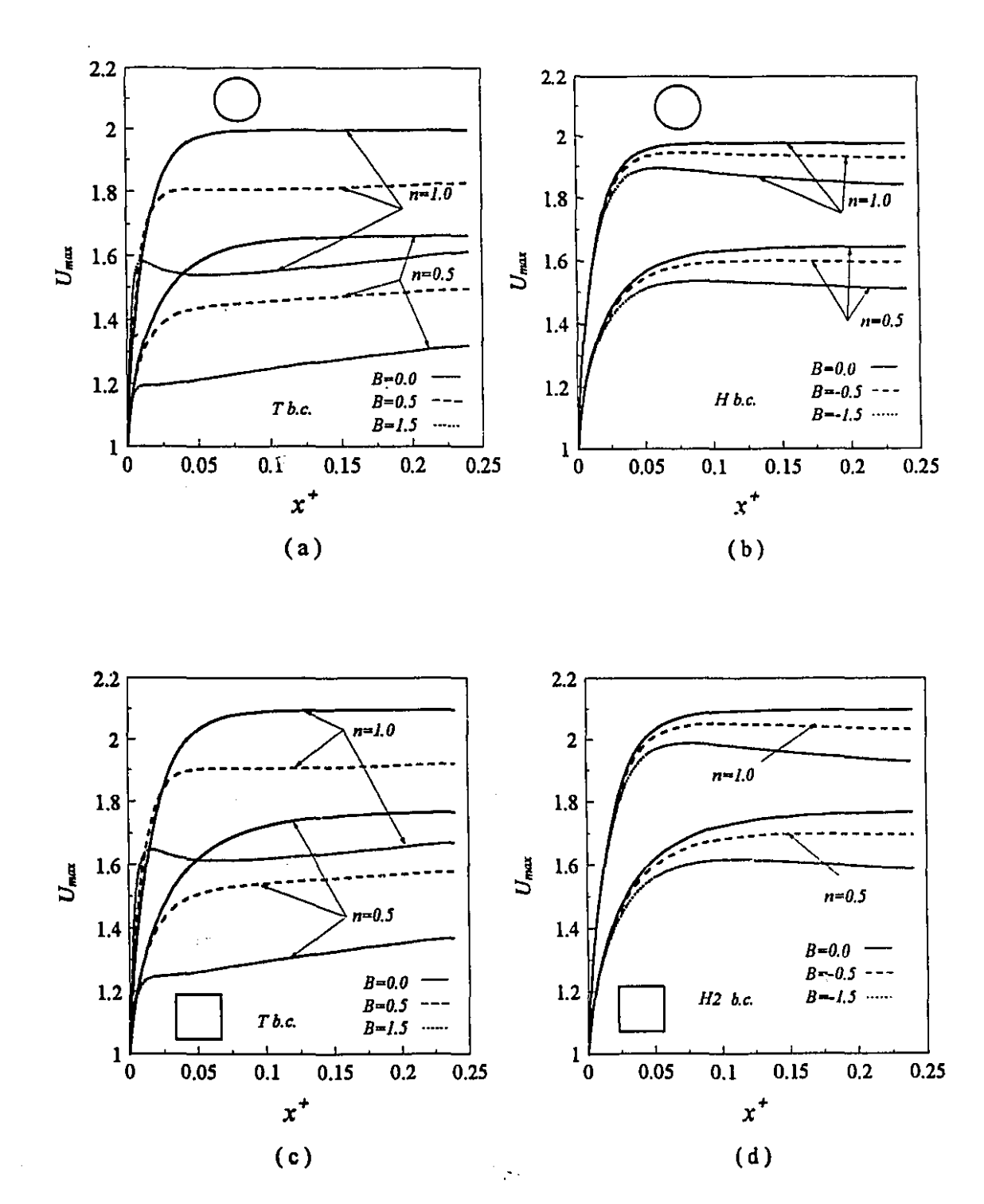


Figure 4.1 (a - h) Effect of temperature-dependent viscosity on the velocity profile for different power law indices and various geometries; Re=500 and Pr=10.



2.2

2.2

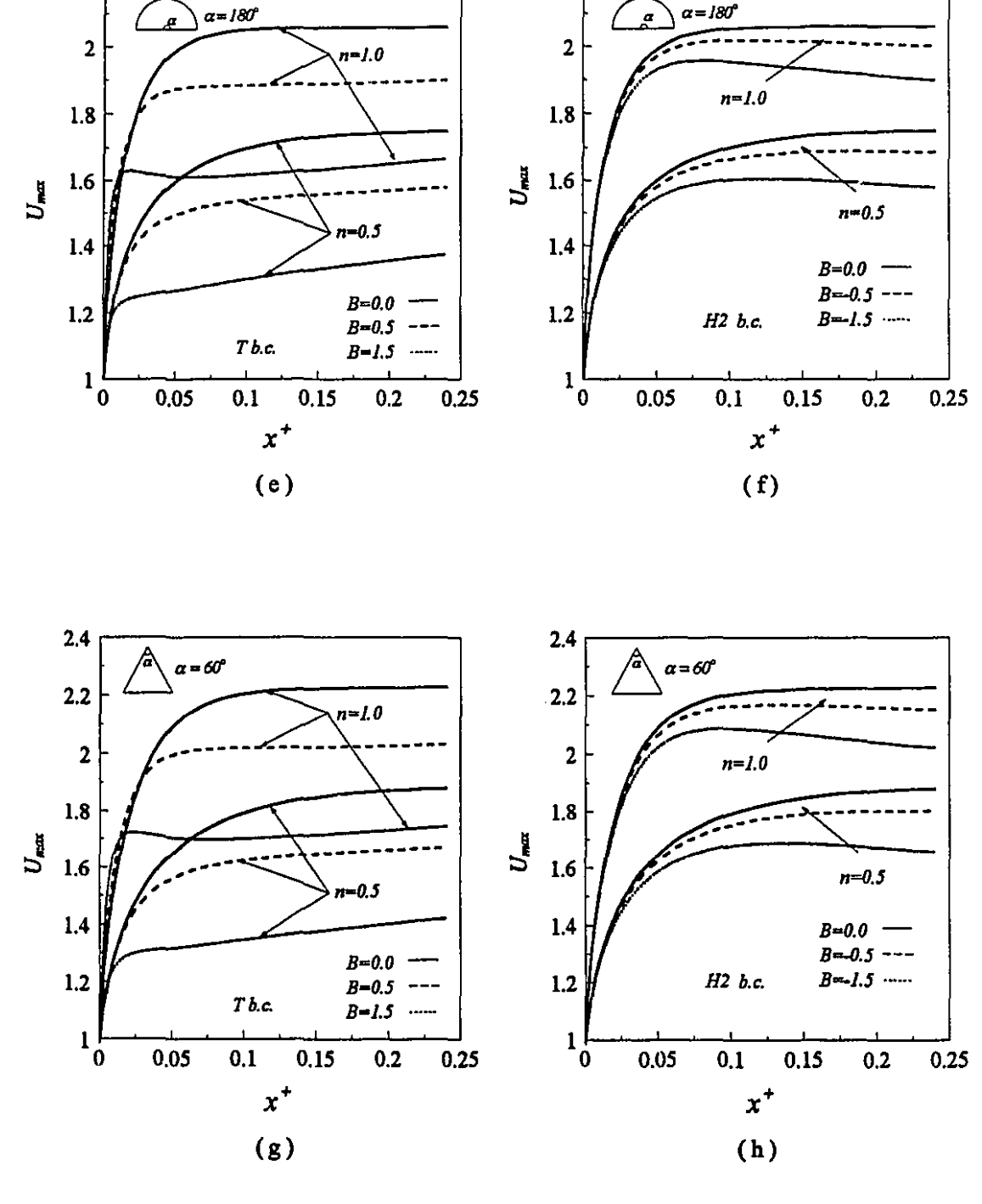
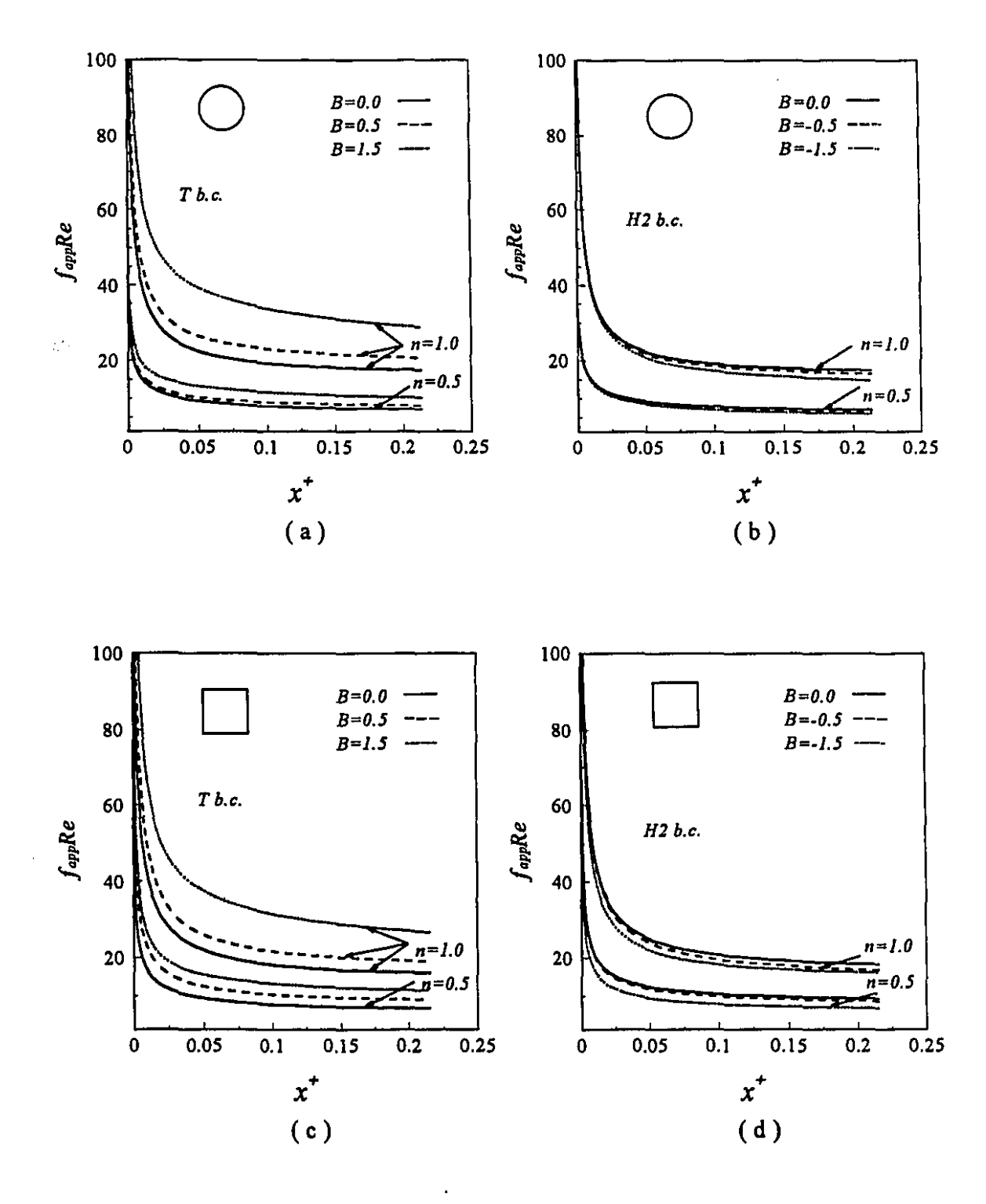


Figure 4.2 (a - h) Effect of temperature-dependent viscosity on the dimensionless maximum velocity for different geometries, Re=500, Pr=10.



٠,

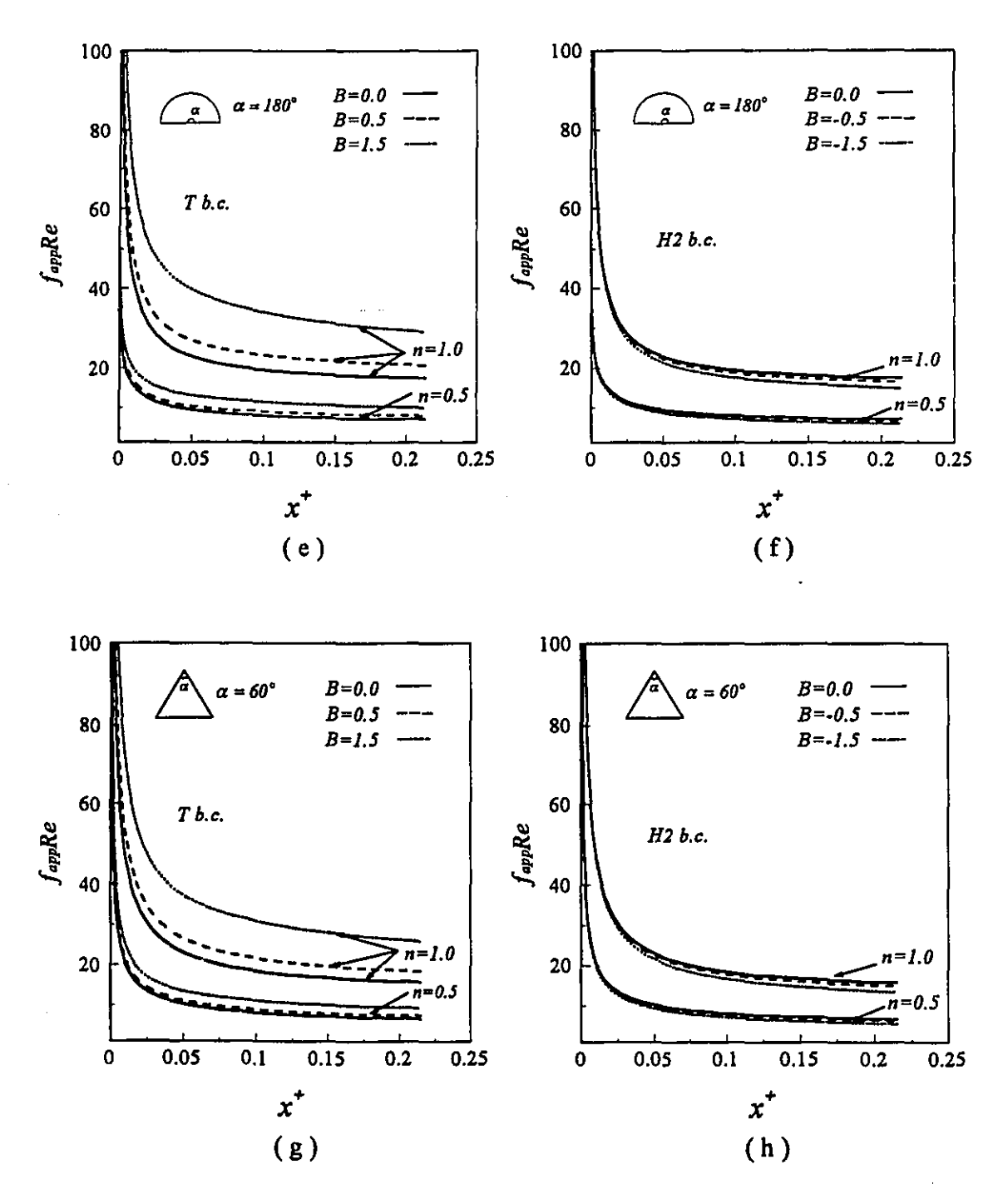
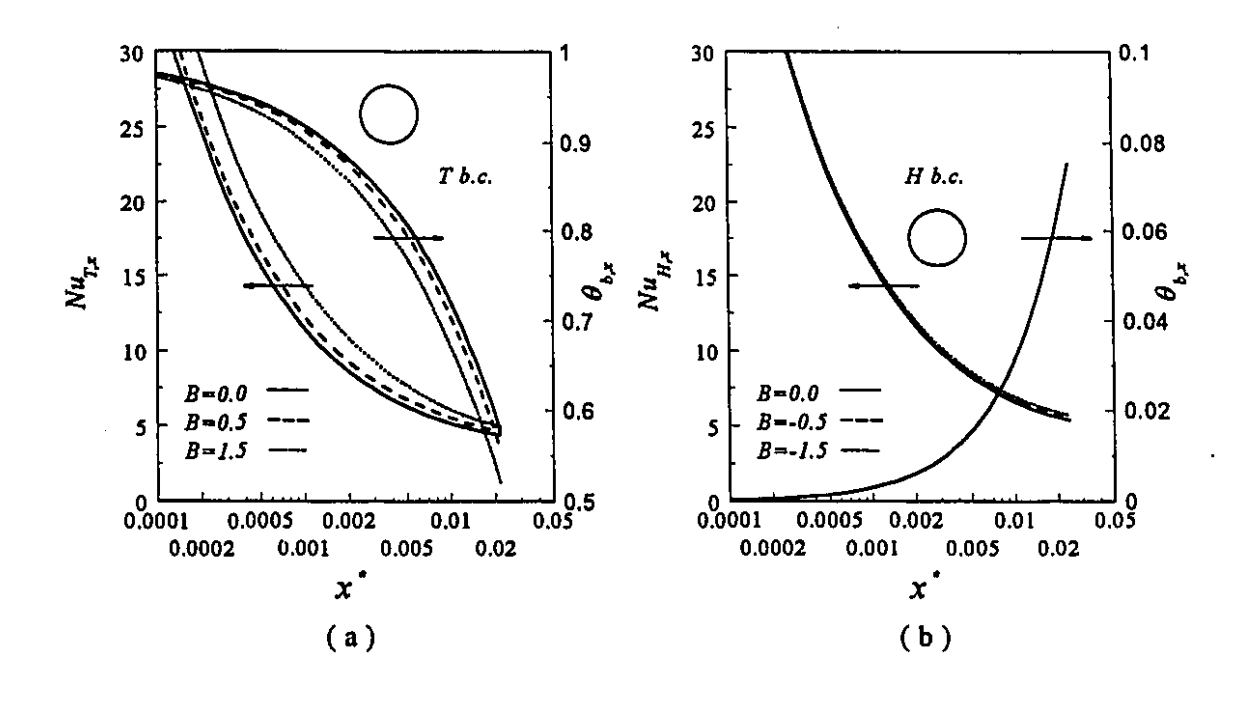
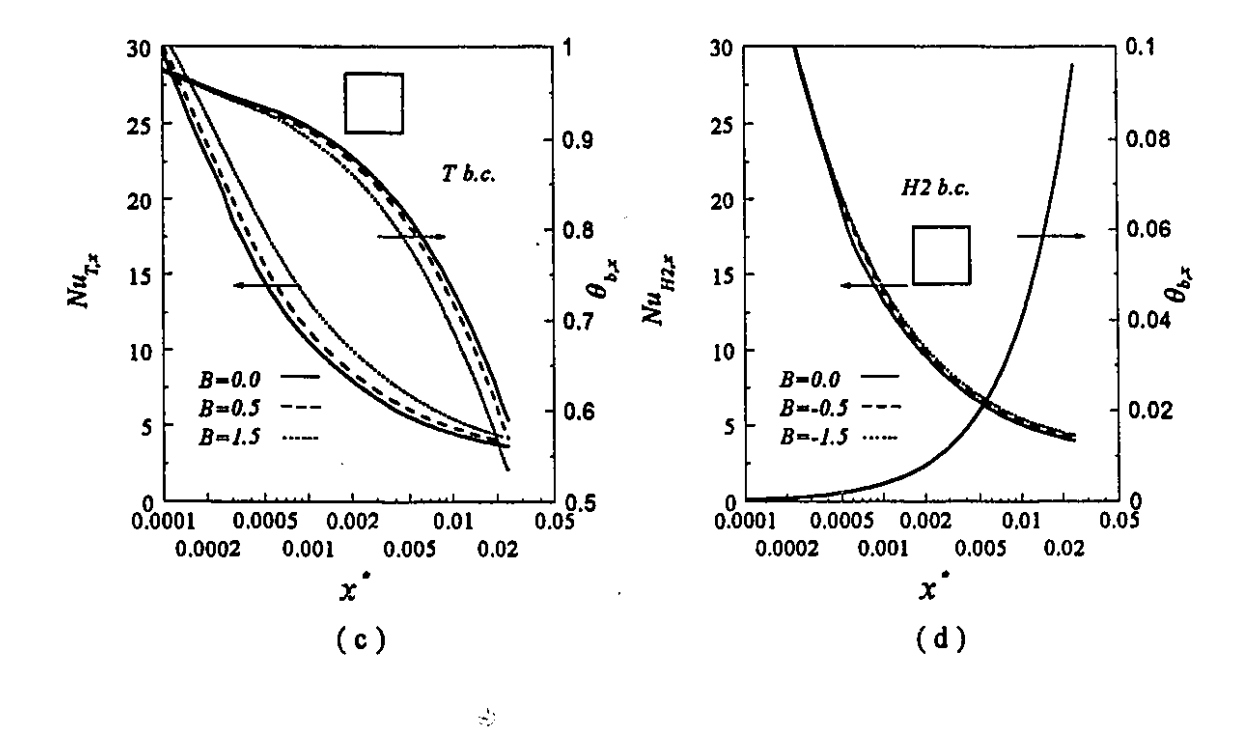


Figure 4.3 (a - h) Effect of temperature-dependent viscosity on the apparent friction factor for different geometries, Re=500, Pr=10.





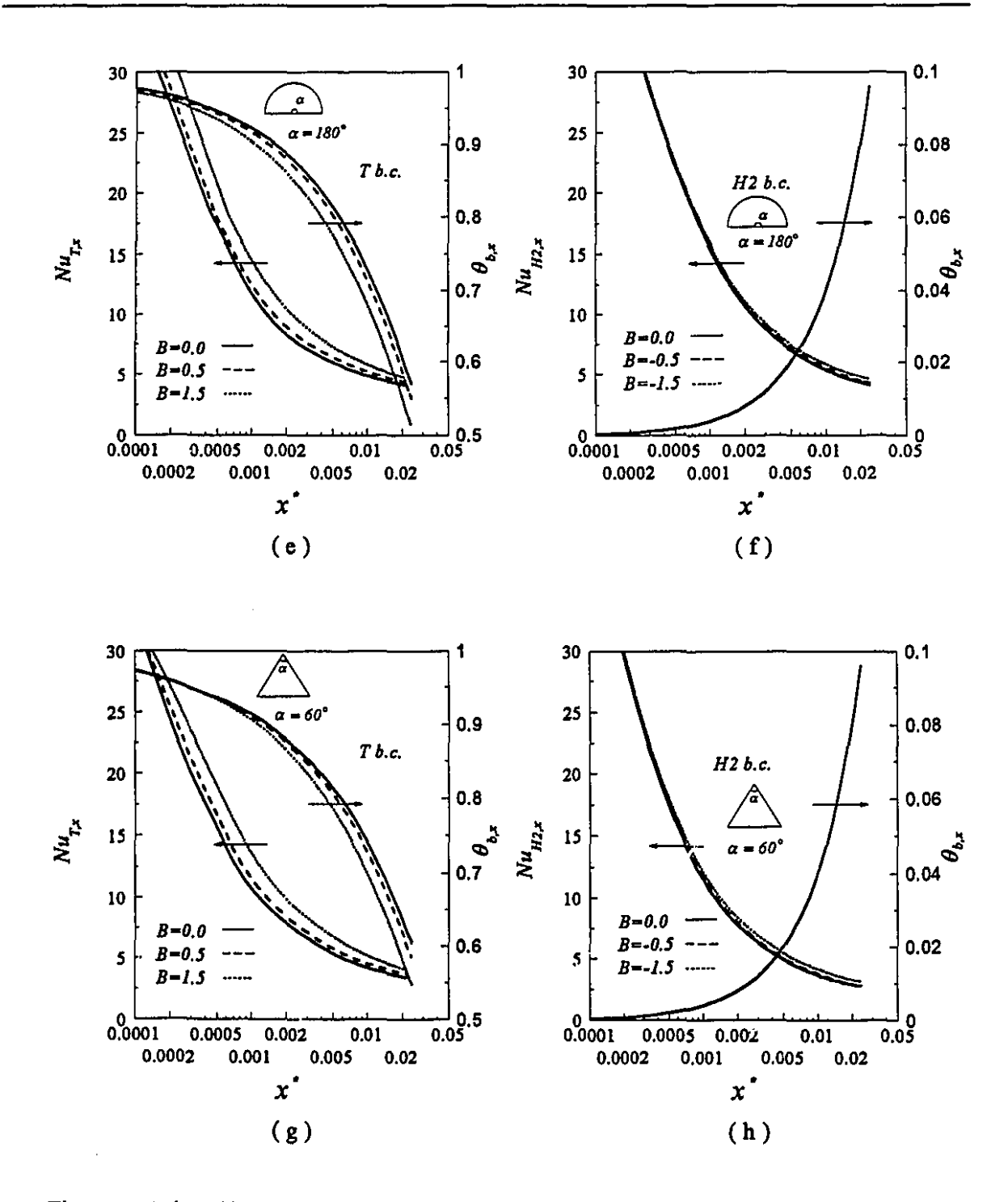


Figure 4.4 (a - h) Effect of temperature-dependent viscosity on Nusselt number for different geometries, n=0.5, Re=500, Pr=10.

4.2 Effect of viscous dissipation

The Brinkman number is used as a criterion which signifies the importance of viscous dissipation. It is defined in chapter 2 (Equation 2.20) for both T and H2 boundary conditions.

The effect of viscous dissipation on the dimensionless center-plane temperature profile for various duct geometries is displayed in Fig. 4.5 (a - h) while the local bulk temperature and Nusselt number variations for n=0.5, different boundary conditions, and for different Brinkman numbers are presented in Fig. 4.6 (a - h) and Tables B5 through B8 (Appendix B). The effect of Brinkman number on Nusselt numbers for n=1.0 can be seen from Fig. B2 (a - h) and Tables B5 through B8.

For both T and H2 boundary conditions, since the highest shear rate occurs near the wall, the effect of viscous dissipation is most significant in this region. Viscous heating increases the bulk temperature and results in a decrease of the local Nusselt number.

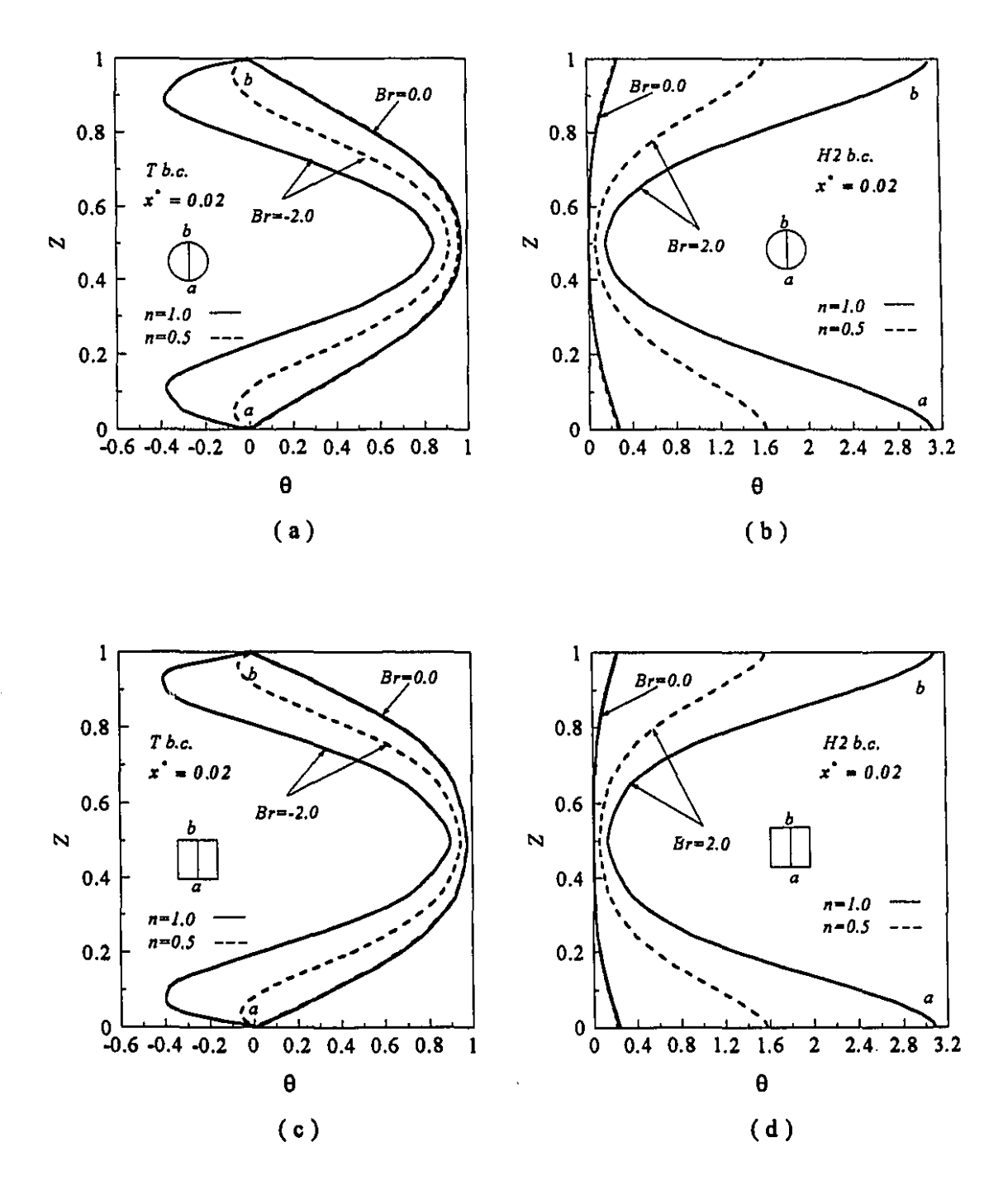
For the T boundary condition the Brinkman number is negative when the fluid is being heated. For this boundary condition, in the entrance region due to the highest velocity gradient close the walls viscous heating is appreciable, while $(T_w - T_b)$ is also large; thus changes in temperature difference due to viscous heating are not appreciable. Competition between these two facts influences the value of the local Nusselt number. Generally due to increase in fluid temperature near the wall, the heat flux from the wall decreases causing lowering of the Nusselt number. For example at $x^*=0.0002$ for n=0.5 and for Br=-2.0 the local Nusselt number decreases about 17.8 %, 14.4 %, 22.0 % and 19.3 % due to viscous dissipation effects for circular, square, semi-circular and equilateral triangular ducts, respectively.

For the T boundary condition since the temperature difference between the wall and the fluid bulk is highest in the entrance region, the bulk temperature and fluid temperature close the wall are still far from the wall temperature. Further downstream, due to the combined effects of viscous heating and wall heating, the temperature of the fluid close to the wall approximates the wall temperature. Hence the temperature gradient

at the wall is nearly zero and the local Nusselt number therefore approaches zero. The zero Nusselt number situations for n=0.5 and Br=-2.0 occur at $x^*=0.00701$, 0.00789, 0.00702, and 0.00614 for circular, square, semi-circular and equilateral triangular ducts, respectively. However, the bulk temperature still is lower than that of the wall (i.e. the dimesionless bulk temperature is positive). As the fluid proceeds downstream the fluid temperature adjacent to the wall becomes higher than the wall temperature, which changes the heating mode to cooling mode (negative heat flux) and Nusselt number assumes a negative value.

Fig. 4.7 (a - h) shows $Nu_{T,x}$, dimensionless bulk fluid temperature and the dimensionless heat flux through the wall for different duct geometries. As can be observed from this figure, further into the duct, where the heat flux through the wall still is negative, the fluid bulk temperature increases to reach the wall temperature, i.e. the dimensionless bulk fluid temperature becomes zero. Consequently, the conventionally defined Nusselt number becomes infinite. At locations further downstream, the bulk temperature becomes greater than the wall temperature (i.e. dimensionless bulk temperature is negative). Since the heat flux is also negative, the Nusselt number changes to a positive value again. At further downstream locations competition between the heat flux and bulk temperature decreases the Nusselt number to an asymptotic value (Fig. 4.7).

For the constant heat flux boundary condition, the Brinkman number is positive for heating. Since in the entrance region, the velocity gradient close to the walls is large and the temperature difference between the wall and the fluid bulk is very small, thus the relative increase in the bulk and wall temperatures is appreciable and the most effect of viscous dissipation is felt in this region. Further downstream the trade-off between the increases of θ_w and θ_b retards the effect of viscous dissipation. For example at $x^*=0.01188$ for n=0.5 and Br=2.0, $Nu_{H2,x}$ decreases about 80 %, 75 %, 76 %, and 68 % due to the viscous heating for circular, square, semi-circular and equilateral triangular ducts, respectively.



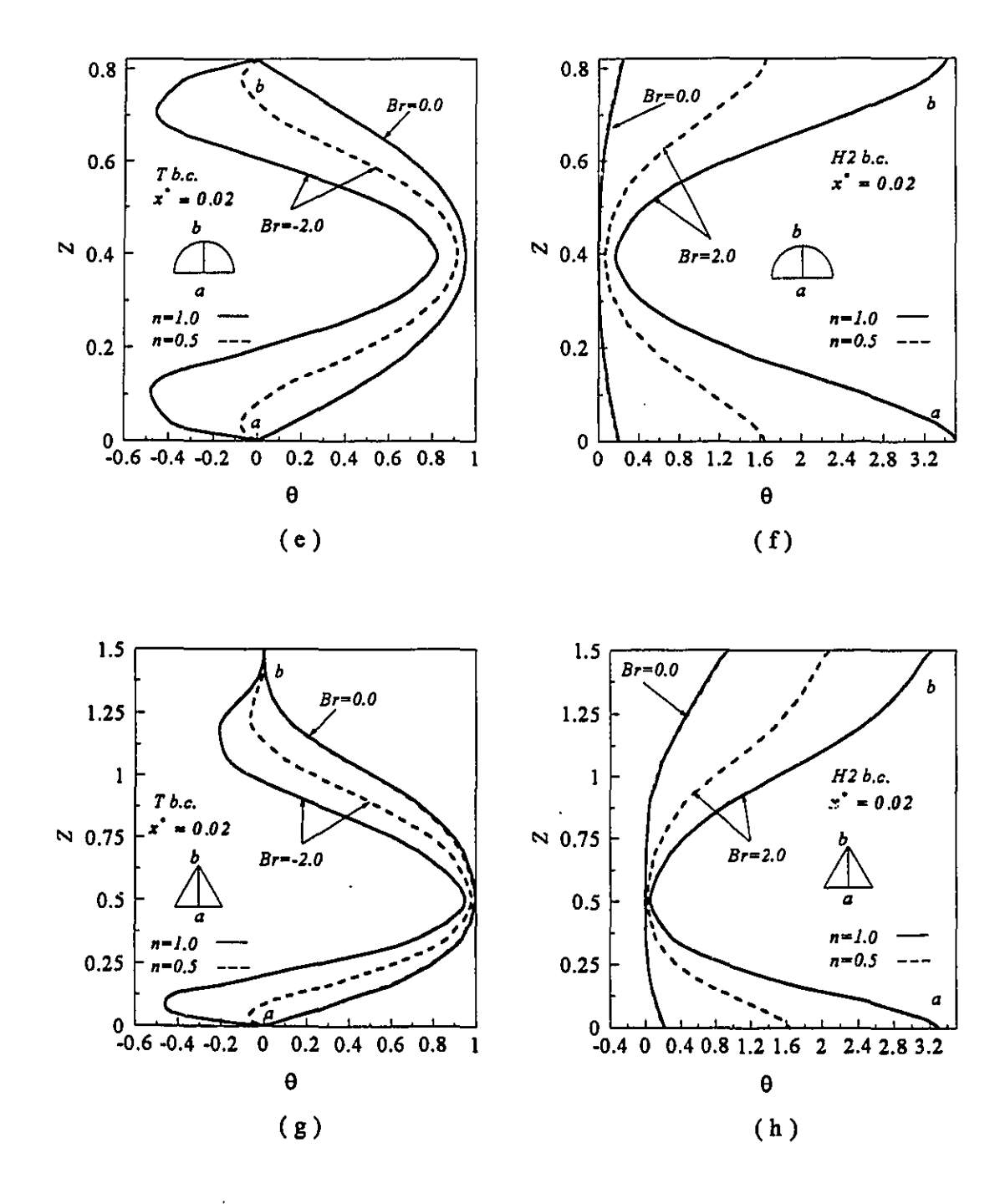
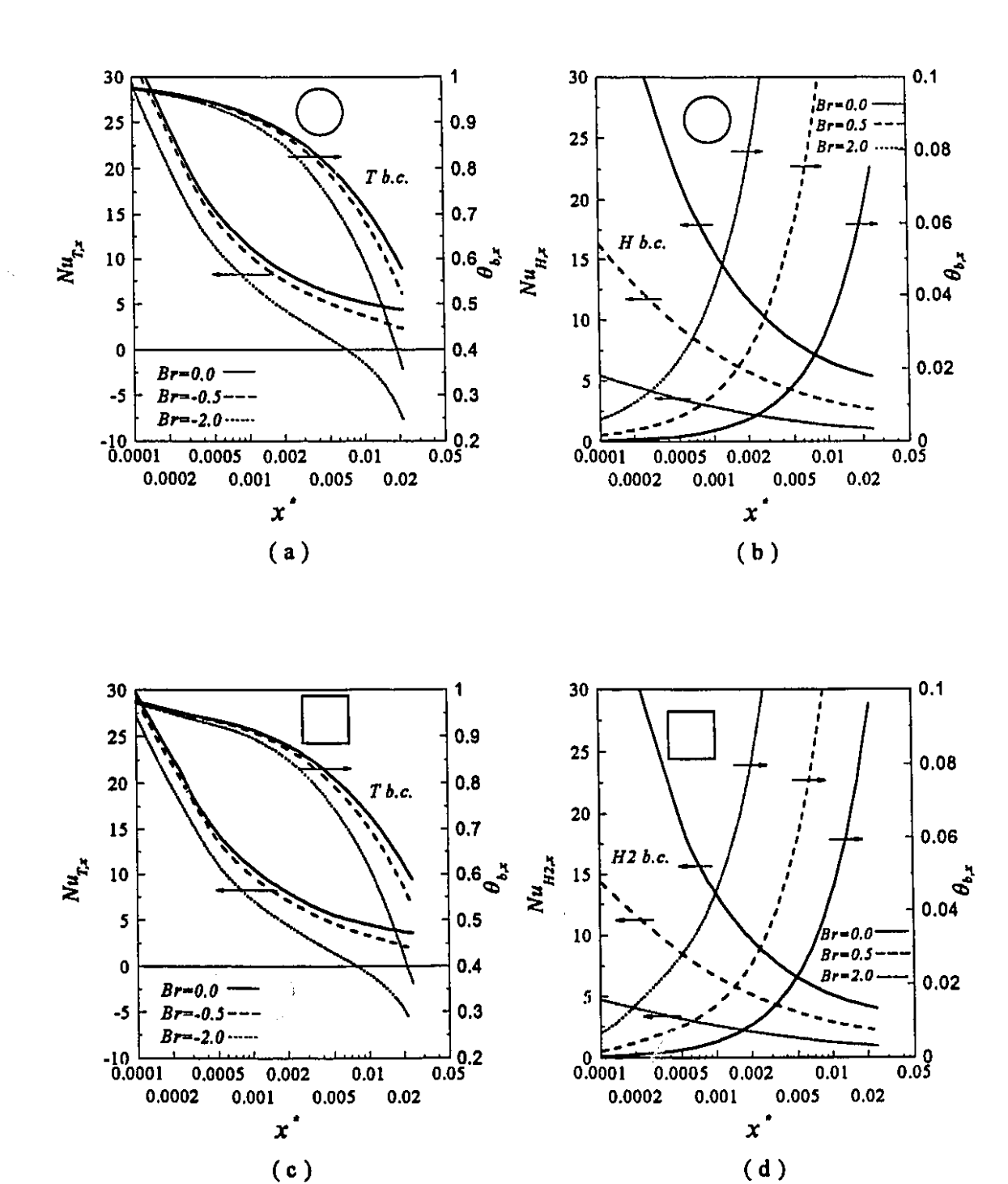


Figure 4.5 (a - h) Effect of viscous dissipation on center-plane dimensionless temperature profiles for different power law indices and various geometries, Re=500, Pr=10.

ċ



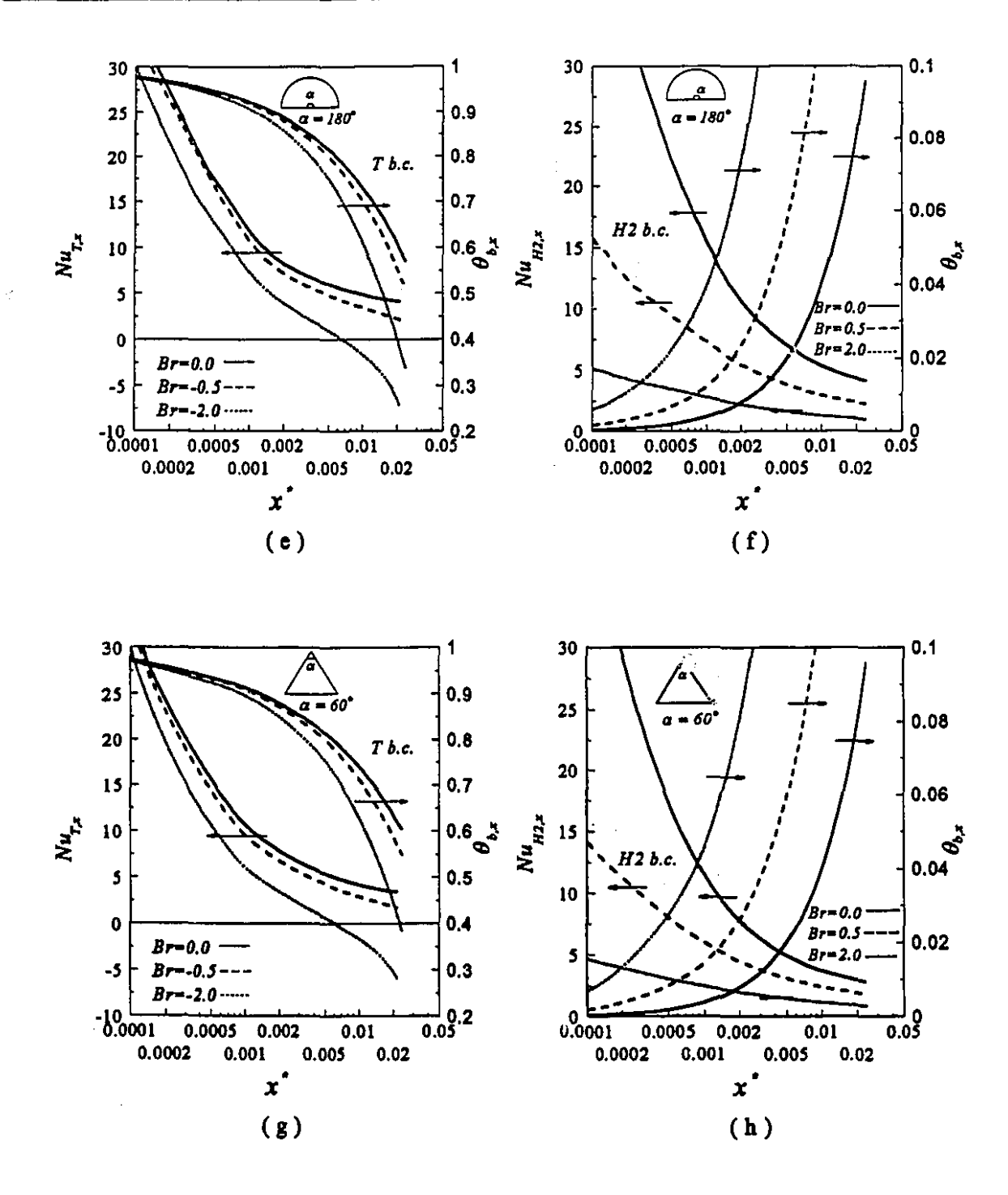
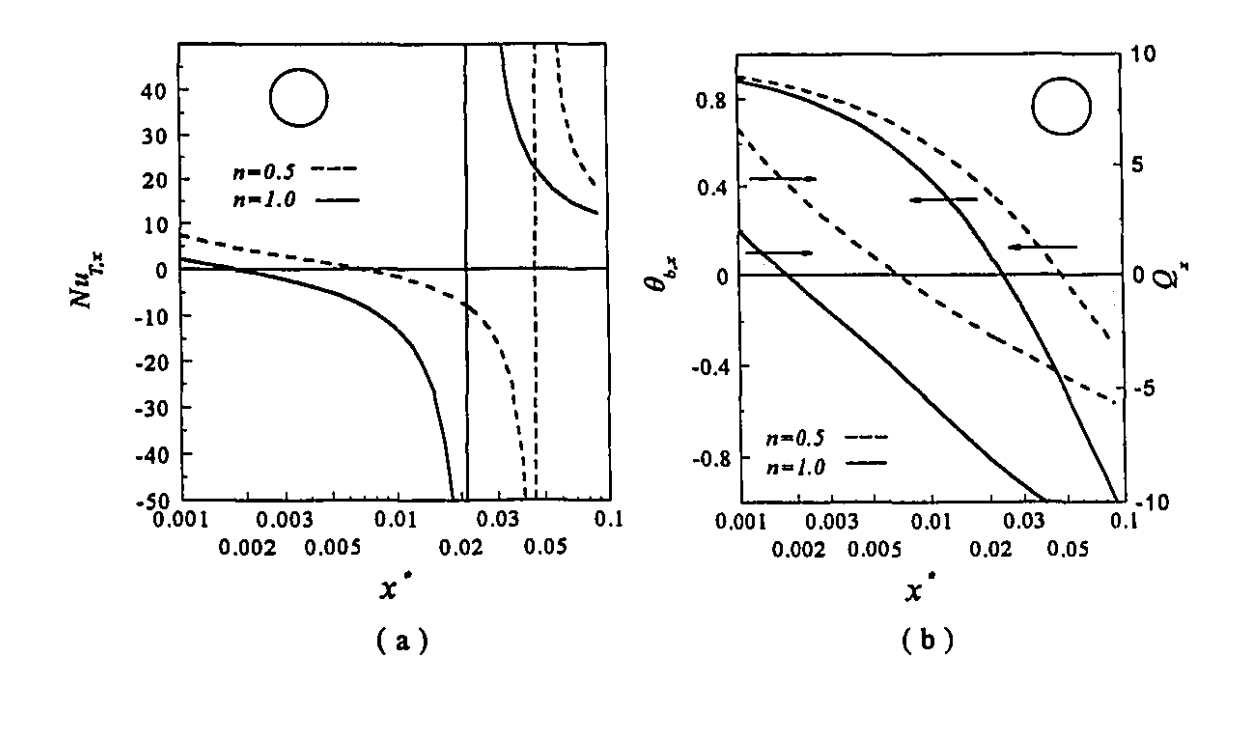
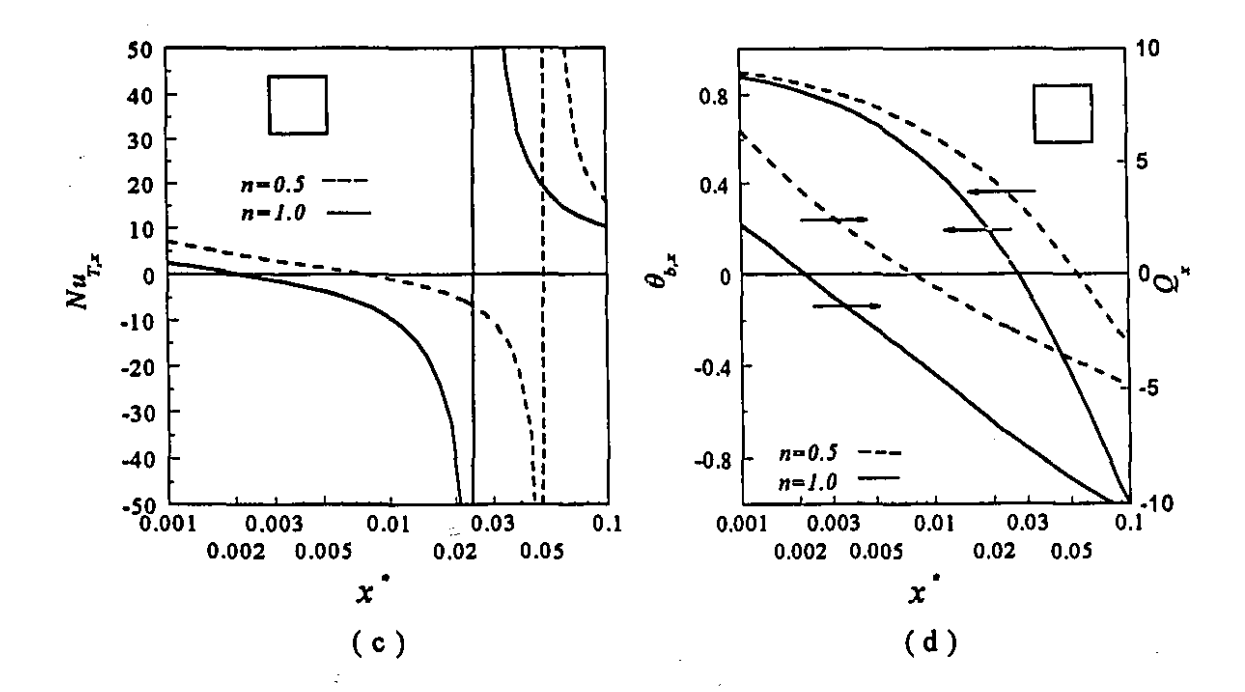


Figure 4.6 (a - h) Effect of viscous dissipation on Nusselt number and dimensionless bulk temperature for different geometries, n=0.5, Re=500, Pr=10.





F1 22

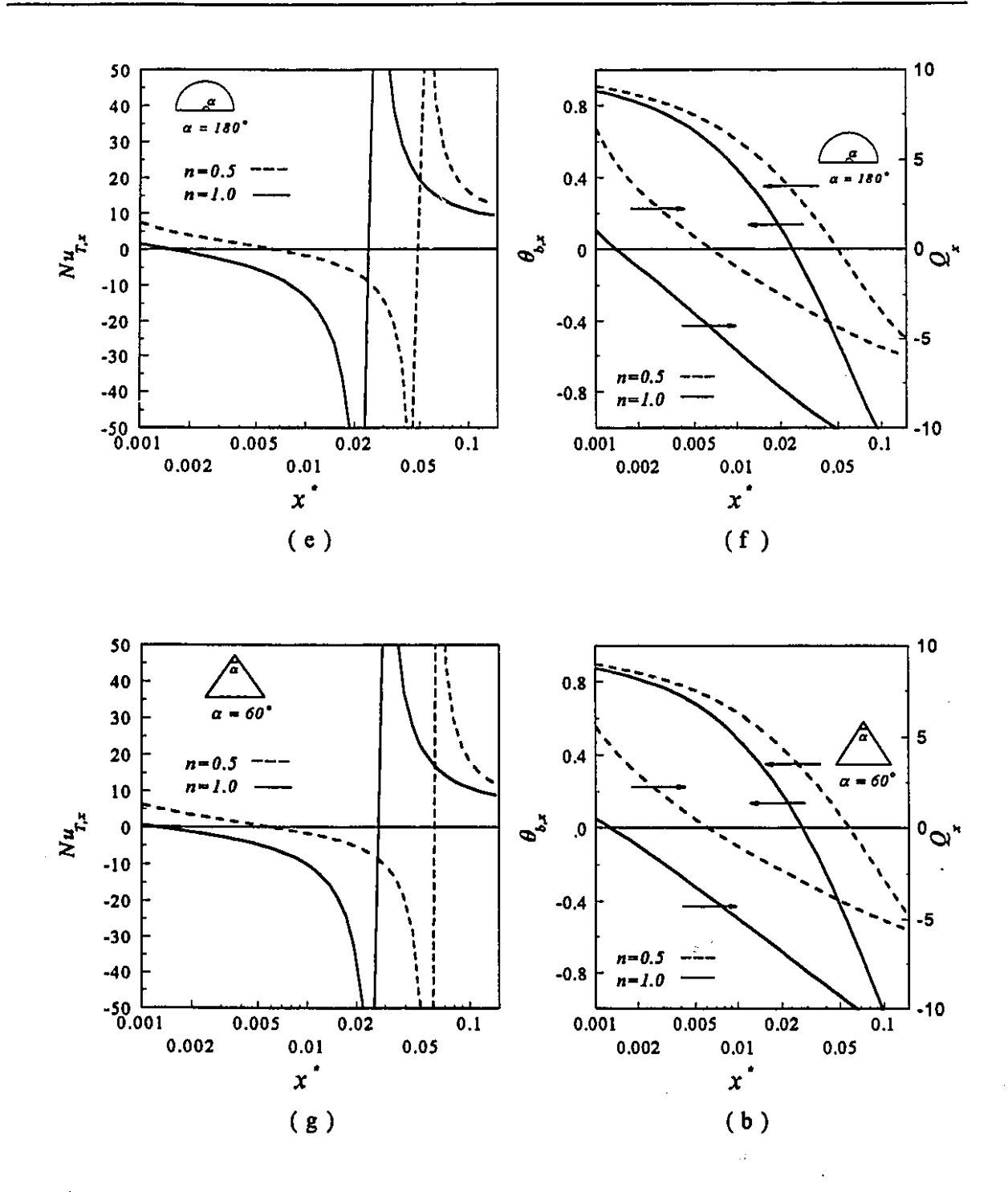


Figure 4.7 (a - h) Effect of viscous dissipation on thermal characteristics for T boundary condition for different geometries, Re=500, Pr=10, Br=-2.0.

1

4.3 Simultaneous effects of temperaturedependent apparent viscosity and viscous dissipation

Fig. 4.8 (a - h) and B3 (a - h) demonstrate the simultaneous effects of temperature-dependent viscosity and viscous dissipation on Nusselt number for both T and H2 boundary conditions for n=0.5 and n=1.0, respectively.

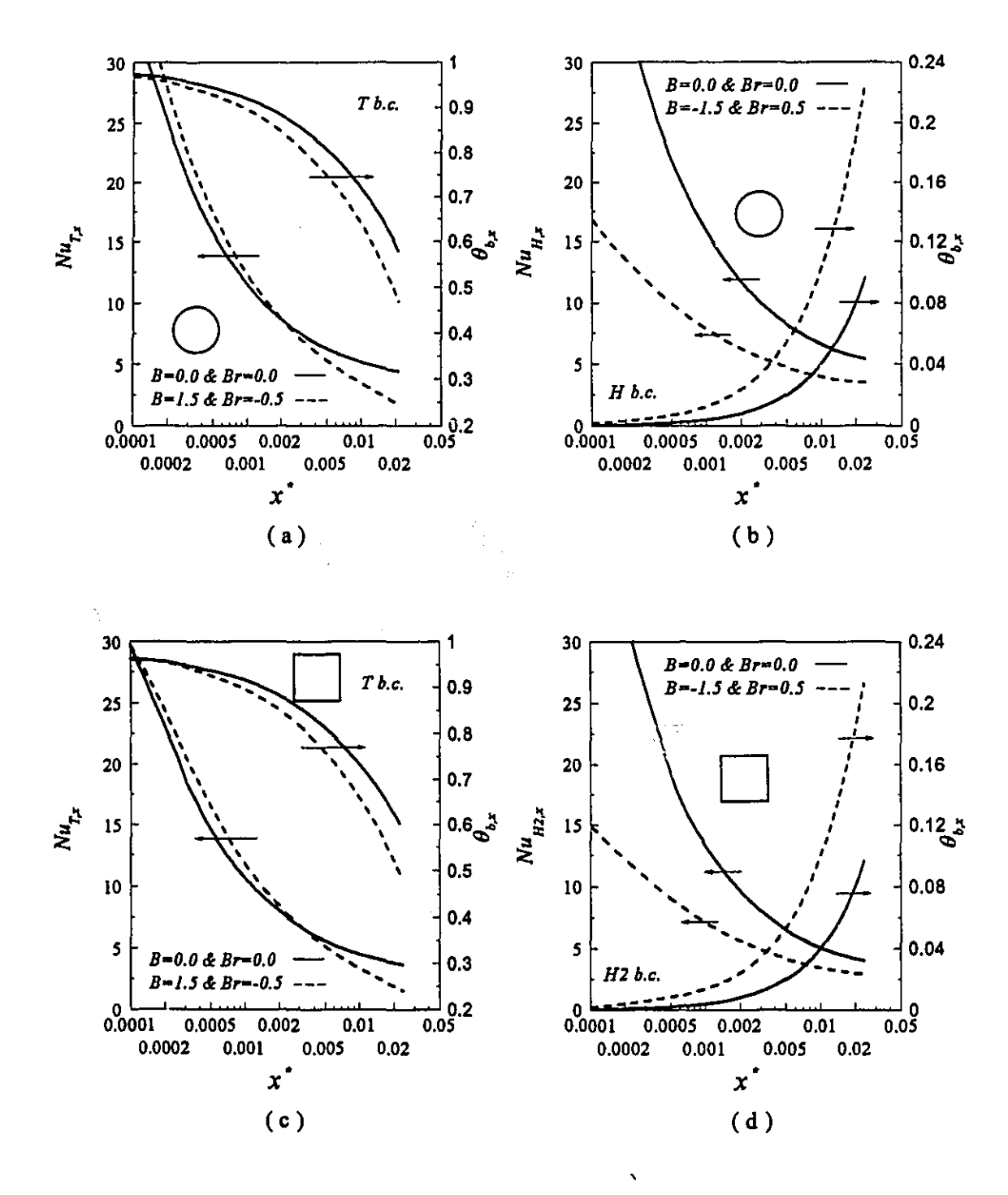
When temperature-dependent viscosity is included in the simulation, both the axial velocity and velocity gradient close to the walls increase which cause higher viscous heating when compared to the isoviscous case. Viscous heating increases the fluid temperature close to the walls, therefore the velocity and velocity gradient next to the walls increase due to the temperature-dependence of viscosity. Higher velocity close to the walls enhances the heat transfer for the T boundary condition and decreases the wall temperature for the H2 boundary condition while viscous dissipation has a reverse effect. Depending on the boundary condition and geometry as well as the value of the power law index, competition between these two opposing effects determines the Nusselt number.

In the entrance region for the T boundary condition the effects of temperature-dependent viscosity as well as viscous heating on heat transfer are significant but in this part the effect of viscous dissipation is less significant than that downstream. Therefore for the T boundary condition, for some geometries (depending on the power law index) the temperature-dependence of viscosity has a dominant effect in the entrance region while the effect of viscous dissipation becomes dominant further downstream.

For the H2 boundary condition the effect of temperature-dependent viscosity is smallest in the entrance part while the effect of viscous heating is the greatest. Thus for the H2 boundary condition the effect of simultaneous temperature-dependence of viscosity and viscous dissipation is more pronounced in the entrance section of the channel while this effect decreases as the fluid proceeds downstream.

5/12

Ġ.



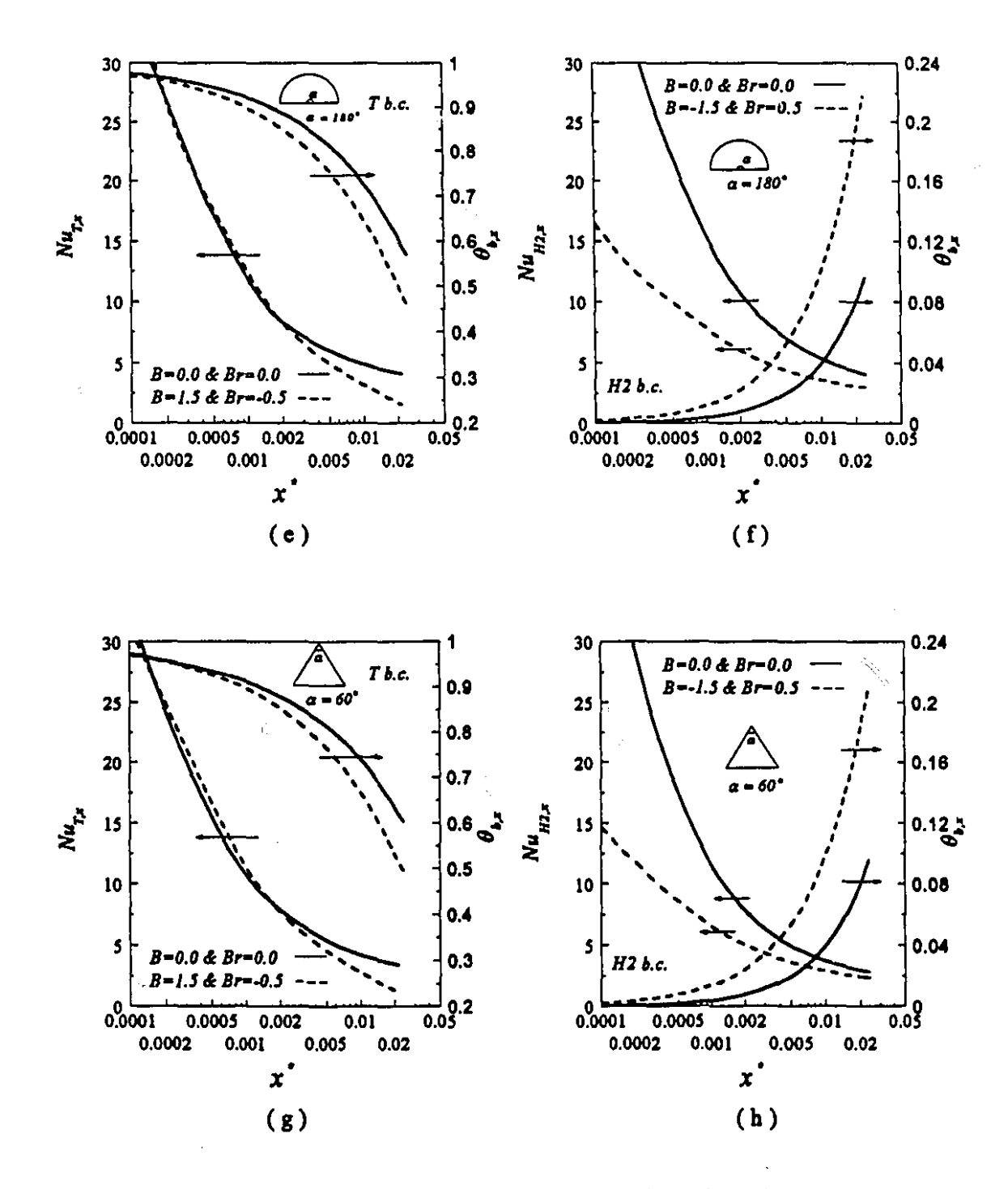


Figure 4.8 (a - h) Simultaneous effects of temperature-dependent viscosity and viscous dissipation on Nusselt number and dimensionless bulk temperature for different geometries, n=0.5, Re=500, Pr=10.

1

4.4 Effect of Prandtl number

For the T boundary condition the local Nusselt number depends on the heat transfer from the walls as well as the dimensionless local bulk temperature. Fig. 4.9 (a - b) presents the dimensionless heat flux through the wall, dimensionless bulk temperature, and Nusselt number vs. X for different Prandtl numbers. A lower Prandtl number implies faster thermal development which results in higher bulk temperature (lower dimensionless bulk temperature) and lower wall heat flux (Fig. 4.9 (a)). Competition between these produces a lower Nusselt number for lower Prandtl numbers in the entrance region (Fig. 4.9 (b)). Far downstream where the fully developed condition occurs, the local Nusselt number approaches a constant value independent of the Prandtl number. Fig. 4.10 (a - b) shows Q_x , $\theta_{b,x}$, $Nu_{T,x}$ based on x^* as dimensionless axial distance. From this figure it is clear that a lower Prandtl number results in higher Q_x but lower $\theta_{b,x}$ causing higher $Nu_{T,x}$ at a given x^* .

Fig. 4.11 (a - b) and Fig. 4.12 (a - b) present the effects of Prandtl number on the local dimensionless wall and bulk temperatures as well as $Nu_{H2,x}$ as functions of X and x^* , respectively. For the H2 boundary condition due to the faster thermal development for lower Prandtl number fluids both $\theta_{b,x}$ and $\theta_{w,x}$ are higher at the same X. Competition between the increasing $\theta_{b,x}$ and $\theta_{w,x}$ due to the lowering of Prandtl number results in lower $Nu_{H2,x}$ at a given X. When x^* is chosen as the dimensionless axial distance (Fig. 4.12 (a - b)) $\theta_{w,x}$ for a smaller Pr is lower while $\theta_{b,x}$ is the same. Therefore for the same x^* , lower Pr results in higher $Nu_{H2,x}$. Fig. 4.13 (a - h) and Fig. B4 (a - h) present Nusselt number distribution for different Prandtl numbers and for various ducts for n=0.5 and n=1.0, respectively. These results are tabulated in Table B9 through Table B12 in Appendix B.

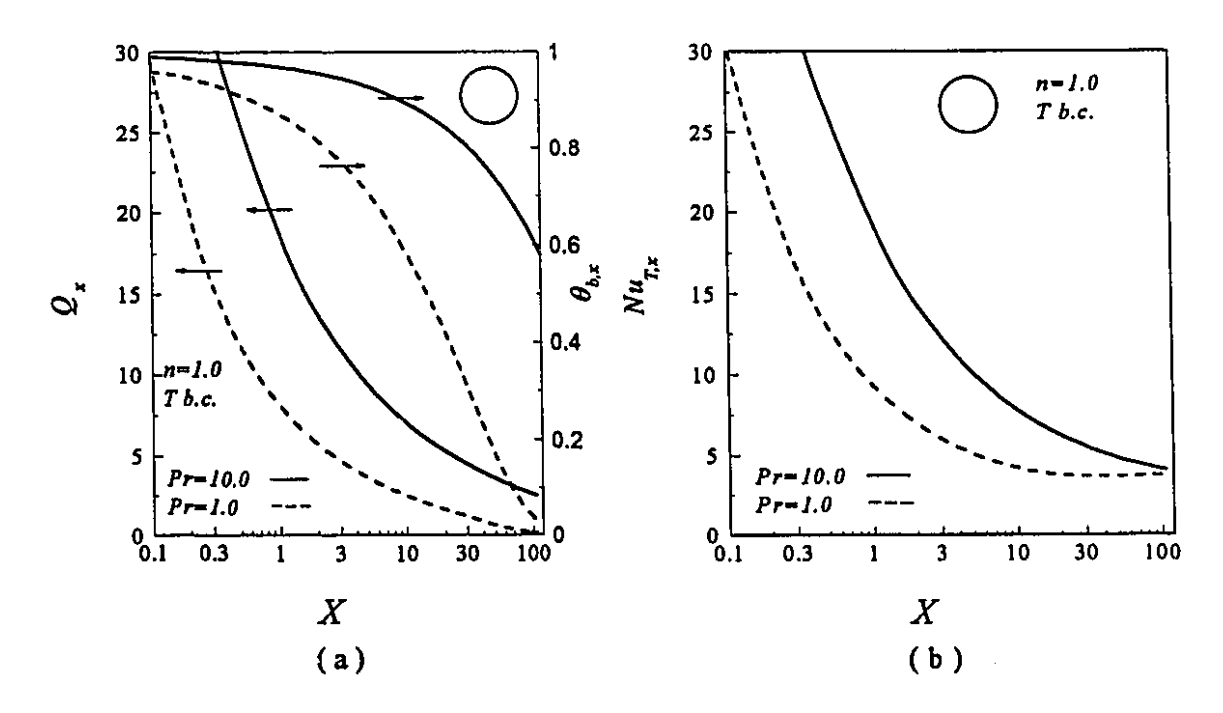


Figure 4.9 (a - b) Heat transfer characteristics vs. X for T boundary condition for different Prandtl number, Re=500.

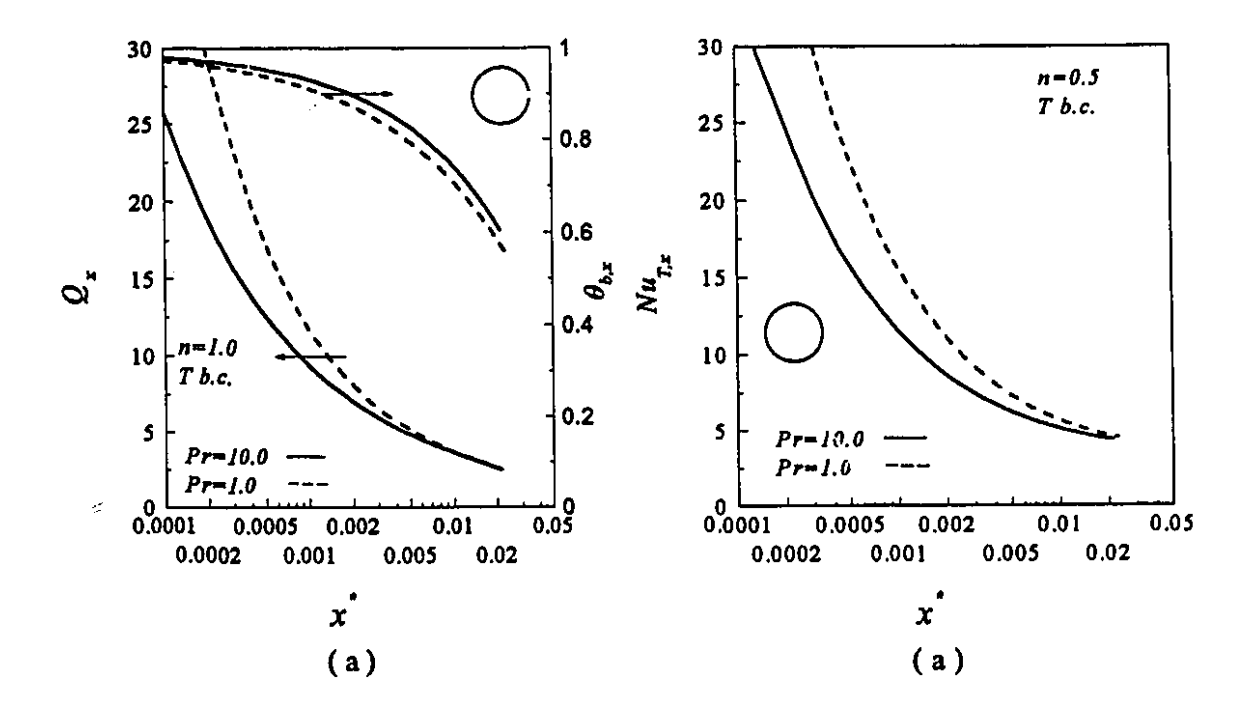


Figure 4.10 (a - b) Heat transfer characteristics vs. x^* for T boundary condition for different Prandtl number, Re=500.

Ó

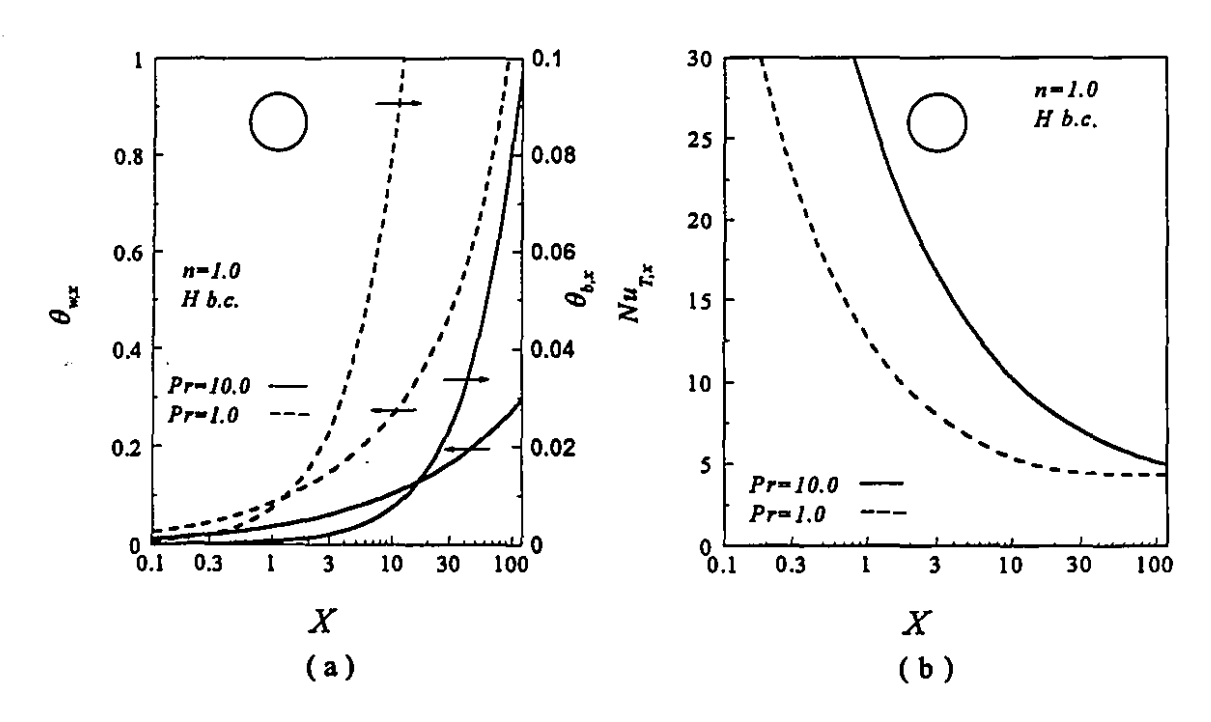


Figure 4.11 (a - b) Heat transfer characteristics vs. X for H boundary condition for different Prandtl number, Re=500.

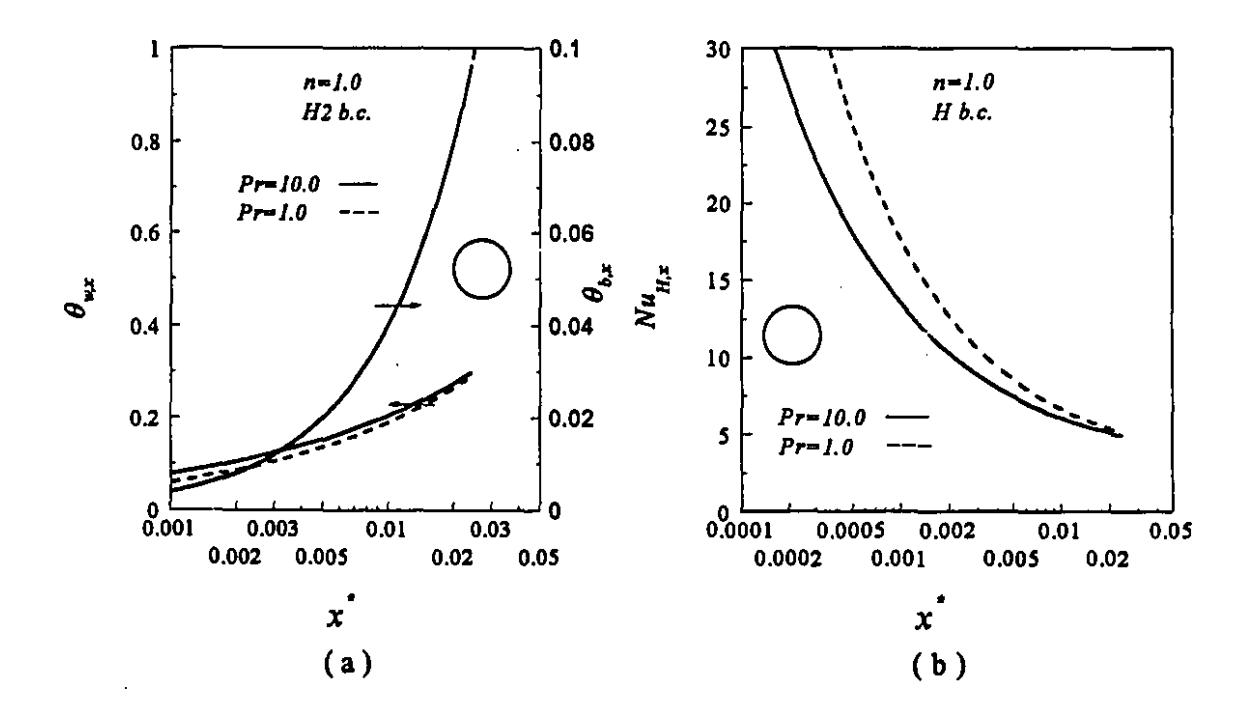
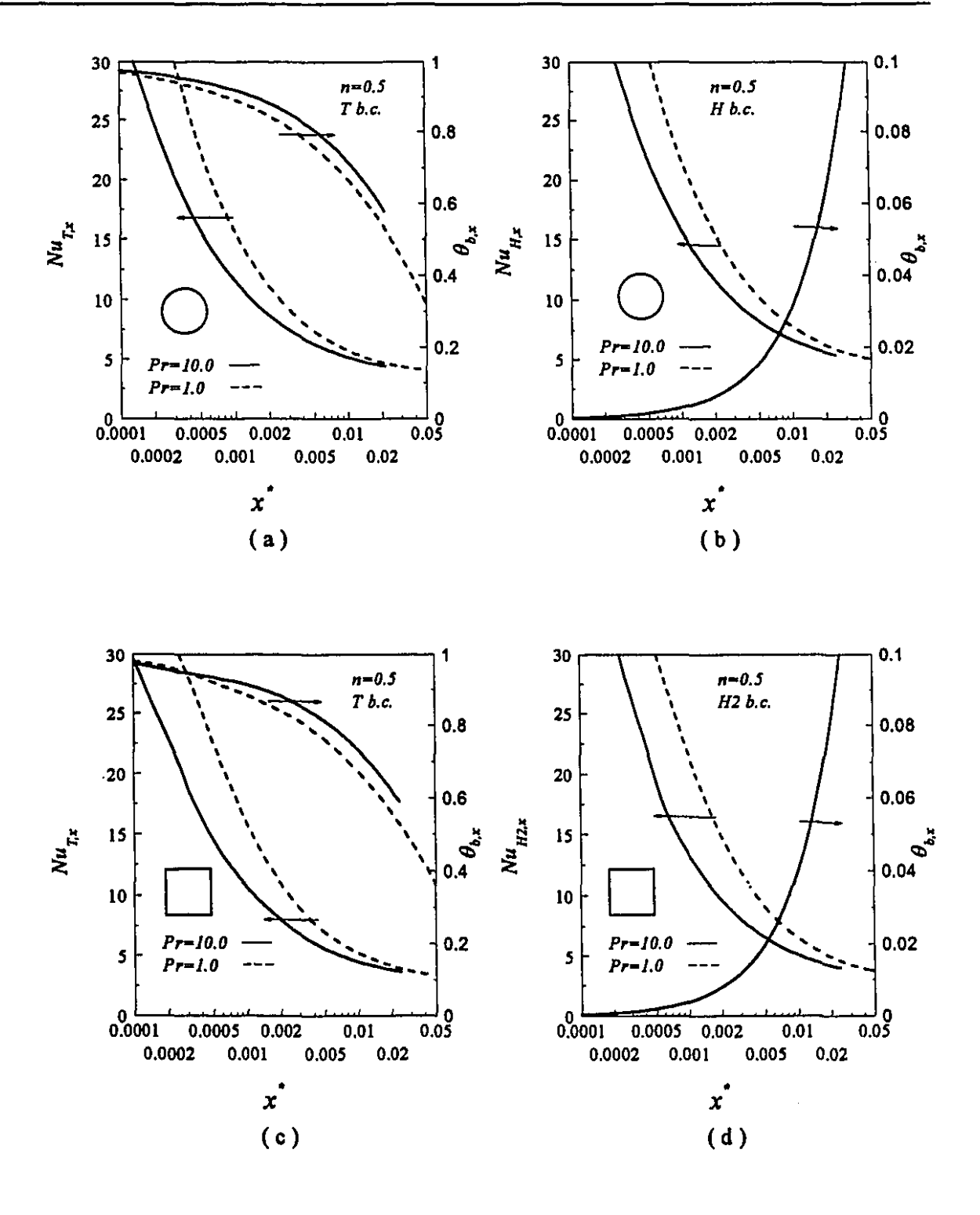


Figure 4.12 (a - b) Heat transfer characteristics vs. x° for H boundary condition for different Prandtl number, Re=500.



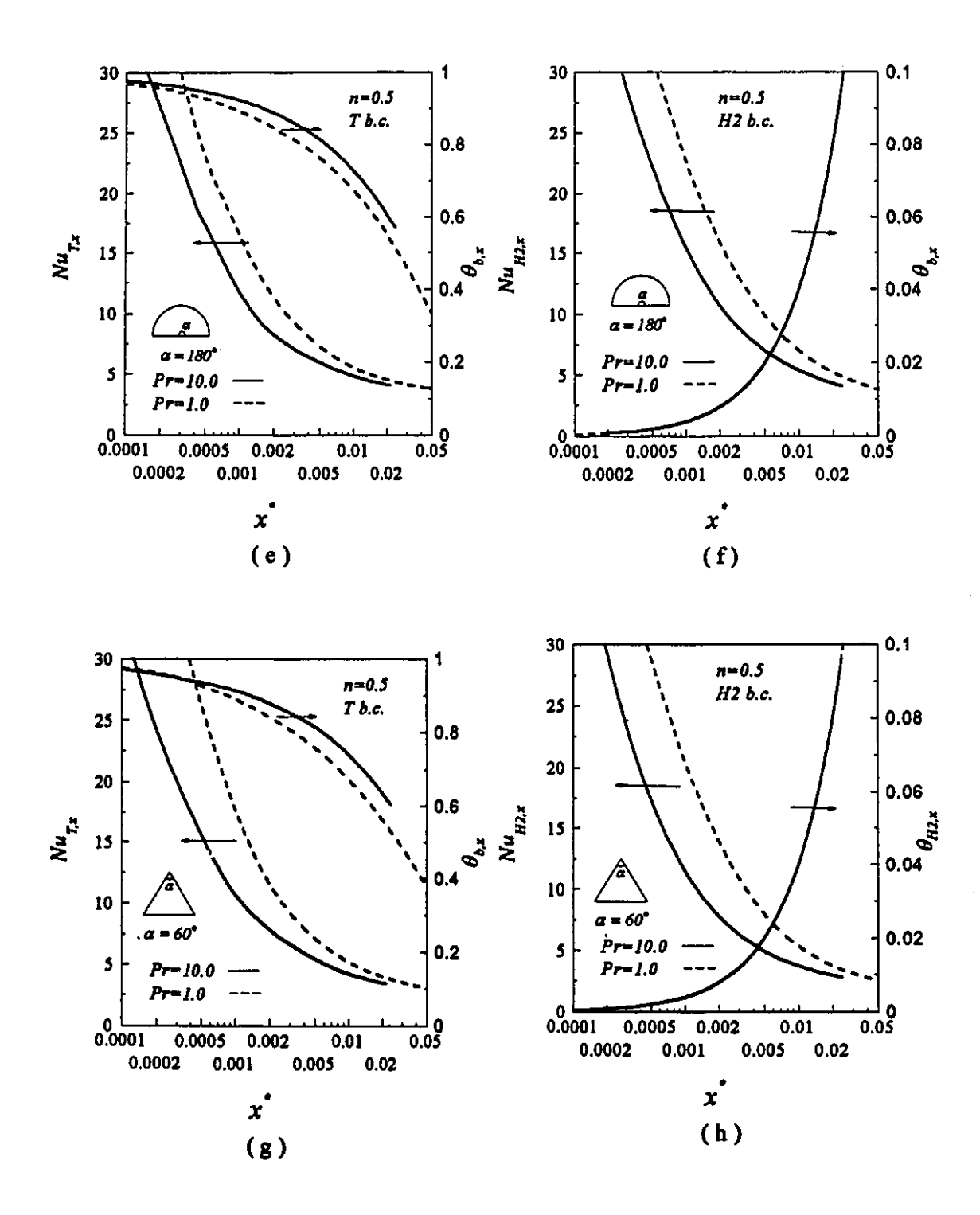


Figure 4.13 (a - h) Effect of Prandtl number on Nusselt number and dimensionless bulk temperature for different geometries, Re=500.

L,

4.5 Conclusions

The numerical simulations considered the effects of temperature-dependent viscosity, viscous dissipation, simultaneous effects of temperature-dependent viscosity and viscous dissipation, and Prandtl number on simultaneously developing flow and heat transfer. Results are given for T and H2 boundary conditions and for fluids of different power law indices.

Viscosity variation with temperature affects the local Nusselt number and also the pressure drop. For heating, the increase in the local Nusselt number for constant temperature boundary conditions is noticeably higher than that for the constant heat flux boundary conditions.

Viscous heating has a very significant effect on heat transfer which can even change the direction of heat flux for the case of uniform temperature boundary conditions.

Results indicates that the Prandtl number is a very important parameter; the lower the Prandtl number the higher Nusselt number in the developing region of the channel (for the same x^*).

Chapter 5

Miscellaneous Geometrical Effects

This chapter covers the results of numerical experiments to evaluate miscellaneous geometrical effects on the flow and heat transfer characteristics. The effects considered are: effect of rounding the corners of a square duct, aspect ratio of rectangular ducts, apex angle of circular-sector channels, and the geometric parameter of cross-shaped channels. Also, circular-sector ducts and triangular channels with the same apex angles are compared. Results are presented for both T and H2 boundary conditions and various power law indices but at fixed values of the Reynolds and Prandtl numbers.

5.1 Effect of rounding corners of a square duct

Two radii of curvature, a/20 and a/6, were chosen for the purpose of simulating the effect of rounding of the corners. Here a is the side of the rounded corners square duct. Fully developed values of the flow characteristics and Nusselt number are presented in Table 5.1. This table also includes the corresponding results for a square duct with sharp corners to compare the effect of "rounding" of the corners.

Fig. 5.1 (a - d) and Fig. 5.2 (a - d) present U_{max} and $f_{app}Re$ as well as the local Nusselt number, respectively, for different rounded corner square ducts.

Generally in the fully developed region rounding of the corners increases velocity and velocity gradient around the corner; therefore requirement mass conservation results in a reduction in the maximum velocity. For example from Table 5.1 rounding corner of square duct $(R.C.=\alpha/6)$ for n=0.5 decreases U_{max} from 1.760 to 1.707.

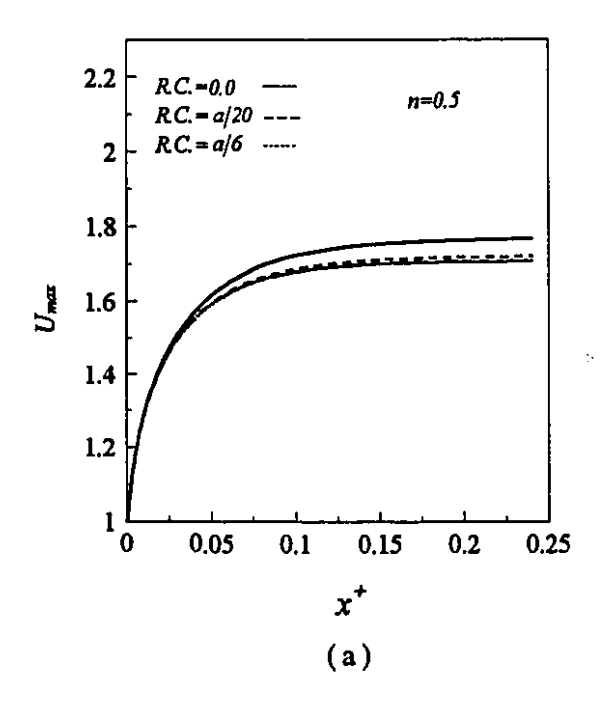
Table 5.1 Comparison of flow and heat transfer characteristics for rounded corner square ducts for different power law indices.

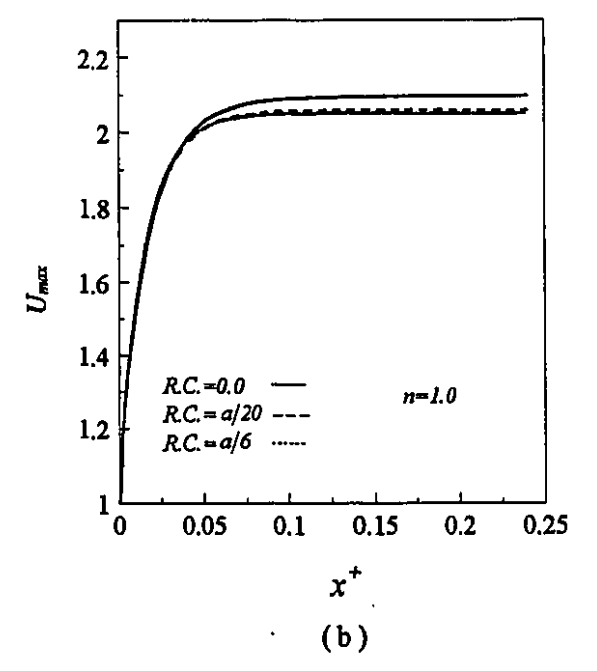
		f.Re	Umax	K(∞)	L ⁺	Nu _T	Nu _{H2}
n=0.5	R.C.=0.0	5.772	1.760	0.901	0.131	3.190	3.310
	R.C.=a/20	5.924	1.719	0.742	0.121	3.270	3.461
	R.C.=a/6	6.193	1.707	0.721	0.116	3.431	3.764
	R.C.=0.0	14.234	2.092	1.670	0.071	2.979	3.090
n=1.0	R.C.=a/20	14.604	2.060	1.419	0.065	3.047	3.221
	R.C.=a/6	15.500	2.051	1.408	0.060	3.188	<i>3.4</i> 88
n=1.25	R.C.=0.0	22.248	2.209	2.222	0.050	2.925	3.032
	R.C.=a/20	22.895	2.150	1.895	0.045	2.991	3.160
	R.C.=a/6	24.120	2.141	1.872	0.042	3.129	3.417

Also rounding corners reduces the hydrodynamic entrance length which is due to change in the shear stress around the corners. f_{app} Re is affected by the velocity gradient, apparent viscosity, and change in the surface in the corner region due to the rounding of the corner. Close to the entrance, coupling between these three effects causes a decrease in f_{app} Re in comparison with a square duct with sharp corners. As the fluid proceeds downstream the difference in f_{app} Re decreases and finally for the duct with rounded corners f_{app} Re becomes greater than that for a duct with sharp corners. From Fig. 5.1 (c - d) at x^+ =0.002 due to rounding of the corners (R.C.=a/6) $f_{app}Re$ decreases 23.3 % and 14.5 % while at fully developed condition it increases by 7.3 % and 8.9 % for n=0.5 and n=1.0, respectively.

The rounding of corners of a square duct affects heat transfer which is reflected in the value of the local Nusselt number. The velocity gradients along the perimeter close to the corners are important factors in determining the local Nusselt number. Very close to the entrance the difference of velocity gradient in the corner region between the sharp and rounded corners is very small but it increases further downstream. Thus the increase of the

radius of rounding of the corner enhances the Nusselt number far from the inlet. At the fully developed condition for n=0.5 this effect increases Nu_T and Nu_{H2} by 7.6 % and 13.7%, respectively, due to the rounding of the corners of the square duct (R.C.=a/6). As discussed in chapter 3, Nu_{H2} is affected more noticeably than Nu_T by the presence of sharp corners. The ratio $\frac{Nu_{H2}}{Nu_T}$ for n=0.5 at the fully developed condition is 1.04, 1.06, and 1.10 for R.C.=0 (sharp corner), a/20, and a/6, respectively. For engineering purpose the effect of rounding is rather small.





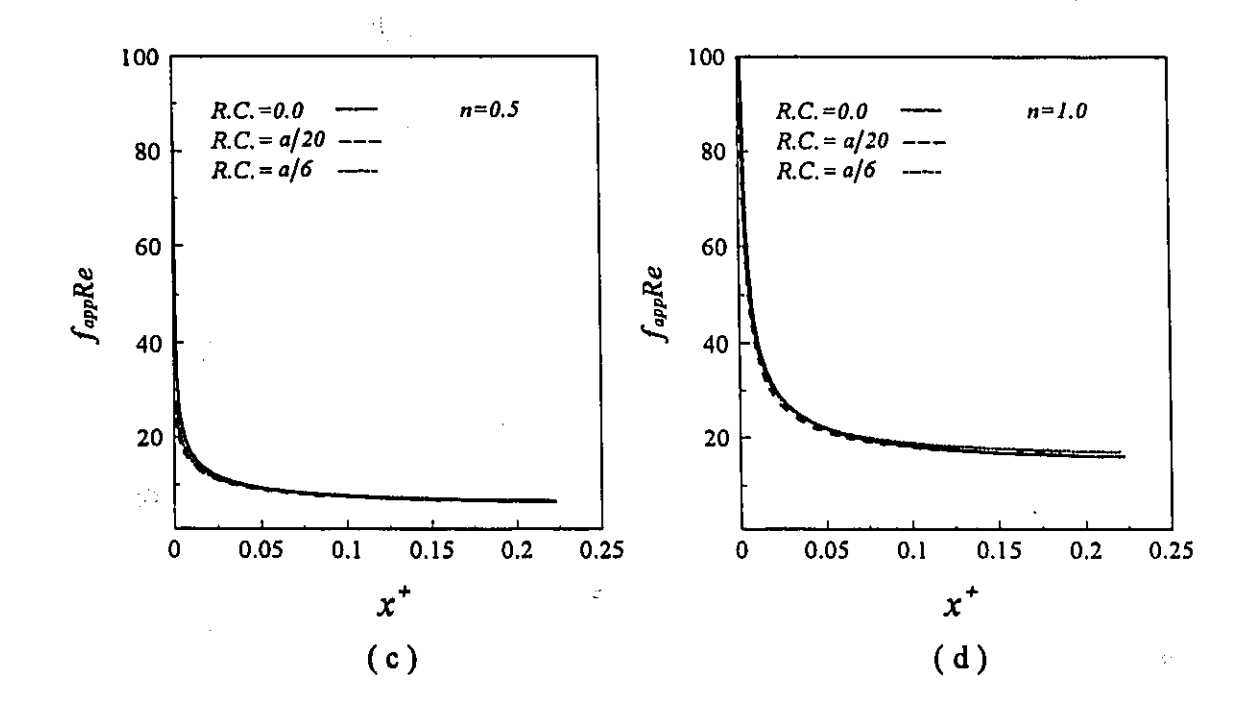
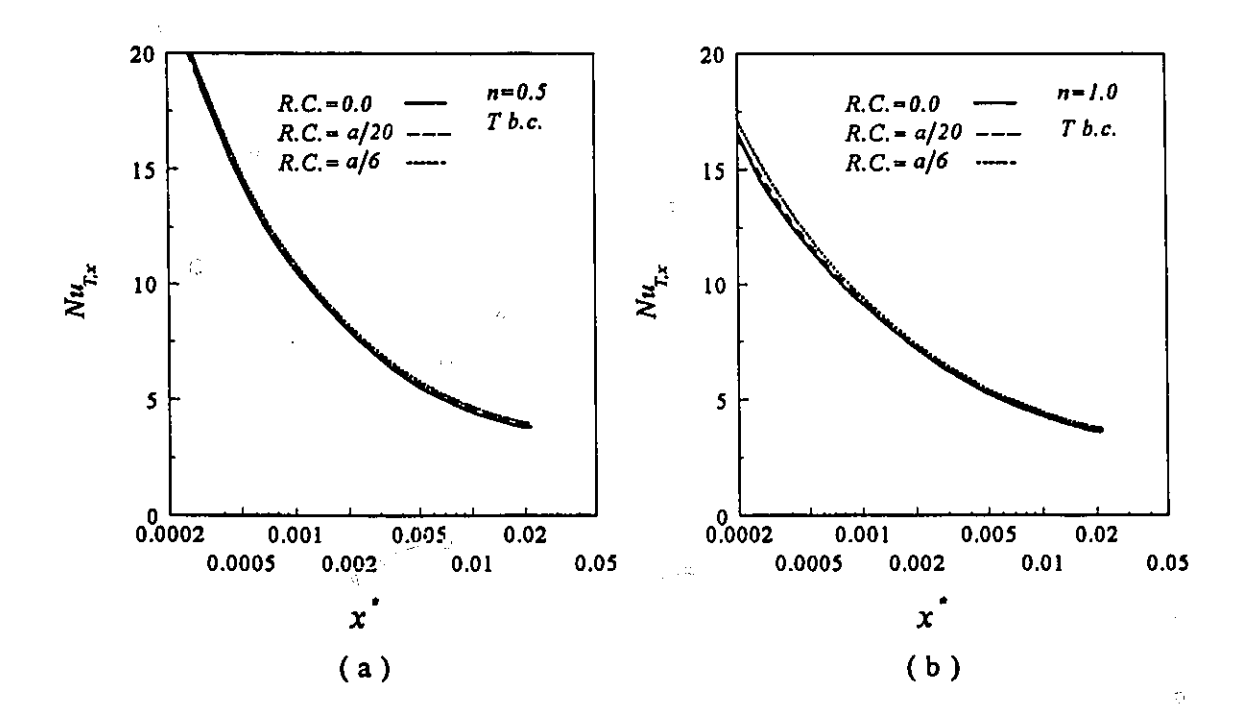


Figure 5.1 (a - d) Effect of rounding corners of a square duct on the dimensionless maximum velocity and apparent friction factor, Re=500.



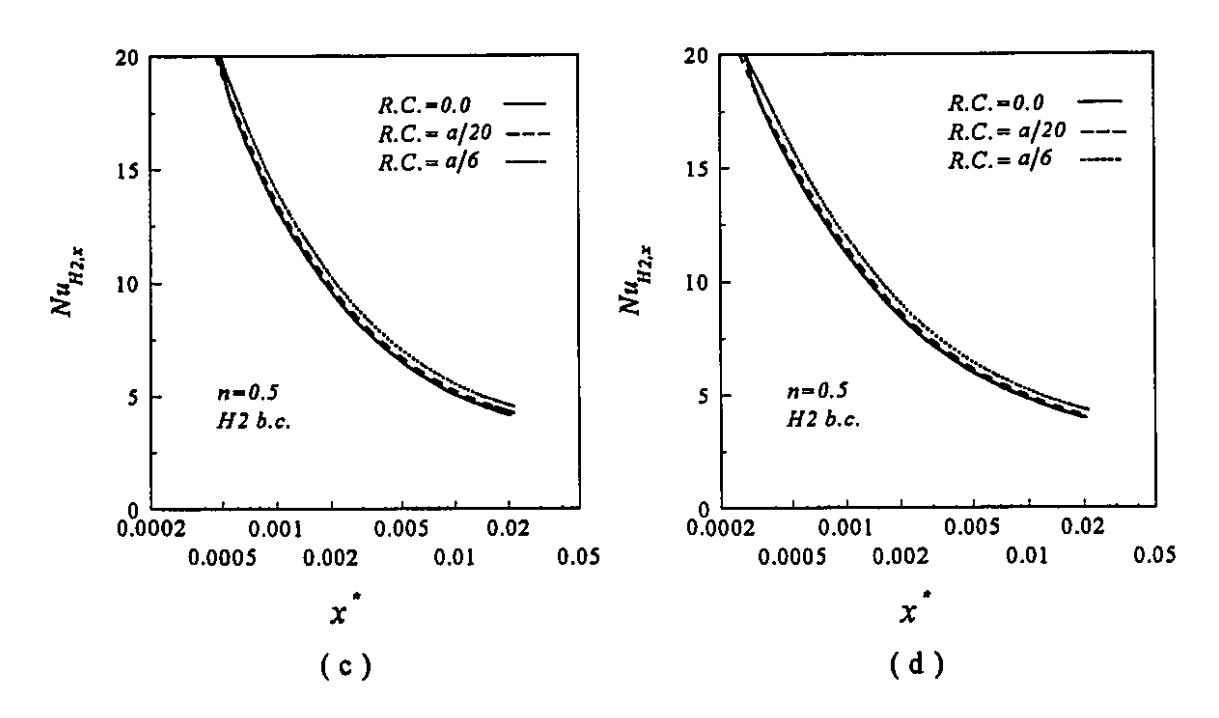


Figure 5.2 (a - d) Effect of rounding corners of a square duct on the local Nusselt number distribution, Re=500, Pr=10.

5.2 Effect of aspect ratio of rectangular ducts

Rectangular channels with aspect ratios of 0.0 (parallel plates), 0.2,0.5, and 1.0 (square duct), were simulated to investigate the effect of the aspect ratio on the fluid flow and heat transfer characteristics. The effects of the aspect ratio on fully developed characteristics, on U_{max} , f_{app} Re and on the local Nusselt number subjected to both T and H2 boundary conditions are displayed in Table 5.2, Fig. 5.3 (a - d) and Fig. 5.4 (a - d), respectively. In the fully developed region the channel with a smaller aspect ratio has higher velocity and velocity gradient close to the wall, and lower dimensionless maximum axial velocity. Due to the flatter velocity for pseudoplastic fluids the effect of aspect ratio on maximum velocity for these fluids is less pronounced than for Newtonian fluids. For example, the dimensionless maximum velocity in the fully developed region for Newtonian fluids ranges from 1.491 (parallel plates) to 2.092 (square duct) while for n=0.5 it ranges from 1.327 to 1.760. The higher velocity gradient close to the walls for the lower aspect

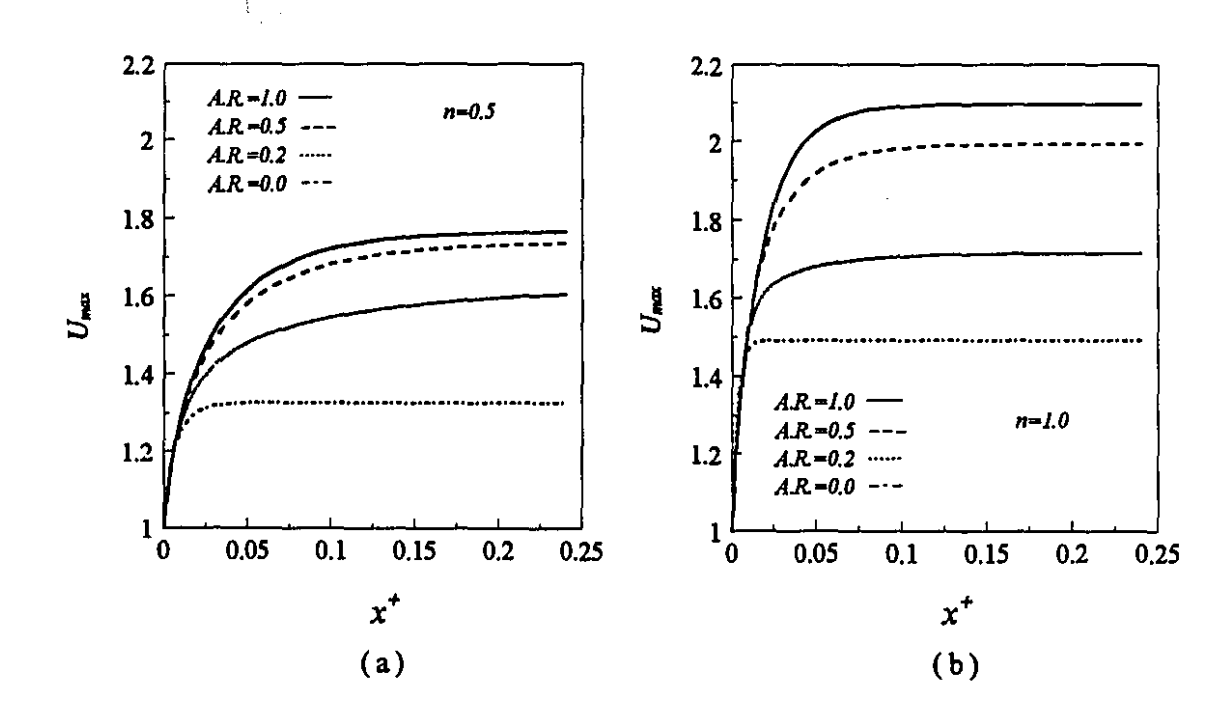
ratio duct as expected results in a higher fully developed friction factor (Fig. 5.3). From Table 5.2 the range of fully developed f.Re is from 5.772 (for square duct) to 7.994 (for parallel plates) and from 14.234 (for square duct) to 23.879 (for parallel plates) for n=0.5 and n=1.0, respectively.

Table 5.2 Comparison of flow and heat transfer characteristics for rectangular ducts with different aspect ratio.

		f.Re	Umax	K (∞)	L^{+}	Nu _T	Nu_{H2}
	A.R.=0.0	7.994	1.327	0.351	0.025	7.950	<i>8.758</i>
n=0.5	A.R. = 0.2	6.860	1.600	0.639	0.165	4.922	2.717
	A.R. = 0.5	6.060	1.734	0.801	0.147	3.600	3.150
	A.R.=1.0	5.772	1.760	0.901	0.131	3.190	3.310
n=1.0	A.R. = 0.0	23.879	1.491	0.763	0.011	7.541	8.235
	A.R. = 0.2	19.077	1.714	1.103	0.074	4.831	2.924
	A.R.=0.5	15.570	1.992	1.475	0.084	3.388	3.021
	A.R.=1.0	14.234	2.092	1.670	0.071	2.979	3.090
n=1.25	A.R.=0.0	40.694	1.546	1.089	0.050	7.442	8.109
	A.R. = 0.2	31.456	1.749	1.417	0.034	4.817	2.996
	A.R.=0.5	24.805	2.053	1.935	0.052	3.350	2.998
	A.R.=I.0	22.248	2.209	2.222	0.050	2.925	3.032

Decreasing the aspect ratio also enhances the local Nusselt number as the velocity close to the wall increases. For example at $x^*=0.0002$ for n=0.5, $Nu_{T,x}$ and $Nu_{H2,x}$ vary from 23 (square duct) to 26 (parallel plates) and from 32 (square duct) to 36 (parallel plates), respectively. As we can see from Fig. 5.4, the enhancement is not the same for different boundary conditions and the magnitude of the relative increase in Nusselt number for various boundary conditions is different. In the entrance region, for the small aspect ratio duct (0.2), $Nu_{H2,x}$ is greater than $Nu_{T,x}$ while this trend reverses further downstream. In other words, for a duct with an aspect ratio approaching zero, due to the effect of imposed constant heat flux on the short sides, $Nu_{H2,x}$ does not approach the value for parallel plates. For example, for n=0.5 at the fully developed condition $Nu_T=7.950$, 4.922,

3.600, 3.190 and $Nu_{H2} = 8.758$, 2.717, 3.150 and 3.310 for ducts with aspect ratios of 0.0, 0.2, 0.5 and 1.0 respectively. For n=0.5, $\frac{Nu_{H2}}{Nu_T}$ is 1.10, 0.55, 0.88, 1.04 which shows the significant effect of sharp corner on Nu_{H2} for A.R.=0.2. Also as explained in Chapter 3 at fully developed region for the rectangular duct of aspect ratio 0.2, due to the opposite effect of power law index on velocity profiles on short sides, increasing n increases Nu_{H2} .



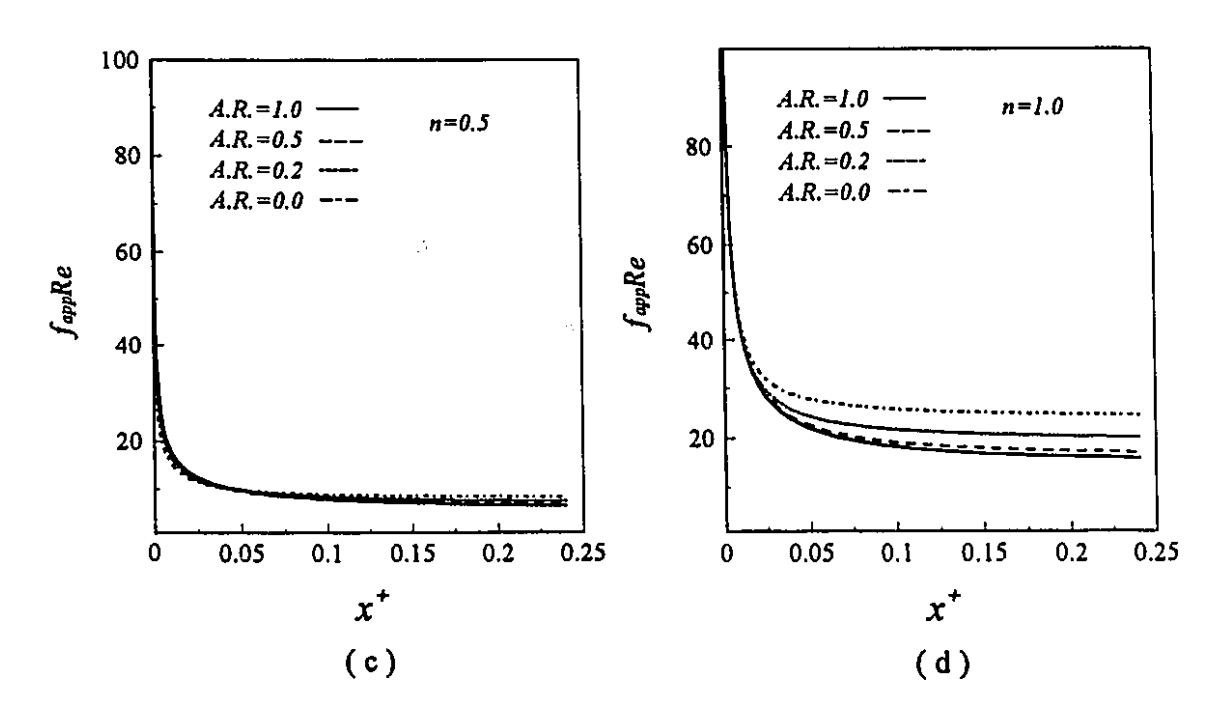
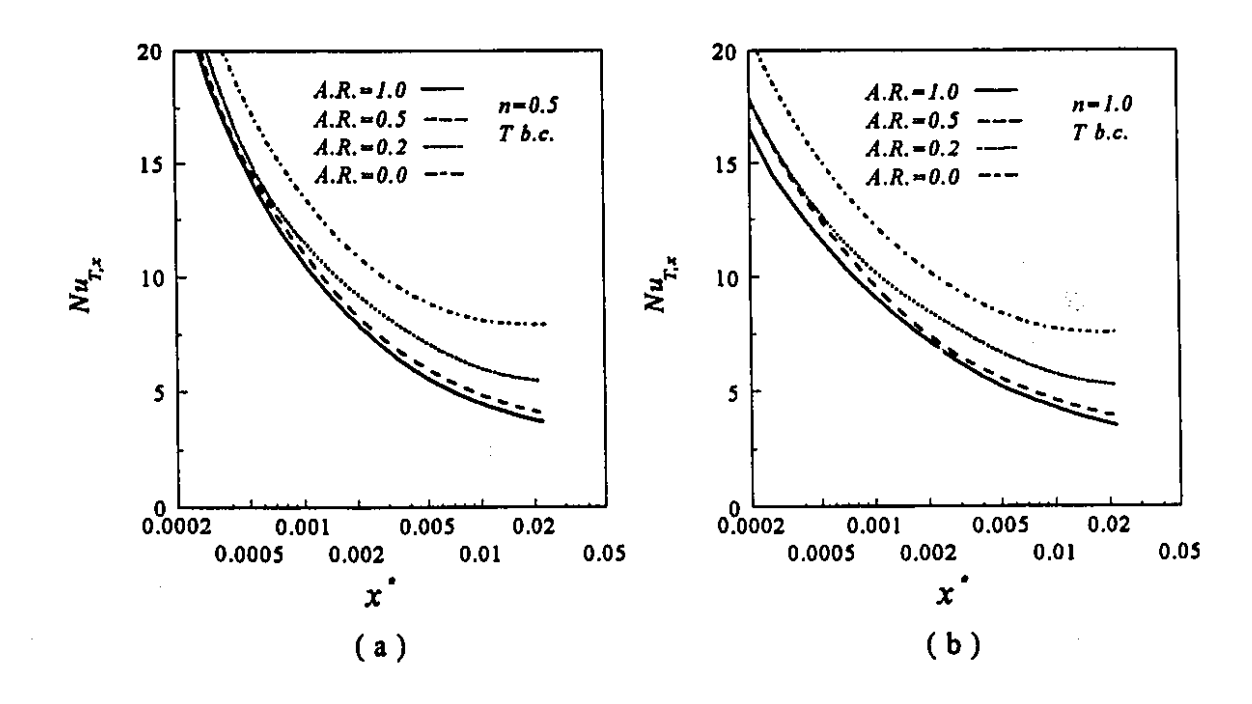


Figure 5.3 (a - d) Effect of aspect ratio of a rectangular duct on dimensionless maximum velocity and apparent friction factor, Re=500.



٠,

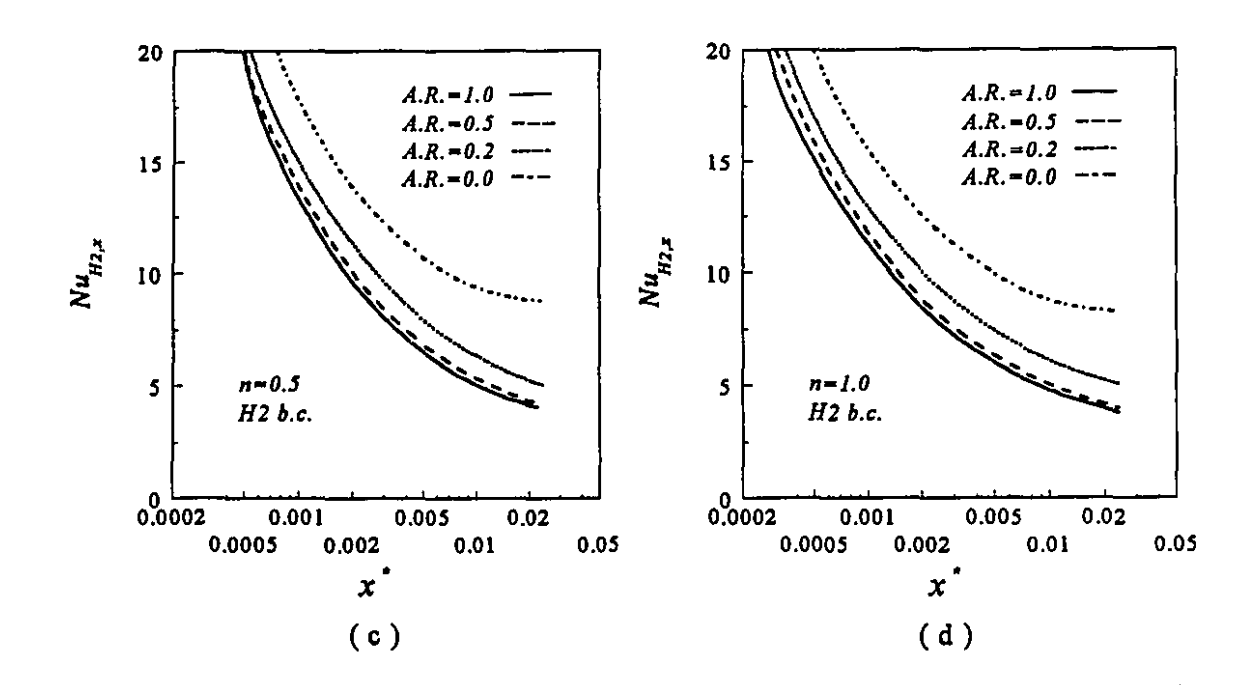


Figure 5.4 (a - d) Effect of aspect ratio of a rectangular duct on the local Nusselt number distribution, Re=500, Pr=10.

5.3 Effect of apex angle of circular-sector ducts

Fig. 5.5 (a - d) shows U_{max} , f_{app} Re for circular-sector ducts of three different apex angles (α). The fully developed flow and heat transfer characteristics are tabulated in Tables 5.3. From Fig. 5.5 the effect of α on U_{max} and $f_{app}Re$ shows different behavior depending on the power law index. For example, for n=0.5 and $\alpha=60^{\circ}$, f_{app} Re (at $x^+=0.0020$) and f.Re (fully developed condition) is about 17.2 % and 10.1 % higher than those for a semi-circular duct, but for n=1.0 these values are about 4.2 % and 10.2 % lower, respectively. For $\alpha=90^{\circ}$, at $x^+=0.0020$ for fluids with n=0.5 and n=1.0, f_{app} Re is 5.0 % and 7.8 % lower than the corresponding values for the semi-circular duct. At the hydrodynamically fully developed condition the corresponding values for f.Re are 4.4 % and 6.6 %, respectively.

Fig. 5.6 (a - d) displays the local Nusselt number and dimensionless bulk temperature distribution for circular-sector ducts of different apex angles. From Fig. 5.6 it

is clear that the effect of the apex angle on $Nu_{T,x}$ is strongly dependent on x° . At the fully developed condition, Nu_{T} for n=0.5 ranges from 2.936 (for $\alpha=60^{\circ}$) to 3.480 ($\alpha=180^{\circ}$) and for Newtonian fluids the corresponding range is from 2.820 to 3.318.

Table 5.3 Comparison of flow and heat transfer characteristics for circular-sector ducts with different apex angles.

		f.Re	U_{max}	$K(\infty)$	$L^{\scriptscriptstyle +}$	Nu _T	Nu _{H2}
	$\alpha = 60^{\circ}$	5.761	1.792	0.837	0.143	2.936	2.510
n=0.5	$\alpha = 90^{\circ}$	5.951	1.744	0.765	0.133	3.206	3.121
	$\alpha = 180^{\circ}$	6.223	1.747	0.764	0.143	3.480	3.038
	$\alpha = 60^{\circ}$	14.248	2.134	1.582	0.077	2.820	2.430
n=1.0	$\alpha = 90^{\circ}$	14.820	2.079	1.451	0.072	3.060	2.980
	$\alpha = 180^{\circ}$	15.860	2.058	1.437	0.076	3.318	2.920
	$\alpha = 60^{\circ}$	22.332	2.242	2.078	0.052	2.789	2.408
$ _{n=1.25} $	$\alpha = 90^{\circ}$	23.216	2.181	1.901	0.048	3.013	2.937
	$\alpha = 180^{\circ}$	25.365	2.146	1.894	0.051	3.265	2.880

For the H2 boundary condition, at the fully developed condition there is a different effect of apex angles on the Nusselt number. At fully developed condition, for all power law indices the duct with $\alpha = 60^{\circ}$ possesses the lowest Nu_{H2} while the duct with $\alpha = 90^{\circ}$ yields the highest Nu_{H2} .

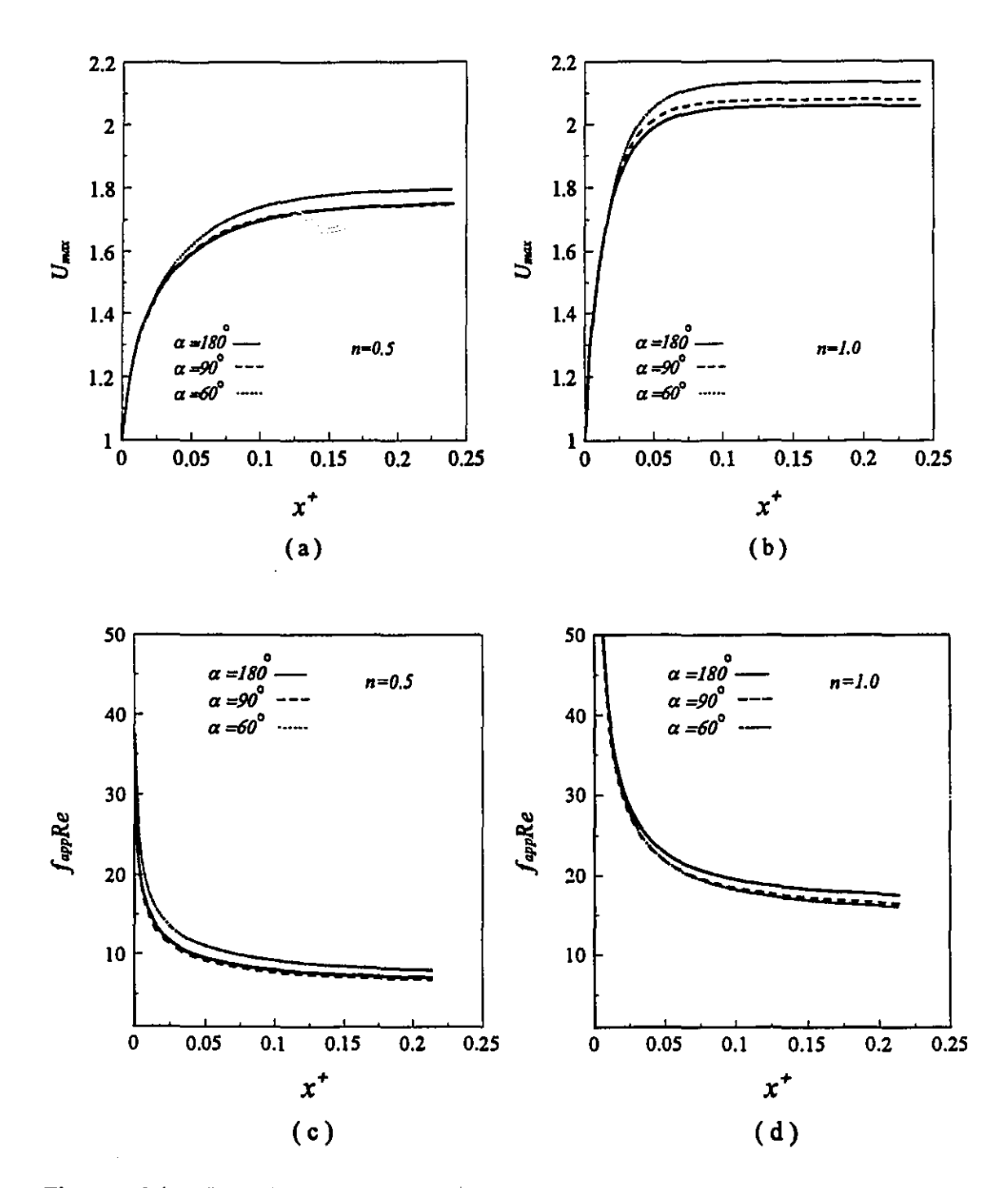


Figure 5.5 (a - d) Effect of apex angle of circular-sector duct on dimensionless maximum velocity and apparent friction factor, Re=500.

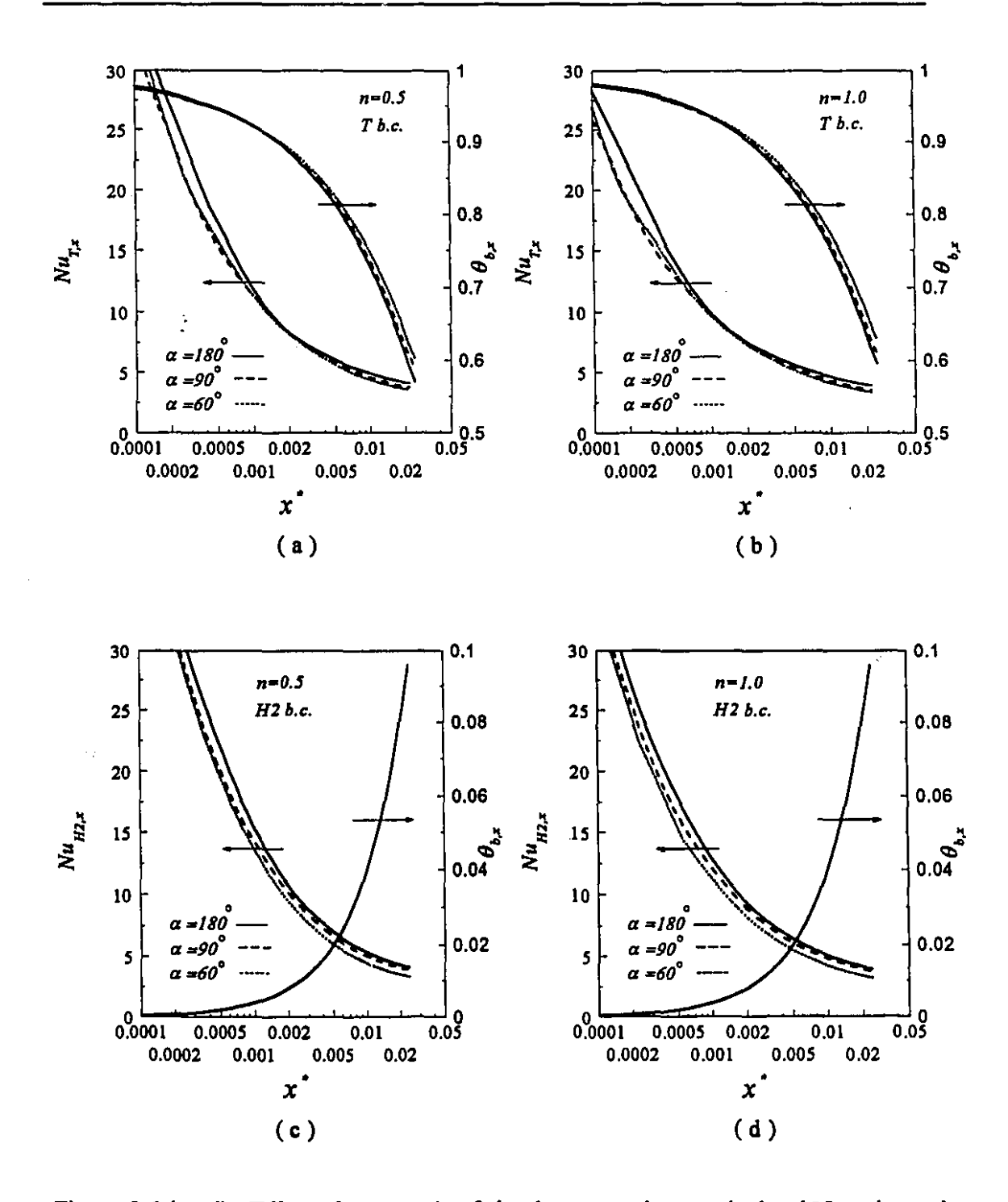


Figure 5.6 (a - d) Effect of apex angle of circular-sector duct on the local Nusselt number distribution, Re=500, Pr=10.

5.4 Comparison between circular-sector and triangular ducts

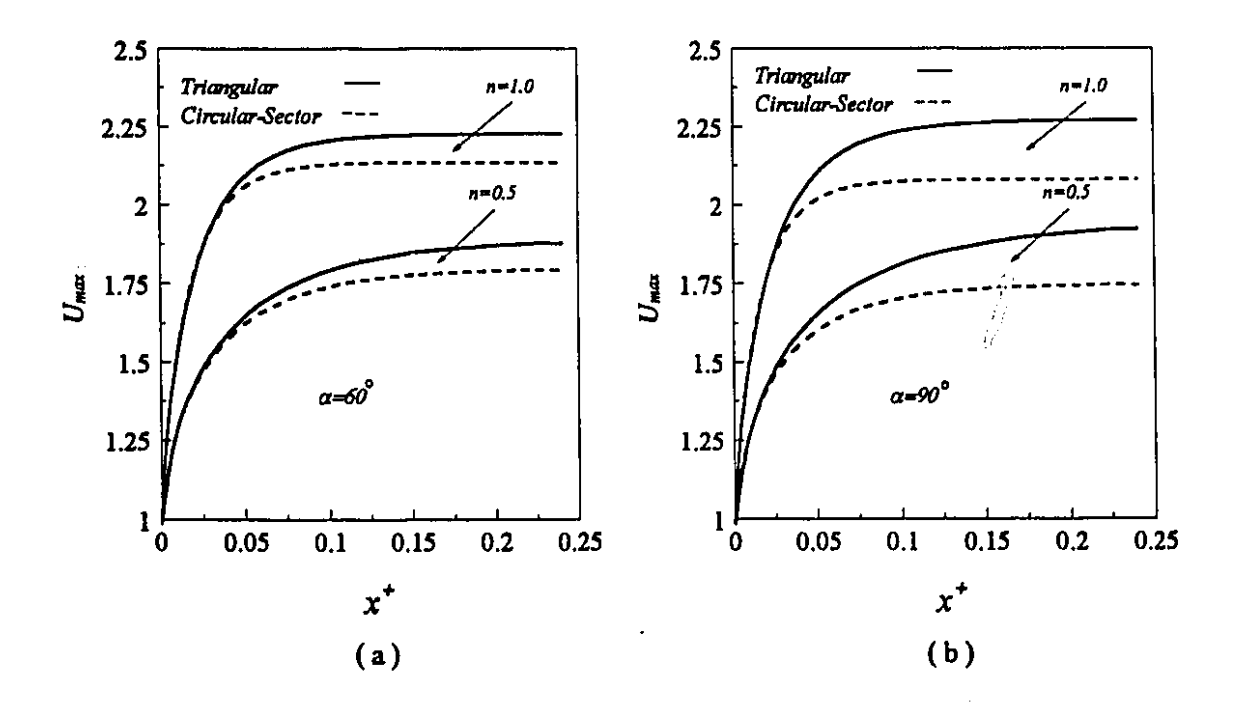
Fig. 5.7 (a - d) compares U_{max} and f_{app} Re for triangular and circular-sector channels with the same apex angles. Fully developed values of the flow characteristics and Nusselt numbers are presented in Table 5.4. For $\alpha = 60^{\circ}$ and $\alpha = 90^{\circ}$, f_{app} Re is lower for circular-sector ducts in the entrance region while it is slightly higher far downstream. For example, at $x^+ = 0.0020$ and $x^+ = 0.02290$ for n=0.5, f_{app} Re for a circular-sector duct ($\alpha = 60^{\circ}$) possesses 40.4 % and 1.3 % lower values than those for an equilateral triangular duct; the corresponding values for $\alpha = 90^{\circ}$ are 55.4 % and 19.9 %, respectively. But the fully developed friction factor for the circular-sector exceeds the corresponding values for the triangular channels (Table 5.4).

Fig. 5.8 (a - d) shows $Nu_{T,x}$ and $Nu_{H2,x}$ for circular-sector and triangular ducts. For both apex angles ($\alpha = 60^{\circ}$ and $\alpha = 90^{\circ}$) $Nu_{H2,x}$ for circular-sector ducts is much higher than those for triangular ducts in the entire duct. For n=0.5 at $x^{\circ} = 0.00020$ and $x^{\circ} = 0.00229$ for the circular-sector duct with $\alpha = 60^{\circ}$ $Nu_{H2,x}$ values are 6.6% and 21.5%, respectively, higher than those for an equilateral triangular duct at the same x° . The corresponding values for $\alpha = 90^{\circ}$ are 15.2% and 54.9%.

For the T boundary condition close to the entrance for n=0.5, $Nu_{T,x}$ is about the same for both circular-sector and triangular channels (for both $\alpha=60^{\circ}$ and $\alpha=90^{\circ}$); further downstream the difference increases reaching a maximum value at the fully developed condition. For n=1.0, at $x^{\circ}=0.00020$ circular sector ducts ($\alpha=60^{\circ}$ and $\alpha=90^{\circ}$) possess 13.9 % and 15.6 % higher $Nu_{T,x}$ values than those for triangular ducts of the same apex angles. Further downstream the difference in $Nu_{T,x}$ between circular sector and triangular channels for n=1.0 decreases.

Table 5.4 Comparison of flow and heat transfer characteristics between circular-sector and triangular ducts with the same apex angles.

		f.Re	U_{max}	K(∞)	L ⁺	NuT	Nu _{H2}
n=0.5	Circular-sector $\alpha = 60^{\circ}$	5.761	1.792	0.837	0.143	2.936	2.510
	Triangular $\alpha = 60^{\circ}$	5.455	1.877	1.159	0.165	2.594	1.951
	Circular-sector $\alpha = 90^{\circ}$	5.951	1.744	0.765	0.133	3.206	3.121
_	Triangular $\alpha = 90^{\circ}$	5.383	1.916	1.236	0.175	2.409	1.370
n=1.0	Circular-sector $\alpha = 60^{\circ}$	14.248	2.134	1.582	0.077	2.820	2.430
	Triangular $\alpha = 60^{\circ}$	13.340	2.230	2.043	0.100	2.503	1.896
	Circular-sector $\alpha = 90^{\circ}$	14.820	2.079	1.451	0.072	3.060	2.980
_	Triangular $\alpha = 90^{\circ}$	13.167	2.268	2.176	0.112	2.350	1.351
n=1.25	Circular-sector $\alpha = 60^{\circ}$	22.332	2.242	2.078	0.052	2.789	2.408
	Triangular $\alpha = 60^{\circ}$	20.978	2.343	2.662	0.069	2.478	1.880
	Circular-sector $\alpha = 90^{\circ}$	23.216	2.181	1.901	0.048	3.013	2.937
	Triangular $\alpha = 90^{\circ}$	20.748	2.377	2.799	0.077	2.335	1.344



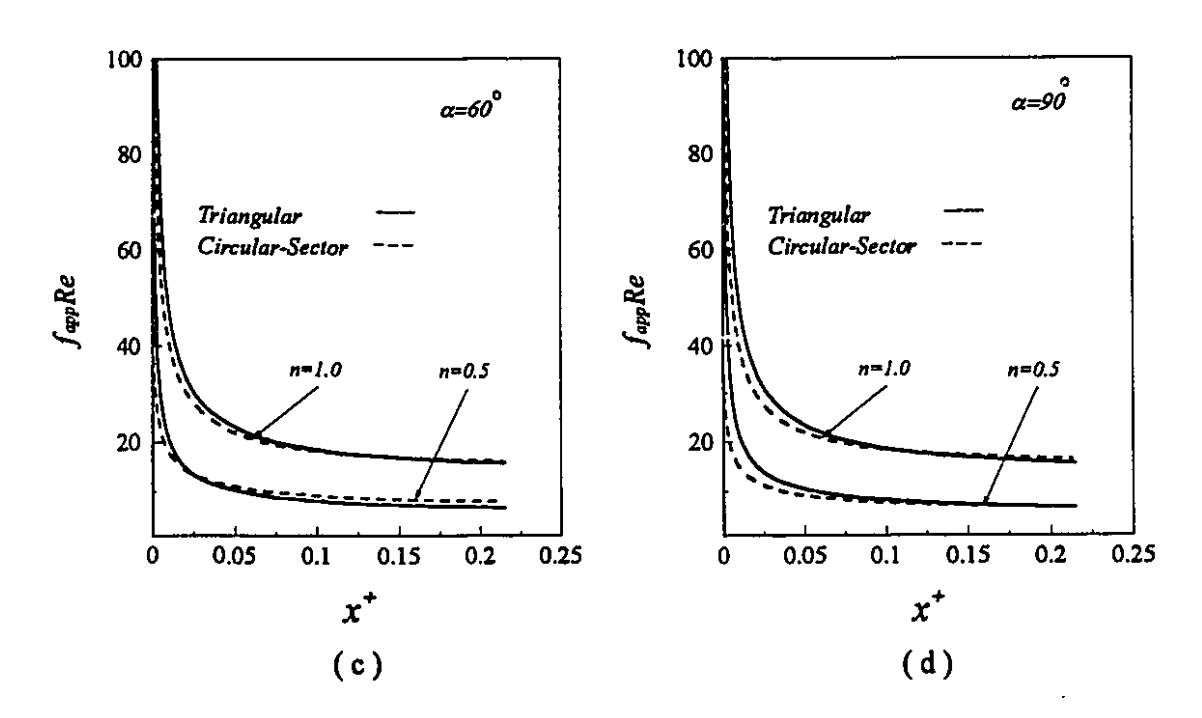
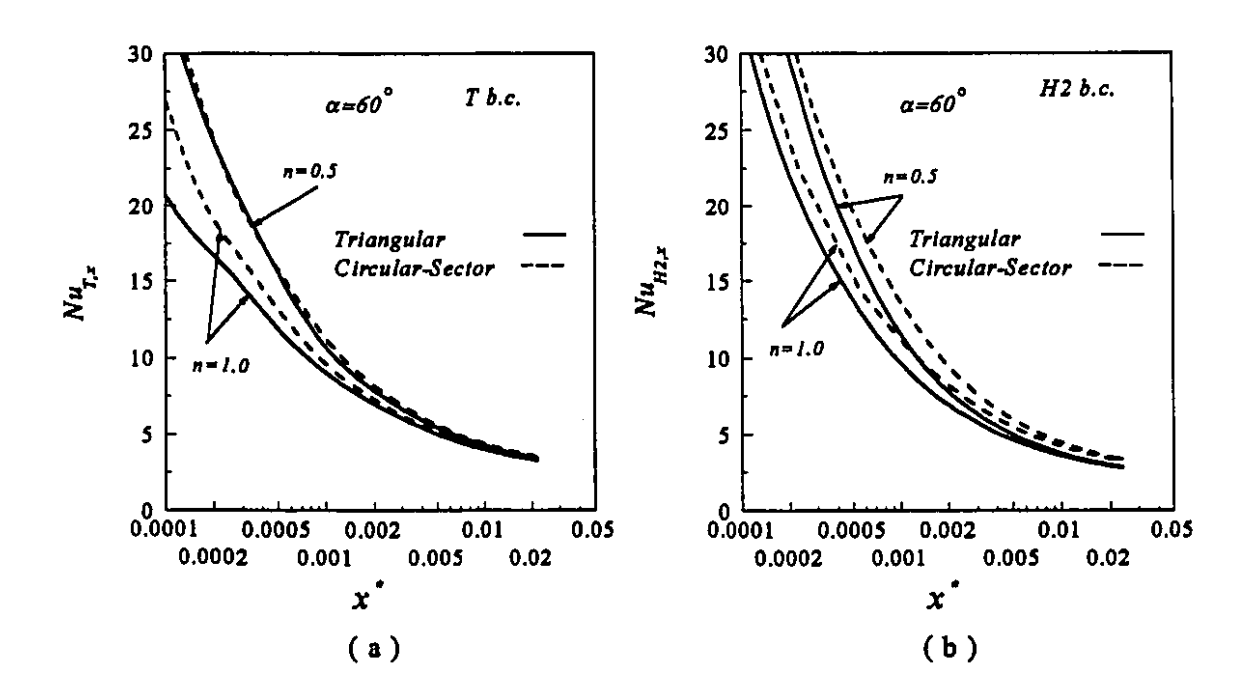


Figure 5.7 (a - d) Comparison of flow characteristics between the circular-sector and triangular ducts with the same apex angles, Re=500.



1!

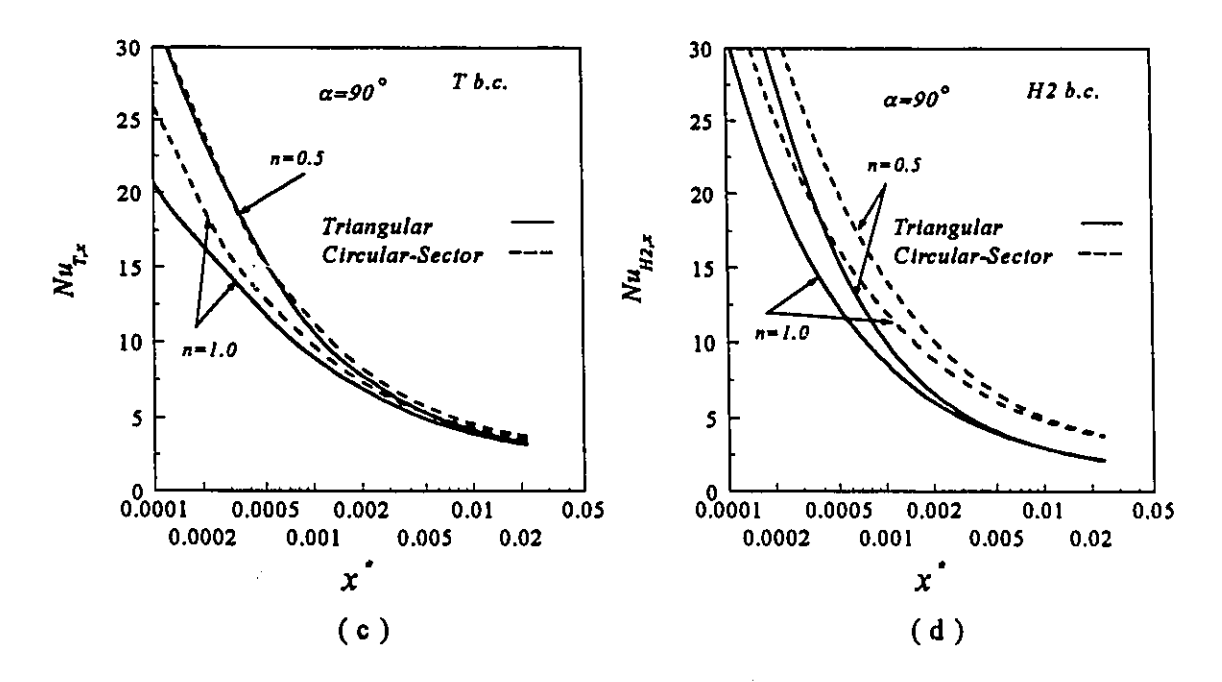


Figure 5.8 (a - d) Comparison of Nusselt number between the circular-sector and triangular ducts of the same apex angles, Re=500, Pr=10.

5.5 Effect of geometric parameter of cross-shaped duct

The effect of the geometric parameter, λ , on the flow and thermal performance of cross-shaped ducts is studied numerically for Re=500 and Pr=10. Fig. 5.9 (a - d) and Fig. 5.10 (a - d) present U_{max} , $f_{app}Re$, and Nusselt number distributions, respectively, for different values of the geometric parameter (λ) defined in Table 2.1. The fully developed values for selected fluid flow and heat transfer characteristics are displayed in Table 5.5. From Fig. 5.9, U_{max} for a square duct ($\lambda=0.0$) falls within the corresponding range for a cross-shape duct with $\lambda=0.25$ and $\lambda=0.50$.

From Fig. 5.9, for n=0.5, the square duct ($\lambda=0.0$) yields the highest f_{app} Re in the entrance region while the cross-shaped duct with $\lambda=0.5$ yields the lowest value. Further downstream the lowest value corresponds to the cross-shaped duct with $\lambda=0.25$. For Newtonian fluids the highest pressure drop is presented by square duct and the lowest value by the cross-shaped channel ($\lambda=0.25$) over most of the axial length.

For both T and H2 boundary conditions the choice of duct geometry with higher Nusselt number depends on the axial length. For example, for n=0.5 at $x^{\bullet}=0.0002$ the highest $Nu_{T,x}$ is obtained with a cross-shaped channel with $\lambda=0.25$ while the lowest one with a square duct. Far downstream, the square duct has the highest $Nu_{T,x}$ while the lowest $Nu_{T,x}$ is due to the cross-shaped channel with $\lambda=0.5$. The fully developed values of Nu_{T} (Table 5.5) emphasize the significant effect of the geometric parameter, λ , on heat transfer.

For the H2 boundary condition, close to the entrance the relative thermal performance of the duct depends on the power law index. For instance, at $x^*=0.0002$ the highest Nusselt number for n=0.5 is due to the square duct while the lowest value is given by the cross-shaped channel with $\lambda=0.5$. Further downstream for both n=0.5 and n=1.0 the square duct has the highest $Nu_{H2,x}$ while the cross-shaped duct with $\lambda=0.5$ yields the lowest value. Different behavior of the fluid flow and heat transfer characteristics can be related to number of the presence of sharp corners and velocity gradient in the corner region.

In general the cross-shaped duct has the advantage of lower friction factor but it results in a lower Nusselt number.

Table 5.5 Comparison of flow and heat transfer characteristics for cross-shaped ducts with different geometric parameters.

		f.Re	Umax	$K(\infty)$	L^{+}	Nu_T	Nu _{H2}
	$\lambda = 0.00$	5.772	1.760	0.901	0.131	3.190	3.310
n=0.5	$\lambda = 0.25$	5.317	1.711	0.727	0.130	2.883	3.170
	$\lambda = 0.50$	5.209	1.821	0.881	0.159	2.508	2.598
	$\lambda = 0.00$	14.234	2.092	1.670	0.071	2.979	3.090
n=1.0	$\lambda = 0.25$	12.625	2.034	1.404	0.074	2.667	2.956
·	$\lambda = 0.50$	12.479	2.171	1.648	0.097	2.338	2.443
	$\lambda = 0.00$	22.248	2.209	2.222	0.050	2.925	3.032
n=1.25	$\lambda = 0.25$	19.356	2.148	1.835	0.053	2.628	2.903
	$\lambda = 0.50$	19.349	2.287	2.121	0.068	2.300	2.413



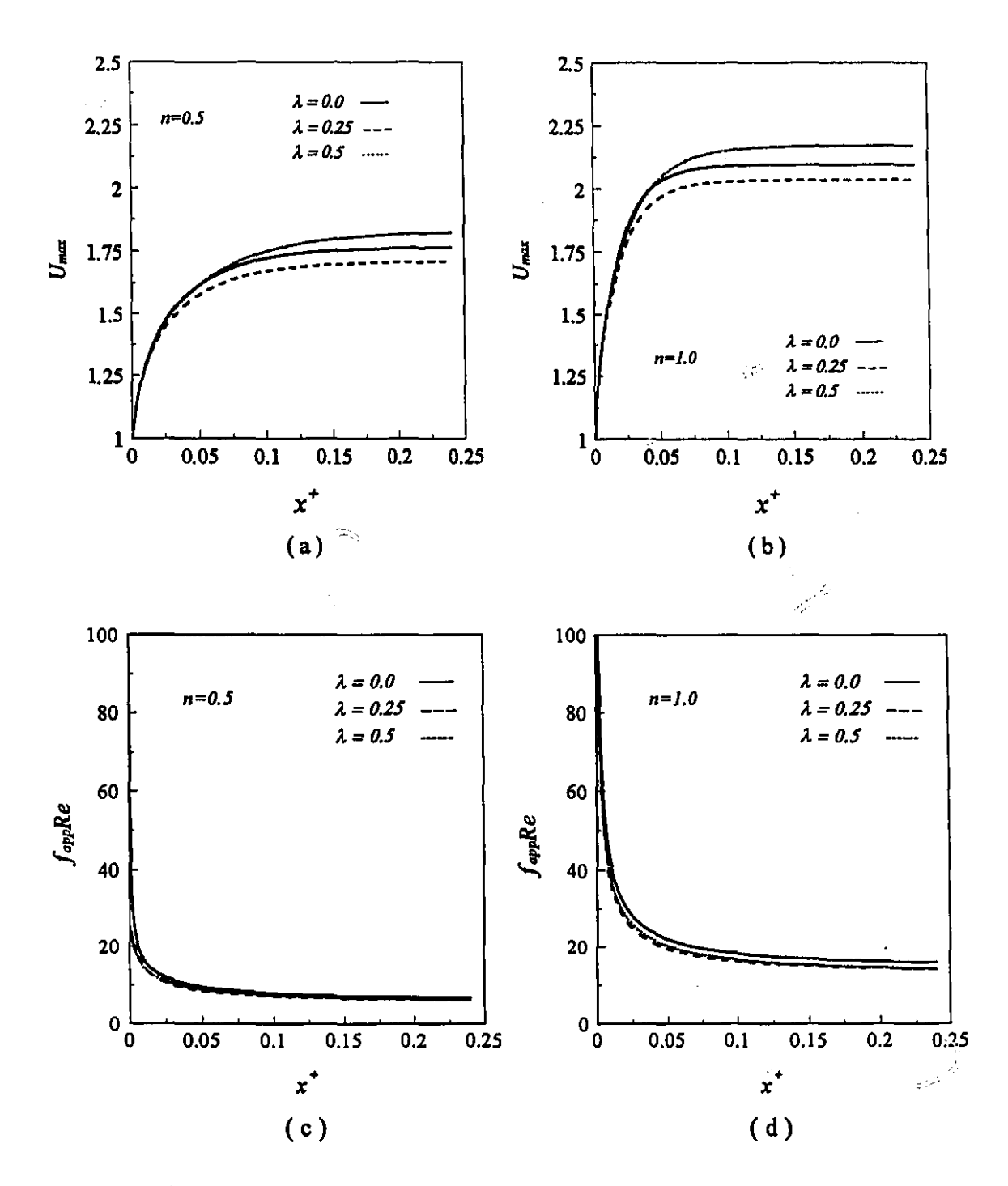


Figure 5.9 (a - d) Effect of geometric parameter of cross-shaped duct on dimensionless maximum velocity and apparent friction factor, Re=500.

ź.;

-

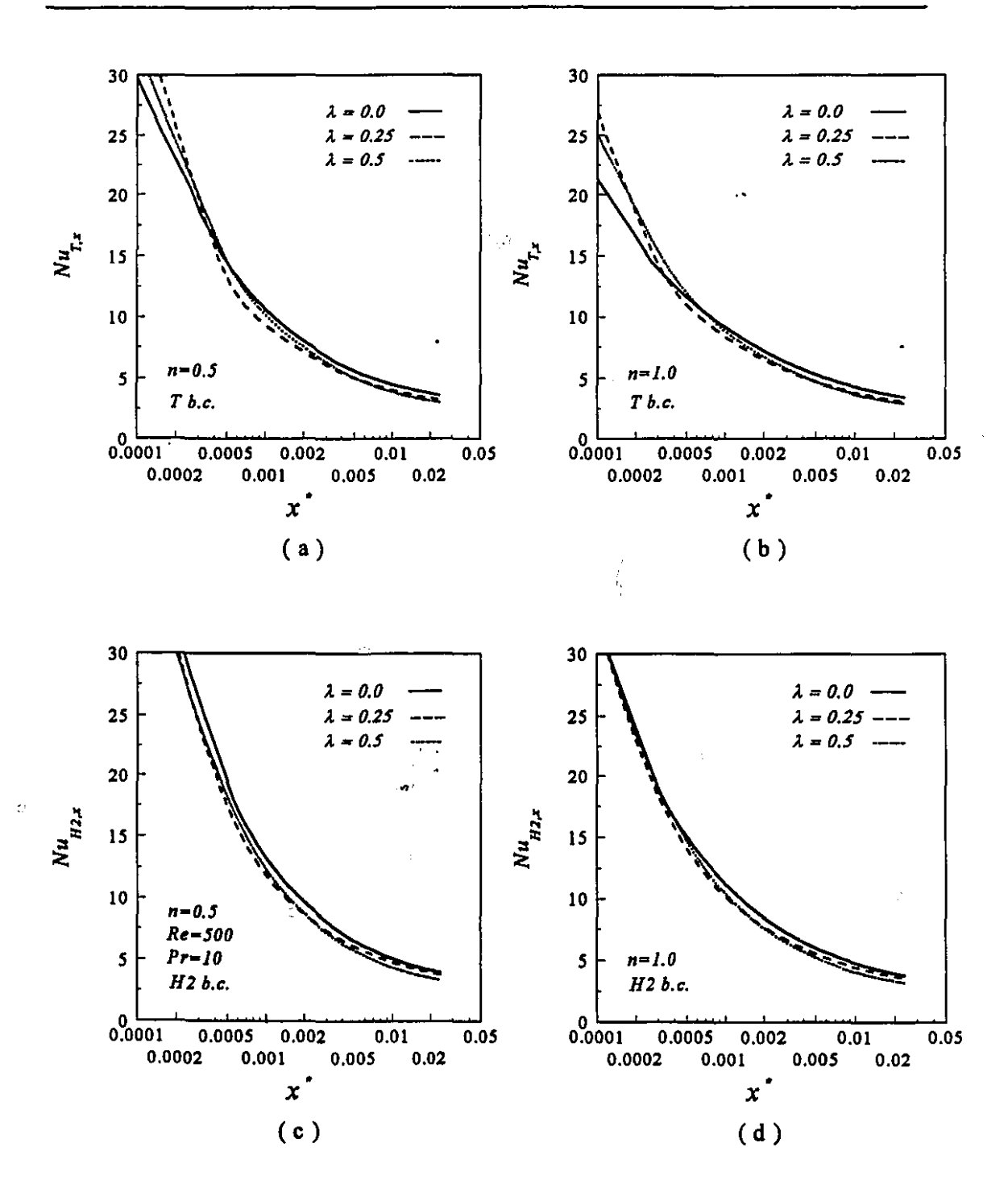


Figure 5.10 (a - d) Effect of the geometric parameter of cross-shaped duct on the local Nusselt number distribution, Re=500, Pr=10.

5.6 Conclusions

The results of numerical simulations are presented which include some miscellaneous effects not documented in earlier chapters. The following conclusions are made from these numerical experiments.

- Rounding of corners of a square duct results in higher fully developed friction factor regardless of the value of n. Also, rounding of corners enhances the fully developed Nusselt number for both T and H2 boundary conditions. The enhancement due to the rounding of corners is greater for Nu_{H2} than for Nu_T .
- The effects of the aspect ratio of a rectangular duct on f_{app} Re and Nusselt number are significant. By decreasing the aspect ratio of a rectangular duct, Nu_{H2} does not simulate the parallel plate channel due to the presence of corners.
- In the entrance region, f_{app} Re for the circular sector duct ($\alpha = 60^{\circ}$ and $\alpha = 90^{\circ}$) is lower than that for the triangular duct of the same apex angles, but it is higher further downstream. Fully developed values of Nu_T and Nu_{H2} for circular sector channels are higher than those for corresponding triangular ducts.

Chapter 6

Comparison of Thermal Performance of Various Ducts

This chapter deals with comparison of the flow and thermal performance of 14 duct geometries examined in this study; it includes results for fully developed as well as simultaneously developing flow and thermal conditions. Different 'goodness factors' are compared for both T and H2 boundary conditions.

1

6.1 Fully developed conditions

The fully developed values of f.Re, U_{max} , $K(\infty)$, and L^+ for 14 duct geometries are presented in Table 6.1. Table 6.2 contains the fully developed Nusselt number values for two thermal boundary conditions (T and H2) and various power law indices.

From Table 6.1 f.Re for n=0.5 ranges from 5.209 to 7.994. For n=1.0 and n=1.25 the ranges of f.Re are 12.479 to 23.879 and 19.349 to 40.692 respectively. The highest f.Re for all n values belong to parallel plate channels and the lowest to the cross-shaped channel ($\lambda = 0.5$). The parallel plate channel is followed by the rectangular channel with an aspect ratio of 0.2.

The fully developed dimensionless maximum axial velocity for the channels studied (Table 6.1) range from 1.327 to 1.916, 1.497 to 2.268 and from 1.547 to 2.377 for n=0.5, 1.0 and 1.25, respectively. The highest values are for right isosceles triangular ducts and the lowest for parallel plates for all power law indices. The hydrodynamic entrance length for parallel plates is the shortest while the right isosceles triangular duct requires the

4

highest length for development. The hydrodynamic entrance length (Table 6.1) varies from 0.025 to 0.175, from 0.011 to 0.112, and from 0.007 to 0.077 for n=0.5, 1.0, and 1.25, respectively. For Newtonian fluids the flow entrance region for parallel plates is about 10 times smaller than that for the right isosceles triangular channel. Hydrodynamic entrance length is one of the parameters which affects the incremental pressure drop. The results also show the incremental pressure drop for parallel plates is the smallest while that for the right triangular channels is the highest. For example, $K(\infty)$ for n=1.0 varies from 0.763 to 2.176; the ratio of the highest to lowest value of $K(\infty)$ is about 2.9 emphasizing the significant effect of the entrance region on the pressure drop for a right triangular duct.

For the duct geometries studied for n=0.5, Nu_T ranges from 2.409 for the right triangular duct to 7.950 for parallel plates (Table 6.2). For n=1.0 and n=1.25 the highest values 7.541 and 7.442 belong to parallel plate channel, while the lowest ones, 2.338 and 2.300, are for the cross-shaped channel ($\lambda=0.5$). Therefore for isothermal walls the parallel plate channel is superior in heat transfer performance relative to other channels.

For the H2 boundary condition the parallel plate channel has the highest Nu_{H2} while the right isosceles triangular duct has the lowest Nu_{H2} for all power law indices. The ratio of highest Nu_{H2} to the lowest values are 6.4, 6.1 and 6.0 for n=0.5, 1 and 1.25 respectively. Nu_{H2} for channels with sharp corners is lower than that circular tubes or parallel plate channels. As mentioned in Chapter 3 the effect of sharp corners in the duct cross-section on Nusselt number is more pronounced for the H2 boundary condition than for the T boundary condition.

Table 6.1 Fluid flow characteristics for different power law indices and various geometric configurations for fully developed conditions.

Geometry			n=0.50			n=1.00				n=1.25			
			U _{max}	<i>K</i> (∞)	L ⁺	f.Re	U _{max}	<i>K</i> (∞)	L ⁺	f.Re	U _{max}	<i>K</i> (∞)	L ⁺
	Circle	6.321	1.665	0.632	0.098	16.005	1.996	1.268	0.054	25.231	2.108	1.701	0.037
	Square	5.772	1.760	0.901	0.131	14.234	2.092	1.670	0.071	22.248	2.209	2.222	0.050
	Rounded Corner R.C.=a/20	5.924	1.719	0.742	0.121	14.604	2.060	1.419	0.065	22.895	2.150	1.895	0.045
	Rounded Corner R.C.=a/6	6.193	1.707	0.721	0.116	15.500	2.051	1 408	0.060	24.120	2.141	1.872	0.042
	A.R.=0.5	6.060	1.734	0.801	0.147	15.570	1.992	1.475	0.084	24.805	2.053	1.935	0.052
	A.R.=0.2	6.860	1.600	0.639	0.165	19.077	1.714	1.103	0.074	31.456	1.749	1.417	0.034

 Parallel Plates	7.994	1.327	0.351	0.025	23.879	1.491	0.763	0.011	40.692	1.547	1.089	0.007
α = 180°	6.223	1.747	0.764	0.143	15.860	2.058	1.437	0.076	25.365	2.146	1.894	0.051
α = 90°	5.951	1.744	0.765	0.133	14.820	2.079	1.451	0.072	23.216	2.181	1.901	0.048
α = 60°	5.761	1.792	0.837	0.143	14.248	2.134	1.582	0.077	22.332	2.242	2.078	0.052
$\alpha = 60^{\circ}$	5.455	1.877	1.159	0.165	13.340	2.230	2.043	0.100	20.978	2.343	2.662	0.069
α = 90°	5.383	1.916	1.236	0.175	13.167	2.268	2.176	0.112	20.748	2.377	2.799	0.077
λ = 0.25	5.317	1.711	0.727	0.130	12.625	2.034	1.404	0.074	19.356	2.148 	1.835	0.053
A = 0.5	5.209	1.821	0.881	0.159	12.479	2.171	1.648	0.097	19.349	2.287	2.121	0.068

P

Table 6.2 Nusselt number for different power law indices and various geometric configurations for fully developed conditions.

Geometry			Nu _T		Nu _{H2}			
		n=0.50	n=1.00	n=1.25	n=0.50	n=1.00	n=1.25	
	Circle	3.950	3.659	3.590	4.744	4.363	4.272	
	Square	3.190	2.979	2.925	3.310	3.090	3.032	
	Rounded Corner R.C.=a/20	3.270	3.047	2.991	3.461	3.221	3.160	
	Rounded Corner R.C.=a/6	3.431	3.188	3.129	3.764	3.488	3.417	
	A.R.=0.5	3.600	3.388	3.350	3.150	3.021	2.998	
	A.R.=0.2	4.922	4.831	4.817	2.717	2.924	2.996	
	Parallel Plates	7.950	7.541	7.442	8.758	8.235	8.109	

K

α = 180°	3.480	3.318	3.265	3.038	2.920	2.880
α = 90°	3.206	3.060	3.013	3.121	2.980	2.937
$\alpha = 60^{\circ}$	2.936	2.820	2.789	2.510	2.430	2.408
α = 60°	2.594	2.503	2.478	1.951	1.896	1.880
α = 90°	2.409	2.350	2.335	1.370	1.351	1.344
λ = 0.25	2.883	2.677	2.628	3.170	2.956	2.903
λ = 0.5	2.508	2.338	2.300	2.598	2.443	2.413

6.2 Effect of cross-sectional factor on fully developed friction factor and Nusselt number

Table 6.3 presents the ratio of the cross-sectional area based on the hydraulic diameter definition over the actual geometric area (here called the cross-sectional factor) for the noncircular duct geometries examined. In Table 6.3 the inset circle describes the fictitious area calculated according to the classical definition of the hydraulic diameter of

the channel. Also, Fig. 6.1 shows the fully developed values of f.Re and Nusselt numbers vs. their respective cross-sectional factors. Bejan (1984) has noted an approximate proportionality between the fully developed values of f.Re and Nu and the degree to which D_h misjudges the wall-to-wall distance. As can be seen from Fig. 6.1 the values are scattered. It is clear that the flow and heat transfer characteristics are affected in a complex way by the effects of channel geometry and a simplistic model based on Bejan's factor can not be expected to hold over a wide range of duct geometries. The relationship appears reasonably good if information on some noncircular ducts is removed from the figure.

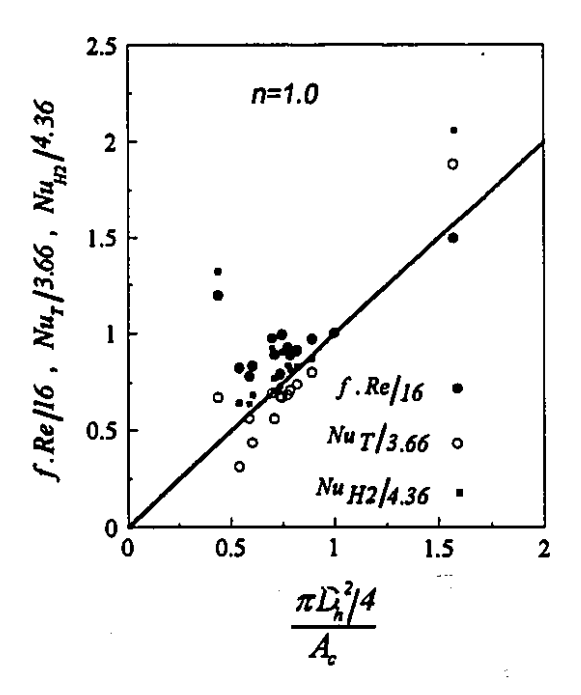


Figure 6.1 Fully developed values of f.Re and Nusselt numbers vs. cross-sectional factor.

Ĥ

Table 6.3 Cross-sectional factors for various duct geometries.

Geometry		$\frac{\pi D_h^2/4}{A_c}$	Geometry		$\frac{\pi D_h^2/4}{A_c}$
	Circle	1.000		$\alpha = 180^{\circ}$	0.747
	Square	0.785		α = 90°	0.774
	Rounded Corner R.C.=a/20	0.819		$\alpha = 60^{\circ}$	0.709
	Rounded Corner R.C.=a/6	0.889		α = 60°	0.605
	A.R.=0.5	0.698		α = 90°	0.539
	A.R.=0.2	0.436		$\lambda = 0.25$	0.736
	Parallel Plates	1.571		$\lambda = 0.5$	0.589

6.3 Comparison of $f_{app}Re$ for different geometries

Values of f_{app} Re in the entrance region at different dimensionless axial locations are tabulated in Tables A1 to A12 (Appendix A) for different power law indices and various cross-sectional configurations.

Due to the short length of channels used in heat exchangers the entrance region can be very important and most of the pressure drop could occur in this section of the channel. This fact is confirmed by the computed results of this study. For example at x^+ =0.0229 for n=0.5, $f_{app}Re$ =11.80, 12.20, 11.64, 11.99, 14.09, 11.20 for parallel plates, square, circular, semicircular, equilateral triangular and cross-shaped (λ = 0.5) ducts, respectively. These imply 48 %, 111 %, 84 %, 93 %, 158 %, and 115 % higher values of $f_{app}Re$ than their respective fully developed values (f.Re).

Fig. 6.2 (a - c) presents f_{app} Re for different duct geometries. This figure refers to the parallel plate channel, the right isosceles triangular duct, and cross-shaped channel $(\lambda = 0.25)$ since these represent the limiting geometries in term of their f_{app} Re values. The remaining duct geometries fall within these bounds. The circular tube is also included in Fig. 6.2 (a - c) for comparison. The right isosceles triangular channel offers the highest pressure drop in the entrance region regardless of the value of n. At $x^+=0.0229$ for n=0.5 among 14 geometries studied the highest f_{app} Re, 14.46, is for the right isosceles triangular channel while the lowest value, 10.90, is for the cross-shaped ($\lambda = 0.25$) configuration. For n=1.0 and n=1.25 at $x^+=0.0229$ the highest values of f_{app} Re, 32.38 and 52.79, are for parallel plates and the lowest values, 25.62 and 37.70, for the cross-shaped duct ($\lambda = 0.25$).

٠,٠

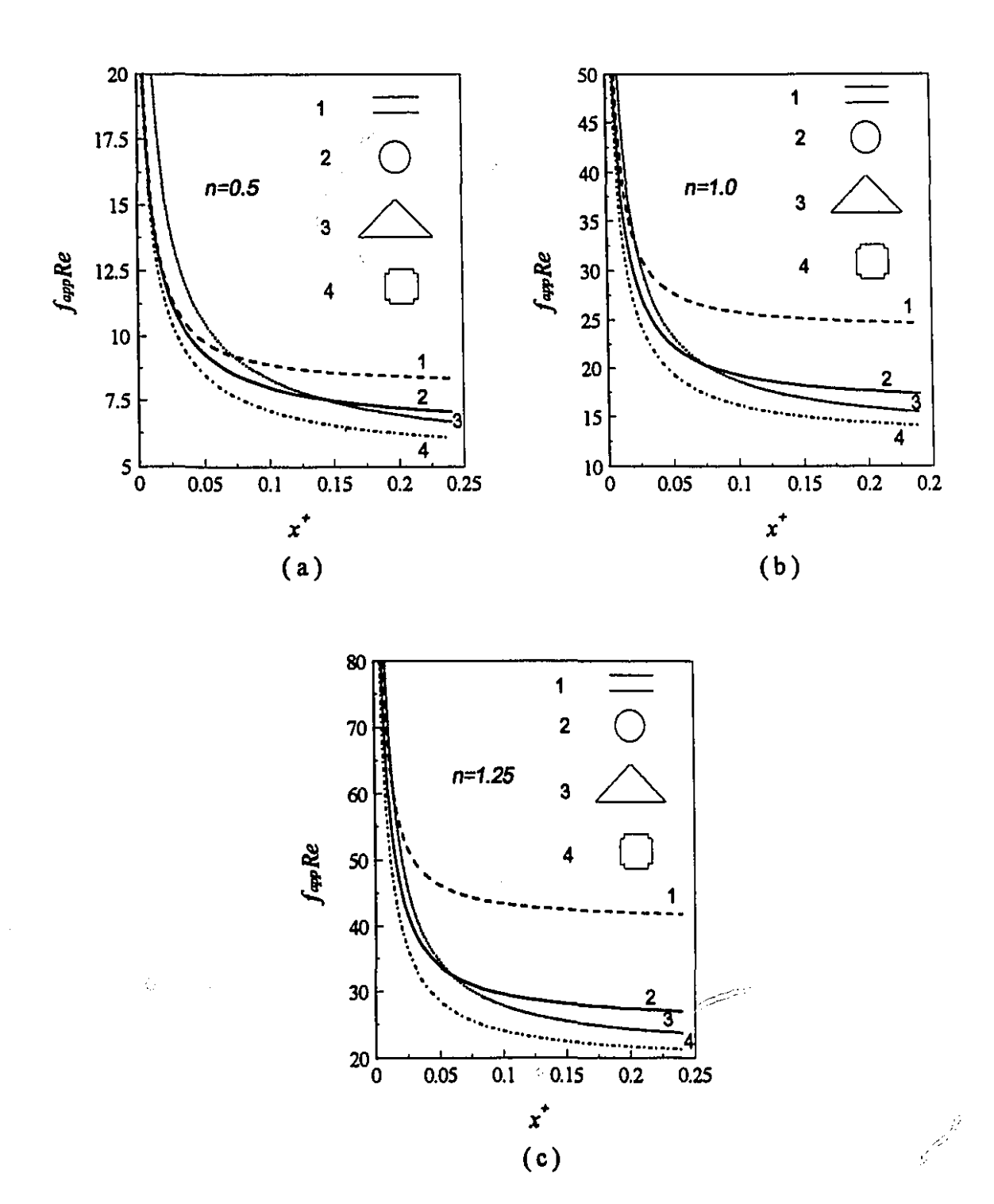


Figure 6.2 (a - c) f_{app} Re vs. x^+ for different geometries at Re=500 (a)- n=0.5, (b)- n=1.0, (c)- n=1.25.

ji

~

6.4 Comparison of entrance region Nusselt numbers for different geometries

Computed Nusselt numbers for different geometries and various power law indices are presented in Fig. 6.3 (a - c) and Fig. 6.4 (a - c) for the T and H2 boundary conditions, respectively. The highest values of $Nu_{T,x}$ and $Nu_{H2,x}$ over the entire length of the duct belong to the parallel plate channel for all power law indices except for $Nu_{T,x}$ of n=1.25 very close the entrance. The lowest value of $Nu_{T,x}$ for n=0.5 is for the square duct close to the inlet and for the cross shape ($\lambda=0.25$) over rest of the channel except further downstream which isosceles right triangular duct possesses a minimum value. For the H2 boundary condition lowest values of $Nu_{H2,x}$ are yielded by the right isosceles triangular duct while the highest values are for parallel plates over the entire length of the duct.

 $Nu_{T,x}$ and $Nu_{H2,x}$ for different power law indices and various geometries are tabulated in Table A13 through A24 (Appendix A).

Service .

-

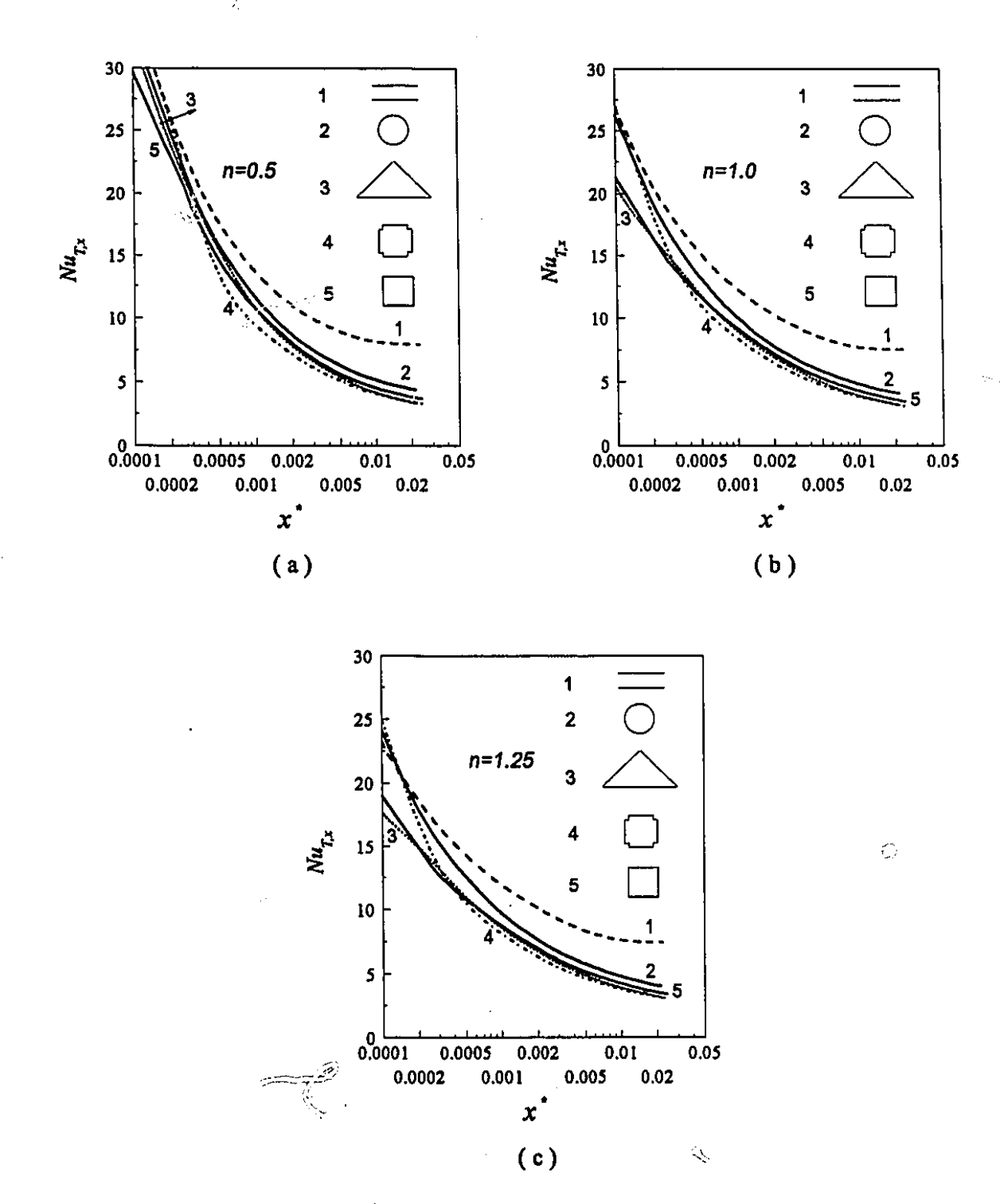


Figure 6.3 (a - c) Nu_T vs. x^* for different geometries, Re=500, Pr=10 (a)- n=0.5, (b)- n=1.0, (c)- n=1.25.

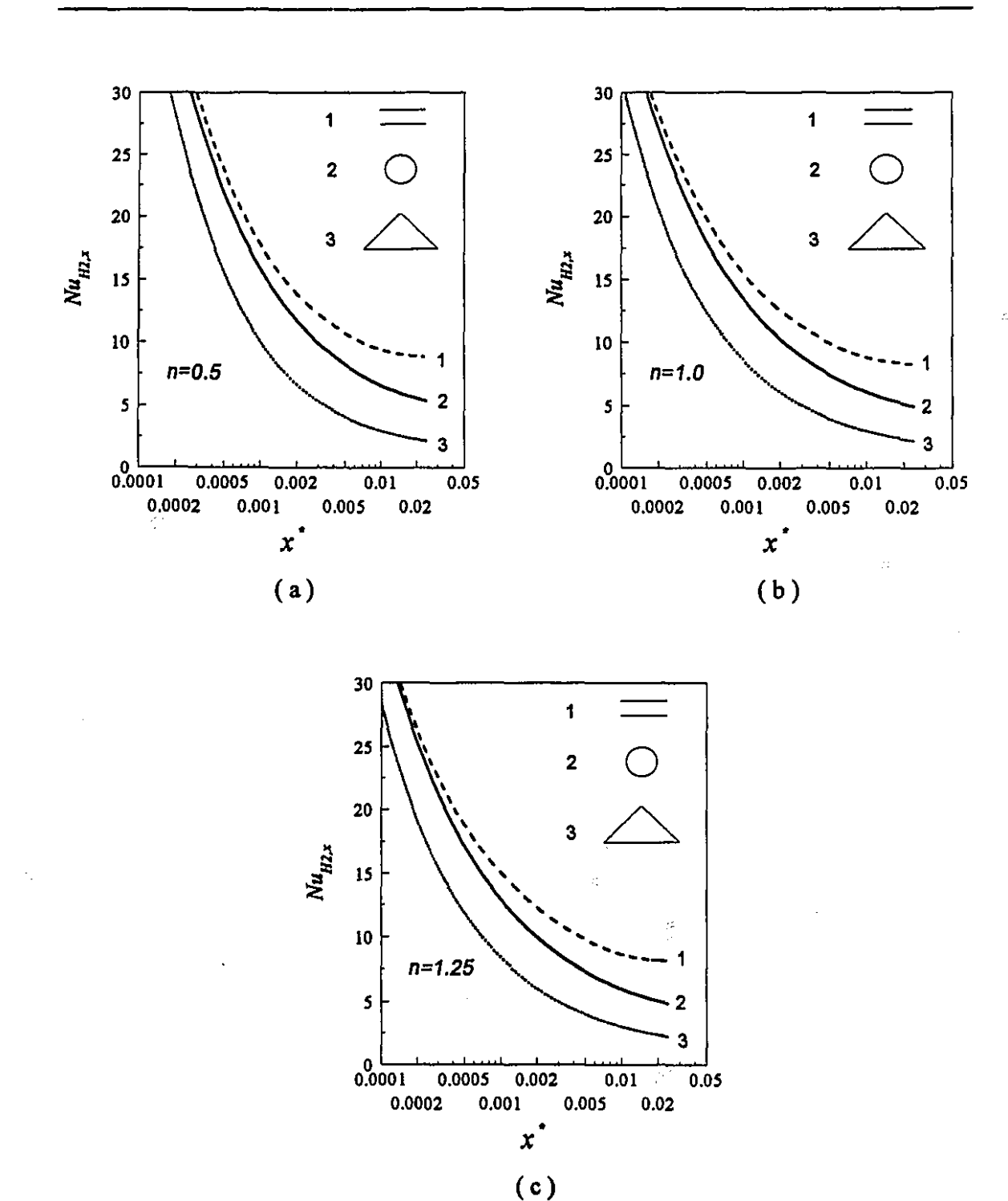


Figure 6.4 (a - c) Nu_{H2} vs. x^{\bullet} for different geometries, Re=500, Pr=10 (a)- n=0.5, (b)- n=1.0, (c)- n=1.25.

Ĵ,

6.5 Goodness factor comparison

Since a variety of surface configurations is being used in compact heat exchanger design, surface selection which governs the channel geometry for fluid flow is an important task. Compact heat exchangers are manufactured for different applications and therefore have different performance criteria depending on the application, e.g. minimum material cost, minimum operating cost, minimum volume, minimum pressure drop, maximum heat transfer rate, etc. Surface selection depends on the objective function chosen which should be minimized or maximized.

Several goodness factors have been defined in the literature for compact heat exchanger surface performance comparisons. These have been reviewed by Shah (1983b), Webb and Bergles (1983), Webb (1981), Kays and London (1984). Among the selection criteria proposed, two important ones for compact surfaces are: minimum cross-sectional area (flow area) and minimum volume for a specified duty. These two criteria can be obtained by comparison of the flow area goodness factor (Nu/f.Re) and also by comparison of the volume goodness factor (heat transfer coefficient (h) and pumping power (P)) which are defined in the following sections.

6.5.1 Area goodness factor comparison

Nu/f. Re can be expressed in the following form:

$$\frac{Nu}{f.Re} = \frac{k_o h A u_e^n}{2K \Delta p D_h^{n-l} A_c} = \frac{h A m^n k_o}{2\rho^n K \Delta p A_c^{n-l} D_h^{n-l}}$$
(6.1)

The left hand side of equation (6.1) is a constant for the fully developed condition for a specified fluid and boundary condition and duct geometry. Equation (6.1) shows that Nu/f. Re is inversely proportional to A_c if the following parameters are kept constant. 1) Reynolds number, 2) heat transfer per unit temperature difference, 3) Δp , 4) hydraulic

When one of the performance criterion has been defined quantitatively and should be minimized or maximized, it is called an "objective function".

diameter. Clearly, a duct with higher Nu/f. Re is desirable because it needs a smaller flow cross-sectional area. A smaller flow area can produce a significant saving in the mass of the heat exchanger.

Table 6.4 presents computed Nu/f. Re values for different power law indices for both T and H2 boundary conditions. From this Table for n=0.5, Nu_T/f . Re varies from 0.448 for the right isosceles triangular duct to 0.994 for parallel plates. The ranges of Nu_T/f . Re for n=1.0 and n=1.25 are 0.178 to 0.316 and 0.112 to 0.183, respectively. The highest value belongs to parallel plate channel and the lowest value to the right isosceles triangular duct. For the H2 boundary condition for all power law indices, again the parallel plate channel has the highest values viz. 1.10, 0.345, and 0.199, and the right triangular channel possesses the lowest values viz. 0.255, 0.103, and 0.065 for n=0.5, 1.0 and 2.25, respectively. The ratio of the highest value of the area goodness factor to the lowest value for the H2 boundary condition is always higher than that for the T boundary condition. For n=0.5 this ratio is 4.314 for the H2 boundary condition while for the T boundary condition it is only 2.219. This also emphasizes the significant effect of sharp corners on Nu_{H2} .

Based on Table 6.4 the parallel plate channel needs a smaller flow area to produce the same heat transfer per unit temperature difference and the same pressure drop when the hydraulic diameter and Reynolds number are constant. For instance, for n=0.5 equation (6.1) gives:

for the T boundary condition:
$$\frac{\left(Nu_T/f.Re\right)_{P,P}}{\left(Nu_T/f.Re\right)_{R,T}} = \frac{\left(A_c\right)_{R,T}}{\left(A_c\right)_{P,P}} = 2.219$$
 (6.2)

$$\frac{(A_c)_{p,p}}{(A_c)_{R,T}} = 0.451 \tag{6.3}$$

for the H2 boundary condition:
$$\frac{(Nu_{H2}/f.Re)_{P.P}}{(Nu_{H2}/f.Re)_{R.T}} = \frac{(A_c)_{R.T}}{(A_c)_{P.P}} = 4.314$$
 (6.4)

$$\frac{(A_c)_{p,p}}{(A_c)_{R,T}} = 0.232 \tag{6.5}$$

The subscripts P.P and R.T refer the parallel plate channels and the right isosceles triangular ducts, respectively. Therefore parallel plate channels need 54.9 % and 76.8 % smaller cross-sectional area in comparison with the right triangular duct for the T and H2 boundary conditions, respectively.

If we consider constant flow rate condition instead of constant Reynolds number, Nu_T/f . Re is inversely proportional to A_c^{n+1} (Equation 6.1). In this case the parallel plate channel for T and H2 boundary conditions need 41.2 % and 62.3 %, respectively, smaller cross-sectional area in comparison with right isosceles triangular duct.

===

Table 6.4 Nu/f. Re for various power law indices and duct geometries for fully developed condition, constant property fluids.

Geometry			Nu_T/f . Re	?	Nu_{H2}/f . Re			
		n=0.50	n=1.00	n=1.25	n=0.50	n=1.00	n=1.25	
	Circle	0.625	0.229	0.142	0.751	0.273	0.169	
	Square	0.553	0.209	0.131	0.573	0.217	0.136	
:	Rounded Corner R.C.=a/20	0.552	0.209	0.131	0.584	0.221	0.138	
	Rounded Corner R.C.=a/6	0.554	0.206	0.130	0.608	0.225	0.142	
	A.R.=0.5	0.594	0.218	0.135	0.520	0.194	0.121	
	A.R.=0.2	0.718	0.253	0.153	0.396	0.153	0.095	
	Parallel Plates	0.994	0.316	0.183	1.100	0.345	0.199	

a = 180°	0.559	0.209	0.129	0.488	0.184	0.114 ୍ର
α = 90°	0.539	0.206	0.130	0.524	0.201	0.127
α = 60°	0.510	0.198	0.125	0.436	0.171	0.108
a = 60°	0.476	0.188	0.118	0.358	0.142	0.090
α = 90°	<i>்</i>	0.178	0.113	0.255	0.103	0.065
λ = 0.25	0.542	0.211	0.136	0.596	0.234	0.150
λ = 0.5	0.482	0.187	0.119	0.499	0.196	0.125

6.5.2 Volume goodness factor comparison

The heat transfer coefficient (h) and pumping power (\overline{P}) can be written in the

following form:
$$Q' = h A \left(T_w - T_b \right) = h \beta' V' \left(T_w - T_b \right) , h = \frac{Nu K}{D_h}$$
 (6.6)

$$\overline{P} = \frac{\Delta p \ m'}{\rho} \quad , \quad E' = \frac{\overline{P}}{A} = \frac{\Delta p \ m'}{\rho A}$$
 (6.7)

-5

where β' is surface compactness. We assume our objective is to reduce the overall exchanger volume (by selecting appropriate geometric configuration) at the same flow rate, the same heat transfer per unit temperature difference, and also the same compactness (the same hydraulic diameter) and pressure drop. The following discussion shows the calculation of the appropriate dimensions for parallel plates in comparison with the right triangular duct for n=0.5 based on fully developed results. This result is shown as an illustration.

For the same Q' and temperature difference $(T_w - T_b)$ from equation 6.6:

$$h \beta' V' = constant \implies h \approx \frac{1}{V'} \text{ or } \frac{1}{A}$$
 (6.8)

Therefore higher h indicates lower heat transfer area (also lower volume). Hence for a constant property fluid Nu can be used instead of h for comparison.

From Table 6.2 for n=0.5:

Ŕ

$$\frac{(Nu_T)_{P,P}}{(Nu_T)_{R,T}} = 3.300 = \frac{A_{R,T}}{A_{P,P}} \quad \text{and} \quad \frac{(Nu_{H2})_{P,P}}{(Nu_{H2})_{R,T}} = 6.393 = \frac{A_{R,T}}{A_{P,P}}$$
(6.9)

Therefore, for the T boundary condition:

$$A_{P,P} = 0.303 A_{R,T}$$
, and

for the H2 boundary condition:

$$A_{PP} = 0.156 A_{PT}$$

Thus for the same pumping power parallel plates need 69.7 % and 84.4 % lower heat transfer area (and also smaller volume) in comparison with the right triangular duct for the T and H2 boundary conditions, respectively.

For the same pressure drop and flow rate, from the computed area goodness factor, 41.2 % and 62.3 % less flow area is required for the parallel plate channel in comparison with a right triangular duct. Since flow rate and pressure drop are the same the pumping power will also be the same for both channels. Since the hydraulic diameter is the same for both ducts, the length necessary for parallel plates is less than that required by the corresponding right triangular channel. Thus,

$$D_{h} = \frac{4 A_{c}}{p'} = \frac{4 A_{c} \overline{L}}{A} \quad , \quad \frac{A_{p,p}}{A_{R,T}} = \frac{(A_{c})_{p,p}}{(A_{c})_{R,T}} \frac{\overline{L}_{p,p}}{\overline{L}_{R,T}}$$
(6.10)

Using the results obtained for area and volume goodness factors, for the T boundary

condition:
$$\frac{L_{P,P}}{L_{R,T}} = 0.515 \text{ , and} \qquad (6.11)$$

for the H2 boundary condition:
$$\frac{L_{p,p}}{L_{R,T}} = 0.414 \tag{6.12}$$

Therefore the length necessary for parallel plates is 48.5 % and 58.6 % shorter than that for the right triangular duct for T and H2 boundary conditions, respectively.

Based on the new dimensions, the operating Reynolds number and Prandtl number are necessarily different for parallel plates:

$$Re = \frac{\rho u^{2-n} D_h^n}{k_a} = \frac{m^{2-n} D_h^n}{k_a A_a^{2-n} \rho^{1-n}}$$
 (6.13)

$$Pr = \frac{k_o C_p \left(\frac{u_o}{D_h}\right)^{n-1}}{K} = \frac{k_o C_p \ m^{n-1}}{K D_h^{n-1} A_c^{n-1} \rho^{n-1}}$$
(6.14)

Bor the T boundary condition:
$$\frac{Re_{p,p}}{Re_{R,T}} = \frac{(A_c)_{R,T}^{2-n}}{(A_c)_{p,p}^{2-n}} = 2.219$$
 (6.15)

$$\frac{Pr_{p,p}}{Pr_{R,T}} = \frac{\left(A_c\right)_{R,T}^{n-1}}{\left(A_c\right)_{P,P}^{n-1}} = 0.767 \tag{6.16}$$

For the H2 boundary condition:
$$\frac{Re_{p,P}}{Re_{R,T}} = \frac{(A_c)_{R,T}^{2-n}}{(A_c)_{p,P}^{2-n}} = 4.314$$
 (6.17)

$$\frac{Pr_{p,p}}{Pr_{R,T}} = \frac{\left(A_c\right)_{R,T}^{n-1}}{\left(A_c\right)_{R,p}^{n-1}} = 0.614 \tag{6.18}$$

Thus the operating Re for parallel plates is higher than that for the right isosceles triangular duct while the operating Pr is lower for both T and H2 boundary conditions.

If the objective is to have the same E' (pumping power per unit heat transfer area), for constant flow rate the pressure drop will be different in each duct. From equation 6.7:

For the T boundary condition:
$$\frac{\Delta p_{P,P}}{\Delta p_{R,T}} = \frac{A_{P,P}}{A_{R,T}} = 0.303 \tag{6.19}$$

For the H2 boundary condition:
$$\frac{\Delta p_{P,P}}{\Delta p_{R,T}} = \frac{A_{P,P}}{A_{R,T}} = 0.156 \tag{6.20}$$

Thus parallel plate channels will have 69.7 % and 84.4 % lower pressure drop than the right triangular duct for T and H2 boundary conditions, respectively. Consequently, the parallel plate channel possesses the advantage of 69.7 % less heat transfer area and 69.7 % lower pressure drop for the T boundary condition and 84.4 % less heat transfer area as well as pressure drop for the H2 boundary condition in comparison with the right triangular duct. To obtain these advantages the cross sectional area for parallel plates is larger, however. From equation 6.1 for n=0.5:

for the T boundary condition:
$$\frac{(Nu_T/f.Re)_{P,P}}{(Nu_T/f.Re)_{R,T}} = \frac{(A_c)_{R,T}^{1.5}}{(A_c)_{P,P}^{1.5}} \frac{\Delta p_{R,T}}{\Delta p_{P,P}} = 2.219$$
 (6.21)

and
$$\frac{(A_c)_{P,P}}{(A_c)_{R,T}} = 1.303$$
 (6.22)

For the H2 boundary condition:
$$\frac{(Nu_{H2}/f)_{P,P}}{(Nu_{H2}/f)_{R,T}} = \frac{(A_c)_{R,T}^{1.5}}{(A_c)_{P,P}^{1.5}} \frac{\Delta p_{R,T}}{\Delta p_{P,P}} = 4.314$$
 (6.23)

and
$$\frac{(A_c)_{p,p}}{(A_c)_{p,T}} = 1.302 \tag{6.24}$$

Thus for both boundary conditions parallel plate channels will require about 30.2 % larger flow area in comparison with that for the right triangular duct.

Similar calculation can be made for the developing section of different geometries based on the mean Nusselt number and apparent friction factor which needs iterative solutions and the results are additionally dependent on the length of channel used. These are not presented in this thesis. The mean Nusselt number for different power law indices and various geometries are given in Tables C1 through C12.

Generally the parallel plate channel has better thermal performance but heat exchangers taking advantage of this simplest geometry seem to be impractical. Table 6.4

shows the thermal performance of various geometries. For the T boundary condition the rectangular duct with small aspect ratio is better geometry than others after parallel plates. For H2 boundary condition the circular duct, rounded corner square duct or the cross shape channel ($\lambda = 0.25$) are better geometries. Thus best practical geometry after the circular tube with high thermal performance (for H2 boundary condition) is the rounded corner square or cross-shape channel (depends on power law index).

In choosing heat exchanger configuration many other criteria must be considered, e.g. structural stability, operating costs, manufacturing costs, etc.. Therefore selection of the geometry is not only governed by the thermal performance and pressure drop considerations. The total capital and operating expenses must also be considered.

It should be noted that triangular cross section channels and other ducts with low thermal performance may fulfill other specific criteria and may find other special applications. Note that the difficulty and cost of fabrication of the non-circular ducts as well as their maintenance problems are not considered in this discussion. For engineering design these factors must be considered as well.

6.6 Conclusions

This chapter compares the flow and heat transfer characteristics in the entrance region and also under fully developed conditions between different geometries. For fully developed condition, f.Re for parallel plates has the highest value while the lowest value belongs to cross-shaped channel ($\lambda = 0.5$) for all values of the power law index. Highest fully developed Nusselt number for both T and H2 boundary conditions is obtained with the parallel plate channel while the right isosceles triangular has the lowest value of Nu_{H2} . Lowest Nu_T is due to the right isosceles triangular duct and cross-shaped channels ($\lambda = 0.5$) depending on the value of the power law index.

In the entrance region the parallel plate channels give the highest $Nu_{H2,x}$ and $Nu_{T,x}$ values.

Based on the goodness criteria discussed in this chapter, for the T boundary condition the rectangular channel with small aspect ratio is a practical geometry with high thermal performance among geometries studied. For the H2 boundary condition, next to the circular tube rounded corner square duct and cross-shaped channel ($\lambda=0.25$) are better geometries than others. It should be noted the parallel plate channel has the highest thermal performance but this geometry is not necessarily the best from the overall engineering viewpoint.

Chapter 7

Experimental Studies

This chapter deals with an experimental study of developing laminar flow and heat transfer to Newtonian and viscous non-Newtonian fluids flowing in straight ducts of semi-circular and equilateral triangular cross-sections. The thermal boundary condition employed is constant heat flux on the lower plate while the other sides are insulated.

The objectives of the experimental study were:

- 1- To measure the critical Reynolds number and static pressure distribution in the entrance region for semi-circular and equilateral triangular ducts.
- 2- To obtain the local Nusselt number distribution over a range of Reynolds and Rayleigh numbers.
- 3- To validate the numerical predictions.

7.1 Experimental apparatus

A basic schematic diagram of the once-through experimental rig is shown in Fig. 7.1. The flow loop consists of a Monyo-type pump, an overhead tank, a calming section, the test section, a motionless mixer, and two reservoir tanks.

7.1.1 Flow system

The working fluid is drawn from the supply reservoir tank (380 liter capacity) by a 0.5 h.p. Monyo-type pump to an overhead tank (Fig. 7.1). The Monyo-type pump is used in order to reduce possible shear degradation of the polymer solution. The constant head

tank is made of PVC (180 cm high and 20 cm diameter). It eliminates fluctuations in the flow rate caused by the pump. A vent is connected to the top of the overhead tank to debubble the solution.

Fluid travels by gravity from the overhead tank to the calming section through a flexible hose and a valve. The calming section is a PVC tube of 10 cm diameter and 60 cm length and helps to establish a uniform velocity profile just upstream of the test section. The calming section is connected to the plexiglas tube of circular cross-section at one end and a semicircular or equilateral triangular cross-section at the other end. The length of this tube is 60 cm and its cross-section changes from circular to semi-circular or triangular gradually to minimize flow distortion due to transition in its cross-sectional shape.

A stainless steel honeycomb is installed in the pipe just upstream of the test section to obtain a uniform velocity profile at the inlet to the test section. The fluid passes through the test section and a motionless mixer and then to a second reservoir of 380 liter capacity.

The mass flow rate is determined by measuring the weight of fluid flowing in a given time. The test section was placed on two supports and is designed to be inclined and / or rotated for future studies.

The dye injection technique was used to determine the critical Reynolds number. A dye was injected through a hypodermic needle at various locations of cross-section in the duct.

1 & 8- Reservoir Tanks

2- Monyo-type Pump

3- Overhead Tank

4- Calming Section

5- Plexiglas Tube

6- Test Section

11- Pressure Taps

7- Motionless Mixer 12- Pressure Taps Collector

9- Balance

13- Pressure Transducer

10- Test Section Supports

14- Thermocouples

15- Thermocouples switch box

16- Power Supply

17- Computer (Data acquisition system)

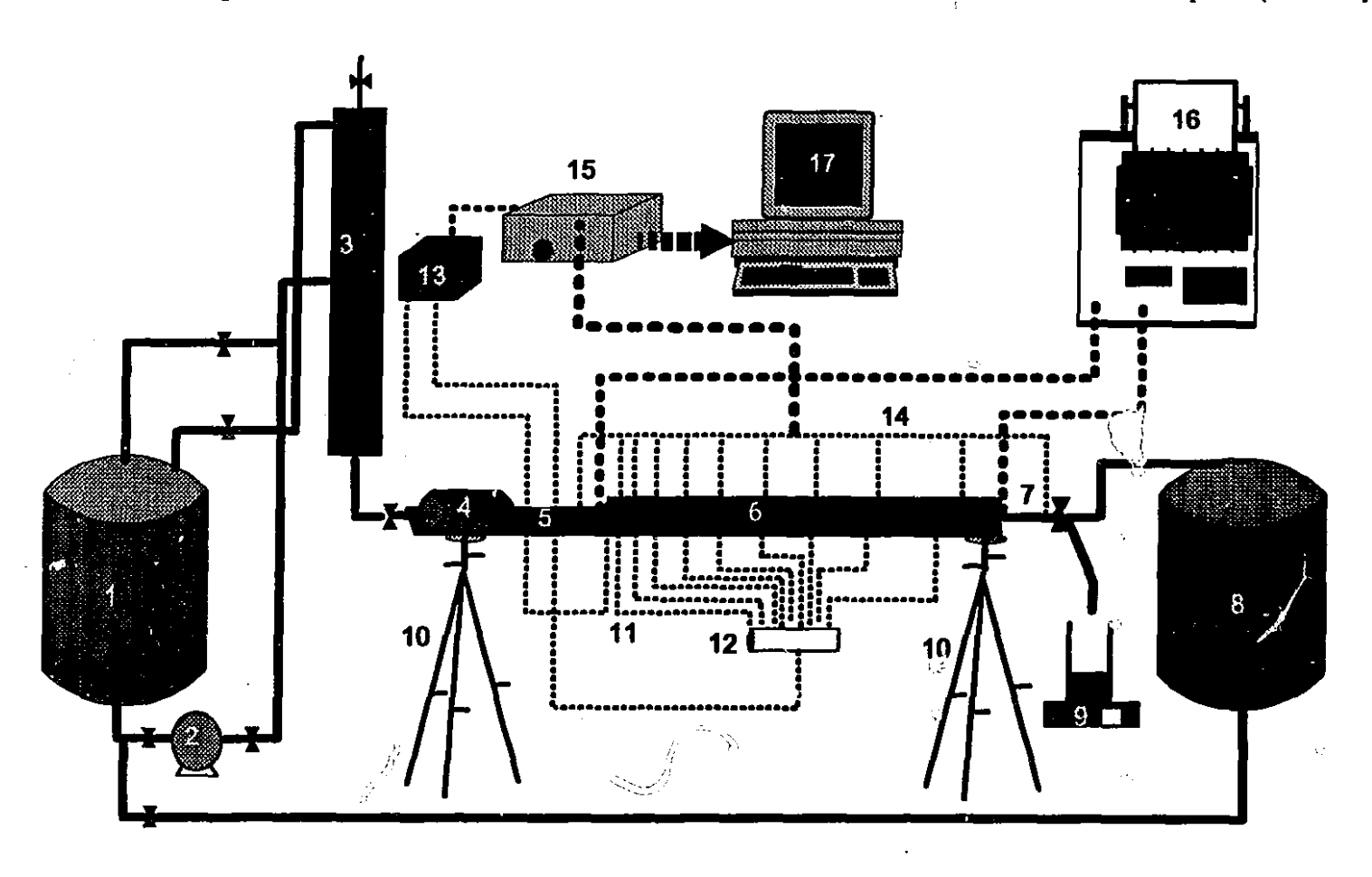


Figure 7.1 Experimental apparatus

Ξ.

7.1.2 Test section

The test sections used in this study were: (1) a semi-circular cross-sectional channel of 29 mm radius and 250 cm long and (2) an equilateral triangular duct with 29.6 mm sides and 250 cm long. Both test sections were made of plexiglas to permit flow visualization.

Ten pressure taps were installed on the top side of the test sections to measure the static pressure variation along the length of the channels. Close to the entrance, due to the high axial pressure gradients, the distance between adjacent pressure taps was small; it was increased further downstream. For each tap, a 3 mm hole was drilled through the duct wall and the burr was carefully removed. After drilling holes the inside walls of the channels were polished. A capillary stainless steel tube was used to fabricate the pressure taps. The taps were connected to a small cylindrical drum by plastic tubes and valves. The drum was coupled to a pressure transducer. The pressure tap in the inlet was connected directly to pressure transducer in order to measure the pressure drop from the inlet. The pressure transducer was calibrated before use. An inclined manometer with a Meriam fluid (specific gravity equal to 1.75) was used for a second check of the pressure transducer calibration.

For heat transfer studies the bottom plate of the test sections was held at constant heat flux while the other walls were insulated. A heater which maintained a uniform heat flux and minimized wall conduction effects was required to meet the constant heat flux boundary condition (H2). A stainless steel foil (Goodfellow Co., FE080240) of very small thickness (0.05 mm) was used to minimize the temperature variation across the thickness of the wall and also axial and peripheral thermal conduction. This method provided the closest possible approximation to the constant heat flux boundary condition (H2) on the heated surface. The foil was bonded to the surface of the plexiglas and was heated by connecting it to a d.c. power supply. To minimize heat losses a polystyrene foam insulation was wrapped around the ducts.

The test section was heated by passing a direct electrical current through the foil. The rate of heat generated is $I^2\overline{R}$ where I is the current and \overline{R} is the electrical resistance of the foil. The electrical resistance of the foil is dependent on its resistivity, its length, width, and thickness. The temperature coefficient of resistance is given in Appendix D (D.1). Due to the very small magnitude of the temperature coefficient of resistance the resistance variation with temperature is negligible. Also, because of the uniform width of the foil in the entire channel, the resistance varies linearly with axial distance.

A 10 kW power supply was used to supply dc power to the foil. The test section was isolated thermally and electrically from both upstream and downstream parts of the flow rig. Each end of the test section was connected to bus bars which provided electrical connections to the test section. The electrical resistance of the test fluid (distilled water and Carbopol 934 solutions) in comparison with the foil is negligible; therefore the amount of electrical current flowing through the fluid could be ignored.

Twenty seven, 24 gage iron-constantan thermocouples were located through 1.5 mm holes drilled on the bottom plate of both test sections to measure the temperature of the heating foil. The thermocouples measured the foil temperature at 9 axial stations, each station employing three thermocouples. The locations of the thermocouples were along the midplane of the bottom plate and along two rows at locations 9 mm and 14 mm from the center. To check for symmetry about the midplane some thermocouples are positioned symmetrically on the opposite side. Due to the larger temperature variation closer to the entrance, thermocouples in this region were more closely spaced. The spacing between thermocouples increased with downstream distance. A thin layer of Omega resin 400 was used to cement each thermocouple bead to the foil and to prevent any electrical interference which might affect the thermocouples reading. All thermocouples (and also pressure transducer) were connected to the selector switch box (Fig. 7.1) which is capable to measuring seven reading simultaneously.

Two ungrounded iron-constantan thermocouples were used to measure the inlet and outlet fluid temperatures. Any temperature gradients in the fluid leaving the test section were destroyed by the motionless mixer. The resulting "mixing cup" temperature of the fluid was measured by the exit thermocouple. The motionless mixer contained of four baffles and was insulated by a fiber glass blanket.

٠.,

From the averaged bottom plate temperature at various axial locations and the inlet and outlet fluid temperatures, the local bottom place Nusselt number was calculated as shown in Appendix D (D.2).

7.2 Test fluids

Distilled water and partially neutralized 0.5 % by weight aqueous solutions of Carbopol 934 (carboxy polymethylene a product of B.F.Goodrich chemical company) were used as the test fluids. Carbopol 934 solutions are viscous power law fluids as shown by Yoo (1974), Lawal (1985) and also verified in the present work.

The Carbopol 934 solution was prepared in the supply reservoir tank (380 liter capacity). A mechanical mixer (0.5 hp) was used to mix a pre-determined quantity of Carbopol powder which was added gradually to distilled water. Special care was taken to avoid agglomeration of the powder. After all the powder was added to the distilled water, stirring of the solution was continued for at least 8 hours to obtain a homogous solution and to bring its rheological properties to steady values before experiments were performed. The solution were allowed to stand for about twenty four hours; small lumps of Carbopol powder floating in the solution were removed by screen.

For partial neutralization, a sodium hydroxide solution was added to the Carbopol solution while stirring. The solution was mixed vigorously to assure a homogenous solution. The neutralization step enhances the apparent viscosity and decreases the power law index of the solution; the values of both apparent viscosity and power law index depend on the degree of neutralization.

7.2.1 Physical properties of Carbopol solutions

For Carbopol 934 solutions the physical properties, e.g. density, thermal conductivity and heat capacity have been reported by several investigators (Yoo (1974), Cho and Hartnett (1985) and Irvine, Jr (1983)). The measurements of Yoo (1974) indicate

that the density and thermal conductivity of Carbopol 934 solution (0.5 %) differ by 0.5 % and 1.7 % respectively from the properties of distilled water. Also as reported by Yoo (1974), the heat capacity of Carbopol solution (0.5 %) is the same as heat capacity of distilled water.

7.2.2 Rheological measurements

The Carbopol solution was sampled before and after each experimental run. The rheological properties (consistency index, and power law index) were measured over a range of temperatures using a Haake rotational viscometer (Model RV20, Haake Hess-Technik, Karlsruhe, Germany). The shear rate range was 10-500 sec⁻¹ which corresponds to the range of conditions encountered in the experiments.

Typical plots of the shear stress vs. shear rate obtained from the rheometer are shown in Fig. 7.2 (a - b) for a 0.5 % Carbopol solution at two neutralization levels. These log-log plots confirm the validity of the power law model for these solutions. The power law index is obtained from the slope of the curve and the consistency index from the intercept. The flow curves were obtained at various temperatures (20, 25, 35, 50° C). Additional information about Fig. 7.2 is given in Appendix D (D.3). The data shown in Appendix D indicates the power law index is constant at all temperatures while the consistency index varies appreciably with temperature. The following correlations were obtained for the two solutions to represent the temperature dependence of the consistency index.

$$k = a' e^{b'T} \tag{7.1}$$

For solution #1: $a' = 0.821 \text{ grsec}^{n-2}/\text{cm}$, $b' = -0.00334 \, ^{\circ} \text{C}^{-1}$

For solution #2: $a' = 2.929 \text{ grsec}^{n-2}/\text{cm}$, $b' = -0.00364 \, {}^{\circ}\text{C}^{-1}$

1)

The rheological measurements for two fluid samples taken before and after selected experimental runs confirmed that no degradation of the Carbopol solutions occurred during the experiments. The absence of degradation was expected because of the

flow loop is a once through system and also because a Monyo-type pump was used in the experiments.

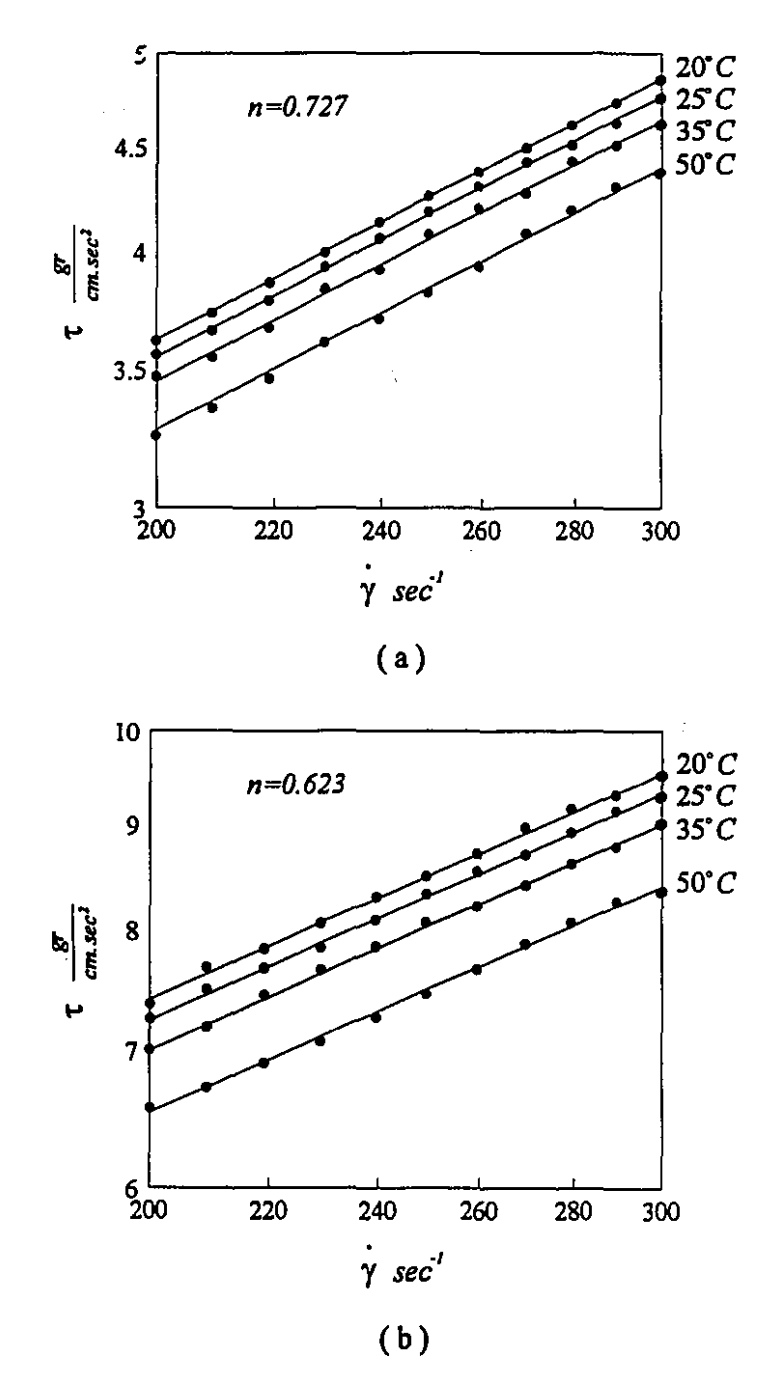


Figure 7.2 (a - b) Shear stress vs. shear rate for partially neutralized Carbopol 934 solutions neutralized to different levels.

7.3 Results and discussion

For both channels the critical Reynolds number and pressure drop measurements were obtained under isothermal conditions. For the heat transfer study a uniform heat flux was applied to the lower plate while the rest of the duct walls were insulated. To check reproducibility of the pressure drop and Nusselt number results runs were made under identical conditions. The results were found to be repeatable within 2.4 % for pressure drop and within 3.3 % for the local Nusselt number.

The ranges of dimensionless parameters were:

Newtonian fluid (distilled water):

$$Re = \frac{\rho u_e D_h}{\mu} = 542 - 1074$$

$$Pr = \frac{\mu C_p}{K} = 6.52 - 6.84$$

$$Gr = \frac{\rho^2 D_h^4 \overline{\beta} q'' g}{\mu^2 K} = 9.03 \times 10^5 - 3.49 \times 10^6$$

$$Ra = Gr. Pr = 6.13 \times 10^6 - 2.27 \times 10^7$$
(7.2)

Viscous non-Newtonian fluids (Carbopol 934 solutions)

For pressure drop study:

$$Re = \frac{\rho u_e^{2-n} D_h^n}{k_0} = 234 - 1155$$

For heat transfer study:

$$Re = \frac{\rho u_e^{2-n} D_h^n}{k_o} = 3.16 - 19.65$$

$$Pr = \frac{k_o C_p \left(\frac{u_e}{D_h}\right)^{n-1}}{K} = 383 - 1412$$

$$Gr = \frac{\rho^2 D_h^{2n+2} \overline{\beta} q^n g u_e^{2-2n}}{k_o^2 K} = 14.33 - 431.65$$

$$Ra = Gr. Pr = 2.02 \times 10^4 - 1.72 \times 10^5$$
(7.3)

All physical properties appearing in the dimensionless numbers are calculated at the inlet fluid temperature.

7.3.1 Critical Reynolds number

Transition from laminar to turbulent flow in triangular ducts was studied by Eckert et al. (1956) using a smoke injection technique. They located a smoke probe at different locations from the apex of triangular ducts and measured the critical Reynolds number. They used two isosceles triangular ducts with apex angles of 11.5° and 24.8°. Based on their data over a wide range of Reynolds number both laminar and turbulent flows co-exist side by side within the channel, extending from laminar flow close to the corners to turbulent flow at the centroid of the triangular ducts. This fact is confirmed recently by Mikic et al. (1994) for an isosceles triangular duct with a 12° apex angle.

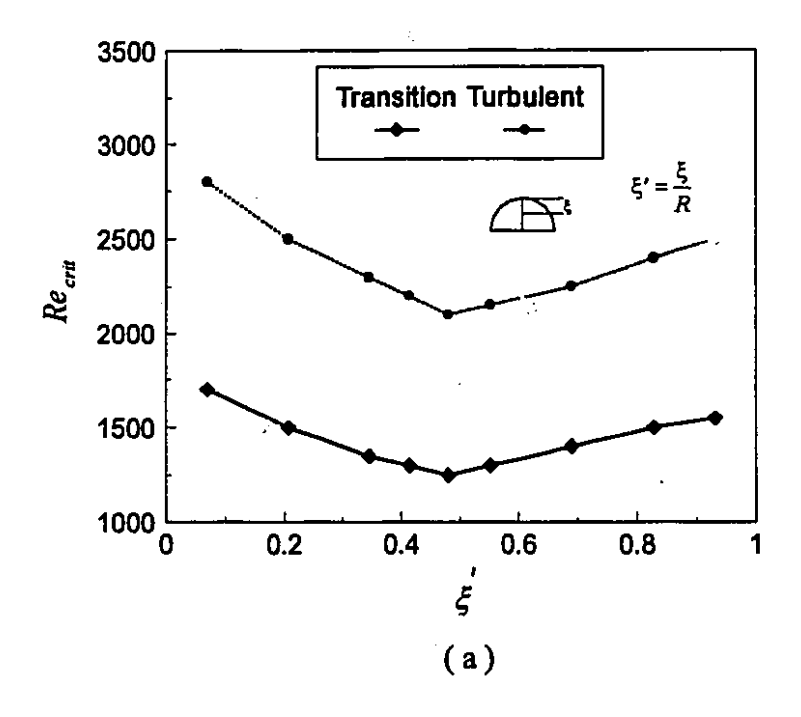
In the present investigation dye injection was used to visualize the distilled water flow and to obtain the critical Reynolds number. The dye solution was prepared using TELON Blue powder (Bayer Co.) dissolved in distilled water.

The dye was injected through a small stainless steel probe bent at a 90° angle. The injection leg was located parallel to the flow direction; it could be moved along the symmetry lines of the semi-circular and equilateral triangular ducts. At each specific location of the probe the critical Reynolds number was measured which showed a wide range of Re_{crit} depending on the distance from the corner.

Dye injection indicated existence of fully laminar flow everywhere in the semi-circular test section for Re < 1250 and in the triangular duct for Re < 1000. Fig. 7.3 (a - b) presents measured Re_{crit} vs. distance from the corner for the equilateral triangular duct and the top point of the semi-circular duct on the symmetry lines of the channels. For the semi-circular duct for Re > 1250 dye injection displayed very small amplitude oscillations at a specific location of the cross-section (Y=0.00, Z=0.39) on the symmetry line. This point is a position where (as shown by numerical results) the maximum axial velocity occurs. For the triangular duct Re_{crit} is 1000 at the centroid (Y=0.87, Z=0.50). As the probe moved toward the apex of the semi-circular and the corner of the triangular duct the critical Reynolds number increased. The maximum critical Reynolds number for semi-circular and equilateral triangular channels are 1700 and 2450, respectively. For

1250 < Re < 1700 (for semi-circular duct) and 1000 < Re < 2450 (for equilateral triangular duct) both laminar and turbulent flows exist simultaneously in different locations of the cross-section. For a triangular channel with an apex angle of 11.5° the data of Eckert et al. (1956) indicate a very wider range of the critical Reynolds number (400 < Re < 8000) in comparison with the present results for an equilateral triangular duct. It appears that the critical Reynolds number depends on the magnitude of the apex angle for a triangular duct.

At all locations of the probe, the amplitude and frequency of fluid oscillations increases with increase of *Re*. The Reynolds numbers at which the flow changes to fully turbulent condition are presented in Fig. 7.3 (a - b) for the two non-circular ducts examined.



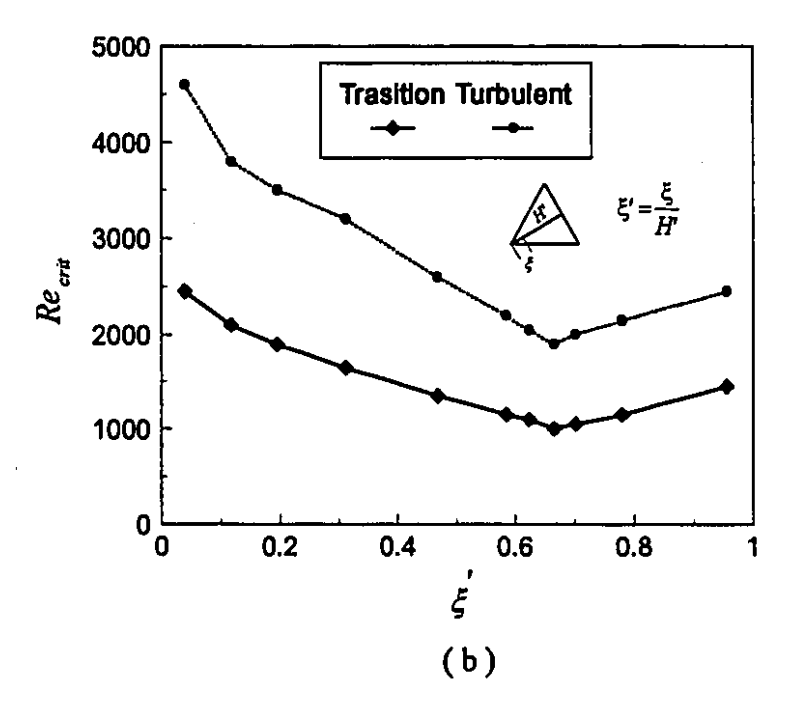


Figure 7.3 (a - b) Critical Reynolds numbers at different locations over duct cross-section (a)- semi-circular duct, (b)- equilateral triangular duct.

`. _____

Salati

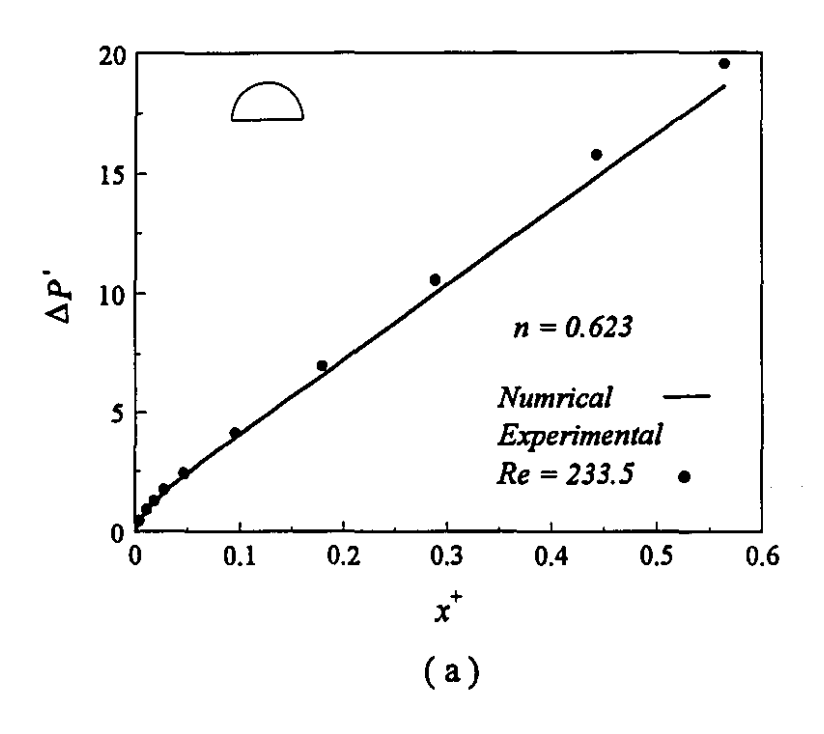
7.3.2 Pressure drop measurements

Fig. 7.4 (a - b) compares the experimental static pressure drop and corresponding numerical simulation results for Carbopol solution (n=0.623). The experimental measurements are in good agreement with the numerical results for both channels. The experimental data are somewhat higher (maximum 5.5 %) than those predicted by the numerical model due to the possibly uncertainty in the experimental values. The Re values are in the fully laminar range for both ducts.

The experimental values of the pressure drop for both channels for the viscous non-Newtonian fluids studied are plotted in Fig. 7.5 (a - b) through Fig. 7.8 (a - b). These results are also tabulated in Appendix D (D.5). The pressure drop is normalized by the dynamic pressure, $\frac{1}{2}\rho u_e^2$ and plotted as a function of the dimensionless axial distance, X, as well as $x^+ = \frac{x/D_h}{Re}$. The data are for different Reynolds numbers.

As seen from Figures 7.5 and 7.6, the dimensionless pressure drop decreases with increasing of Reynolds number. Also the pressure drop per unit length close to the entrance is higher than that downstream. From Fig. 7.7 and Fig. 7.8 it is clear that when $\Delta P'$ is plotted against $x^+ = \frac{x/D_h}{Re}$ resulting plots are independent of Re for both semi-circular and triangular ducts.

/}



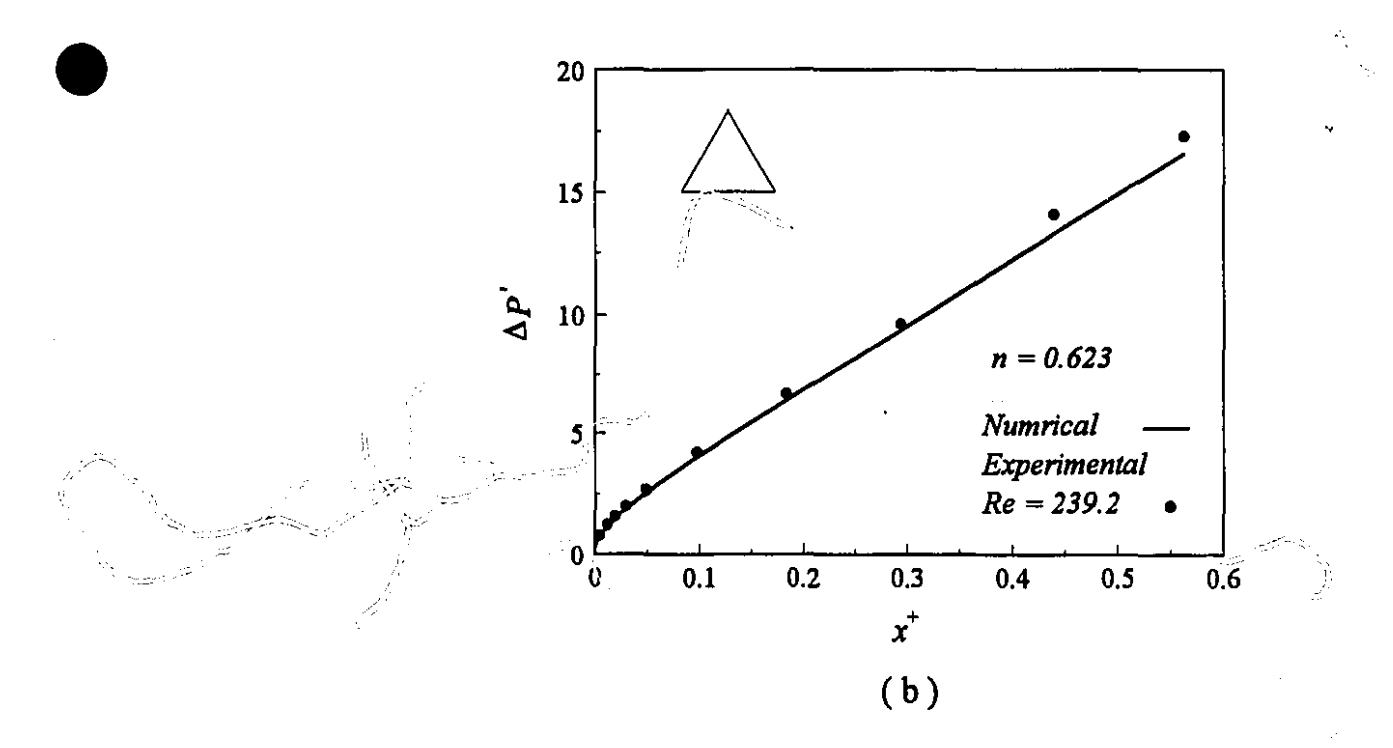
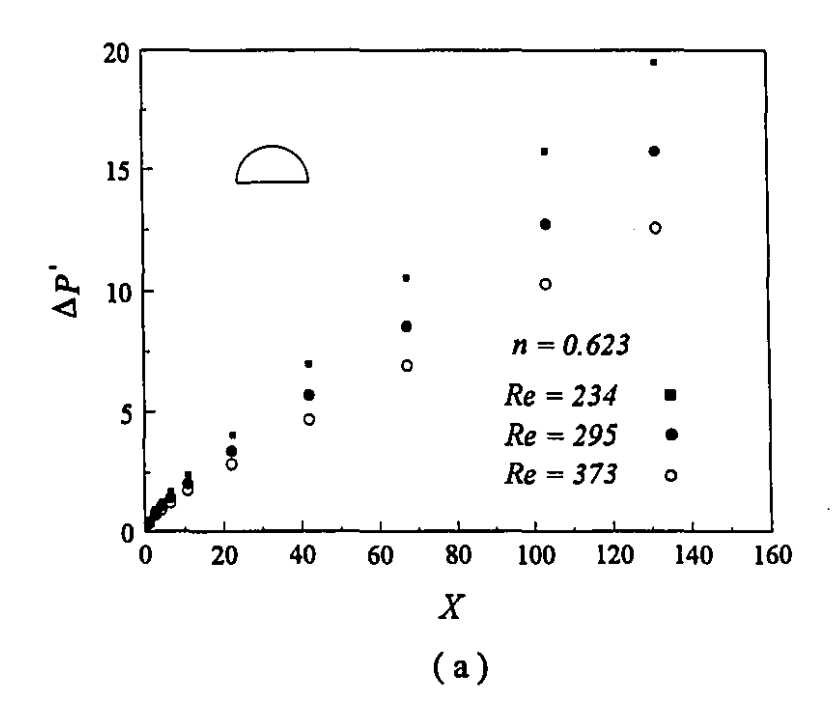


Figure 7.4 (a - b) Comparison of numerical and experimental results for $\Delta P'$ (a)- semi-circular duct, (b)- equilateral triangular duct.



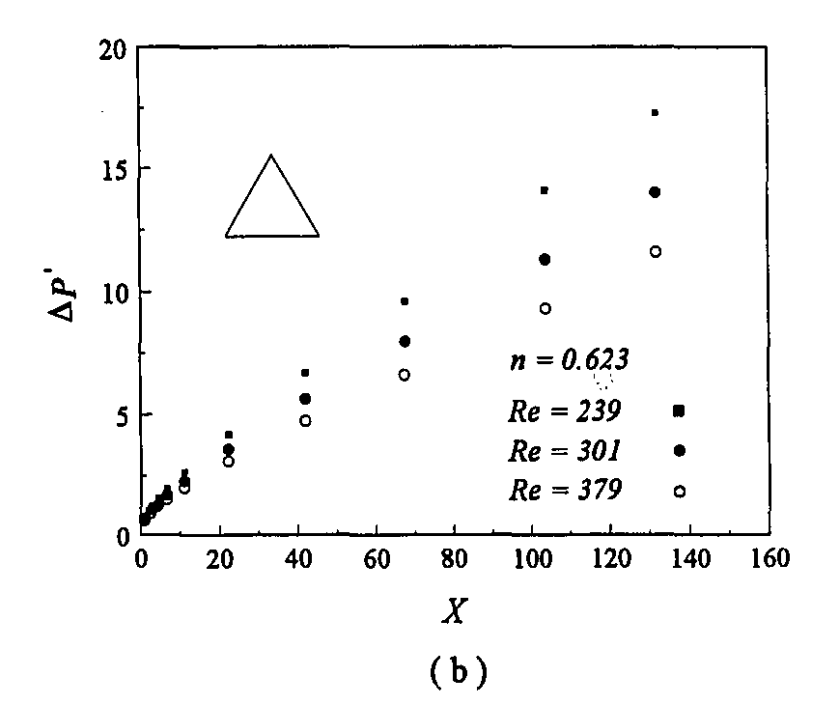
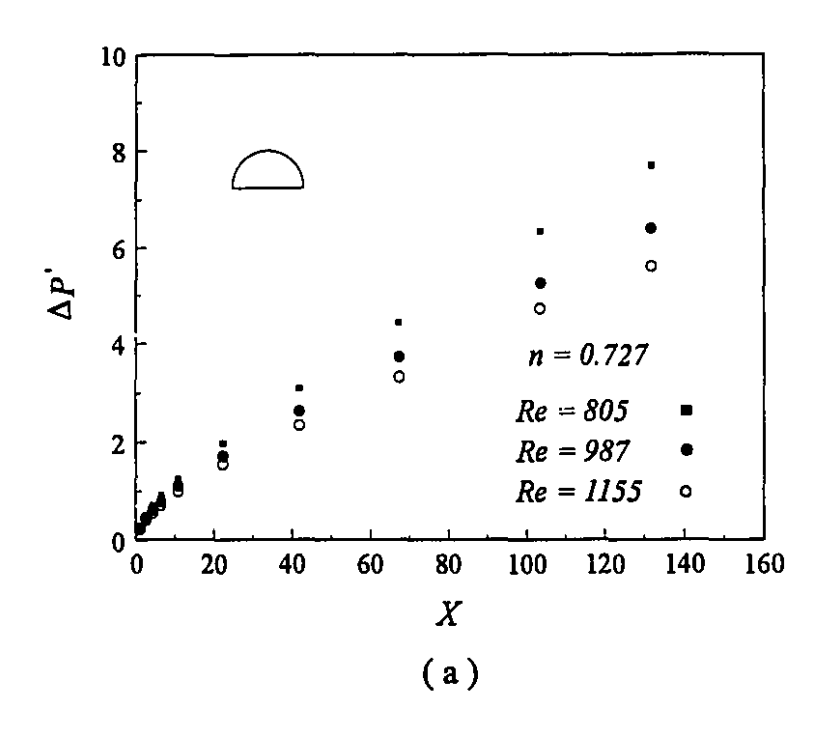


Figure 7.5 (a - b) Dimensionless pressure drop vs. dimensionless axial distance X for n=0.623, (a)-semi-circular duct, (b)-equilateral triangular duct.

15



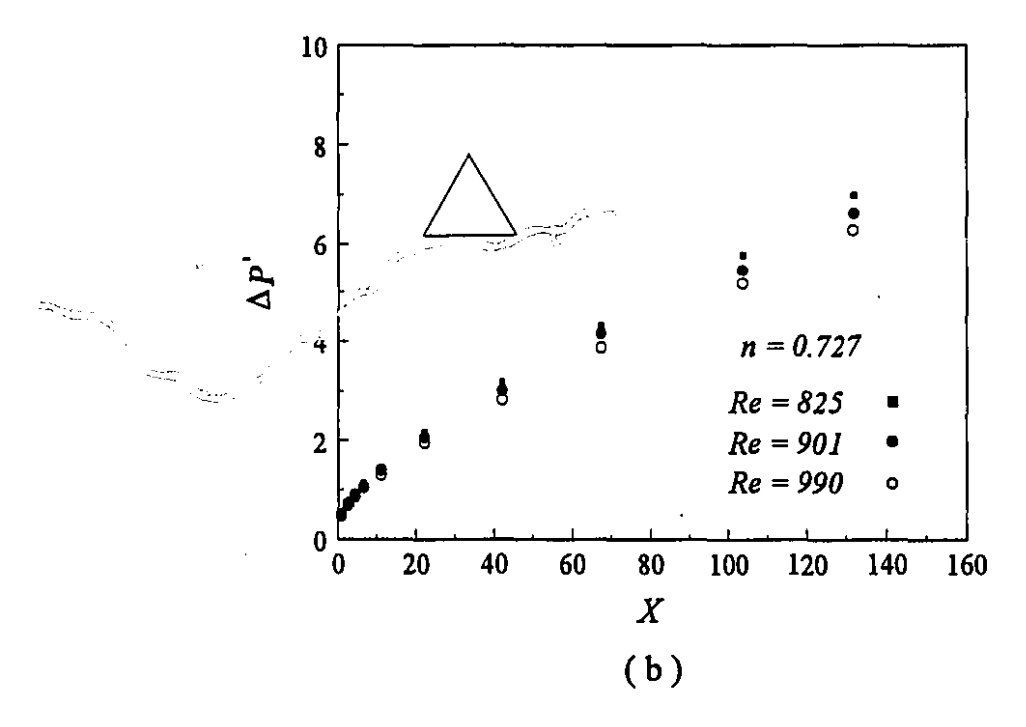
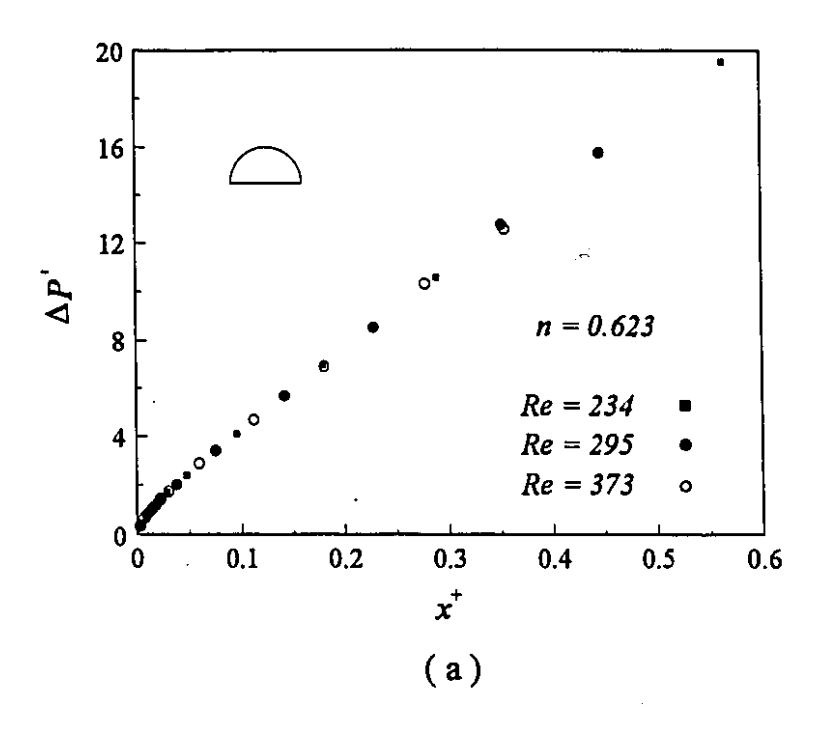


Figure 7.6 (a - b) Dimensionless pressure drop vs. dimensionless axial distance X for n=0.727, (a)- semi-circular duct, (b)- equilateral triangular duct.



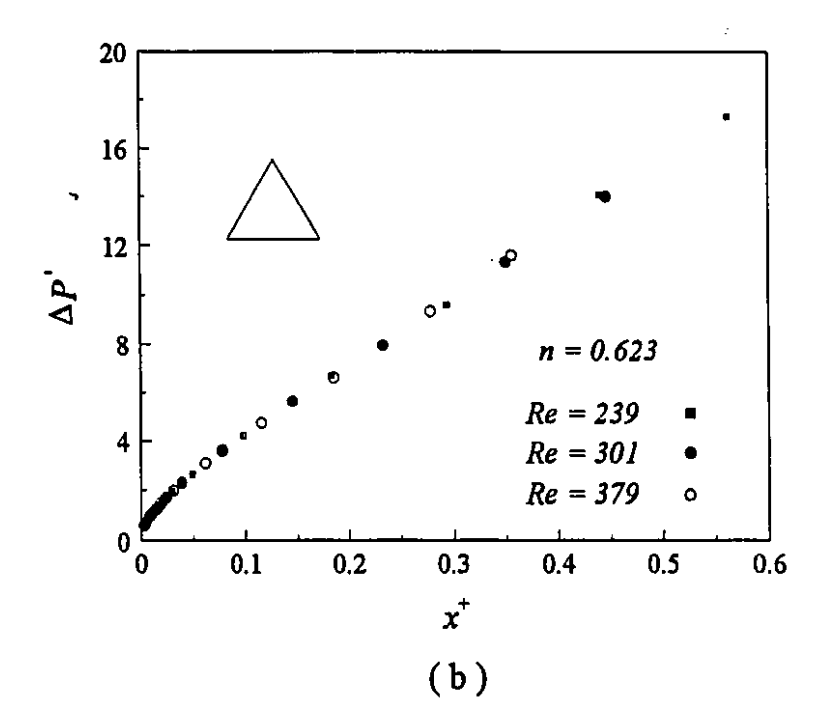
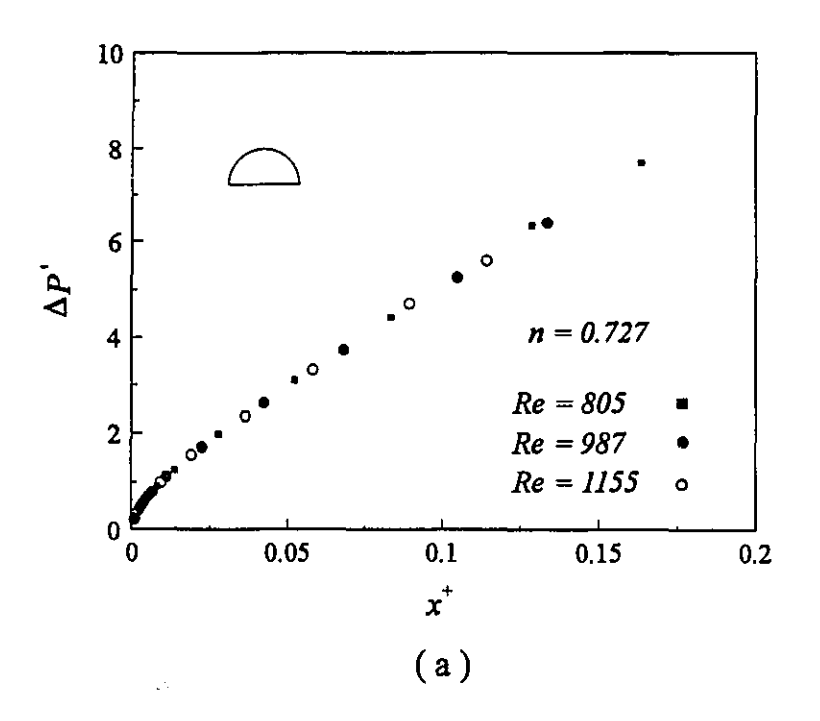


Figure 7.7 (a - b) Dimensionless pressure drop vs. dimensionless axial distance x^+ for n=0.623, (a)- semi-circular duct, (b)- equilateral triangular duct.



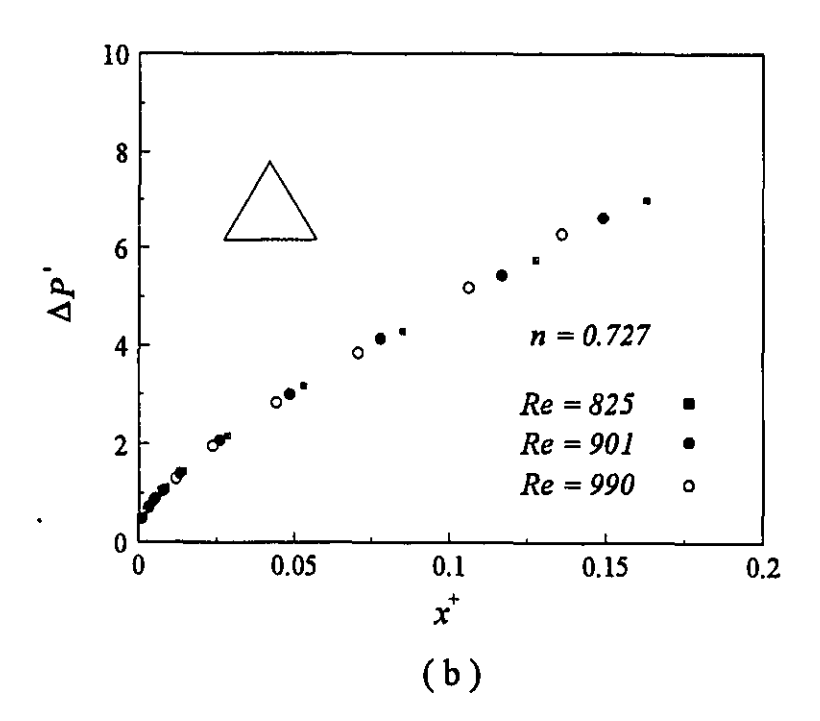


Figure 7.8 (a - b) Dimensionless pressure drop vs. dimensionless axial distance x^+ for n=0.727, (a)- semi-circular duct, (b)- equilateral triangular duct.

57.4

7.3.3 Heat transfer results

Heat transfer experiments were performed with distilled water and Carbopol solutions by heating the foil bonded on to the lower plate of the semi-circular and triangular channels. The measured quantities were: the inlet and outlet temperatures of the fluid, bottom plate temperatures at different spanwise locations as well as various axial distances and the flow rate. Bottom plate temperatures at each axial station integrated over-the width of channel to obtain mean bottom plate temperature. The local Nusselt number was calculated based on the average bottom plate temperature (Appendix D, D.2). Appendix D (D.4) presents results of the uncertainty analysis for Nusselt number.

7.3.3.1 Newtonian fluids

A typical mean bottom plate temperature distribution (Tw_x) and the corresponding local Nusselt number distribution based on the bottom plate temperature ($Nu_{b,x}$) are presented in Fig. 7.9 and Fig. 7.10, respectively. All data related to Nusselt number are given in Appendix D (D.5).

Inspection of these figures reveals that in the entrance region as Tw_x increases $Nu_{b,x}$ decreases. Natural convection effects are small in this section of the channel due to the small temperature difference between the wall and fluid. As the fluid proceeds downstream, the temperature difference between the wall and the fluid increases and promotes secondary flow over the bottom plate. The heated fluid near the bottom plate becomes lighter and moves along the side wall while the cooler fluid descends. Introduction of the cooler fluid in the vicinity of the bottom plate causes a reduction in Tw_x (Fig. 7.9) and enhancement in Nusselt number (Fig. 7.10). Thus a local maximum in Tw_x and a local minimum in $Nu_{b,x}$ appear. Further downstream, reduction of the bottom plate temperature due to natural convection effect causes the temperature difference (Tw_x - $T_{b,x}$) to diminish and Nusselt number increases. This phenomenon is repeated and Tw_x displays local maxima and minima. Also, $Nu_{b,x}$ possesses local minima and maxima.

Similar behavior of wall temperature and consequently the local Nusselt number was reported by Incropera et al. (1987) based on their experimental work and by Mahaney et al. (1988) in their numerical study of mixed convection in rectangular channels.

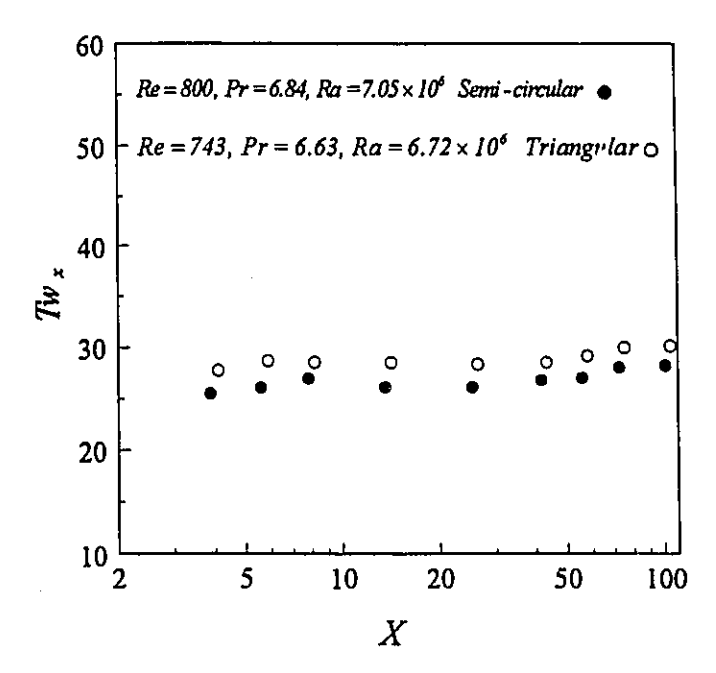


Figure 7.9 Mean bottom plate wall temperature vs. dimensions axial distance X for semi-circular and equilateral triangular ducts.

المرتبع تنا

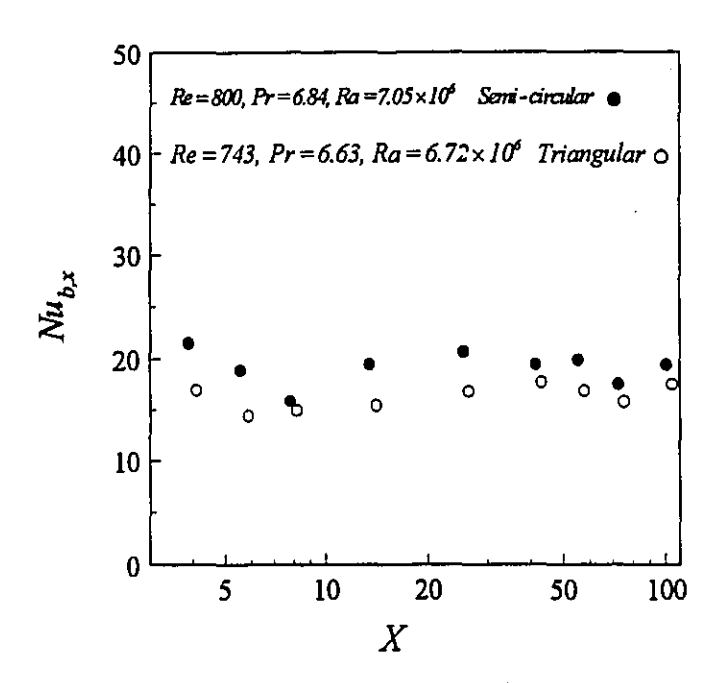
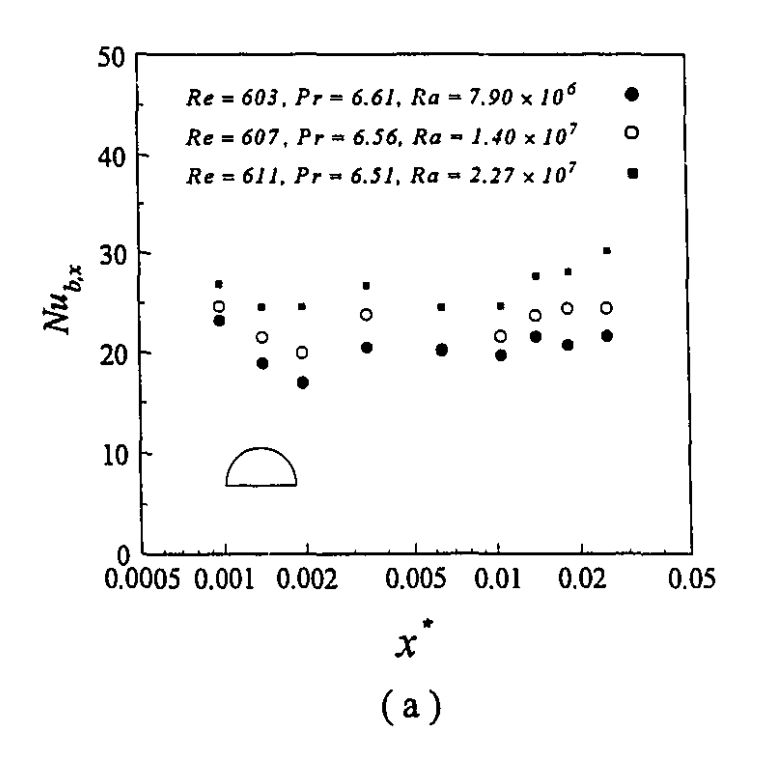


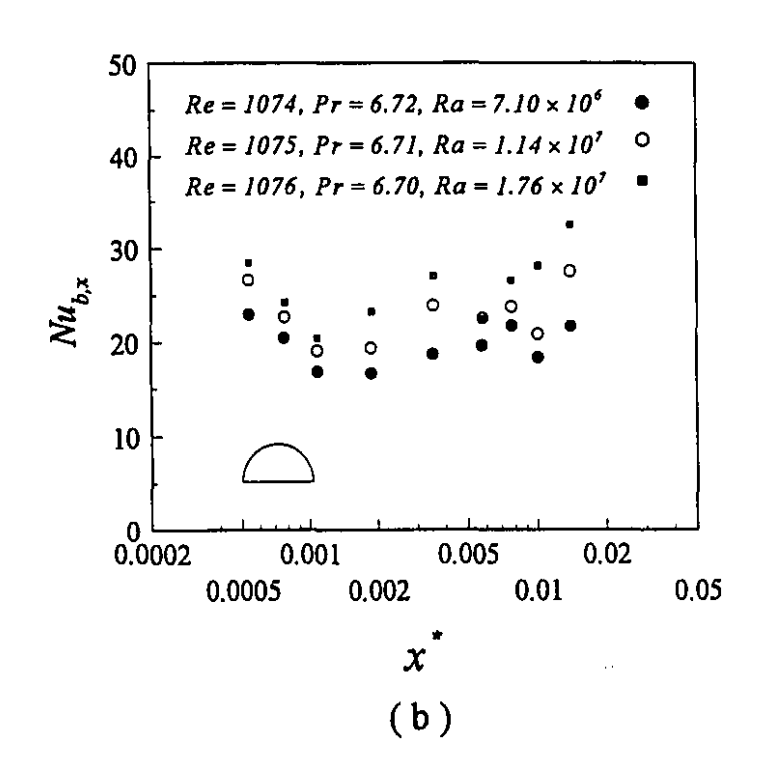
Figure 7.10 Bottom plate Nusselt number vs. dimensionless axial distance X for semi-circular and equilateral triangular ducts.

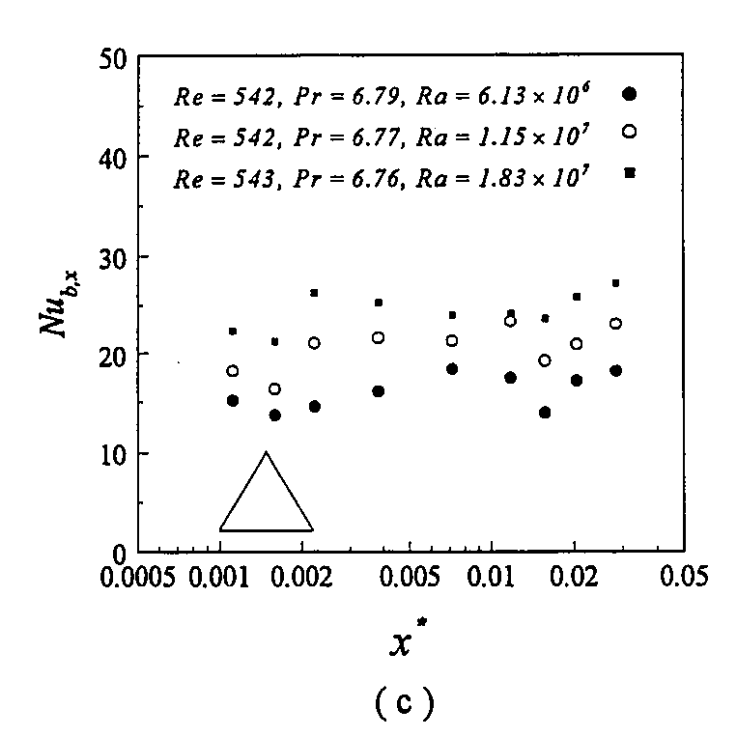
7.3.3.1.1 Effect of Rayleigh number

Fig. 7.11 (a - d) portrays typical axial variations of $Nu_{b,x}$ for different Rayleigh numbers but for approximately the same Reynolds number. The corresponding data are tabulated in Appendix D (D.5).

As shown in Fig. 7.11 increasing the Rayleigh number for the same Reynolds number strongly increases Nusselt number due to the presence of secondary flows. The magnitude of the local minima and maxima in Nusselt number decreases with diminishing Rayleigh number.







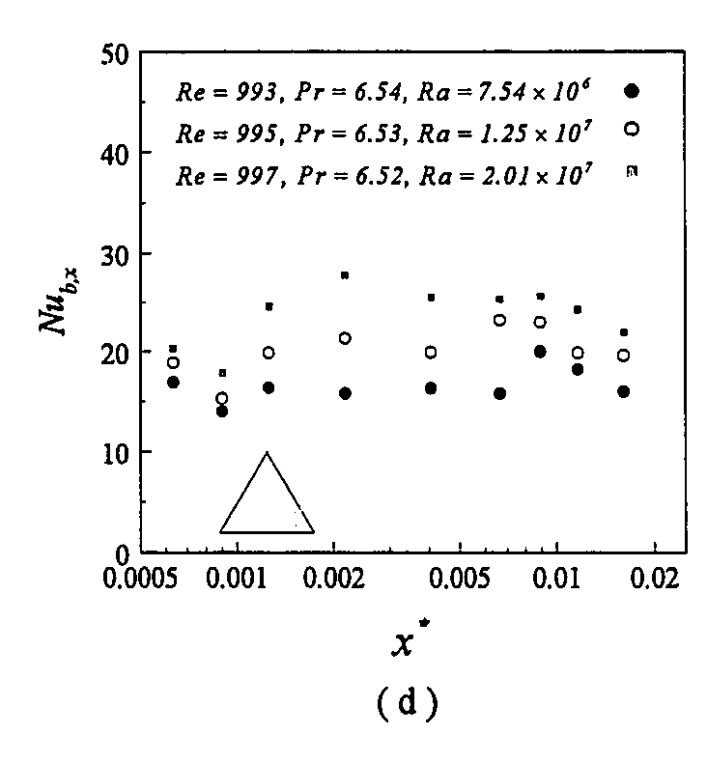


Figure 7.11 (a - d) Nusselt number vs. dimensionless axial distance x^* for different Reynolds and Rayleigh numbers for semi-circular and equilateral triangular ducts.

7.3.3.2 Viscous non-Newtonian fluids

A comparison of the local Nusselt number distribution obtained numerically and experimentally for a viscous non-Newtonian fluid (n=0.623) is shown in Fig. 7.12 (a - b) for both semi-circular and triangular channels. The measured $Nu_{b,x}$ values are seen to be in good agreement with the numerical predictions with a maximum deviation of 8.6 %.

Nusselt number vs. x^* are presented in Fig. 7.13 (a - b) for two Carbopol solutions (n=0.623, n=0.727) for the semi-circular and equilateral triangular ducts. These results and other heat transfer results for viscous non-Newtonian fluids obtained from this experimental study are tabulated in Appendix D (D.5).

Due to limitation of the apparatus higher values of Ra could not be achieved for further evaluation. For the small Rayleigh numbers used (for n=0.623) natural convection does not have a strong effect on heat transfer (Fig. 7.13a and Fig. 7.13c). For Carbopol solution with n=0.727 (Fig. 7.13b and Fig. 7.13d) due to the higher Ra effect of natural convection in downstream becomes noticeable. At $x^{\bullet}=0.0156$ and n=0.727 for the semicircular duct increasing Ra from 1.11×10^5 to 1.72×10^5 increases $Nu_{b,x}$ 12.6% and for triangular duct increasing Ra from 1.02×10^5 to 1.64×10^5 enhances Nusselt number about 8.5%.

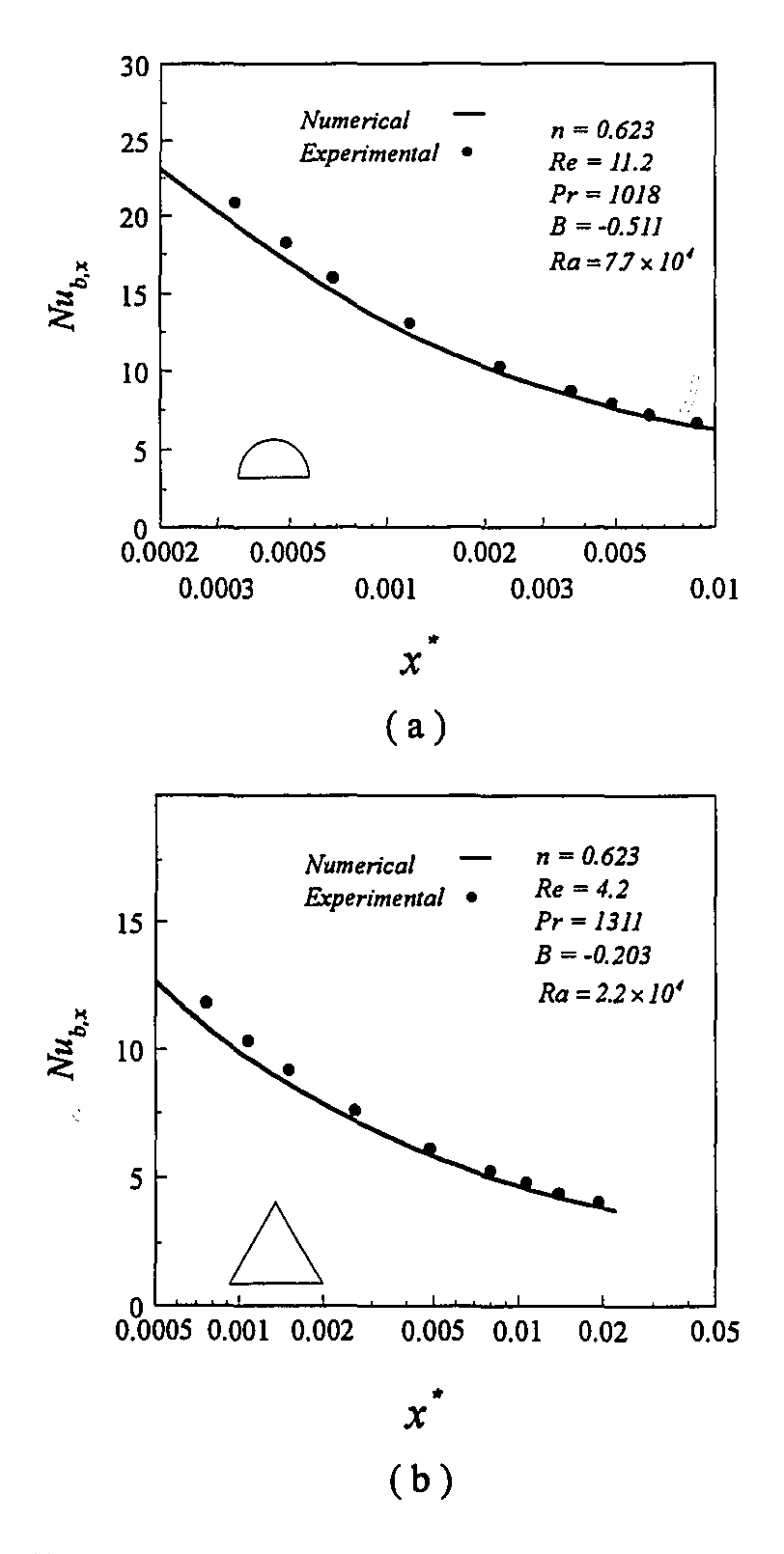
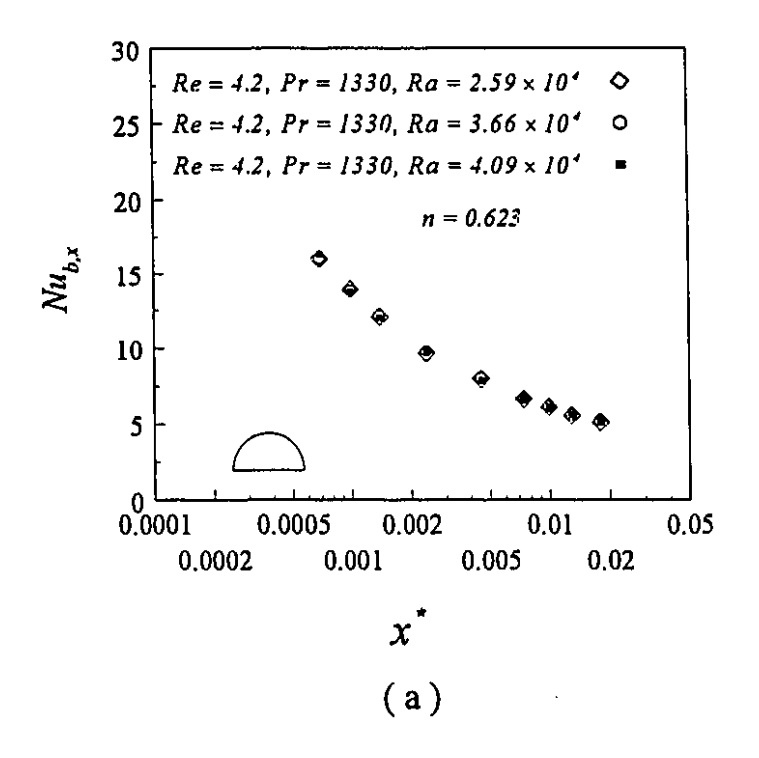
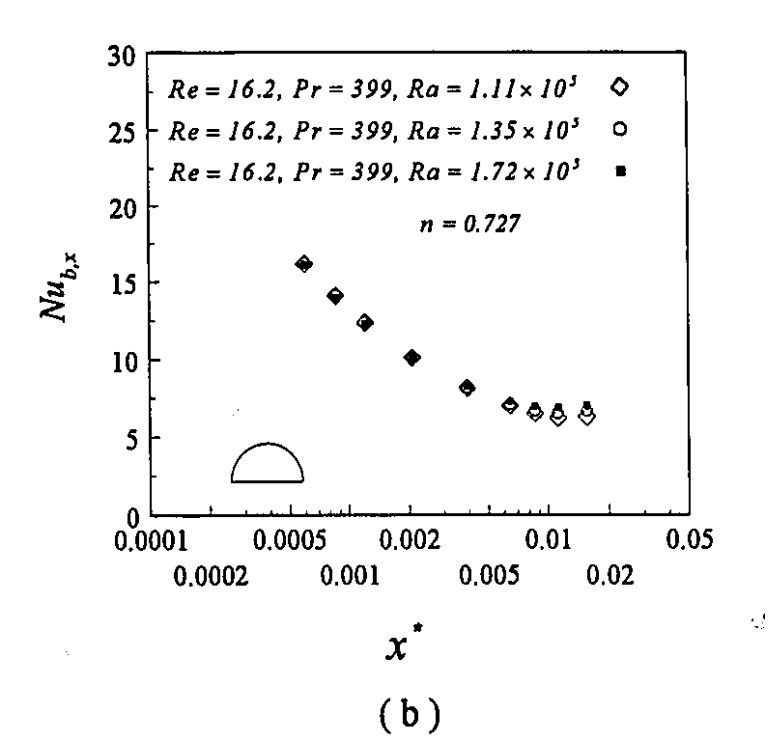
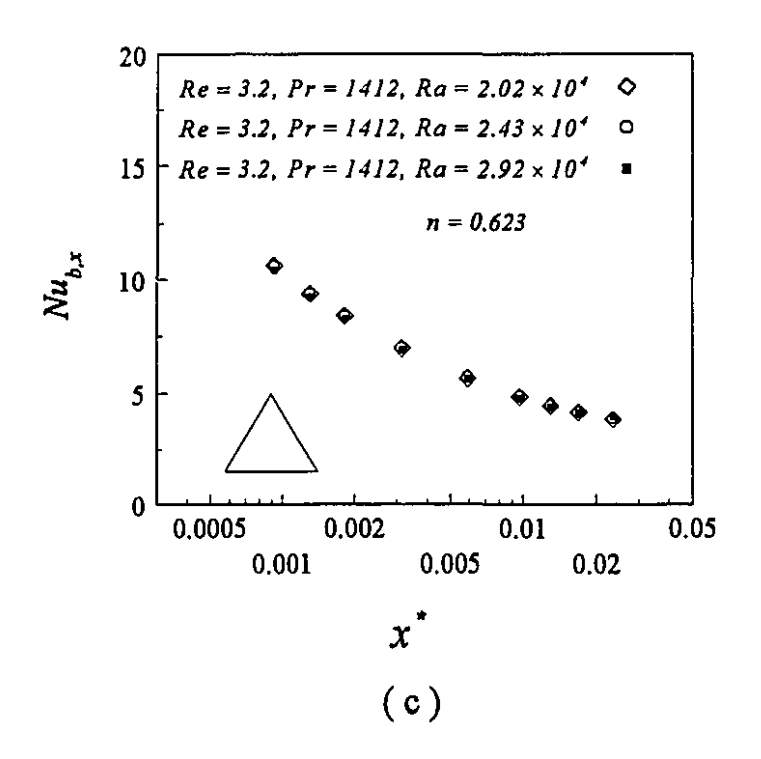


Figure 7.12 (a - b) Comparison of the local Nusselt number distribution from numerical and experimental results (n=0.623), (a)- semi-circular duct, (b)- equilateral triangular duct.







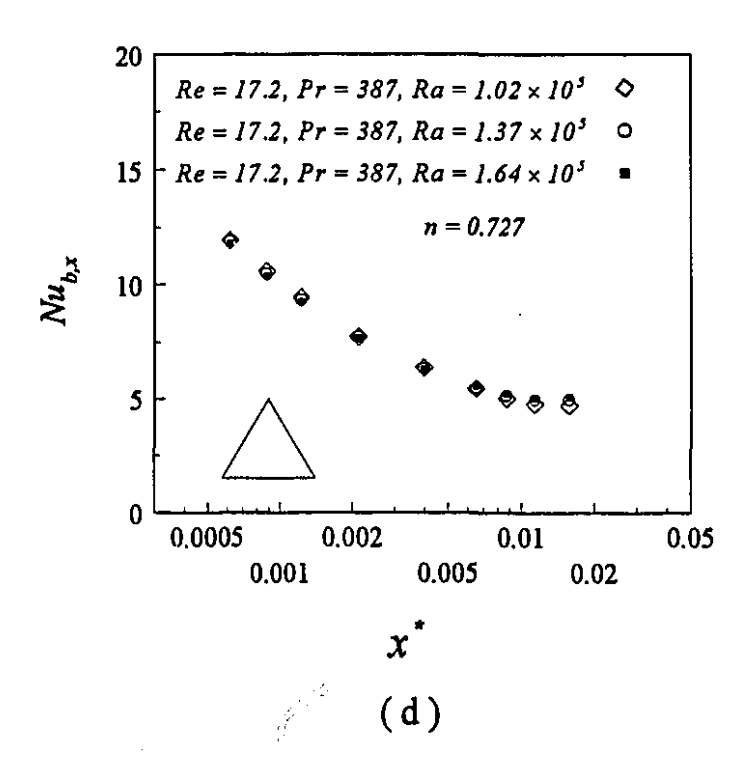


Figure 7.13 (a - d) Local Nusselt number vs. dimensionless axial distance x^* for different Rayleigh numbers.

7.4 Conclusions

An experimental study was performed to measure the critical Reynolds number, pressure drop, and local heat transfer distribution in simultaneously developing laminar flow of Newtonian and purely viscous non-Newtonian fluids in semi-circular and equilateral triangular ducts. The thermal boundary condition employed was constant heat flux on the bottom plate while other walls of the duct are insulated.

The measured critical Reynolds numbers indicate which for Re < 1250 and Re < 1000 the flow is fully laminar over the entire cross-section for semi-circular and triangular ducts, respectively. The measured pressure drop and Nusselt number results are in good agreement with numerical predictions. Results show that the Rayleigh number influences the Nusselt number. At higher Rayleigh numbers (for distilled water) the mean bottom plate temperature and Nusselt numbers show local maxima and minima. Also, results indicate isothermal dimensionless pressure drop can be scaled with x^+ which makes it almost independent of the Reynolds number.

Chapter 8

Conclusions, Contributions to Knowledge and Recommendations

8.1 Conclusions

The Galerkin finite element method was used to solve numerically the governing equations for a steady laminar three dimensional simultaneously developing flow of Newtonian and viscous non-Newtonian fluids flowing through various non-circular cross-section ducts subjected to the constant temperature and constant heat flux conditions. For each geometry results were compared with available data in the literature to validate the code. The numerical results include the effects of the power law index, temperature dependence of viscosity, viscous dissipation, simultaneous effects of temperature-dependent viscosity and viscous dissipation, and Prandtl number. The following general conclusions apply to all duct geometries unless stated otherwise.

Based on this comprehensive numerical study the following conclusions are made:

1- Lower power law index results in higher Nusselt number and reduced dimensionless pressure drop. The effect of Prandtl number on heat transfer is significant. Higher Prandtl

number produces higher Nusselt number (at the same $X^{\frac{1}{2}}$) but a lower Nusselt number (at the same $x^{\frac{n}{2}}$).

When the apparent friction factor and Nusselt number are plotted vs. x^{*-3} and x^{*} respectively for different Reynolds numbers, the Reynolds number dependence is eliminated.

2- For the case of heating, inclusion of the temperature-dependence of viscosity increases the pressure drop for the T boundary condition while decreasing it for the H2 boundary condition. For both T and H2 thermal boundary conditions, the temperature-dependence of viscosity enhances Nusselt number but this influence for the T boundary condition is more pronounced than that for the H2 boundary condition.

For the heating case, for both T and H2 conditions, inclusion of the viscous dissipation effects reduces Nusselt number. For the H2 boundary condition, close to the entrance of the duct, this effect is more significant than further downstream. For the T boundary condition when viscous dissipation is significant, the heating process can change to the cooling process under certain set of parameter values.

3- From a comparison of the thermal performance criteria for the various duct geometries studied it is concluded that the parallel plate channel is superior to all other configurations from the heat transfer point of view for the same flow rate, hydraulic diameter, and pressure drop. Therefore when reduction in the heat transfer area is the main objective, since the parallel plate geometry is not always practical, use of rectangular ducts of small aspect ratio (for the T boundary condition) and circular tubes or rounded corner square ducts are recommended for the constant heat flux boundary conditions.

$$\frac{2}{D_h Re Pr}$$

$$\frac{3}{2} \quad x^+ = \frac{x}{D_h Re}$$

 $[\]frac{1}{2} \quad X = \frac{x}{D_h}$

An experimental study was performed to obtain new data to validate the numerical work. The critical Reynolds numbers for semi-circular and equilateral triangular ducts were measured by a flow visualization technique. Pressure drop measurements for viscous non Newtonian fluids and heat transfer experiments for distilled water as well as Carbopol 934 solutions were carried out. The constant heat flux condition was applied in the experimental tests.

From the experimental study the following conclusions are drawn.

- 1- The critical Reynolds number for the semi-circular duct varies from 1250 to 1700 depending on the transverse location at a given axial cross section. This range for the equilateral triangular duct is 1000 to 2450. Laminar flow simulations are strictly applicable only up to the lower limit of the critical Reynolds number.
- 2- The effect of Rayleigh number on heat transfer to distilled water in two noncircular ducts was found to be significant. High Rayleigh number (2x10⁷) results in a local maximum and a minimum in the Nusselt number distribution at different axial distances for the two channels used.

According to the limited experimental data the pressure drop and Nusselt number for viscous non-Newtonian fluids can be scaled by x^+ and x^* , respectively, which makes the distribution curves independent of the Reynolds number. Experimental pressure drop and local Nusselt number distribution curves agreed closely with the numerical results for both semi-circular and equilateral triangular ducts.

8.2 Contributions to knowledge

1- Quantitative laminar fluid flow and heat transfer characteristics are presented for the combined entrance region for fourteen different channels. Results are obtained for both constant temperature and constant heat flux boundary conditions. The effects of the power law index on flow and heat transfer performance and the effect of Prandtl number on heat transfer are discussed quantitatively.

- 2- The effect of rounding the corners of a square duct, the effect of aspect ratio of rectangular channels, effect of apex angle of a circular sector duct, and effect of the geometric parameter of a cross-shape channel on fluid flow and heat transfer performance are examined and discussed.
- 3- A quantitative discussion is made which includes the effects of temperature-dependent viscosity, viscous dissipation, and the simultaneous effects of temperature-dependent viscosity and viscous dissipation, and Prandtl number. Presented results cover velocity profiles, apparent friction factor, and Nusselt number distribution for different temperature-viscosity functions and a range of Brinkman numbers.
- 4- The experimental study has produced new results for the critical Reynolds number, pressure drop and Nusselt number distribution for laminar flow through semi-circular and equilateral triangular ducts. The range of the critical Reynolds numbers based on the location of the dye probe was obtained for both channels. The effect of the Rayleigh number on the Nusselt number distribution for distilled water is discussed quantitatively. Pressure drop and Nusselt numbers obtained for various viscous non-Newtonian fluids indicate the capability of these parameters to be scaled by x^+ and x^+ , respectively. The experimental results verified accuracy of the numerical model.

8.3 Recommendations for future research

It is recommended that further attention be given to the following:

- 1- Extension of the study of fluid flow and heat transfer to other non-Newtonian fluids such as: Bingham plastic and viscoelastic non-Newtonian fluids. Such studies need to be carried out both numerically and experimentally. Extension to include time-dependent flow or boundary conditions is also of practical interest.
- 3- Free convection effects on the fluid flow and heat transfer characteristics in the entrance region of non-circular channels for non-Newtonian fluid have not been studied before; even for the Newtonian case very few investigations have been reported. Also, as an extension of the present study experiments should be carried out at higher Rayleigh

numbers for both Newtonian and non-Newtonian fluids. Also, effects of transversely mounted fins to enhance heat transfer would be of significant practical interest.

- 4- The present work should be extended to reacting flows as well as to non-Newtonian fluids containing particulate solids. The latter is an important problem in continuous processing of liquids foods.
- 5- Extension of the present study to the turbulent flow regime would be of engineering interest. There are opportunities for both fundamental and applied contributions in this area.
- 6- Effects of variable cross-sectional area as well as geometry in the flow direction should be of potential interest in the design of novel heat exchangers.

Laminar and turbulent heat transfer in Newtonian and non-Newtonian fluids flowing in curved ducts as well as coils of ducts of non-circular ducts may find new applications in future.

References

- 1. Abou-Ellail, M. M. M. and Morcos, S. M. 1983. Buoyancy Effects in the Entrance Region of Horizontal Rectangular Channels. J. of Heat Transfer, 105, 924-928.
- 2. Al-Ali, H. H. and Selim, M. S. 1992. Analysis of Laminar Flow Forced Convection Heat Transfer with Uniform Heating in the Entrance Region of a Circular Tube. The Canadian Journal of Chemical Engineering, 70, 1101-1107.
- 3. Aparecido, J. B. and Cotta, R. M. 1990. Thermally Developing Laminar Flow Inside Rectangular Ducts. *Int. J. Heat Mass Transfer*, **33**, 341-347.
- 4. Asako, Y. and Faghri, M. 1988. Three-Dimensional Laminar Flow Heat Transfer and Fluid Flow Characteristics in the Entrance Region of a Rhombic Duct. J. of Heat Transfer, 110, 855-861.
- 5. Ben-Ali, T. M., Soliman, H. M. and Zariffeh, E. K. 1989. Further Results for Laminar Heat Transfer in Annular Sector and Circular Sector Ducts. *J. of Heat Transfer*, 111, 1090-1093.
- 6. Bhatti, M. S. and Savery, C.W. 1977. Heat Transfer in the Entrance Region of a Straight Channel: Laminar Flow with Uniform Wall Heat Flux. *Trans. ASME*, 99, 142-144.
- 7. Bird, R. B., Armstrong, R. C. and Hassager, O. 1977. Dynamics of Polymeric Liquids. 1, Wiley, New York.
- 8. Bodoia, J. R. and Osterle, J. F. 1961. Finite Difference Analysis of Plane Poiseuille and Couette Flow Developments. *Appl. Sci. Res. Sect. A*, 10, 265-276.
- 9. Brooks, N. and Hughes, J. R. 1982. Streamline Upwind / Petrov-Galerkin Formulations for Convection Dominated Flows with Particular Emphasis on the Incompressible Navier-Stokes Equations. Computer Methods in Applied Mechanics and Engineering, 32, 199-259.
- 10. Burke, J. P. and Berman, N. S. 1969. Entrance Flow Development in Circular Tubes at Small Axial Distances. Am. Soc. Mech. Eng., pap. 69-WA / FE-13.

į.

- 11. Campos Silva, J. B., Cotta, R. M., and Aparecido, J. B. 1992. Analytical Solutions to Simultaneously Developing Laminar Flow inside Parallel Plate Channels. *Int. J. Heat Mass Transfer*, 35, 887-895.
- 12. Chadrupatla, A. R. and Sastri, V. M. K. 1977. Laminar Forced Convection Heat Transfer of a Non-Newtonian Fluid in a Square Duct. *Int. J. Heat Mass Transfer*, 20, 1315-1324.
- 13. Chandrupatla, A.R. 1977. Analytical and Experimental Studies of Flow and Heat Transfer Characteristics of a Non-Newtonian Fluid in a Square Duct. *Ph.D. Thesis, Indian Institute of Technology, Madras, India.*
- 14. Cho, Y. I., and Hartnett, J. P. 1985. Non-Newtonian Fluids. *Handbook of Heat Transfer Applications* edited by Rohsenow, W. M., Hartnett, J. P. and Gonic, E. N., McGraw Hill Book Co..
- 15. Conley, N., Lawal, A. and Mujumdar, A. S. 1985. An Assessment of the Accuracy of Numerical Solutions to the Graetz Problem. *Int. Comm. Heat Mass Transfer*, 12, 209-218.
- 16. Eckert, E. R. G., Irvine, Jr. T. F. and Minneapolis, M. 1956. Flow in Corners of Passages with Noncircular Cross Sections. *Transactions of the ASME*, 78, 709-718.
- 17. Engleman, M. S. 1991. FIDAP Theoretical Manual, Fluid Dynamics International Inc., 500 Davis St. Suite 600, Evanston, IL.
- 18. Etemad, S. Gh., Mujumdar, A. S. and Huang, B. 1994. Viscous Dissipation Effects in Entrance Region Heat Transfer foe a Power law Fluid Flowing between Parallel Plates. *Int. J. Heat and Fluid Flow*, 15, 122-131.
- 19. Filkova, I., Lawal, A., Koziskov, B. and Mujumdar, A. S. 1987. Heat Transfer to a Power-Law Fluid in Tube Flow: Numerical and Experimental Studies. *Journal of Food Eng.*, 6, 143-151.
- 20. Flores, A. F., Gottifredi, J. C., Morales, G. V., and Quiroga, O. D. 1991. Heat Transfer to Power Law Fluids Flowing in Pipes and Flat Ducts with Viscous Heat Generation. *Chem. Eng. Sci.*, 46, 1385-1392.
- 21. Gao, S. X. and Hartnett, J. P. 1992. Non-Newtonian Fluid Laminar Flow and Forced Convection Heat Transfer in Rectangular Ducts. *Int. Comm. Heat Mass Transfer*, 19, 673-686.

- Goldstein, R. J. and Kreid, D. K. 1967. Measurement of Laminar Flow Development in a Square Duct Using a Laser-Doppler Flowmeter. J. Appl. Mech., 34, 813-818.
- 23. Hartnett, J. P. and Kostic, M. 1985. Heat Transfer to a Viscoelastic Fluid in Laminar Flow through a Rectangular Channel. *Int. J. Heat Mass Transfer*, 28, 1147-1155.
- 24. Hartnett, J. P., and Kostic, M. 1989. Heat Transfer to Newtonian and Non-Newtonian Fluids in Rectangular Ducts. *Advances in Heat Transfer*, Edited by Hartnett, J. P., And Irvine, Jr. T. F., 247-356.
- 25. Heinrich, J. C. and Yu, C. C. 1988. Finite Element Simulation of Buoyancy-Driven Flows with Emphasis on Natural Convection in a Horizontal Circular Cylinder. Computer Methods in Applied Mechanics and Engineering, 69, 1-27.
- Hong, S. W. and Bergles, A. E. 1976. Laminar Flow Heat Transfer in the Entrance Region of Semi-Circular Tubes with Uniform Heat Flux. Int. J. Heat Mass Transfer, 19, 123-124.
- 27. Hornbeck, R.W. 1965. An All-Numerical Method for Heat Transfer in the Inlet of a Tube. Am. Soc. Mech. Eng., pap. 65-WA/HT-36.
- 28. Hughes, T. J. R., Liu, W. K. and Brooks, A. 1979. Finite Element analysis of incompressible viscous flows by the penalty function formulation. *j. Comput. Phys.*, 30, 1-60.
- 29. Huhn, J. 1992. Heat Transfer in the Inlet Region of Tubes and Channels with Laminar Flow. *Recent Advances in Heat Transfer*. Edited by Sunden, B. and ZuKauskas, A. Elsvier Science Publisher B.V., 516-523.
- 30. Hwang, C. L., and Fan, L. T. 1964. Finite Difference Analysis of Forced Convection Heat Transfer in Entrance Region of a Flat Rectangular duct. *Appl. Sci. Res.*, A13, 401-422.
- 31. Incropera, F. P. and Schutt, J. A. 1985. Numerical Simulation of Laminar Mixed Convection in the Entrance Region of Horizontal Rectangular Ducts. *Numerical Heat Transfer*, 8, 707-729.
- 32. Incropera, F. P., Knox, A. L. and Maughan, R. M. 1987. Mixed Convection Flow and Heat Transfer in the Entry Region of a Horizontal Rectangular Duct. *J. of Heat Transfer*, 109, 434-439.

- 33. Irvine, Jr. T. F. 1983. Fundamentals of Low Reynolds Number Non-Newtonian Flows. Low Reynolds Number Flow Heat Exchangers. Edited by Kakac, S., Shah, R. K., and Bergles, A. E., Hemisphere Publishing Corporation, 559-592.
- 34. Irvine, Jr. T. F. and Karni, J. 1987. Non-Newtonian Fluid Flow and Heat Transfer. *Handbook of Single-Phase Convective Heat Transfer* Edited by Kakac, S., Shah, R. K., and Aung, W., John Wiley & Sons, 20.1-20.57.
- 35. Isazadeh, M. A. 1993. Numerical Solution of Reacting Laminar Flow Heat and Mass Transfer in Ducts of Arbitrary Cross-Sections for Power Law Fluids. *Ph.D. Thesis, McGill university, Montreal, Quebec, Canada.*
- 36. Jensen, M. K. 1989. Simultaneously Developing Flow in an Isothermal Circular Duct. *Int. Comm. Heat Mass Transfer*, **16**, 811-820.
- 37. Joshi, S. D. and Bergles, A. E. 1980. Experimental Study of Laminar Heat Transfer to In-Tube Flow of Non-Newtonian Fluids, J. of Heat Transfer, 102, 397-401.
- 38. Kakac, S. and Yener, Y. 1983. Laminar Forced Convection in the Combined Entrance Region of Ducts. Low Reynolds Number Flow Heat Exchangers. Edited by Kakac, S., Shah, R. K., and Bergles, A. E., Hemisphere Publishing Corporation, 165-204.
- 39. Kays, W. M. 1955. Numerical Solutions for Laminar Flow Heat Transfer in Circular Tubes. *Trans. ASME*, 77, 1265-1274.
- 40. Kays, W. M. and London, A. L. 1984. Compact Heat Exchangers, McGraw Hill Book Co., New York.
- 41. Kays, W. M., and London, A. L. 1984. Compact Heat Exchangers. McGraw Hill Co..
- 42. Klemp, K., Demmer, T., and Herwing, H. 1992. Entrance Flows of Non-Newtonian Fluids with Temperature Dependent Viscosity. *Transport Phenomena in Heat and Mass Transfer*, Edited by Reizes, J. A. Elsevier Science Publishers B.V., 316-327.
- 43. Kline, J. S. and McClintock, F. A. 1953. Describing Uncertainties in Single-Sample Experiments. *Mechanical Eng.*, 75, 3-8.
- 44. Kozicki, W., Chou, C. H. and Tiu, C. 1966. Non-Newtonian Flow in Ducts of Arbitrary Cross-Sectional Shape. *Chem. Eng. Sci.*, 21, 665-679.

- 45. Lakshminarayanam, R. and Haji-Sheikh, A. 1992. Entrance Heat Transfer in Isosceles and Right Triangular Ducts. J. Thermodynamics, 6, 167-171.
- 46. Lawal, A. 1985. Laminar Flow and Heat Transfer to Variable Property Power-Law Fluids in Arbitrary Cross-Sectional Ducts. Ph.D. Thesis, McGill university, Montreal, Quebec, Canada.
- 47. Lawal, A. 1989. Mixed Convection Heat Transfer to Power Law Fluids in Arbitrary Cross-Sectional Ducts. J. of Heat Transfer, 111, 399-406.
- 48. Lawal, A. and Mujumdar, A. S. 1984. Forced Convection Heat Transfer to a Power Law Fluid in Arbitrary Cross-Section Duct. *The Canadian J. of Chem. Eng.*, 62, 326-333.
- 49. Lawal, A. and Mujumdar, A. S. 1985. Developing Flow and Heat Transfer to Power Law Fluids in Square, Trapezoidal and Pentagonal Ducts. *Int. Comm. Heat Mass Transfer*, 12, 23-31.
- 50. Lawal, A. and Mujumdar, A. S. 1989a. Viscous Dissipation Effects on Thermal Entrance Heat Transfer to Power Law Fluids in Arbitrary Cross-Sectional Ducts. *The Chemical Eng. J.*, 41, 57-66.
- 51. Lawal, A. and Mujumdar, A. S. 1989b. Laminar Duct Flow and Heat Transfer to Purely Viscous Non-Newtonian Fluids. Advances in Transport Processes. Edited by Mujumdar, A. S. and Mashelkar, R. A. Wiley Eastern, New Dehli, 352-443.
- 52. Lawal, A. and Mujumdar, A. S. 1992. The Effects of Viscous Dissipation on Heat Transfer to Power Law Fluids in Arbitrary Cross-Sectional Ducts. Warme-und Stoffübertragung, 27, 437-446.
- 53. Lei, Q. M. 1990. Numerical and Experimental Study of Laminar Mixed Convection in a Horizontal Semicircular Duct. *Ph.D. Thesis, University of Manitoba, Winnipeg, Canada.*
- 54. Lei, Q. M. and Trupp, A. C. 1989a. Maximum Velocity Location and Pressure Drop of Fully Developed Laminar Flow in Circular Sector Ducts. J. of Heat Transfer, 111, 1085-1087.
- 55. Lei, Q. M. and Trupp, A. C. 1989b. Further Analysis of Laminar Flow Heat Transfer in Circular Sector Ducts. J. of Heat Transfer, 111, 1088-1090.

- Lei, Q. M. and Trupp, A. C. 1990. Forced Convection of Thermally Developing Laminar Flow in Circular Sector Ducts. *Int. J. Heat Mass Transfer*, **33**, 1675-1683.
- 57. Lei, Q. M. and Trupp, A. C. 1991. Experimental Study of Laminar Mixed Convection in the Entrance Region of a Horizontal Semicircular Duct. *Int. J. Heat Mass Transfer*, 34, 2361-2372.
- 58. Lin, T. 1977. Numerical Solutions of Heat Transfer to Yield Power Law Fluids in the Entrance Region. M. S. thesis, University of Wisconsin, Milwaukee.
- 59. Lin, T., and Shah, V. L. 1978. Numerical Solution of Heat Transfer to Yield Power Law Fluids Flowing in the Entrance Region. *Int. Heat Transfer Conf.* 6th. Toronto, 5, 317-321.
- 60. Mahaney, H. V., Incropera, F.P. and Ramadhyani, S. R. 1987. Development of Laminar Mixed Convection Flow in a Horizontal Rectangular Duct with Uniform Bottom Heating. *Numerical Heat Transfer*, 12, 137-155.
- 61. Mahaney, H. V., Incropera, F.P. and Ramadhyani, S. R. 1988. Effect of Wali Heat Flux Distribution on Laminar Mixed Convection in the Entrance Region of a Horizontal Rectangular Duct. *Numerical Heat Transfer*, 13, 427-450.
- Manglik, R. M. and Bergles, A. E. 1987. A correlation for Laminar Flow Enhanced Heat Transfer in Uniform Wall Temperature Circular Tubes with Twisted-Tape Inserts. Advances in Enhanced Heat Transfer, ASME Edited by Jensen, M. K. and Carey, V. P., HTD 68, 19-25.
- 63. Manglik, R. M. and Bergles, A. E. 1988. Laminar Flow Heat Transfer in a Semi-Circular Tube with Uniform Wall Temperature. *Int. J. Heat Mass Transfer*, 31, 625-636.
- 64. Mansour, A. R. 1989. An Analytical Solution of Laminar Heat Transfer to Power-Law Non-Newtonian Fluids in Circular Ducts, Graetz-Nusselt Problem. *Int. Comm. Heat Mass Transfer*, 16, 199-204.
- 65. McKillop, A. A. 1964. Heat Transfer for Laminar Flow on Non-Newtonian Fluids in Entrance Region of a Tube. *Int. J. Heat Mass transfer*, 7, 853-862.
- 66. McKillop, A. A., Harper, J. C. and Bader, H. J. 1970. Variable Viscosity Entrance-Region Flow on Non-Newtonian Liquids, *Int. J. Heat Mass transfer*, 13, 901-909.

- 67. Mercer, W. E., Pearce, W. M. and Hitchcock, J. E. 1967, Laminar Forced Convection in the Entrance Region Between Parallel Plates. J. of Heat Transfer, 251-257.
- 68. Metzner, A. B. 1965. Heat Transfer in Non-Newtonian Fluids. Advances in Heat Transfer edited by Irvine, Jr. T. F. and Hartnett, J. P. Academic press, New York.
- 69. Mikic, B. B., Vujisic, Li. B. and Kapat, J. 1994. Turbulent Transition and Maintenance of Turbulence; Implication to Heat Transfer Augmentation. *Int. J. Heat Mass Transfer*, 37, 425-431.
- Montgomery, S. R. and Wibulswas, P. 1967. Laminar Flow Heat Transfer for Simultaneously Developing Velocity and Temperature Profiles in Ducts of Rectangular Cross Section. Appl. Sci. Res., 18, 247-259.
- 71. Natio, E. 1975. Laminar Heat Transfer in the Entrance Region between Parallel Plates-The Case of Uniform Heat Flux. *Heat Transfer-Jpn. Res.*, 4(2), 63-74.
- 72. Natio, E. 1985. The Effect of Buoyancy on Laminar Flow and Heat Transfer in the Entrance Region between Horizontal Parallel Plates. *Int. Chem. Eng.*, 25, 315-323.
- 73. Neti, S. and Eichhorn, R. 1983. Combined Hydrodynamic and Thermal Development in a Square Duct. *Numerical Heat Transfer*, 6, 497-510.
- 74. Nguyen, T. V. 1991. Low Reynolds Number Simultaneously Developing Flows in the Entrance Region of Parallel Plates. *Int. J. Heat Mass Transfer*, 34, 1219-1225.
- 75. Nguyen, T. V. 1992. Laminar Heat Transfer Number for Thermally Developing Flow in Ducts. *Int. J. Heat Mass transfer*. **35**, 1733-1741.
- 76. Nguyen, T. V. 1993. Incremental Heat Transfer Number in the Entry Region of Circular Tube. *Int. J. Heat Mass transfer*, **36**, 3659-3662.
- 77. Nguyen, T. V., Maclaine-cross, I. L. 1991., Simultaneously Developing, Laminar Flow, Forced Convection in the Entrance Region of Parallel Plates. J. of Heat Transfer, 113, 837-842.
- 78. Nonino, C., DelGiudice, S. and Comini, G. 1988. Laminar Forced Convection in Three Dimensional Duct Flows. *Numerical Heat Transfer*, 13, 451-466.

- 79. Pagliarini, G. 1989. Steady Laminar Heat Transfer in the Entry Region of Circular Tubes with Axial Diffusion of Heat and Momentum. *Int. J. Heat Mass transfer*, 32, 1037-1052.
- 80. Parikh, R. S. and Mahalingam, R. 1988. Laminar Tube Flow Heat Transfer in Non-Newtonian Fluids under Arbitrary Wall Heat Flux. *Int. Comm. Heat Mass Transfer*, 15, 1-16.
- 81. Patankar, S. V., and Spalding, D. B. 1970. Heat and Mass Transfer in Boundary Layers, 2nd Edition, Intertext Books, London.
- 82. Pawlek, R.A. and Tien. C. 1964. Laminar Heat Transfer to Non-Newtonian Fluids in the Entrance Region of a Circular Conduit. *Can. J. Chem. Eng.*, 42, 222-227.
- 83. Pittman, J. F. 1989. Finite Elements for Field Problems. Fundamentals of Computer Modeling for Polymer Processing edited by Tucker III. Ch. L. Hanser Publishers, New York.
- 84. Poirier, N. A. and Mujumdar, A. S. 1989. Numerical Solution of Graetz Problem: Achieving Accuracy in the Entrance Region. *Int. Comm. Heat Mass Transfer*, 16, 205-214.
- 85. Prusa, J. and Manglik, R. M. 1994. Asymptotic and Numerical Solutions for Thermally Developing Flows of Newtonian and Non-Newtonian Fluids in Circular Tubes with Uniform Wall Temperature. *Numerical Heat Transfer*, 26, 199-217.
- 86. Rostami, A. A., and Mortazavi, S. S. 1990. Analytical Prediction of Nusselt Number in a Simultaneously Developing Laminar Flow Between Parallel Plates. *Int. J. Heat and Fluid Flow*, March, 11, 44-47.
- 87. Salazar, A. J. and Campo, A. 1990. Prediction of the Thermal Entry Length without Solving the Complete Entrance Length Problem. *Int. J. Heat and Fluid Flow*, 11, 48-53.
- 88. Samant, A. B. and Marner, W. J. 1971. Heat Transfer to a Bingham Plastic in the Entrance Region of a Circular Tube. *Nuclear Sci. and Eng.*, 43, 241-246.
- 89. Schneider, G. E. and LeDain, B. L. 1981. Fully Developed Laminar Heat Transfer in Triangular Passages. *J. Energy*, 5, 15-21.
- 90. Shah, R. K. 1975. Laminar Flow Friction and Forced Convection Heat Transfer in Ducts of Arbitrary Geometry. *Int. J. Heat Mass Transfer*, 18, 849-862.

- 91. Shah, R. K. 1983a. Fully Developed Laminar Flow Forced Convection in Channels. Low Reynolds Number Flow Heat Exchangers. Edited by Kakac, S., Shah, R. K., and Bergles, A. E., Hemisphere Publishing Corporation, 75-108.
- 92. Shah, R. K. 1983b. Compact Heat Exchanger Surface Selection, Optimization, and Computer-Aided Thermal Design. Low Reynolds Number Flow Heat Exchangers. Edited by Kakac, S., Shah, R. K., and Bergles, A. E., Hemisphere Publishing Corporation, 845-874.
- 93. Shah, R. K., and Bhatti, M. S. 1987. Laminar Convection Heat Transfer in Ducts. *Handbook of Single-Phase Convective Heat Transfer* Edited by Kakac, S., Shah, R. K., and Aung, W., John Wiley & Sons, 3.1-3.137.
- 94. Shah, R. K., and London, A. L. 1978. Laminar Flow Forced Convection in Ducts. Advances in Heat Transfer edited by Irvine, Jr. T.F. and Hartnett, J. P. Academic press, New York.
- 95. Shin, S. and Cho, Y. I. 1994. Laminar Heat Transfer in a Rectangular Duct with a Non-Newtonian Fluid with Temperature-Dependent Viscosity. *Int. J. Heat Mass Transfer*, 37, Suppl. 1, 19-30.
- 96. Shome, B. and Jensen, M. K. 1993. Correlations for Simultaneously Developing Laminar Flow and Heat Transfer in a Circular Tube. *Int. J. Heat Mass transfer*, 36, 2710-2713.
- 97. Siegel, R. and Sparrow, E. M. 1959. Simultaneous Development of Velocity and Temperature Distributions in a Flat Duct with Uniform Wall Heating. A.I.Ch.E. J., 5, 73-75.
- 98. Skelland, A. H. P. 1967. Non Newtonian Flow and Heat Transfer. John Wiley & sons Inc..
- 99. Soliman, H. M., Munis, A. A. and Trupp, A. C. 1982. Laminar Flow in the Entrance Region of Circular Sector Ducts. J. Appl. Mech., 49, 640-642.
- Sparrow, E. M., Hixon, C. W. and Shavit, G. 1967. Experiments on Laminar Flow Development in Rectangular Ducts. j. Basic Eng., 89, 116-124.
- Trupp, A. C. and Lau, A. C. Y. 1984. Fully Developed Laminar Heat Transfer in Circular Sector Ducts with Isothermal Walls. J. of Heat Transfer, 106, 467-469.
- Trupp, A. C. and Lei, Q. M. 1989. Laminar Flow Heat Transfer in Circular Sector Ducts with Uniform Heat Flux. *Transactions of the CSME*, 13, 31-34.

- 103. Victor, S. A. and Shah, V. L. 1976. Steady State Heat Transfer to Blood Flowing in the Entrance Region of a Tube. *Int. J. Heat Mass Transfer*, 19, 777-783.
- 104. Vradis, G. C., Dougher, J. and Kumar, S. 1993. Entrance Pipe Flow and Heat Transfer for Bingham Plastic. *Int. J. Heat Mass Transfer*, 36, 543-552.
- Webb, R. L. 1981. Performance Evaluation Criteria for Use of Enhanced Heat Transfer Surfaces in Heat Exchanger Design. *Int. J. Heat Mass Transfer*, 24, 715-726.
- Webb, R. L. and Bergles, A. E. 1983. Performance Evaluation Criteria for Selection of Heat Transfer Surface Geometries Used in Low Reynolds Number Heat Exchangers. Low Reynolds Number Flow Heat Exchangers. Edited by Kakac, S., Shah, R. K., and Bergles, A. E., Hemisphere Publishing Corporation, 735-752.
- 107. Weber, M. E. 1995. Personal Communication. Chem. Eng. Dept., McGill University, Montreal, Quebec, Canada.
- 108. Wibulswas, P. 1966. Laminar-Flow Heat-Transfer in Non-Circular Ducts. *Ph.D. Thesis, London University, London.*
- 109. Xie, C. and Hartnett, J. P. 1992. Influence of Variable Viscosity of Mineral Oil on Laminar Heat Transfer in a 2:1 Rectangular Duct. *Int. J. Heat Mass Transfer*, 35, 641-648.
- 110. Yang, H. and Camarero, R. 1991. Internal Three-Dimensional Viscous Flow Solutions Using Vorticity-Potential Method. *Int. J. for Numerical Methods in Fluids*, 12, 1-15.
- 111. Yau, J, and Tien, Chi. 1963. Simultaneous Development of Velocity and Temperature Profiles for Laminar Flow of a Non Newtonian Fluid in the Entrance Region of Flat Ducts. *The Canadian Journal of Chemical Engineering*, 139-145.
- Yoo, S. 1974. Heat Transfer and Friction Factors for non-Newtonian Fluids in Turbulent Pipe Flow. *Ph.D. Thesis, University of Illinois, Chicago, Illinois.*
- 113. Zienkiewicz, O. C. 1977. Finite Element Method. McGraw Hill, New York.

Appendix A

A.1 U_{max} and $f_{app}Re$ for different geometries

Table A1 f_{app} . Re and U_{max} for different power law indices and at different axial locations: circular tube.

x ⁺		f _{app} .Re			U_{max}	
	n=0.50	n=1.00	n=1.25	n=0.50	n=1.00	n=1.25
0.00201	24.035	81.659	136.366	1.097	1.204	1.268
0.00334	21.021	64,535	103.992	1.147	1.291	1.375
0.00546	18.187	<i>51.587</i>	80.931	1.211	1.394	1.499
0.00884	15.658	41.772	64.232	1.283	1.522	1.652
0.01425	13.476	34.318	<i>52.044</i>	1.363	1.677	1.849
0.02289	11.641	28.683	43.167	1.449	1.828	2.009
0.02898	10.853	26.425	39.718	1.492	1.889	2.058
0.05873	8.974	21.494	32.558	1.601	1.985	2.107
0.11878	7.756	18.763	28.847	1.654	1.996	2.107
0.21346	7.151	17.544	27.224	1.662	1.996	2.107

Table A2 f_{app} . Re and U_{max} for different power law indices and at different axial locations: parallel plates.

x ⁺	f_{app} Re			U_{max}		
	n=0.50	n=1.00	n=1.25	n=0.50	n=1.00	n=1.25
0.00201	26.239	88.869	150.196	1.103 .	1.232	1.315
0.00334	22.227	69.583	114.327	1.146	1.318	1.422
0.00546	18.826	55.451	89.294	1.192	1.402	1.504
0.00884	15.976	44.978	71.761	1.239	1.460	1.539
0.01425	13.637	37.437	60.116	1.281	1.485	1.546
0.02289	11.799	32.384	<i>52.790</i>	1.310	1.491	1.546
0.02898	11.063	30.594	50.240	1.319	1.491	1.546
0.05873	9.534	27.184	45.399	1.327	1.491	1.546
0.11878	8. <i>748</i>	25.503	43.009	1.327	1.491	1.546
0.21346	8.407	24.773	41.970	1.327	1.491	1.546

Table A3 f_{app} . Re and U_{max} for different power law indices and at different axial locations: square duct.

x ⁺		f _{app} .Re			U_{max}	
	n=0.50	n=1.00	n=1.25	n=0.50	n=1.00	n=1.25
0.00201	30.469	87.795	139.272	1.077	1.182	1.247
0.00334	24.690	68.352	106.497	1.125	1.269	1.352
0.00546	20.526	54.190	82.595	1.191	1.367	1.460
0.00884	17.132	43.453	65.115	1.269	1.486	1.599
0.01425	14.396	35.234	52.270	1.356	1.639	1.794
0.02289	12.204	29.011	42.812 -	. 1.453	1.811	2.003
0.02898	11.285	26.531	39.106	1.504	1.891	2.086
0.05873	9.054	20.928	31.036	1.648	2.052	2.202
0.11878	7.548	17.621	26.635	1.740	2.094	2.215
0.21346	6.768	16.121	24.710	1.765	2.096	2.215

, · (*)

Table A4 f_{app} -Re and U_{max} for different power law indices and at different axial locations: rectangular duct (A.R.=0.5).

x+ ,		f _{app} .Re			$U_{ extit{max}}$	
ļ	n=0.50	n=1.00	n=1.25	n=0.50	n=1.00	n=1.25
0.00201	31.087	93.586	154.835	1.082	1.190	1.250
0.00334	25.597	72.220	115.698	1.134	1.274	1.348
0.00546	21.056	56.499	88.353	1.196	1.376	1.479
0.00884	17.454	44.874	68.963	1.266	1.501	1.636
0.01425	14.610	36.247	54.957	1.348	1.636	1.788
0.02289	12.340	29.818	44.868	1.438	1.763	1.910
0.02898	11.387	27.268	41.006	1.483	1.818	1.957
0.05873	9.161	21.766	33.070	1.611	1.941	2.038
0.11878	7.730	18.690	28.906	1.701	1.987	2.053
0.21346	6.999	17.299	27.073	1.734	1.992	2.053

Table A5 f_{app} . Re and U_{max} for different power law indices and at different axial locations: rectangular duct (A.R.=0.2).

x^+	f _{app} .Re			U_{max}		
	n=0.50	n=1.00	n=1.25	n=0.50	n=1.00	n=1.25
0.00201	31.189	89.739	143.027	1.082	1.181	1.233
0.00334	25.539	69.902	109.971	1.131	1.269	1.368
0.00546	21.219	55.573	85.961	1.189	1.384	1.505
0.00884	17.545	44.795	58.186	1.254	1.493	1.612
0.01425	14.627	<i>36.588</i>	55.442	1.323	1.577	1.676
0.02289	12.376	30.586	46.773	1.391	1.630	1.713
0.02898	11.460	28.317	43.640	1.422	1.649	1.724
0.05873	9.407	23.757	37.538	1.498	1.689	1.745
0.11878	8.193	21.406	34.468	1.560	1.709	1.749
0.21346	7.610	20.370	33.117	1.600	1.714	1.749

Table A6 f_{app} -Re and U_{max} for different power law indices and at different axial locations: semi-circular duct.

x ⁺		f _{app} .Re			U_{max}	
	n=0.50	n=1.00	n=1.25	n=0.50	n=1.00	n=1.25
0.00201	24.860	86.872	147.089	1.083	1.193	1.258
0.00334	21.229	<i>68.354</i>	110.858	<i>1.131</i>	1.282	1.364
0.00546	18.488	54.121	85.429	1.195	1.386	1.491
0.00884	16.125	43.472	67.272	1.272	1.516	1.651
0.01425	13.927	35.494	54.175	1.357	1.662	1.829
0.02289	11.992	29.526	44.734	1.448	1.807	1.980
0.02898	11.153	27.150	41.090	1.494	1.873	2.039
0.05873	9.149	21.956	33.466	1.624	2.012	2.135
0.11878	7.816	18.971	29.386	1.716	2.056	2.146
0.21346	7.118	17.607	27.584	1.747	2.058	2.146

Table A7 f_{app} -Re and U_{max} for different power law indices and at different axial locations: circular sector duct ($\alpha = 90^{\circ}$).

x^{+}	f _{app} .Re			U_{max}		
	n=0.50	n=1.00	n=1.25	n=0.50	n=1.00	n=1.25
0.00201	23.611	80.087	134.609	1.081	1.181	1.245
0.00334	20.683	<i>63.753</i>	102.964	1.130	1.269	1.351
0.00546	17.917	51.114	80.283	1.192	1.371	1.474
0.00884	15.473	41.459	63.730	1.266	1.499	1.628
0.01425	13.371	34.062	51.510	1.350	1.654	1.822
0.02289	11.584	28.393	42.503	1.443	1.817	2.007
0.02898	10.803	26.090	38.956	1.492	1.891	2.075
0.05873	8.883	20.928	31.365	1.630	2.039	2.172
0.11878	7.552	17.899	27.253	1.718	2.077	2.181
0.21346	6.847	16.519	25.442	1.744	2.079	2.181

Ó

Table A8 f_{app} -Re and U_{max} for different power law indices and at different axial locations: circular sector duct ($\alpha = 60^{\circ}$).

x ⁺		f _{app} .Re			U_{max}	
	n=0.50	n=1.00	n=1.25	n=0.50	n=1.00	n=1.25
0.00201	29.125	83.239	140.778	1.080	1.178	1.239
0.00334	25.257	65.361	107.578	1.129	1.264	1.348
0.00546	21.705	52.359	83.529	1.192	1.368	1.473
0.00884	18.649	42.433	65.770	1.268	1.499	1.629
0.01425	16.068	34.703	52.704	1.355	1.659	1.827
0.02289	13.904	28.747	43.121	1.453	1.832	2.030
0.02898	12.957	26.326	39.350	1.505	1.913	2.109
0.05873	10.599	20.868	31.218	1.655	2.083	2.228
0.11878	8.925	17.605	26.744	1.759	2.132	2.242
0.21346	8.017	16.100	24.765	1.792	2.134	2.242

Table A9 f_{app} . Re and U_{max} for different power law indices and at different axial locations: equilateral triangular duct ($\alpha = 60^{\circ}$).

<i>x</i> ⁺	f _{app} .Re			U_{max}		
	n=0.50	n=1.00	n=1.25	n=0.50	n=1.00	n=1.25
0.00201	48.868	117.092	186.682	1.069	1.174	1.237
0.00334	36.049	86.408	135.086	1.119	1.267	1.346
0.00546	27.681	65.177	100.239	1.185	1.367	1.457
0.00884	21.757	50.254	76.046	1.266	1.490	1.606
0.01425	17.357	39.502	58.973	1.357	1.646	1.804
0.02289	14.087	31.650	46.877	1.460	1.825	2.019
0.02898	12.776	28.560	42.219	1.515	1.915	2.120
0.05873	9.792	21.774	32.239	1.685	2.129	2.302
0.11878	7.852	17.710	26.617	1.820	2.216	2.341
0.21346	6.815	15.786	24.099	1.876	2.226	2.343

Table A10 f_{app} . Re and U_{max} for different power law indices and at different axial locations: right isosceles triangular duct ($\alpha = 90^{\circ}$).

x ⁺	f _{app} Re			U_{max}		
	n=0.50	n=1.00	n=1.25	n=0.50	n=1.00	n=1.25
0.00201	52.971	123.910	193.684	1.067	1.168	1.227
0.00334	38.499	90.729	139.625	1.116	1.261	1.338
0.00546	. 29.178	67.930	103.105	1.183	1.362	1.453
0.00884	22.679	51.972	77.859	1.264	1.486	1.604
0.01425	17.945	40.581	60.155	1.356	1.643	1.804
0.02289	14.462	32.344	47.641	1.460	1.823	2.020
0.02898	13.075	29.117	42.824	1.517	1.914	2.121
0.05873	9.947	22.051	32.519	1.692	2.142	2.320
0.11878	7.924	17.811	26.676	1.843	2.250	2.373
0.21346	6.832	<i>15.771</i>	24.030	1.916	2.268	2.377

Table A11 f_{app} . Re and U_{max} for different power law indices and at different axial locations: cross-shaped duct ($\lambda = 0.25$).

x ⁺	f _{app} .Re			U_{max}		
	n=0.50	n=1.00	n=1.25	n=0.50	n=1.00	n=1.25
0.00201	21.585	75.242	121.824	1.077	1.176	1.277
0.00334	20.045	59.327	93.329	1.129	1.257	1.327
0.00546	17.858	47.279	72.621	1.194	1.349	1.436
0.00884	15.198	38.077	57.349	1.265	1.459	1.559
0.01425	12.825	31.015	46.048	1.342	1.598	<i>1.731</i>
0.02289	10.898	25.621	37.702	1.429	1.757	1.930
0.02898	10.083	23.436	34.394	1.475	1.833	2.014
0.05873	8.141	18.521	27.209	1.605	1.990	2.136
0.11878	6.843	15.605	23.253	1.688	2.032	2.149
0.21346	6.169	14.271	21.508	1.711	2.034	2.148

Table A12 f_{app} . Re and U_{max} for different power law indices and at different axial locations: cross-shaped duct ($\lambda=0.5$).

x +		f _{app} .Re			U_{max}	
	n=0.50	n=1.00	n=1.25	n=0.50	n=1.00	n=1.25
0.00201	21.003	75.238	124.781	1.071	1.169	1.223
0.00334	19.239	59.997	96.731	1.121	1.254	1.331
0.00546	17.225	48.480	76.024	1.184	1.356	1.456
0.00884	14.998	39.496	60.220	1.259	1.478	1.599
0.01425	12.957	32.331	48.334	1.345	1.623	1.768
0.02289	11.202	26.726	39.524	1.443	1.788	1.971
0.02898	10.420	24.436	36.028	1.495	1.872	2.067
0.05873	8.447	19.216	28.317	1.653	2.078	2.248
0.11878	7.030	15.968	23.852	1.774	2.162	2.287
0.21346	6.242	14.411	21.837	1.821	2. <u>171</u>	2.287

A.2 Nusselt numbers for different geometries

Table A13 $Nu_{T,x}$ and $Nu_{H2,x}$ for different power law indices and different axial distances, Re=500 and Pr=10: circular tube.

x'		$Nu_{T,x}$	·		Nu _{H2,x}	
	n=0.50	n=1.00	n=1.25	n=0.50	n=1.00	n=1.25
0.000201	24.804	19.350	17.934	34.376	27.147	25.289
0.000334	19.150	15.510	14.668	26.752	21.549	20.263
0.000546	15.107	12.734	12.171	21.039	17.388	16.497
0.000884	12.170	10.540	10.157	16.783	14.210	13.582
0.001425	9.917	8.812	8.562	13.559	11.727	11.287
0.002289	8.217	7.465	7.307	11.096	9. 788	9.484
0.002898	7.532	6.905	<i>6.781</i>	10.094	8.985	8. <i>735</i>
0.005873	5.960	5.577	5.512	7.792	7.104	6.965
0.011878	4.931	4.644	4.584	6.292	5.821	5.720
0.0213460	4.398	4.119	4.054	5.474	5.074	4.985
Fully Developed	3.950	3.659	3.590	4.744	4.363	4.272

Table A14 $Nu_{T,x}$ and $Nu_{H2,x}$ for different power law indices and different axial distances, Re=500 and Pr=10: parallel plates.

x'		$Nu_{T,x}$			$Nu_{H2,x}$	
	n=0.50	n=1.00	n=1.25	n=0.50	n=1.00	n=1.25
0.000201	26.105	20.679	18.661	36.216	28.634	26.180
0.000334	20.823	17.329	16.079	28.414	23.218	21.513
0.000546	17.005	14.727	13.971	22.787	19.266	18.189
0.000884	14.187	12.713	12.297	18.662	16.229	15.576
0.001425	12.100	11.167	10.934	15.587	13.907	13.509
0.002289	10.570	9.947	9.777	13.291	12.118	11.843
0.002898	9.971	9.427	9.272	12.377	11.374	11.133
0.005873	8. <i>679</i>	8.226	8.103	10.354	= 9.634	9.457
0.011878	8.061	7.648	7.544	9.203	8.615	8.472
0.0213460	7.952	7.551	7.451	8.829	8.293	8.164
Fully Developed	7.950	7.541	7.442	8.758	8.235	8.109

Table A15 $Nu_{T,x}$ and $Nu_{H2,x}$ for different power law indices and different axial distances, Re=500 and Pr=10: square duct.

x.		Nu _{T,x}			Nu _{H2,x}		
	n=0.50	n=1.00	n=1.25	n=0.50	n=1.00	n=1.25	
0.000201	22.898	16.494	14.887	32.180	23.959	22.137	
0.000334	17.808	13.466	12.288	24.783	17.992	16.712	
0.000546	13.943	11.305	10.501	18.321	14.512	<i>13.713</i>	
0.000884	11.229	9.567	9.056	14.160	11.901	11.341	
0.001425	9.214	<i>8.131</i>	7.787	11.297	9.743	9.359	
0.002289	7.589	6.887	6.643	9.107	8.032	7.773	
0.002898	6.883	6.331	6.136	8.129	7.327	7.106	
0.005873	5.291	5.013	4.918	6.132	5.684	5.541	
0.011878	4.304	4.115	4.048	4.804	4.563	<i>4.451</i>	
0.0213460	3.746	3.548	3.494	4.090	3.915	<i>3.799</i>	
Fully Developed	3.190	2.979	2.925	3.310	3.090	3.032	

Table A16 $Nu_{T,x}$ and $Nu_{H2,x}$ for different power law indices and different axial distances, Re=500 and Pr=10: rectangular duct (A.R.=0.5).

x.		$Nu_{T,x}$			$Nu_{H2,x}$	
	n=0.50	n=1.00	n=1.25	n=0.50	n=1.00	n=1.25
0.000201	24.422	17.836	16.167	33.089	24.974	23.270
0.000334	18.056	14.523	13.644	24.447	19.365	18.334
0.000546	14.262	12.075	11.598	18.710	15.414	14.748
0.000884	11.661	10.104	9.817	14.755	12.467	12.008
0.001425	9.590	8.434	8.270	11.788	10.188	9.860
0.002289	7.925	7.113	7.037	9.499	8.399	8.180
0.002898	7.246	6.577	6.530	8.566	7.662	7.490
0.005873	5.699	5.325	5.312	6.450	5.961	5.873
0.011878	4.686	4.439	4.416	5.067	4.791	4.745
0.0213460	4.132	3.935	3.900	4.294	4.101	4.069
Fully Developed	3.600	3.388	3.350	3.150	3.021	2.998

Table A17 $Nu_{T,x}$ and $Nu_{H2,x}$ for different power law indices and different axial distances, Re=500 and Pr=10: rectangular duct (A.R.=0.2).

x'	Nu _{T,x}			Nu _{H2,x}		
	n=0.50	n=1.00	n=1.25	n=0.50	n=1.00	n=1.25
0.000201	24.005	17.815	16.432	33.396	26.139	24.727
0.000334	<i>18.881</i>	14.658	<i>13.804</i>	26.115	20.703	19.749
0.000546	14.645	<i>12.360</i>	11.842	20.167	16.609	15.929
0.000884	12.069	10.611	10.358	15.882	13.547	13.103
0.001425	10.292	9.289	9.197	12.841	11.264	10.998
0.002289	8.919	8.218	<i>8.173</i>	10.606	9.543	9.382
0.002898	8.320	7.724	7.684	9.699	8.826	8.699
0.005873	6.811	6.432	6.390	7.549	7.072	7.008
0.011878	5.846	5.586	5.545	6.048	5.829	<i>5.788</i>
0.0213460	5.468	5.266	5.299	5.192	5.117	5.088
Fully Developed	4.922	4.831	4.817	2.717	2.924	2.996

Table A18 $Nu_{T,x}$ and $Nu_{H2,x}$ for different power law indices and different axial distances, Re=500 and Pr=10: semi-circular duct.

x'		Nu _{T,x}		_	Nu _{H2,x}	
	n=0.50	n=1.00	n=1.25	n=0.50	n=1.00	n=1.25
0.000201	26.952	21.957	19.533	34.739	. 27.022	24.947
0.000334	21.305	17.361	15.968	27.027	21.426	20.158
0.000546	16.597	13.402	12.626	21.332	17.157	16.207
0.000884	12.698	10.447	9.969	16.600	13.603	12.937
0.001425	9.712	8.474	<i>8.233</i>	12.806	10.845	10.417
0.002289	7.872	7.172	7.039	10.014	8.793	8.535
0.002898	7.209	6.641	6.539	8.934	7.937	7.776
0.005873	5.687	5.351	5.305	6.570	6.089	6.012
0.011878	4.660	4.435	4.403	5.062	4.813	4.785
0.0213460	4.108	3.908	3.872	4.212	4.052	4.034
Fully Developed	3.480	3.318	3.265	3.038	2.920	2.880

Table A19 $Nu_{T,x}$ and $Nu_{H2,x}$ for different power law indices and different axial distances, Re=500 and Pr=10: circular sector duct ($\alpha=90^{\circ}$).

x'	"	Nu _{T,x}			Nu _{H2,x}	
	n=0.50	n=1.00	n=1.25	n=0.50	n=1.00	n=1.25
0.000201	24.333	19.022	17.440	32.252	25.371	23.629
0.000334	18.703	<i>15.050</i>	14.213	24.840	19.808	18.697
0.000546	14.713	12.426	11.869	19.330	15.779	15.055
0.000884	11.930	10.260	9.835	15.212	12.723	12.226
0.001425	9.636	8.417	<i>8.135</i>	12.060	10.313	9.971
0.002289	7.813	6.998	6.827	9.536	8.386	8.192
0.002898	7.085	6.422	6.292	8.520	7.592	7.457
0.005873	5.436	5.067	5.018	6.216	5.769	<i>5.737</i>
0.011878	4.346	4.112	4.094	4.759	4.569	4.549
0.0213460	3.754	3.538	3.543	3.982	3.867	<i>3.833</i>
Fully Developed	3.206	3.060	3.013	3.121	2.980	2.937

Table A20 $Nu_{T,x}$ and $Nu_{H2,x}$ for different power law indices and different axial distances, Re=500 and Pr=10: circular sector duct ($\alpha=60^{\circ}$).

x.		$Nu_{T,x}$			Nu _{H2,x}	
	n=0.50	n=1.00	n=1.25	n=0.50	n=1.00	n=1.25
0.000201	24.328	18.959	17.971	31.535	24.254	23.136
0.000334	18.857	<i>15.706</i>	14.795	24.248	19.028	18.255
0.000546	15.168	12.664	11.921	18.813	14.542	14.470
0.000884	11.970	10.138	9.688	14.605	11.832	11.537
0.001425	9.527	8.329	<i>8.071</i>	11.311	9.549	9.295
0.002289	7.748	6.934	6.761	8.821	7.721	7.556
0.002898	7.005	6.320	6.180	7.819	6.959	6.830
0.005873	5.231	4.850	4.797	5.577	5.170	5.124
0.011878	4.124	3.910	<i>3.881</i>	4.183	3.993	3.981
0.0213460	3.554	3.370	<i>3.335</i>	3.440	3.318	3.306
Fully Developed	2.936	2.820	2.789	2.510	2.430	2.408

Table A21 $Nu_{T,x}$ and $Nu_{H2,x}$ for different power law indices and different axial distances, Re=500 and Pr=10: equilateral triangular duct ($\alpha=60^{\circ}$).

x*		Nu _{T,x}			Nu _{H2,x}		
	n=0.50	n=1.00	n=1.25	n=0.50	n=1.00	n=1.25	
0.000201	24.181	16.639	15.148	29.576	21.930	20.704	
0.000334	19.122	14.038	12.874	21.997	16.856	16.211	
0.000546	14.855	11.484	10.702	16.513	13.116	12.719	
0.000884	11.390	9.473	8.996	12.355	10.236	10.008	
0.001425	9.084	7.925	7.643	9.364	8.094	7.987	
0.002289	7.449	6.679	6.501	7.261	6.502	6.459	
0.002898	6.767	6.125	5.979	6.443	5.855	5.828	
0.005873	5.095	4.732	4.669	4.619	4.353	4.344	
0.011878	4.005	<i>3.813</i>	3.794	3.493	3.388	3.363	
0.0213460	3.442	3.294	3.271	2.853	2.815	2.784	
Fully Developed	2.594	2.503	2.478	1.951	1.896	1.880	

Table A22 $Nu_{T,x}$ and $Nu_{H2,x}$ for different power law indices and different axial distances, Re=500 and Pr=10: right isosceles triangular duct ($\alpha=90^{\circ}$).

x.		Nu _{T,x}			Nu _{H2,x}		
_	n=0.50	n=1.00	n=1.25	n=0.50	n=1.00	n=1.25	
0.000201	23.841	16.454	14.912	27.995	20.657	19.067	
0.000334	18.879	13.842	12.706	20.296	15.461	14.566	
0.000546	14.664	11.386	10.617	14.756	11.849	11.313	
0.000884	11.331	9.405	8.943	10.830	9.184	8.866	
0.001425	9.017	7.865	7.586	8.077	7.187	7.027	
0.002289	7.363	6.601	6.424	6.158	5.697	5.633	
0.002898	6.676	6.044	5.903	5.417	5.094	5.060	
0.005873	5.013	4.663	4.607	3.780	3.701	<i>3.721</i>	
0.011878	3.910	<i>3.731</i>	3.701	2.755	2.781	2.825	
0.0213460	3.328	3.202	<i>3.178</i>	2.207	2.260	2.299	
Fully Developed	2.409	2.350	2.335	1.370	1.351	1.344	

Table A23 $Nu_{T,x}$ and $Nu_{H2,x}$ for different power law indices and different axial distances, Re=500 and Pr=10: cross-shaped duct ($\lambda=0.25$).

x'		Nu _{T,x}			Nu _{H2,x}		
	n=0.50	n=1.00	n=1.25	n=0.50	n=1.00	n=1.25	
0.000201	25.668	18.394	16.861	30.623	22.860	21.241	
0.000334	18.106	13.503	12.562	22.564	17.397	16.287	
0.000546	12.530	10.569	10.086	16.579	13.510	12.779	
0.000884	9.817	8.774	8.474	12.639	10.786	10.312	
0.001425	<i>8.153</i>	7.362	7.152	10.348	8.821	8.505	
0.002289	6.779	6.180	6.033	8.194	7.329	7.110	
0.002898	6.187	5.672	5.553	7.445	6.710	6.528	
0.005873	4.778	4.471	4.415	5.706	5.249	5.150	
0.011878	3.874	3.662	3.622	4.550	4.254	4.193	
0.0213460	3.377	3.184	3.141	3.910	3.674	3.621	
Fully Developed	2.883	2.677	2.628	3.170	2.956	2.903	

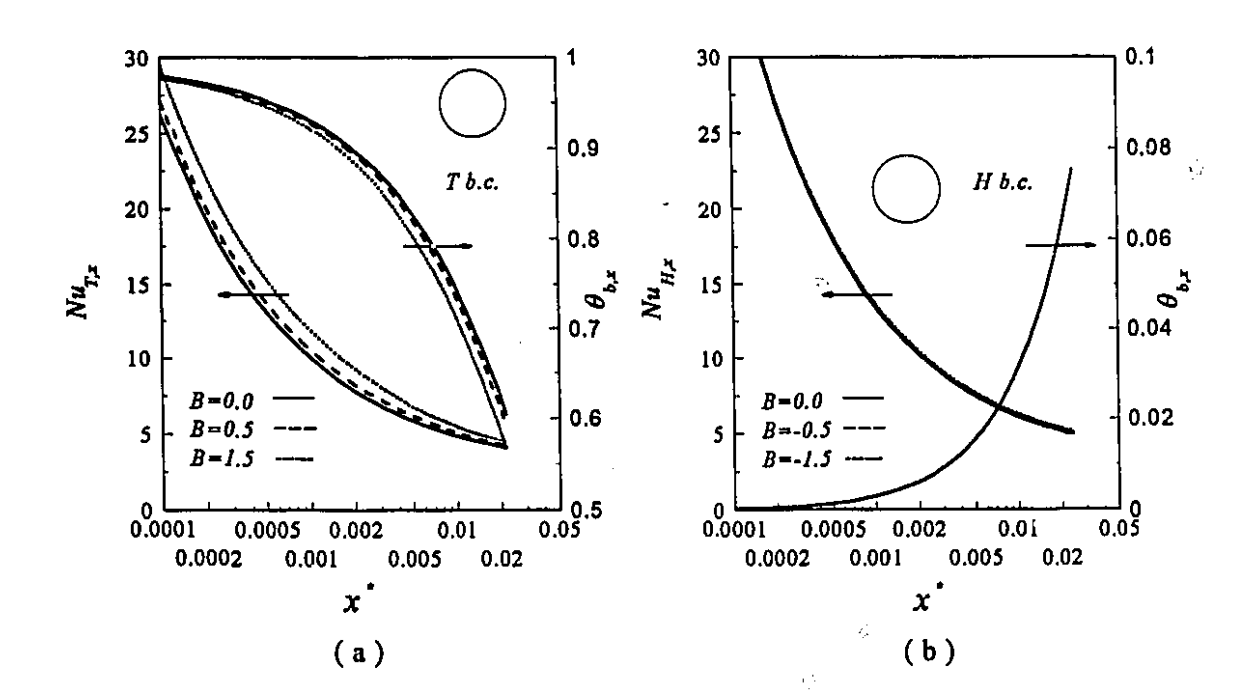
Table A24 $Nu_{T,x}$ and $Nu_{H2,x}$ for different power law indices and different axial distances, Re=500 and Pr=10: cross-shaped duct ($\lambda=0.5$).

x.	Nu _{T,x}			Nu _{H2,x}		
	n=0.50	n=1.00	n=1.25	n=0.50	n=1.00	n=1.25
0.000201	24.364	18.738	17.367	30.140	23.411	21.935
0.000334	<i>18.718</i>	14.537	13.564	22.973	18.097	16.941
0.000546	13.883	11.491	10.844	17.333	14.059	13.222
0.000884	10.779	9.308	<i>8.916</i>	13.219	11.063	10.513
0.001425	8.696	7.676	7.445	10.297	8.856	8.512
0.002289	7.097	6.383	6.226	8.156	7.197	6.978
0.002898	6.413	5.810	5.679	7.297	6.516	6.339
0.005873	4.744	4.404	4.347	5.348	4.923	4.837
0.011878	3.683	3.498	3.475	4.112	3.875	3.837
0.0213460	3.135	2.987	2.960	3.449	3.282	3.254
Fully Developed	2.508	2.338	2.300	2.598	2.443	2.413

Appendix B

B.1 Effect of temperature dependent viscosity on Nusselt number for n=1.0

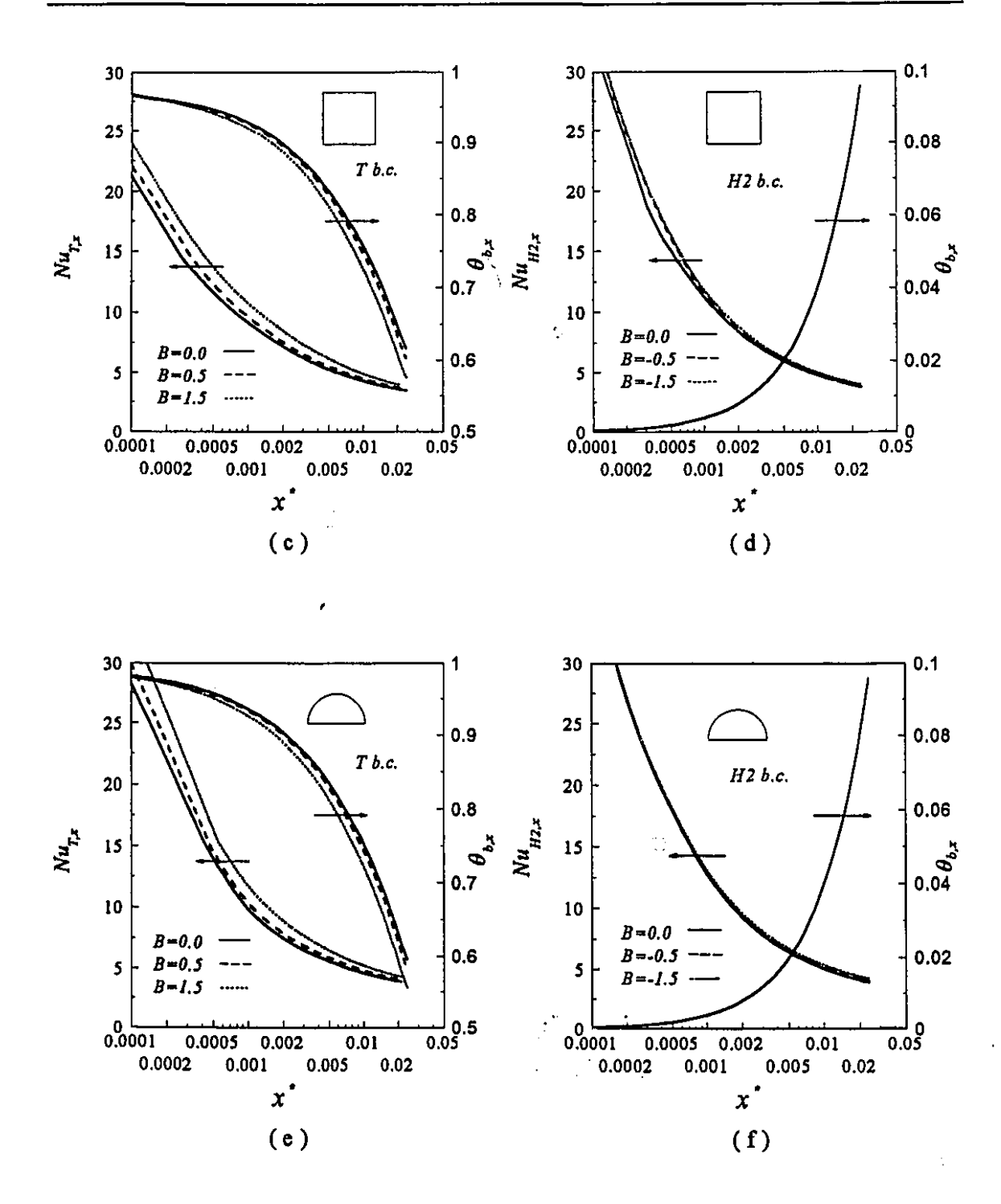
1/2



 $\frac{I_i}{\Pi}$

ă.

1.



 $\tilde{\mathcal{Z}}_{\ell}$

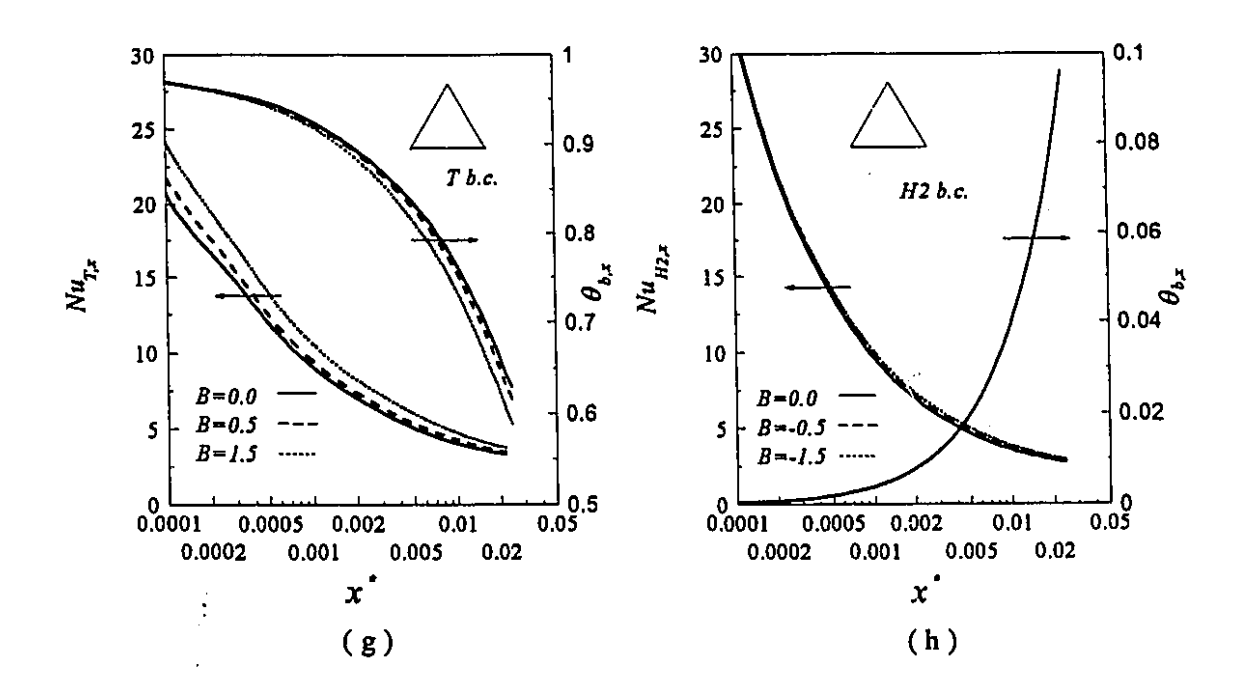
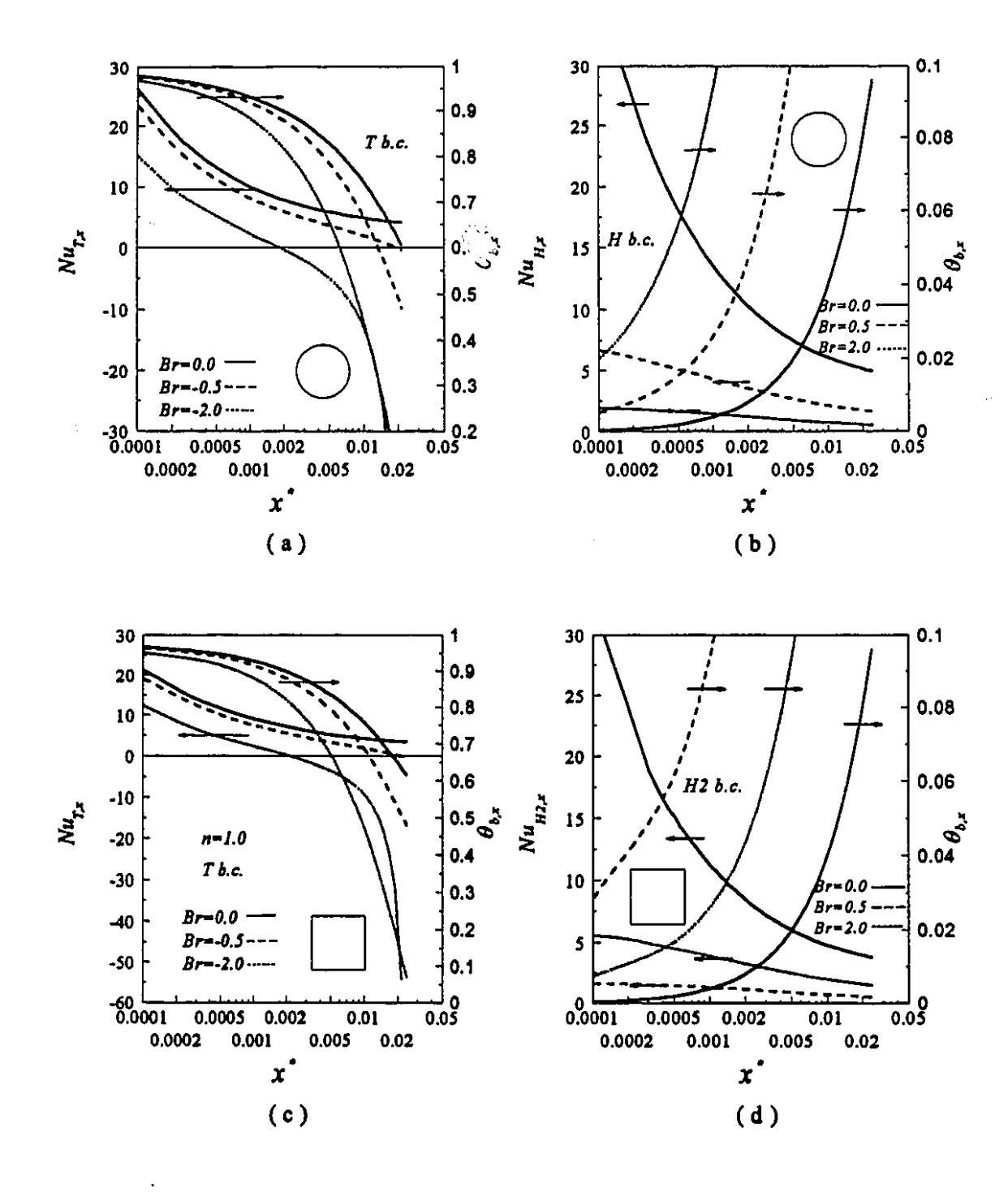


Figure B1 (a - h) Effect of temperature-dependent viscosity on Nusselt number and dimensionless bulk temperature, n=1.0, Re=500, Pr=10.

Ġ

 $\epsilon_{\rm s}^{\rm s}$

B.2 Effect of viscous dissipation on Nusselt number for n=1.0



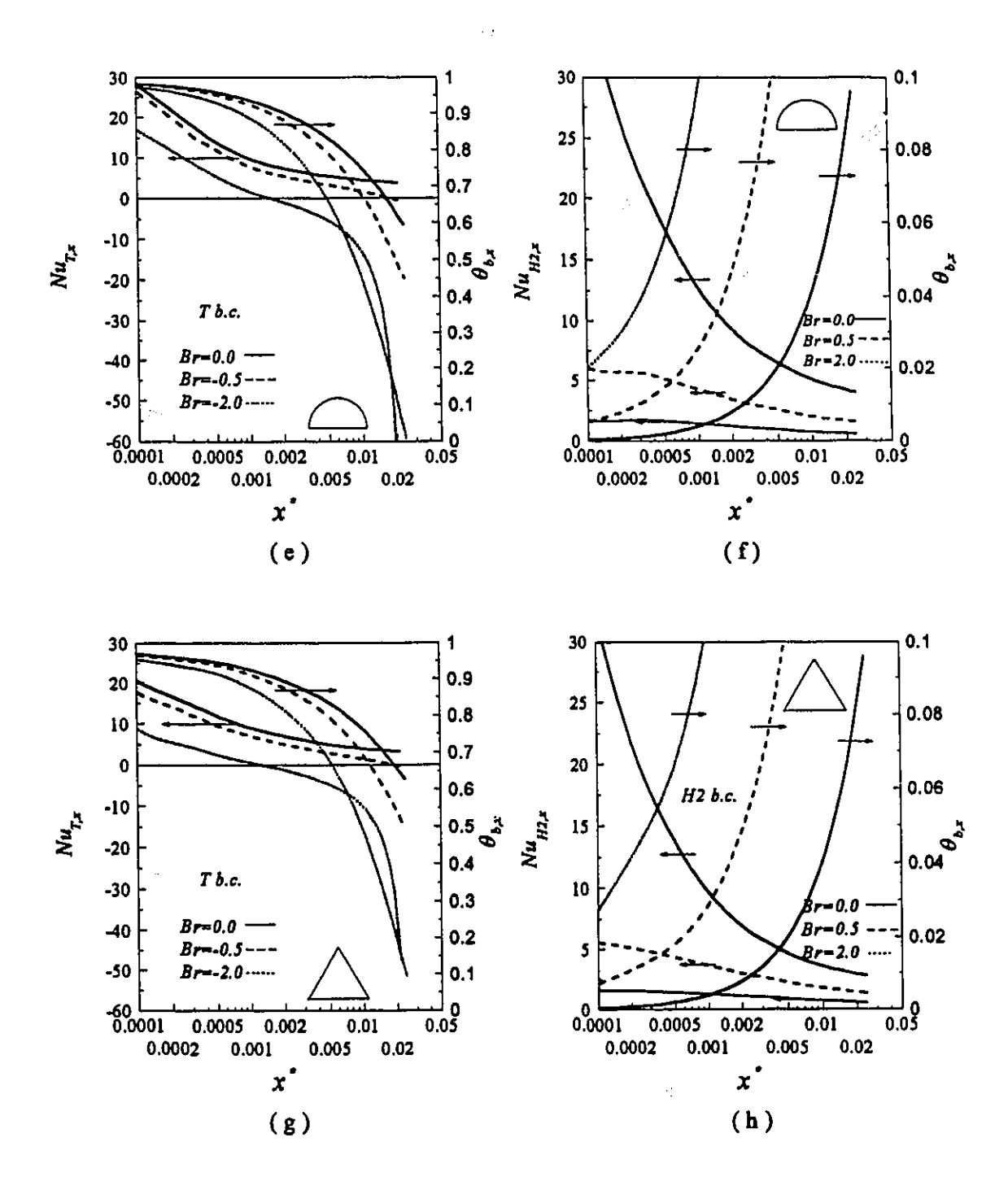
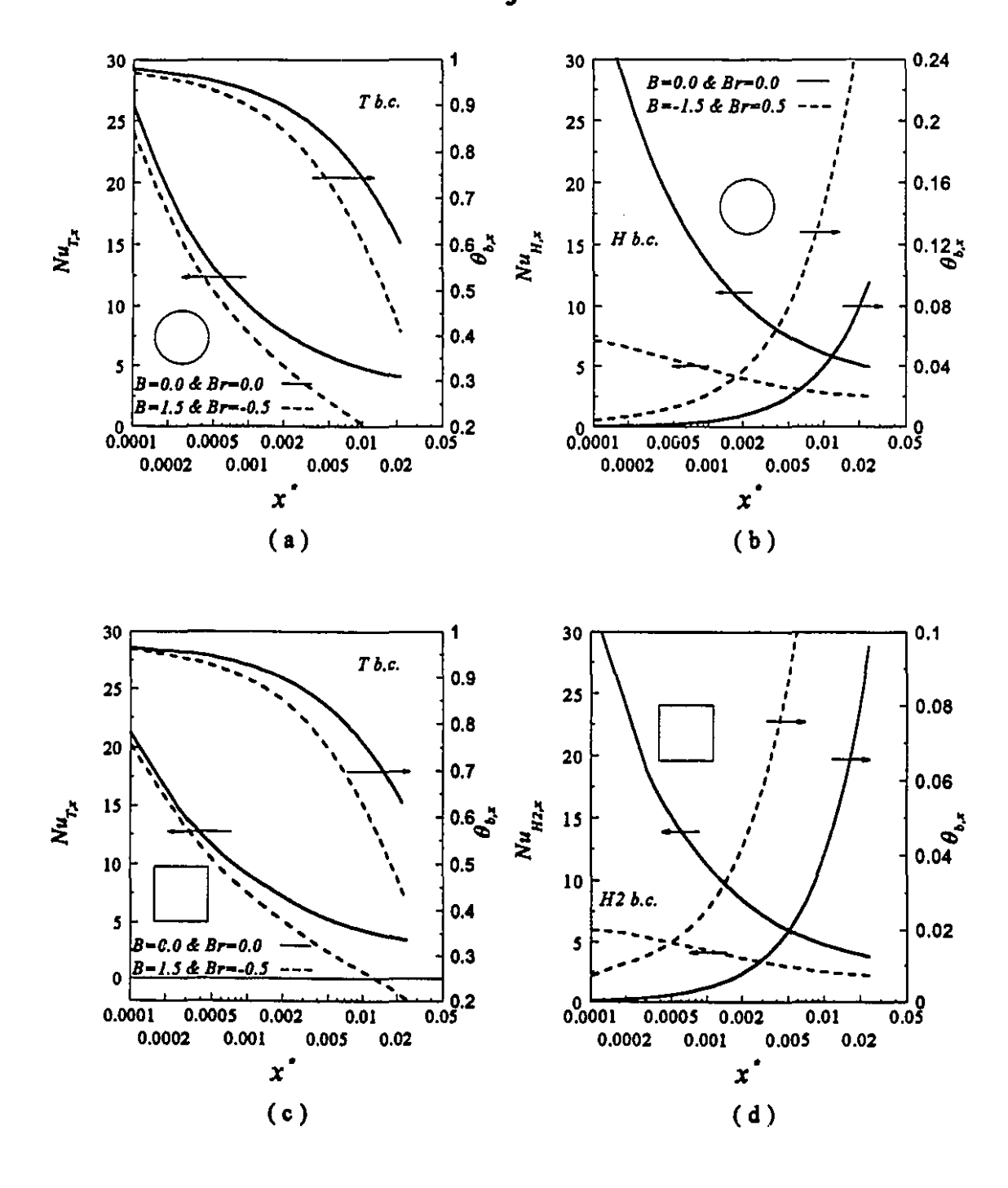


Figure B2 (a - h) Effect of viscous dissipation on Nusselt number and dimensionless bulk temperature, n=1.0, Re=500, Pr=10.

B.3 Simultaneous effects of temperaturedependent viscosity and viscous dissipation on Nusselt number for n=1.0



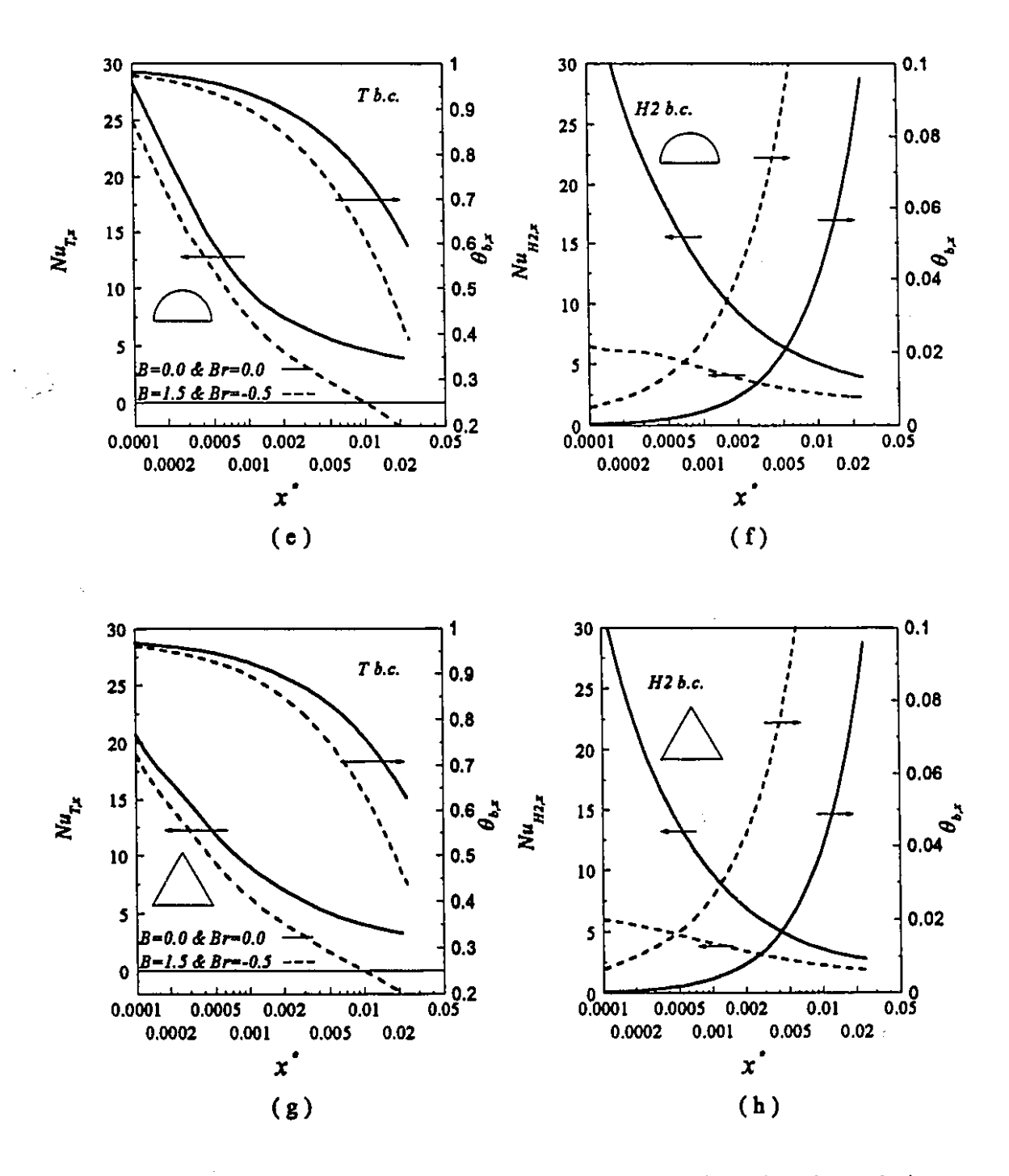
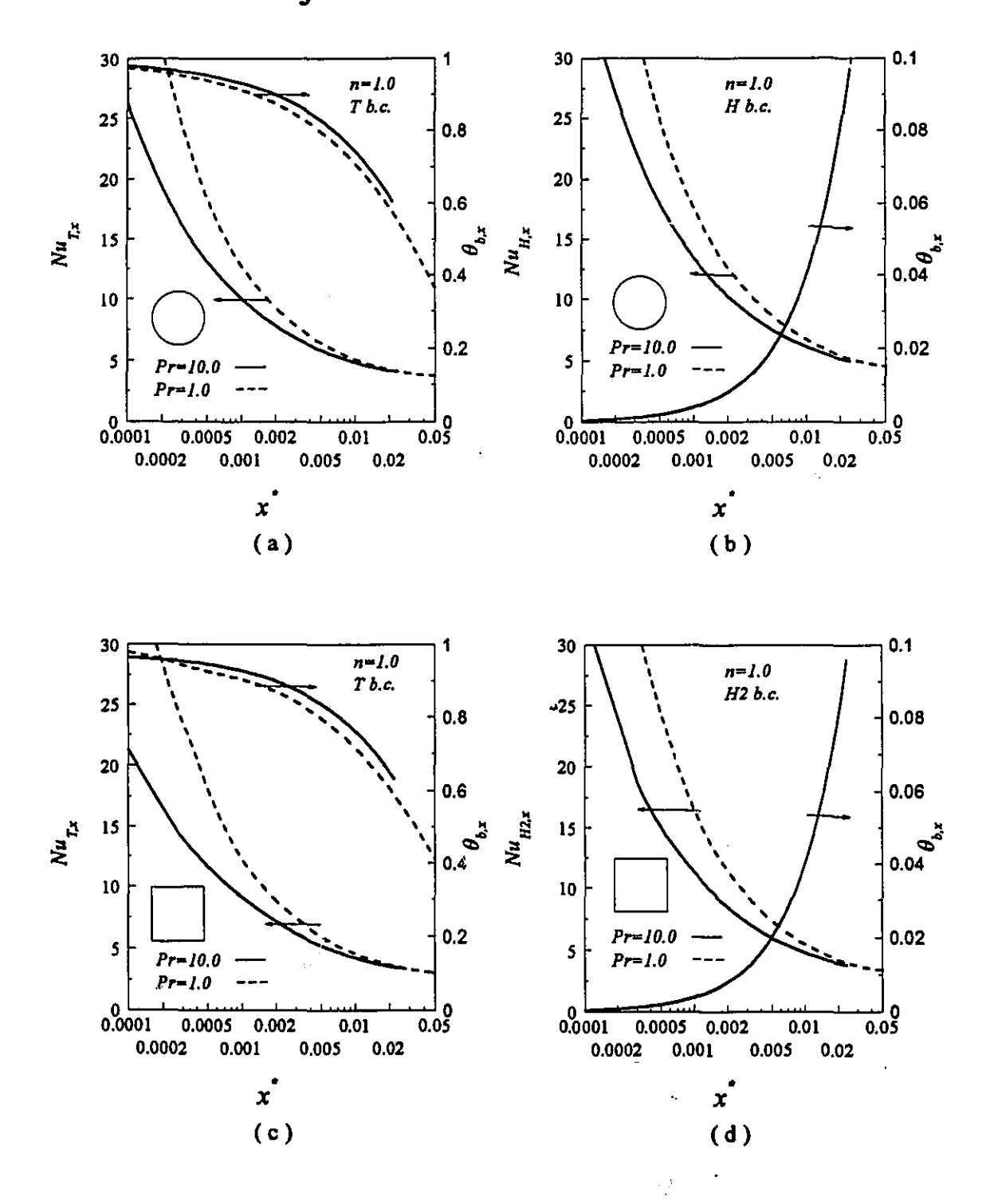


Figure B3 (a - h) simultaneous effects of temperature-dependent viscosity and viscous dissipation on Nusselt number and dimensionless bulk temperature, n=1.0, Re=500, Pr=10.

B.4 Effect of Prandtl number on Nusselt number for n=1.0



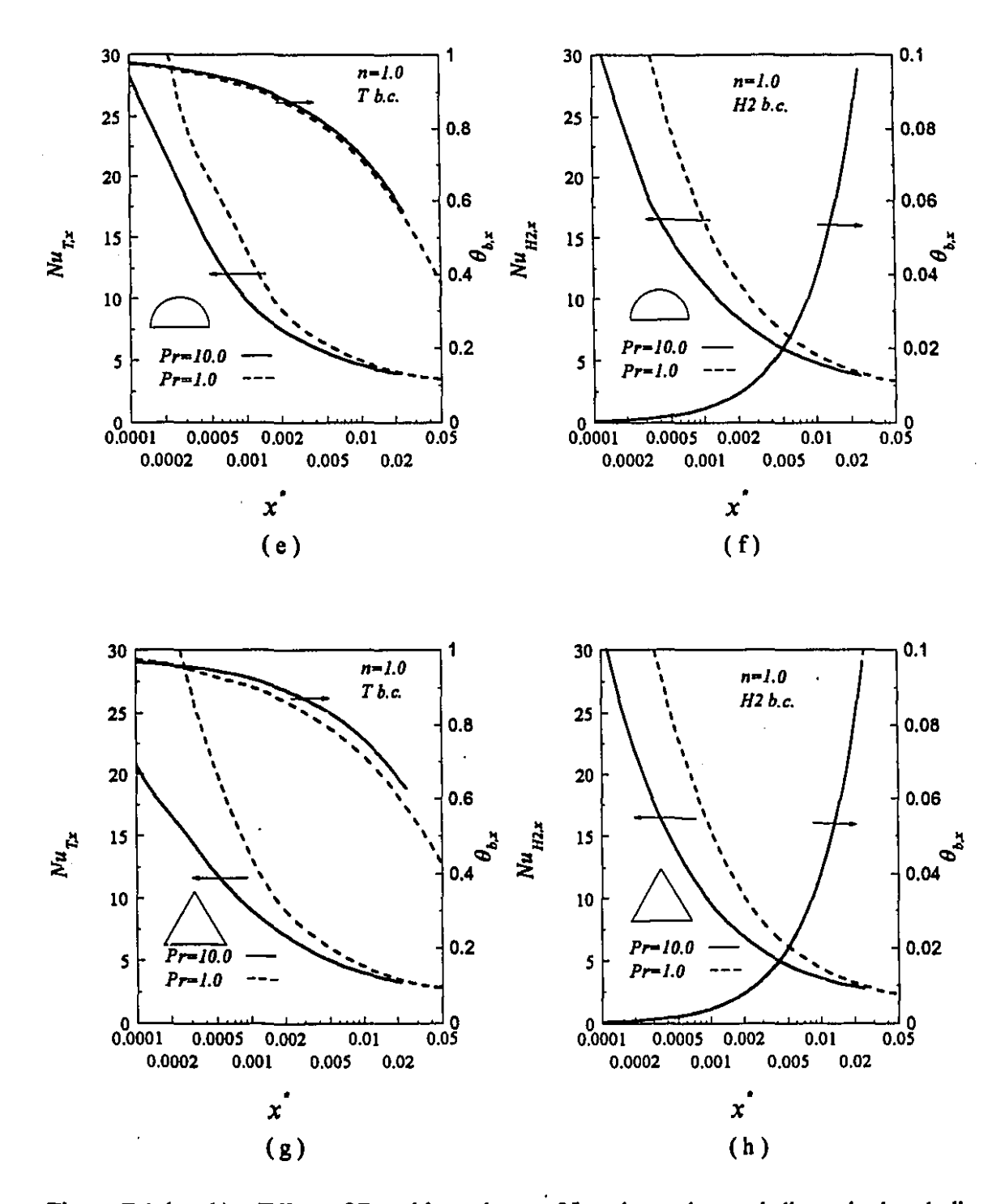


Figure B4 (a - h) Effect of Prandti number on Nusselt number and dimensionless bulk temperature for various geometries, n=1.0, Re=500, Pr=10.

B.5 Effects of temperature-dependent viscosity and viscous dissipation on flow and heat transfer characteristics.

Table B1 f_{app} Re and U_{max} for T and H boundary conditions and for Re=500, Pr=10 and different values of B: circular tube.

		f _{app} Re				U_{max}			
<i>x</i> ⁺	n=0	0.50	n=]	1.00	n=(0.50	n=	1.00	
	B=1.5 T B.C.	B=1.5 HB.C.	B=1.5 T B.C.	B=1.5 H B.C.	B=1.5 T.B.C.	B=-1.5 H B.C.	B=1.5 T B.C.	B=1.5 H B.C.	
0.00201	30.188	23.568	129.660		1.107	1.084	1.296	1.191	
0.00334	26.287	20.506	102.019	64.189	1.144	1.132	1.422	1.277	
0.00546	22.810	17.637	<i>81.708</i>	51.233	1.173	1.192	1.527	1.378	
0.00884	19.886	15.073	66.775	41.402	1.191	1.260	1.577	1.503	
0.01425	17.519	12.852	55.955	33.925	1.196	1.333	1.578	1.654	
0.02289	15.640	10.974	48.185	28.256	1.197	1.409	1.558	1.799	
0.02898	14.847	10.160	45.110	25.975	1.199	1.445	1.549	1.857	
0.05873	12.868	8.183	37.894	20.948	1.220	1.523	1.539	1.942	
0.11878	11.303	6.815	32.495	18.048	1.261	1.534	1.558	1.942	
0.21346	10.225	6.013	28.841	16.606	1.310	1.514	1.601	1.931	

Table B2 f_{app} Re and U_{max} for T and H2 boundary conditions and for Re=500, Pr=10 and different values of B: square duct.

		f_{epp}	Re		U_{max}			
x ⁺	n=(0.50	n=1	.00	n=0.50		n=1.00	
	B=1.5	B =-1.5	B=1.5	B=-1.5	B=1.5	B=-1.5	B=1.5	B =-1.5
	T.B.C.	H2 B.C.	TRC	H2 B.C.	TB.C.	H2 B.C.	TB.C.	H2 B.C.
0.00201	53.135	35.126	150.146	99.198	1.100	1.075	1.266	1.184
0.00334	41.453	27.693	114.399	74.979	1.148	1.124	1.391	1.271
0.00546	33.259	22.316	88.852	57.816	1.189	1.187	1.51 <i>7</i>	1.366
0.00884	27.243	18.054	70.432	45.190	1.224	1.260	1.610	1.480
0.01425	22.754	14.720	57.130	35.814	1.243	1.340	1.647	1.624
0.02289	19.412	12.122	47.656	28.854	1.250	1.427	1.641	1.783
0.02898	18.077	11.039	44.006	26.070	1.253	1.471	1.632	1.855
0.05873	15.012	8.469	35.899	19.800	1.270	1.580	1.614	1.980
0.11878	12.844	6.714	30.308	<i>15.901</i>	1.310	1.615	1.626	1.973
0.21346	11.445	5.695	26.679	<i>13.771</i>	1.361	1.592	1.663	1.935

Table B3 f_{app} Re and U_{max} for T and H2 boundary conditions and for Re=500, Pr=10 and different values of B: semi-circular duct.

		f _{epp} Re				Umax			
x ⁺	n=(0.50	n=]	1.00	n=(0.50	n=	1.00	
	B=1.5	B=1.5	B=1.5	B=1.5	B=1.5	B=-1.5	B=1.5	B=1.5	
	TBC.	H2 B.C.	TB.C.	H2B.C.	TB.C.	H2 B.C.	TB.C.	H2 B.C.	
0.00201	30.833	24.402	136.799	<i>85.823</i>	1.102	1.091	1.294	1.190	
0.00334	26.822	20.746	107.495	<i>67.330</i>	1.145	1.128	1.418	1.277	
0.00546	23.412	17.951	<i>85.762</i>	53.108	1.183	1.190	1.522	1.379	
0.00884	20.462	15.540	69.647	42.422	1.215	1.263	1.595	1.504	
0.01425	17.927	13.303	57.884	34.367	1.236	1.342	1.628	1.643	
0.02289	15.836	11.320	49.353	28.293	1.249	1.423	1.628	1.777	
0.02898	14.950	10.453	45.985	25.852	1.254	1.462	1.622	1.835	
0.05873	12.803	8.342	38.260	20.391	1.274	1.561	1.610	1.944	
0.11878	11.183	6.857	<i>32.701</i>	16.968	1.313	1.603	1.622	1.945	
0.21346	10.089	5,968	29.023	15.027	1.363	1.583	1.658	1.905	

Table B4 f_{app} Re and U_{max} for T and H2 boundary conditions and for Re=500, Pr=10 and different values of B: equilateral triangular duct.

		f_{epp}	,Re		U_{max}			
x ⁺	n=	0.50	n=i	1.00	n=	0.50	n=.	1.00
	B=1.5	B=-1.5	B=1.5	B=-1.5	B=1.5	B=-1.5	B=1.5	B=-1.5
	TB.C.	H2 B.C.	TB.C.	H2 B.C.	TBC.	H2 B.C.	TB.C.	H2 B.C.
0.00201	60.508	48.425	173.211	117.616	1.093	<i>1.068</i>	1.245	1.172
0.00334	44.317	35.500	128.679	86.323	1.145	1.115	1.375	<i>1.263</i>
0.00546	33.819	27.065	97.747	64.688	1.194	1.179	1.512	1.359
0.00884	26.594	21.096	75.885	49.498	1.240	1.255	1.629	1.477
0.01425	21.430	16.660	60.316	38.542	1.276	1.339	<i>1.701</i>	1.626
0.02289	17.667	13.345	49.195	30.528	1.299	1.432	1.722	1.793
0.02898	16.183	12.010	44.909	27.363	1.305	1.480	1.719	1.875
0.05873	12.889	8. <i>936</i>	35.619	20.323	1.322	1.615	1.700	2.053
0.11878	10.737	6.866	29.600	15.882	1.359	1.685	1.704	2.082
0.21346	9.420	5.657	25.851	13.438	1.412	1.664	1.739	2.031

Table B5 $Nu_{T,x}$ and $Nu_{H,x}$ for Re=500, Pr=10 and specific values of B and Br: circular tube.

		Nu	I _{T,x}		Nu _{H,x}			
x.	n=(0.50	n=.	1.00	n=(0.50	n=)	1.00
ļ	B=1.5	Br=-2.0	B=1.5	Br=-2.0	B=-1.5	Br=2.0	B=-1.5	Br=2.0
	Br=0.0	B=0.0	Br=0.0	B=0.0	Br=0.0	B=0.0	Br=0.0	B=0.0
0.000201	29.478	20.385	22.128	9.861	34.671	4.548	27.220	1.831
0.000334	23.304	14.870	17.964	7.003	27.063	3.944	21.622	1.722
0.000546	18.629	10.954	14.852	4.776	21.351	3.410	17.460	1.600
0.000884	15.144	8. <i>079</i>	12.418	2.764	17.084	2.948	14.280	1.456
0.001425	12.448	<i>5.782</i>	10.469	0.923	13.854	2.536	11.796	1.303
0.002289	10.309	3.908	8.871	-0.919	11.393	2.171	9.855	1.150
0.002898	9.405	3.074	8.174	-1.935	10.392	<i>2.007</i>	9.051	1.075
0.005873	7.232	0.654	6.437	-6.167	8.094	1.586	7.169	0.861
0.011878	5.741	-2.430	5.183	-16.869	6.601	1.263	5.886	0.679
0.021492	4.953	<i>-7.733</i>	4.495	-128.326	5.789	1.067	5,140	0.567

Table B6 $Nu_{T,x}$ and $Nu_{H2,x}$ for Re=500, Pr=10 and specific values of B and Br: square duct.

	Nu _{T,x}			Nu _{H2,x}				
x.	n=(0.50	n=]	1.00	n=(0.50	n=i	1.00
	B=1.5	Br=-2.0	B=1.5	Br=-2.0	B=-1.5	Br=2.0	B=-1.5	Br=2.0
	Br=0.0	B=0.0	Br=0.0	B=0.0	Br=0.0	_B=0.0	Br=0.0	B=0.0_
0.000201	25.584	19.610	19.238	8.479	32.532	4.005	24.961	1.562
0.000334	21.297	14.607	15.967	6.048	25.173	3.525	19.633	1.492
0.000546	17.310	10.488	13.320	4.283	19.350	3.081	<i>15.533</i>	1.410
0.000884	14.033	7.720	11.233	2.818	15.043	2.683	12.456	1.322
0.001425	11.510	<i>5.696</i>	9.556	1.372	11.914	2.335	10.140	1.220
0.002289	9.545	3.975	<i>8.132</i>	-0.249	9.588	<i>2.023</i>	<i>8.353</i>	1.100
0.002898	8.702	3.173	7.489	-1.136	8.649	<i>1.878</i>	7.611	1.037
0.005873	6.609	0.935	5.840	-4.485	6.520	1.488	5.888	0.847
0.011878	5.142	-1.567	4.635	-11.994	5.171	1.177	4.747	0.674
0.021492	4.300	-5.365	3.908	-52.71 <i>§</i>	4.445	0.978	4.086	0.553

Table B7 $Nu_{T,x}$ and $Nu_{H2,x}$ for Re=500, Pr=10 and specific values of B and Br: semi-circular duct.

		Nu	T,×		Nu _{H2,x}			
x'	n=(0.50	n=]	1.00	n=(0.50	n=j	1.00
	B=1.5	Br=-2.0	B=1.5	Br=-2.0	B=-1.5	Br=2.0	B=-1.5	Br=2.0
	Br=0.0	B=0.0	Br=0.0	B=0.0	Br=0.0	B=0.0	Br=0.0	B=0.0
0.000201	31.756	21.032	25.878	11.907	35.062	4.31.3	27.268	1.681
0.000334	26.230	<i>15.420</i>	20.542	<i>8.242</i>	27.305	<i>3.799</i>	21.665	1.720
0.000546	20.632	11.856	15.387	4.942	21.584	3.397	17.411	1.604
0.000884	15.430	7.930	12.372	2.166	16.873	<i>2.950</i>	13.873	1.434
0.001425	12.241	5.365	10.104	0.212	13.162	2.502	11.119	1.275
0.002289	9.902	3.443	8.475	-1.507	10.463	2.115	9.065	1.126
0.002898	8.994	2.664	7.810	-2.480	9.410	1.954	8.242	1.053
0.005873	6.915	0.389	6.174	-6.578	7.039	1.533	6.356	0.848
0.011878	5.487	-2.475	4.982	-16.791	5.512	1.212	5.091	0.676
0.021492	4.703	-7.241	4.301	-114.663	4.697	1.016	4.354	0.567

: . .

,

Table B8 $Nu_{T,x}$ and $Nu_{H2,x}$ for Re=500, Pr=10 and specific values of B and Br: equilateral triangular duct.

		Nu	T,x		Nu _{H2,x}			
x.	n=(0.50	n=	1.00	n=0	0.50	n=1	1.00
	B=1.5	Br=-2.0	B=1.5	Br=-2.0	B=-1.5	Br=2.0	B=-1.5	Br=2.0
ļ	Br=0.0	B=0.0	Br=0.0	B=0.0	Br=0.0	B=0.0	Br=0.0	B=0.0
0.000201	26.963	19.502	19.508	5.493	29.994	3.952	22.360	1.541
0.000334	22.531	14.102	16.375	3.906	22.540	<i>3.430</i>	17.255	1.486
0.000546	18.220	9.961	13.403	2.172	17.081	<i>2.975</i>	13.517	1.392
0.000884	14.407	6.739	11.037	0.889	12.951	2.571	10.641	1.290
0.001425	11.456	4.600	9.252	-0.292	9.954	2.212	8.48 5	1.187
0.002289	9.308	2.992	7.853	-1.621	7.829	1.905	6.872	<i>1.078</i>
0.002898	8.451	2.264	7.240	-2.410	6.994	1.767	6.213	1.020
0.005873	6.387	0.130	5.632	<i>-5.601</i>	5.098	1.397	4.652	0.838
0.011878	4.911	-2.285	4.424	-12.699	3.864	1.112	3.594	0.674
0.021492	4.069	-5.876	3.708	-47.569	3,227	0.916	3.005	0.556

B.6 Nusselt number for Re=500 and Pr=1.0

Table B9 $Nu_{T,x}$ and $Nu_{H,x}$ for Pr=1.0: circular tube.

x*	Nu	t _{T,x}	Nu	H,x
	n=0.50	n=1.00	n=0.50	n=1.00
0.00201	11.055	9.275	15.612	12.667
0.00334	8. <i>735</i>	7.511	12.284	10.149
0.00546	7.114	6.240	9.881	8.318
0.00884	5.947	5.293	8.121	6.958
0.01425	5.114	4.597	6.835	5.946
0.02289	4.550	4.114	5.918	<i>5.215</i> =
0.02898	4.358	3.948	5.576	4.943
0.05873	4.074	3.725	4.951	4.467
0.11878	4.041	<i>3.659</i>	4.761	4.363
0.21346	4.232	3.659	4.744	4.363

Table B10 $Nu_{T,x}$ and $Nu_{H2,x}$ for Pr=1.0: square duct.

x.	Ni	$Nu_{T,x}$		H2,x
	n=0.50	n=1.00	n=0.50	n=1.00
0.00201	10.931	8.876	14.842	11.387
0.00334	8.439	7.144	11.266	8.903
0.00546	6.683	5.790	8.695	7.081
0.00884	5.471	4.809	6.877	5.742
0.01425	4.600	4.097	5.572	4.766
0.02289	3.968	3.567	4.639	4.060
0.02898	3.733	3.366	4.286	3.791
0.05873	3.336	3.035	3.606	3.272
0.11878	3.232	2.981	3.354	3.105
0.21346	3.213	2,979	3.308	3.088

Table B11 $Nu_{T,x}$ and $Nu_{H2,x}$ for Pr=1.0: semi-circular duct.

x'	Nu	$t_{T,x}$	Nu	H2,x
	n=0.50	n=1.00	n=0.50	n=1.00
0.00201	11.343	9.118	15.883	12.489
0.00334	8.833	7.275	12.255	9.561
0.00546	7.057	6.077	9.472	7.590
0.00884	5.828	5.163	7.441	6.170
0.01425	4.987	4.475	5.989	5.111
0.02289	4.411	3.981	4.932	4.319
0.02898	4.199	3.799	4.546	4.005
0.05873	3.786	<i>3.458</i>	3.666	3.333
0.11878	3.620	3.356	3.196	3.001
0.21346	3.672	3.425	3.052	2.920

Table B12 $Nu_{T,x}$ and $Nu_{H2,x}$ for Pr=1.0: equilateral triangular duct.

\ x'	Nı	t _{T,x}	Nu	H2,x
	n=0.50	n=1.00	n=0.50	n=1.00
0.00201	11.571	9.008	13.913	10.192
0.00334	8.748	7.182	10.200	7.648
0.00546	6.822	5.818	7.583	5.924
0.00884	5.467	4.750	5.728	4.654
0.01425	4.514	3.971	4.418	<i>3.712</i>
0.02289	3.831	3.410	3.496	<i>3.032</i>
0.02898	3.563	3.188	3.144	2.768
0.05873	3.018	2.731	2.414	2.213
0.11878	2.821	2.595	2.069	1.961
0.21346	2.815	2.617	1.982	1.909

Appendix C

C.1 Mean Nusselt number

Table C1 $Nu_{T,m}$ and $Nu_{H2,m}$ for different power law indices and different axial distances, Re=500 and Pr=10: circular tube.

x.	$Nu_{T,m}$		Nu _{H2,m}	
.]	n=0.50	n=1.00	n=0.50	n=1.00
0.000201	44.187	36.125	63.205	49.339
0.000334	<i>34.7</i> 19	28.575	49.924	<i>39.172</i>
0.000546	27.612	22.972	39.618	31.376
0.000884	<i>22.183</i>	18.678	31.561	25.319
0.001425	17.958	15.305	25.254	20.567
0.002289	14.633	12.633	20.312	16.816
0.002898	13.245	11.511	18.260	15.247
0.005873	9.956	8.837	13.431	11.512
0.011878	7.687	6.963	10.128	8.900
0.0213460	6.417	5.883	8.216	7.344

Table C2 $Nu_{T,m}$ and $Nu_{H2,m}$ for different power law indices and different axial distances, Re=500 and Pr=10: Parallel plates.

x*	N	Nu _{T,m}		H2,m
	n=0.50	n=1.00	n=0.50	n=1.00
0.000201	51.620	37.848	65.244	51.020
0.000334	40.276	30.269	51.937	40.888
0.000546	31.879	24.675	41.560	33.168
0.000884	25.576	20.434	33.482	27.194
0.001425	20.806	17.174	27.199	22.536
0.002289	17.193	14.650	22.328	18.901
0.002898	<i>15.732</i>	13.603	20.323	17.391
0.005873	12.421	11.125	15.687	13.822
0.011878	10.326	9.469	12.631	11.386
0.0213460	9.286	<i>8.629</i>	11003	_10.064

Table C3 $Nu_{T,m}$ and $Nu_{H2,m}$ for different power law indices and different axial distances, Re=500 and Pr=10: square duct.

x*	$Nu_{T,m}$		$Nu_{H2,m}$	
	n=0.50	n=1.00	n=0.50	n=1.00
0.000201	56.068	50.171	65.0.21	50.855
0.000334	43.534	<i>35.271</i>	50.202	39.156
0.000546	32.152	25.886	39.004	30.526
0.000884	24.031	<i>19.797</i>	30.37 0	23.999
0.001425	18.563	15.625	23.724	19.017
0.002289	14.716	12.605	18.624	15.191
0.002898	13.191	11.386	16.539	13.618
0.005873	9.661	8.515	11.716	9.939
0.011878	7.205	6.490	8.0501	7.433
0.0213460	<i>5.790</i>	5.294	6.682	5.976

0

والمعارب

Table C4 $Nu_{T,m}$ and $Nu_{H2,m}$ for different power law indices and different axial distances, Re=500 and Pr=10: rectangular duct (A.R.= 0.5).

x*	Nu _{T,m}		Nu _{H2,m}	
_	n=0.50	n=1.00	n=0.50	n=1.00
0.000201	64.518	38.999	60.401	45.806
0.000334	41.652	31.643	47.488	36.177
0.000546	31.338	25.831	37.222	28.748
0.000884	24.827	20.822	29.262	22.998
0.001425	19.489	16.406	23.118	18.514
0.002289	<i>15.288</i>	<i>13.170</i>	18.356	₌ 14.993
0.002898	13.656	11.894	16.389	13.524
0.005873	9.959	8.911	11.790	10.046
0.011878	7.519	6.871	8.676	7.633
0.0213460	6.136	5.682	6.878	6.197

Table C5 $Nu_{T,m}$ and $Nu_{H2,m}$ for different power law indices and different axial distances, Re=500 and Pr=10: rectangular duct (A.R.=0.2).

x'	$Nu_{T_{im}}$		Nu _{H2,m}	
	n=0.50	n=1.00	n=0.50	n=1.00
0.000201	65.927	53.280	64.920	51.790
0.000334	47.990	<i>35.173</i>	50.681	40.291
0.000546	<i>32.197</i>	25.396	39.891	31.752
0.000884	23.686	20.358	31.335	25.280
0.001425	19.270	17.124	24.812 =	20.334
0.002289	16.087	14.403	19.817	16.545
0.002898	14.674	<i>13.168</i>	17.778	14.993
0.005873	11.113	10.085	13.048	11.351
0.011878	8.647	7.973	9.822	8.817
0.0213460	7.325	<i>6.853</i>	7.931	7.311

Table C6 $Nu_{T,m}$ and $Nu_{H2,m}$ for different power law indices and different axial distances, Re=500 and Pr=10: semi-circular duct.

x.	$Nu_{T,m}$		Nu _{H2,m}	
	n=0.50	n=1.00	n=0.50	n=1.00
0.000201	40.953	31.568	64.500	49.960
0.000334	<i>32.978</i>	25.119	50.788	39.478
0.000546	26.372	20.764	40.262	31.507
0.000884	21.132	17.283	31.968	25,234
0.001425	17.112	14.401	25.300	20.221
0.002289	14.023	12.028	19.977	16.241
0.002898	12.736	11.007	17.760	14.582
0.005873	9.619	8.500	12.580	10.669
0.011878	7.385	6.687	9.090	7.972
0.0213460	6.118	5.635	7.086	6.378

Table C7 $Nu_{T,m}$ and $Nu_{H2,m}$ for different power law indices and different axial distances, Re=500 and Pr=10: quarter-circular duct.

x*	Nu _{T,m}		Nu _{H2,m}	
	n=0.50	n=1.00	n=0.50	n=1.00
0.000201	42.945	34.951	61.085	47.666
0.000334	<i>33.297</i>	27.535	47.841	<i>37.458</i>
0.000546	26.570	22.054	37.644	29.673
0.000884	21.341	17.812	29.716	23.677
0.001425	17.162	14.463	23.519	19.001
0.002289	13.877	11.845	18.648	<i>15.311</i>
0.002898 -	12.524	10.768	16.617	13.766
0.005873	9.351	8.230	11.822	10.088
0.011878	g 7.149	6.453	8.547	7.544
0.0213460	5.912	5.432	6.667	6.045

Table C8 $Nu_{T,m}$ and $Nu_{H2,m}$ for different power law indices and different axial distances, Re=500 and Pr=10: circular sector duct ($\alpha=60^{\circ}$).

x ·	$Nu_{T,m}$		$Nu_{H2,m}$	
	n=0.50	n=1.00	n=0.50	n=1.00
0.000201	44.998	36.036	61.201	46.639
0.000334	<i>34</i> .833	28.083	47.651	36.056
0.000546	27.215	22.102	37.313	28.223
0.000884	21.389	17.407	29.290	22.392
0.001425	16.879	13.385	22.993	17.895
0.002289	13.477	11.294	18.048	14.355
0.002898	12.113	10.247	15.996	12.873
0.005873	8.952	7.778	11.184	9.341
0.011878	6.761	6.045	7.929	6.878
0.0213460	5.527	5.041	6.076	5.427

Table C9 $Nu_{T,m}$ and $Nu_{H2,m}$ for different power law indices and different axial distances, Re=500 and Pr=10: equilateral triangular duct ($\alpha=60^{\circ}$).

x'	, Nu	t _{T,m}	Nu	H2,m
	n=0.50	n=1.00	n=0.50	n=1.00
0.000201	53.062	50.036	69.180	54.302
0.000334	41.820	35.429	51.591	40.158
0.000546	31.620	26.338	38.838	30.245
0.000884	24.090	20.546	29.370	23.048
0.001425	18.985	16.360	22.260	17.722
0.002289	<i>15.101</i>	13.001	16.939	13.749
0.002898	<i>13.428</i>	11.583	14.811	12.152
0.005873	9.504	8.358	10.016	8.510
0.011878	6.983	6.296	6.930	6.104
0.0213460	· 5.536	5.084	5.244	4.755

Table C10 $Nu_{T,m}$ and $Nu_{H2,m}$ for different power law indices and different axial distances, Re=500 and Pr=10: right triangular duct ($\alpha=90^{\circ}$).

x.	$Nu_{T,m}$		Nu _{H2,m}	
	n=0.50	n=1.00	n=0.50	n=1.00
0.000201	53.235	50.141	65.270	50.988
0.000334	41.692	35.583	48.561	<i>37.630</i>
0.000546	31.614	26.475	36.303	28.179
0.000884	24.151	20.589	27.178	21.333
0.001425	18.952	16.332	20.370	16.289
0.002289	15.011	<i>12.961</i>	15.317	12.536
0.002898	13.348	11.548	13.307	11.031
0.005873	9.454	8.322	8.81 <i>7</i>	7.609
0.011878	6.903	6.227	5.962	5.358
0.0213460	5.444	5.005	4.400	4.084

Table C11 $Nu_{T,m}$ and $Nu_{H2,m}$ for different power law indices and different axial distances, Re=500 and Pr=10: cross shape duct ($\lambda=0.25$).

x.	$Nu_{T,m}$		Nu _{H2,m}	
	n=0.50	n=1.00	n=0.50	n=1.00
0.000201	47.653	42.367	58.150	46.285
0.000334	40.544	32.541	45.309	<i>35.654</i>
0.000546	30.417	23.941	35.106	27.668
0.000884	22.366	18.111	27.124	21.640
0.001425	17.158	14.382	21.059	17.096
0.002289	13.635	11.672	16.507	13.657
0.002898	12.209	10.533	14.675	12.258
0.005873	<i>8.878</i>	7.841	10.495	9.014
0.011878	6.667 ·	6.023	7.729	6.816
0.0213460	5.404	4.953	6.157	<i>5.533</i>

₹.

Table C12 $Nu_{T,m}$ and $Nu_{H2,m}$ for different power law indices and different axial distances, Re=500 and Pr=10: cross shape duct ($\lambda=0.5$).

x*	Nu	¹ T,m	Nu,	H2,m
	n=0.50	n=1.00	n=0.50	n=1.00
0.000201	47.390	40.190	58.101	47.280
0.000334	38.070	28.682	45.289	36.515
0.000546	27.525	21.246	35.347	28.442
0.000884	20.671	17.084	27.537	22.273
0.001425	16.794	14.346	21.469	17.542
0.002289	13.921	11.990	16.795	13.912
0.002898	12.614	10.900	14.882	12.425
0.005873	9.205	8.085	10.455	8.958
0.011878	6.724	6.041	7.501	6.605
0.0213460	5.318	4.864	5.830	5.245

Appendix D

D.1 Resistance variation with temperature

The electrical resistance, \overline{R}_T , of the foil at a given temperature is a function of its resistivity and physical dimensions.

$$\overline{R}_{T} = \rho_{T} \frac{\overline{L}_{T}}{A_{T}} \tag{D.1}$$

where ρ_T is electrical resistivity, A_T is the cross-sectional area of the foil, and \overline{L}_T is its length. Each of these dimensional factors is a function of temperature as is the resistivity.

The change in resistance of the test section with temperature is defined as its temperature coefficient of resistance.

$$\alpha_R' = \frac{\overline{R}_T - \overline{R}_R}{\overline{R}_R (T - T_R)} = \frac{\Delta \overline{R}}{\overline{R}_R \Delta T}$$
 (D.2)

Now we consider the effects of a change in temperature, from T_R to T, on the dimensions of the foil and consequently on its resistance. These effects may be evaluated by examining the temperature dependence of the dimensional factors in Eq. (D.1).

$$\vec{R}_T = \frac{\rho_T \vec{L}_R \left[1 + \alpha_L (T - T_R) \right]}{a''b'' \left[1 + \alpha_L (T - T_R) \right]^2}$$
 (D.3)

where a'' and b'' are the width and thickness of foil, respectively.

$$\overline{R}_{T} = \rho_{T} \frac{\overline{L}_{R}}{a''b''} \frac{1}{\left[1 + \alpha_{L}(T - T_{R})\right]}$$
 (D.4)

Yi

The resistance variation in the worst case with temperature difference about $50^{\circ}C$ for stainless steel foil (Goodfellow Co., FE080240) can be shown to be:

$$\overline{R}_{T} = \rho_{T} \frac{\overline{L}_{R}}{a''b''} \frac{1}{\left[1 + 11.1 \times 10^{-6} \times 50\right]} = \rho_{T} \frac{\overline{L}_{R}}{a''b''} (0.999)$$
 (D.5)

Thus the influence of dimensional changes can be considered negligible.

$$\alpha_{R}' = \frac{\overline{R}_{T} - \overline{R}_{R}}{\overline{R}_{R}(T - T_{R})} = \frac{\Delta \overline{R}}{\overline{R}_{R} \Delta T} = \frac{\rho_{T} \frac{\overline{L}_{R}}{a''b''} - \rho_{R} \frac{\overline{L}_{R}}{a''b''}}{\rho_{R} \frac{\overline{L}_{R}}{a''b''}} = \frac{\rho_{T} - \rho_{R}}{\rho_{R} \Delta T} = \frac{\Delta \rho}{\rho_{R} \Delta T} = \alpha_{\rho}' \quad (D.6)$$

The temperature coefficient of resistance very closely approximates the temperature coefficient of electrical resistivity. α'_{ρ} for stainless steel foil is $0.0001K^{-1}$; therefore the effect of temperature on electrical resistance is treated as negligible.

D.2 Local bottom plate Nusselt number

For the case of constant heat flux (both axially and peripherally) on the bottom plate, the local heat transfer coefficient is expressed by:

$$h_x = \frac{q''}{Tw_x - T_{b,x}} \tag{D.7}$$

where q'' is the rate of heat flux per unit surface area on the bottom plate and Tw_x and $T_{b,x}$ are the averaged wall temperature and bulk temperature, respectively, at axial location x. Equation D.7 can be rearranged in the following form:

$$h_{x} = \frac{q''}{(Tw_{x} - T_{e}) - (T_{b,x} - T_{e})}$$
 (D.8)

where T_e is the inlet fluid temperature. T_e and Tw_x are measured using thermocouples, and difference $(T_{b,x} - T_e)$ can be calculated from an overall energy balance over the test section. Assuming the wall is well insulated,

$$T_{b,x} - T_{a} = \frac{\overline{Q}_{x}}{mC_{n}} \tag{D.9}$$

where \overline{Q}_x is the heat supplied from the beginning of the heating up to the axial position x.

ij

Due to the uniform thickness of the foil and also small temperature-coefficient of resistance it can be assumed the resistance varies linearly with axial distance since the current is constant.

$$\overline{Q}_{x} = \frac{\overline{Q}x}{\overline{I}.} \tag{D.10}$$

Here \overline{L} is the total length of the foil and \overline{Q} is the amount of energy generated electrically within the duct. The bottom plate Nusselt number was calculated as follows:

$$Nu_{b,x} = \frac{h_x D_h}{K} = \frac{q'' D_h}{K(Tw_x - T_{b,x})}$$
 (D.11)

الله الأست الأست

D.3 Physical and rheological properties of Carbopol solution

As was mentioned in Chapter 7, the physical properties (density, heat capacity and thermal conductivity) of Carbopol 934 solution can be approximated by those for distilled water.

Rheological properties of Carbopol 934 solution (0.5 % by weight) with two different partial neutralization levels were measured at four temperatures. For both solutions and all temperatures straight lines were fitted to the flow curve data with R^2 =0.999 in log-log coordinates. The consistency index is the intercept while the power law index is the slope of the fitted straight line.

Table D1 Consistency index of Carbopol 934 solutions (n=0.727 for solution # 1 and n=0.623 for solution # 2).

Temperature °C	Solution # 1 k grsec ⁿ⁻² /cm	Solution # 2 k grsec ⁿ⁻² /cm
20	0.769	2.728
25	0.754	2.667
35	0.733	2.576
50	0.694	2.443

 $\mathcal{E}_{\mathcal{F}}^{(i)}$

D.4 Error analysis

Suppose the measurements of independent variables x_1 , x_2 ,, x_n are made in the laboratory and the relative uncertainty of each measured quantity is estimated as u_i . If the objective is to calculate some result \overline{Y} (here Nusselt number), we want to analyze how errors in the x_i propagate into the calculation \overline{Y} from measured values.

$$\overline{Y} = f(x_1, x_2, \dots, x_n) \tag{D.12}$$

As shown by Kline and McClintock (1953) the uncertainty for a result \overline{Y} is given by:

$$u_{\overline{Y}}^{2} = \left(\frac{x_{1}}{\overline{Y}} \frac{\partial \overline{Y}}{\partial x_{1}}\right)^{2} u_{x_{1}}^{2} + \left(\frac{x_{2}}{\overline{Y}} \frac{\partial \overline{Y}}{\partial x_{2}}\right)^{2} u_{x_{2}}^{2} + \cdots$$
(D.13)

The local Nusselt number is obtained from:

$$Nu_{b,x} = \frac{q''D_h}{K(Tw_x - T_{b,x})}$$
 (D.14)

The uncertainties associated with the measurement of various parameters are presented in Table D.2. Uncertainty of the heat flux can then be calculated as following:

$$u_{q''}^{2} = \left(\frac{m}{q''}\frac{\partial q''}{\partial m}\right)^{2}u_{m}^{2} + \left(\frac{C_{p}}{q''}\frac{\partial q''}{\partial C_{p}}\right)^{2}u_{C_{p}}^{2} + \left(\frac{\Delta T}{q''}\frac{\partial q''}{\partial \Delta T}\right)^{2}u_{\Delta T}^{2} + \left(\frac{A}{q''}\frac{\partial q''}{\partial A}\right)^{2}u_{A}^{2} \qquad (D.15)$$

Here A is the bottom plate area and ΔT is the increase in the fluid bulk temperature due to heating. The uncertainty in each property is calculated as follows:

$$u_{\rho}^{2} = (0.0005)^{2} + (0.005)^{2} = 2.53 \times 10^{-5}$$

$$u_{K}^{2} = (0.0005)^{2} + (0.017)^{2} = 2.89 \times 10^{-4}$$

$$u_{C_{-}}^{2} = (0.0005)^{2} + (0.01)^{2} = 1.00 \times 10^{-4}$$
(D.16)

The uncertainty of the mass flow rate and bottom plate area are calculated as:

$$u_{\rm m}^2 = \left(\frac{0.1}{2000}\right)^2 + \left(\frac{0.1}{60}\right)^2 = 2.78 \times 10^{-6}$$
 (D.17)

يستر إلمسترا

Since $A = a'' \times \overline{L}$ and a'' = 2.9cm, $\overline{L} = 250cm$ thus:



$$u_A^2 = \left(\frac{0.05}{250}\right)^2 + \left(\frac{0.01}{2.90}\right)^2 = 1.19 \times 10^{-5}$$
 (D.18)

In the worst case ΔT is about $3^{\circ}C$, therefore:

$$u_{q''}^2 = 2.78 \times 10^{-6} + 1.00 \times 10^{-4} + \left(\frac{0.1}{3}\right)^2 + 1.19 \times 10^{-5} = 1.226 \times 10^{-3}$$
 (D.19)

$$T_{b,x} - T_s = \frac{q''Ax}{m'C_n\overline{L}} \tag{D.20}$$

$$u_{(T_{b,s}-T_{s})}^{2} = 1.34 \times 10^{-3} \tag{D.21}$$

$$u_{T}^{2} = 6.25 \times 10^{-6} \tag{D.22}$$

$$u_{T_{b,1}}^2 = 8.77 \times 10^{-6} \tag{D.23}$$

$$u_{(Tw_x-T_{b,x})}^2 = 3.98 \times 10^{-4} \tag{D.24}$$

The uncertainty of the measured Nusselt number is thus given by:

$$u_{Nu}^{2} = 1.226 \times 10^{-3} + 0.0004 + 2.890 \times 10^{-4} + 3.530 \times 10^{-4} = 2.09 \times 10^{-3}$$

$$u_{Nu} = 0.046$$
(D.25)

Equation D.24 shows that the uncertainty in calculating Nusselt number is 4.6 %. It is estimated that the maximum actual error is not greater than 10 %. The reproducibility of local $Nu_{b,H2}$ values was within ± 3.3 % based on reproducibility tests.

Table D2 Uncertainty for different parameters.

Quantity 🚈	Measurement uncertainty	Correlation uncertainty	Uncertainty (other)	Value
Temperature	0.05°C			
m	0.1 gr			2000 gr
t _f	0.1 sec			60 sec
ΔT	0.1°C			3°C
ρ		0.0005	±0.5%	
K		0.0005	±17%	
C_p		0.0005	±1.0%	
$ar{L}$	0.05 cm			250 cm
D_h	0.02 cm			

D.5 Experimental results

D.5.1 Pressure drop

Table D3 Experimental results

n=0.623, Re=234, Flow Rate=16615 cm³ min⁻¹, $T_e=20.1^{\circ}$ C, Semi-circular duct

x cm	0.95	2.61	4.27	6.50	10.98	22.26	41.98	67.40	103.64	131.76
ΔΡ'	0.478	0.930	1.270	1.730	2.409	4.108	6.967	10.556	15.776	19.543

n=0.623, Re=295, Flow Rate=19701 cm³.min⁻¹, $T_e=20.1^{\circ}$ C, Semi-circular duct

x cm	0.95	2.61	4.27	6.50	10.98	22.26	41.98	67.40	103.64	131.76
$\Delta P'$	0.396	0.799	1.090	1.439	2.032	3.399	5.675	8.526	12.725	15.759

n=0.623, Re=372, Flow Rate=23319 cm³.min⁻¹, $T_e=20.1^{\circ}$ C, Semi-circular duct

x cm	0.95	2.61	4.27	6.50	10.98	22.26	41.98	67.40	103.64	131.76
ΔP'	0.340	0.686	0.930	1.225	1.739	2.877	4.678	6.897	10.298	12.556

n=0.727, Re=805, Flow Rate=22301 cm³.min⁻¹, $T_e=20.1^{\circ}$ C, Semi-circular duct

x cm	0.95	2.61	4.27	6.50	10.98	22.26	41.98	67.40	103.64	131.76
ΔP′	0.262	0.513	0.700	0.910	1.243	1.980	3.101	4.428	6.338	7.691

n=0.727, Re=987, Flow Rate=26153 cm³.min⁻¹, $T_e=20.1^{\circ}$ C, Semi-circular duct

x cm	0.95	2.61	4.27	6.50	10.98	22.26	41.98	67.40	103.64	131.76
ΔP'	0.232	0.450	0.613	0.780	1.100	1.710	2.621	3.720	5.236	6.396

$n=0.727$, $Re=1155$, $Flow Rate=29605 cm^3.min^{-1}$,	T _e =20.1° C, Semi-circular duct
---	---

x cm	0.95	2.61	4.27	6.50	10.98	22.26	41.98	67.40	103.64	131.76
ΔP'	0.210	0.399	0.550	0.713	0.988	1.550	2.345	3.309	4.704	5.597

n=0.623, Re=239, Flow Rate=19754 cm³.min⁻¹, $T_e=20.3^{\circ}$ C, Equilateral triangular duct

x cm	1.18	2.92	4.67	6.99	11.65	23.32	43.76	70.06	105.19	134.44
ΔΡ΄	0.784	1.225	1.570	1.965	2.665	4.202	6.680	9.600	14.100	17.300

n=0.623, Re=301, Flow Rate=23364 cm³.min⁻¹, $T_e=20.3^{\circ}$ C, Equilateral triangular duct

x cm	1.18	2.92	4.67	6.99	11.65	23.32	43.76	70.06	105.19	134.44
ΔΡ΄	0.691	1.068	1.308	1.701 g	2.297	3.601	5.625	7.958	11.316	14.013

n=0.623, Re=379, Flow Rate=27567 cm³.min⁻¹, $T_e=20.3^{\circ}$ C, Equilateral triangular duct

ĺ	x cm	1.18	2.92	4.67	6.99	11.65	23.32	43.76	70.06	105.19	134.44
	ΔP′	0.614	0.944	1.214	1.496	2.001	3.090	4.729	6.600	9.319	11.601

n=0.727, Re=825, Flow Rate=26665 cm³.min⁻¹, $T_e=20.1^{\circ}$ C, Equilateral triangular duct

x cm	1.18	2.92	4.67	6.99	11.65	23.32	43.76	70.06	105.19	134.44
ΔΡ΄	0.514	0.757	0.942	1.137	1.437	2.165	3.173	4.299	5.757	6.988

n=0.727, Re=901, $Flow Rate=28581 \ cm^3.min^{-1}$, $T_e=20.1^{\circ} \ C$, Equilateral triangular duct

х ст	1.18	2.92	4.67	6.99	11.65	23.32	43.76	70.06	105.19	134.44
ΔΡ΄	0.496	0.727	0.894	1.060	1.399	2.067	2.999	4.145	5.434	6.622

n=0.727, Re=989, Flow Rate=30756 cm³.min⁻¹, $T_e=20.1^{\circ}$ C, Equilateral triangular duct

x cm	1.18	2.92	4.67	6.99	11.65	23.32	43.76	70.06	105.19	134.44
ΔP'	0.479	0.687	0.855	1.039	1.302	1.950	2.829	3.856	5.180	6.279

D.5.2 Nusselt Number

D. 5. 2.1 Distilled water

Table D3 (continued)

Re=603, Pr=6.61, $Gr=1.20\times10^6$, Flow Rate=644cm³.min⁻¹, $T_e=22.6^\circ$ C, Semi-circular duct

x cm	6.88	9.88	13.85	23.92	45.02	73.80	98.80	128.77	178.76
$Nu_{b,x}$	23.30	18.98	16.99	20.52	20.30	19.72	21.57	20.73	21.64

Re=607, Pr=6.56, $Gr=2.13\times10^6$, Flow Rate=644cm³.min⁻¹, $T_e=22.9^\circ$ C, Semi-circular duct

x cm	6.88	9.88	13.85	23.92	45.02	73.80	98.80	128.77	178.76
$Nu_{b,x}$	24.67	21.58	19.99	23.84	20.18	21.62	23.70	24.43	24.45

Re=611, Pr=6.51, $Gr=3.49\times10^6$, Flow Rate=644cm³.min⁻¹, $T_e=23.2^\circ$ C, Semi-circular duct

х ст	6.88	9.88	13.85	23.92	.45.02	73.80	98.80	128.77	178.76
$Nu_{b,x}$	26.89	24.64	24.62	26.73	24.56	24.72	27.63	28.07	30.21

Re=780, Pr=6.84, $Gr=1.03\times10^6$, Flow Rate=880 cm³.min⁻¹, $T_e=21.4^\circ$ C, Semi-circular duct

	x cm	6.88	9.88	13.85	23.92	45.02	73.80	98.80	128.77	178.76
,	$Nu_{b,x}$	21.52	18.88	15.78	19.44	20.71	19.41	19.85	17.45	19.36

Re=802, Pr=6.82, $Gr=1.83\times10^6$, Flow Rate=880 cm³.min⁻¹, $T_c=21.5^\circ$ C, Semi-circular duct

х ст	6.88	9.88	13.85	23.92	45.02	73.80	98.80	128.77	178.76
Nu _{b,x}	24.90	20.51	18.54	22.75	22.80	22.40	22.88	21.86	23 46

Re=829, Pr=6.56, $Gr=2.92\times10^6$, Flow Rate=880 cm³.min⁻¹, $T_e=22.9^\circ$ C, Semi-circular duct

x cm	6.88	9.88	13.85	23.92	45.02	73.80	98.80	128.77	178.76
$Nu_{b,x}$	24.90	20.51	18.54	22.75	22.80	22.40	22.88	21.86	23.46

Re=1074, Pr=6.72, Gr=1.06 × 10^6 , Flow Rate=1164 cm³.min⁻¹, T_e =22.0° C, Semi-circular duct

x cm	6.88	9.88	13.85	23.92	45.02	73.80	98.80	128.77	178.76
$Nu_{b,x}$	22.97	20.43	16.89	16.64	18.71	19.66	21.78	18.34	21.68

Re=1075, Pr=6.71, $Gr=1.70\times10^6$, Flow Rate=1164 cm³.min⁻¹, $T_e=22.1^\circ$ C, Semi-circular duct

x cm	6.88	9.88	13.85	23.92	45.02	73.80	98.80	128.77	178.76
$Nu_{b,x}$	26.67	22.70	19.09	19.37	23.95	22.55	23.82	20.86	27.57

Re=1076, Pr=6.70, $Gr=2.62\times10^6$, Flow Rate=1164 cm³.min⁻¹, $T_e=22.1^\circ$ C, Semi-circular duct

x cm	6.88	9.88	13.85	23.92	45.02	73.80	98.80	128.77	178.76
$Nu_{b,x}$	28.49	24.31	20.52	23.30	27.08	22.56	26.63	28.16	32.53

Re=542, Pr=6.79, $Gr=9.03\times10^{5}$, $Flow Rate=640 \text{ cm}^3.\text{min}^{-1}$, $T_e=21.7^{\circ}$ C, Equilateral triangular duct

294	2107 W. 17 1W	ngalar a	uc:						
x cn	7.02	10.02	13.99	24.11	45.15	73.96	99.00	129.01	179.01
$Nu_{b,x}$	15.15	13.70	14.54	16.08	18.35	17.45	13.88	17.13	18.11

Re=542, Pr=6.77, $Gr=1.70\times10^6$, $Flow\ Rate=640\ cm^3.min^{-1}$, $T_e=21.7^{\circ}\ C$,

Equilateral triangular duct

x cm	7.02	10.02	13.99	24.11	45.15	73.96	99.00	129.01	179.01
$Nu_{b,x}$	18.17	16.37	21.05	21.62	21.30	23.30	19.18	20.91	23.01

Re=543, Pr=6.76, $Gr=2.71\times10^6$, $Flow\ Rate=640\ cm^3.min^1$, $T_e=21.8^{\circ}\ C$,

Equilateral triangular duct

	7		-6							
x	cm	7.02	10.02	13.99	24.11	45.15	73.96	99.00	129.01	179.01
λ	$u_{b,x}$	22.35	21.25	26.24	25.23	23.96	24.10	23.60	25.78	27.21

Re=743, Pr=6.63, Gr=1.01×10 6 , Flow Rate=860 cm 3 .min $^{-1}$, T_e =22.5 o C, Equilateral triangular duct

x cm	7.02	10.02	13.99	24.11	45.15	73.96	99.00	129.01	179.01
$Nu_{b,x}$	16.90	14.41	14.87	15.33	16.78	17.65	16.79	15.70	17.44

Re=744, Pr=6.62, Gr=1.85 \times 10⁶, Flow Rate=860 cm³.min⁻¹, T_e =22.6° C, Equilateral triangular duct

x cm	7.02	10.02	13.99	24.11	45.15	73.96	99.00	129.01	179.01
$Nu_{b,x}$	19.15	16.49	21.50	25.15	19.74	26.31	21.92	19.85	21.29

Re=745, Pr=6.61, $Gr=2.93\times10^6$, Flow Rate=860 cm³.min⁻¹, $T_e=22.6^\circ$ C, Equilateral triangular duct

x cm	7.02	10.02	13.99	24.11	45.15	73.96	99.00	129.01	179.01
$Nu_{b,x}$	22.55	19.63	26.94	26.26	23.53	26.62	23.62	24.61	23.10

Re=993, Pr=6.54, $Gr=1.15\times10^6$, Flow Rate=1136 cm³.min⁻¹, $T_e=23.0^\circ$ C, Equilateral triangular duct

x cm	7.02	10.02	13.99	24.11	45.15	73.96	99.00	129.01	179.01
$Nu_{b,x}$	16.92	14.01	16.37	15.82	16.33	15.79	19.96	18.22	15.96

Re=994, Pr=6.53, $Gr=1.92\times10^6$, Flow Rate=1136 cm³.min⁻¹, $T_e=23.1^\circ$ C, Equilateral triangular duct

	7.00.000	07 007 17 700	-5 m - ca.	***						
x	ст	7.02	10.02	13.99	24.11	45.15	73.96	99.00	129.01	179.01
λ	$u_{b,x}$	18.92	15.29	19.87	21.31	19.89	23.11	22.94	19.84	19.60

Re=997, Pr=6.51, $Gr=3.08\times10^6$, $Flow\ Rate=1136\ cm^3.min^{-1}$, $T_e=23.2^\circ\ C$,

Equilateral triangular duct

x cm	7.02	10.02	13.99	24.11	45.15	73.96	99.00	129.01	179.01
$Nu_{b,x}$	20.35	17.85	24.54	27.83	25.50	25.30	25.61	24.23	21.94

D.5.2.2 Viscous non-Newtonian fluid

Table D3 (continued)

n=0.623, Re=11.21, Pr=1018, Gr=75.7, B=-0.511, Flow Rate=1831 cm³.min⁻¹,

Q=344 w, $T_e=20.4$ °C, Semi-circular duct

x cm	6.88	9.88	13.85	23.92	45.02	73.80	98.80	128.77	178.76
$Nu_{b,x}$	20.89	18.22	16.00	13.09	10.29	8.70	7.91	7.20	6.63

n=0.623, Re=9.14, Pr=1077, Gr=67.7, B=-0.457, Flow Rate=1579 cm³.min⁻¹, Q=308 w, $T_e=20.4^{\circ}C$, Semi-circular duct

x cm	6.88	9.88	13.85	23.92	45.02	73.80	98.80	128.77	178.76
$Nu_{b,x}$	17.53	15.34	13.50	11.01	8.82	7.47	6.80	6.27	5.71

n=0.623, Re=4.23, Pr=1330, Gr=27.5, B=-0.317, Flow Rate=902 cm³.min⁻¹, <math>Q=213 w, $T_e=20.4$ °C, Semi-circular duct

x cm	6.88	9.88	13.85	23.92	45.02	73.80	98.80	128.77	178.76
$Nu_{b,x}$	16.03	13.86	12.14	9.79	8.01	6.68	6.14	5.63	5.24

-

 $\{\lambda_{i},z\}$

n=0.623, Re=4.23, Pr=1330, Gr=30.8, B=-0.354, Flow Rate=902 cm³.min⁻¹, O=239 w, $T_e=20.4$ °C. Semi-circular duct

x cm	6.88	9.88	13.85	23.92	45.02	73.80	98.80	128.77	178.76
$Nu_{b,x}$	16.33	13.80	12.05	9.83	7.88	6.69	6.13	5.65	5.27

n=0.623, Re=4.23, Pr=1330, Gr=19.4, B=-0.224, Flow Rate=902 $cm^3.min^{-1}$, Q=151 w, $T_e=20.4$ °C, Semi-circular duct

x cm	6.88	9.88	13.85	23.92	45.02	73.80	98.80	128.77	178.76
$Nu_{b,x}$	16.02	13.93 ₀	12.07	9.65	7.97	6.65	6.12	5.59	5.17

n=0.727, Re=19.65, Pr=383, Gr=351, B=-0.309, Flow Rate=1206 cm³.min⁻¹, Q=227 w, $T_e=20.1$ °C, Semi-circular duct

x cm	6.88	9.88	13.85	23.92	45.02	73.80	98.80	128.77	178.76
$Nu_{b,x}$	17.13	14.89	13.07	10.65	8.58	7.36	6.82	ó.52	6.55

n=0.727, Re=11.54, Pr=429, Gr=279, B=-0.309, $Flow\ Rate=794\ cm^3.min^{-1}$, $Q=226\ w$, $T_e=20.1^{\circ}C$, $Semi-circular\ duct$

x cm	6.88	9.88	13.85	23.92	45.02	73.80	98.80	128.77	178.76
$Nu_{b,x}$	14.60	12.69	11.15	9.24	7.59	6.91	6.85	6.87	7.40

n=0.727, Re=16.21, Pr=399, Gr=339, B=-0.324, $Flow\ Rate=1037\ cm^3.min^{-1}$, $Q=238\ w$, $T_a=20.1^{\circ}C$, $Semi-circular\ duct$

x cm	6.88	9.88	13.85	23.92	45.02	73.80	98.80	128.77	178.76
$Nu_{b,x}$	16.17	14.04	12.34	10.11	8.17	7.07	6.64	6.49	6.62

n=0.727, Re=16.21, Pr=399, Gr=278, B=-0.266, Flow Rate=1037 cm³.min⁻¹, Q=195 w, $T_e=20.1$ °C, Semi-circular duct

x cm	6.88	9.88	13.85	23.92	45.02	73.80	98.80	128.77	178.76
$Nu_{b,x}$	16.14	14.07	12.36	10.08	8.15	6.99	6.48	6.20	6.26

n=0.727, Re=16.21, Pr=399, Gr=432, B=-0.413, $Flow\ Rate=1037\ cm^3.min^{-1}$, $Q=303\ w$, $T_e=20.1^{\circ}C$, $Semi-circular\ duct$

x cm	6.88	9.88	13.85	23.92	45.02	73.80	98.80	128.77	178.76
$Nu_{b,x}$	16.17	13.98	12.37	10.14	8.24	7.24	6.96	6.91	7.05

(E)7/--

Sp

n=0.623, Re=5.43, Pr=1218, Gr=25.3, B=-0.284, Flow Rate=1264 cm³.min⁻¹, O=202 w, T_e =20.3°C, Equilateral triangular duct

x cm	7.02	10.02	13.99	24.11	45.15	73.96	99.00	129.01	179.01
$Nu_{b,x}$	12.09	10.59	9.46	<i>7.87</i>	6.43	5.46	4.99	4.62	4.24

n=0.623, Re=4.15, Pr=1311, Gr=16.3, B=-0.203, $Flow Rate=1040 \text{ cm}^3.\text{min}^{-1}$, O=145 w, $T_e=20.3^{\circ}\text{C}$. Equilateral triangular duct

x cm	7.02	10.02	13.99	24.11	45.15	73.96	99.00	129.01	179.01
$Nu_{b,x}$	11.70	10.28	9.16	7.55	6.08	5.21	4.77	4.42	4.06

n=0.623, Re=3.16, Pr=1412, Gr=14.3, B=-0.208, Flow Rate=853 cm³.min⁻¹, O=148 w. $T_0=20.3$ °C. Equilateral triangular duct

x cm	7.02	10.02	13.99	24.11	45.15	73.96	99.00	129.01	179.01
$Nu_{b,x}$	10.61	9.36	8.38	6.97	5.65	4.86	4.46	4.17	3.85

n=0.623, Re=3.16, Pr=1412, Gr=17.2, B=-0.250, Flow Rate=853 cm³.min O=178 w, $T_e=20.3$ °C, Equilateral triangular duct

x cm	7.02	10.02	13.99	24.11	45.15	73.90	99.00	129.01	179.01
$Nu_{b,x}$	10.58	9.38	8.36	6.91	5.73	4.91	4.47	4.19	3.91

n=0.623, Re=3.16, Pr=1412, Gr=20.6, B=-0.299, Flow Rate=853 cm³.min⁻¹, O=214 w. $T_e=20.3$ °C. Equilateral triangular duct

x cm	7.02	10.02	13.99	24.11	45.15	<i>75.96</i>	99.00	129.01	179.01
$Nu_{b,x}$	10.43	9.24	8.28	6.93	5.67	4.95	4.45	4.16	3.95

179.01

4.62

6.12

5.22

4.83

4.61

n=0.727, Re=14.26, Pr=403, Gr=218, B=-0.236, Flow Rate=1100 cm³.min⁻¹, <math>O=184 w. $T_{\bullet}=20.4^{\circ}C$. Equilateral triangular duct

	20.	, -8 -	••••	7	 			
x	cm	7.02	10.02	13.99	45.15	73.96	99.00	129.01

7.53

 $Nu_{b,x}$

11.61

10.20

9.06

n=0.727, Re=11.25, Pr=424, Gr=150, B=-0.180, Flow Rate=913 cm³.min⁻¹, O=140 w. $T_{-}=20.4^{\circ}C$. Equilateral triangular duct

	7.02	1		· · · · · · · · · · · · · · · · · · ·		72.06	00.00	120.01	170.01
x cm	7.02	10.02	15.99	24.11	45.15	73.90	99.00	129.01	1/9.01
$Nu_{b,x}$	11.17	9.80	8.72	7.21	5.85	4.98	4.59	4.36	4.39

n=0.727, Re=17.24, Pr=387, Gr=263, B=-0.263, $Flow\ Rate=1276\ cm^3.min^{-1}$, $Q=204\ w$, $T_s=20.4^{\circ}C$, Equilateral triangular duct

x cm	7.02	10.02	13.99	24.11	45.15	73.96	99.00	129.01	179.01
$Nu_{b,x}$	11.92	10.57	9.43	7.84	6.39	5.45	5.03	4.78	4.71

n=0.727, Re=17.24, Pr=387, Gr=354, B=-0.355, Flow Rate=1276 cm³.min⁻¹, O=275 w. $T_{\bullet}=20.4$ °C. Equilateral triangular duct

x cm	7.02	10.02	13.99	24.11	45.15	73.96	99.00	129.01	179.01
$Nu_{b,x}$	11.93	10.46	9.33	7.74	6.34	5.48	5.15	4.95	4.96

n=0.727, Re=17.24, Pr=387, Gr=423, B=-0.423, $Flow\ Rate=1276\ cm^3.min^{-1}$,

Q=328 w, $T_s=20.4$ °C, Equilateral triangular duct

x cm	7.02	10.02	13.99	24.11	45.15	73.96	99.00	129.01	179.01
$Nu_{b,x}$	11.87	10.39	9.30	7.73	6.33	5.58	5.29	5.08	5.11